

Christer Kobbevik Oldeide

Development of Hybrid Aluminum Carbon Fiber Composite Wheels for a Formula Style Race Car

November 2017



©FSG Soukup



Norwegian University of
Science and Technology

Development of Hybrid Aluminum Carbon Fiber Composite Wheels for a Formula Style Race Car

Christer Kobbevik Oldeide

Master of Science in Mechanical Engineering
Submission date: November 2017
Supervisor: Jan Torgersen, MTP

Norwegian University of Science and Technology
Department of Mechanical and Industrial Engineering

© 2017 - CHRISTER KOBBEVIK OLDEIDE

ALL RIGHTS RESERVED.

Development of Hybrid Aluminum Carbon Fiber Composite Wheels for a Formula Style Race Car

ABSTRACT

Modern short product life cycles and the necessity to rapidly manufacture components with minimal production needs poses stringent requirements on both time and sophistication of modern product design. Light weight components are more and more in demand, which drives industry to utilize advanced materials like Carbon Fiber Reinforced Polymer (CFRP). The ever-increasing demands of conventional design methods often fail to fulfill the necessary requirements for complex, high performing components. For example, conventional design methods for composites are done manually and often based on experience which is time consuming and can result in non-optimal designs. Using simulation based design (SBD) approaches, this thesis presents FE optimization models that can lead to next generation CFRP designs. A two module wheel is presented consisting of a topology optimized aluminum center for easy machinability and a CFRP rim, for which the layup was optimized in a self-developed evolution based material optimization algorithm. The design considerations and developed algorithm are presented in this thesis as well as the results on optimization with the weight target of 700 g and maximization of the total global stiffness which yielded a deflection of maximum 2.27 mm in cornering at 110 km/h. The optimization was based on two quasi static load scenarios gathered from vehicle dynamic simulations performed by collaborators. The optimized rim shell has an increased specific stiffness of around 45 % and a decreased rotational inertia of nearly 70 %, compared to an aluminum rim shell. The combination of the optimized design and a high quality production resulted in high performing rims that worked well throughout the competitions and during tuning of the car. Mechanical tests on the wheel showed the perfect agreement between the simulation and the experimental results. The largest discrepancy was found in large static loads up to 200 kg, where the discrepancy of the total deformation was 15.6 %. To the best of the author's knowledge, this work presents the first complete and successful approach towards the parametric material optimization of a CFRP component linked to an entire product development process from the initial design consideration all the way to mechanical testing and application. It is likely helpful to many researchers and developers of next-generation composite designs.

Utvikling av Hybrid Aluminum Karbonfiberforsterket Polymer Felger for en Formula type racerbil

SAMMENDRAG

Moderne produkters korte livssykluser og krav om rask produksjon og minimerte produksjonsbehov stiller høye krav til et sofistikert design av produktet. Etterspørselen etter lette produkter presser næringslivet til å anvende avanserte materialer, slik som karbonfiberforsterkede polymerer (CFRP). Konvensjonelle designmetoder evner derimot ikke å oppfylle de nødvendige kravene stilt til komplekse komponenter, som skal yte på høyt nivå. For eksempel er design for kompositter ofte gjort manuelt og basert på erfaring, hvilket er tidskrevende og ikke nødvendigvis gir det beste designet. Denne avhandlingen kommer til å presentere FE-optimaliseringsmodeller ved bruk av simuleringsbasert design (SBD), som kan føre til neste generasjons kompositdesign. Designet som er presentert, er et todelt hjul bestående av et topologioptimalisert aluminiumssenter, som også er optimalisert for maskinering, og en CFRP-felg, som er optimert med en egenutviklet og evolusjonsbasert materialoptimaliseringsalgoritme. Designkravene og den utviklede algoritmen er her presentert sammen med resultatene fra optimaliseringen. Optimaliseringen hadde et vektkrav på 700 g, samtidig som den globale stivheten skulle maksimeres. Det resulterte i en maksimal defleksjon på 2.27 mm når belastet med kreftene fra sving ved 110 km/t. Optimeringen ble basert på to kvasistatiske lastscenarioer gitt av analyser av bilens kjøredynamikk, utført av samarbeidspartnere. Den optimerte felgbanen har omrent 45% høyere spesifikk stivhet og nesten 70 % lavere treghetsmoment enn en felgbane av aluminium. Optimalisert design sammen med høy-kvalitets produksjon førte til et sluttprodukt av høy kvalitet, som fungerte bra både under konkurransene og testingen. Mekaniske tester av det fullstendige designet viste perfekt overensstemmelse med simuleringene. Det største avviket var på 15.6 % og inntraff ved store statiske laster opp til 200 kg. Så vidt forfatteren vet er dette arbeidet det første som kan vise til et fullstendig og vellykket design ved parametrisk materialoptimalisering av en CFRP-komponent, som også er en del av en fullstendig produktutviklingsprosess fra konseptualisering til mekanisk testing og faktisk anvendelse av ferdig produkt. Sannsynligvis vil det være hjelpsomt for utviklere av neste generasjons kompositdesign.

Acknowledgments

I WOULD LIKE TO DIRECT SPECIAL THANKS TO MY SUPERVISOR JAN TORGERSEN WHO HAS BEEN HELPFUL, INSPIRING AND MY BIGGEST MOTIVATION THROUGH THE WORK OF THIS THESIS.

For a person who has been active in Revolve NTNU and Formula Student over the last five years, and is generally interested in motorsport, this is a dream come true to be able to write about your favorite topic. As an car enthusiast and a person that dreams about working in the car industry, getting the chance to write for an organization like Revolve NTNU, is possibly the best opportunity to get involved with the car manufacturing and the motorsport, as Formula Student collaborates closely with the car industry and the motorsport society.

I would like to give thanks to Revolve NTNU for giving me this unique chance and to the sponsors, Mjøs Metallvarefabrikk AS, Dassault Systèmes Simulia Corp., Molstad modell and Kongsberg Gruppen for helping me bring this work to life. A special thanks goes to Jon Martin Haaland for helping me getting a better knowledge of vehicle dynamics and also Jørgen Eliassen, Jacob Vigerust, Jens Mildestveit and Simen Ekoråsvåg for general engineering advise. I would also thank my mom and dad, Oddrun and Øystein for encouraging. Without their support I would not have the opportunity to take this degree.

Last but not least, I would thank Maria Bjelland and Maria Dyrseth for the endless hours they spent helping in the production of the carbon fiber reinforced rim shell.

I WOULD LIKE TO DEDICATE MY THESIS TO REVOLVE NTNU
- MY BIGGEST PASSION OVER THE LAST FIVE YEARS

Contents

ABSTRACT	i
SAMMENDRAG	iii
1 INTRODUCTION	1
1.1 Performance of a Wheel	2
1.2 Revolve NTNU and Team Role	5
1.3 Rim Concepts	6
1.4 CFRP layup	8
1.5 Structural Optimization & Simulation Driven Design	9
1.6 Previous Work and Motivation	9
2 METHODS AND PROCEDURE	11
2.1 Load Scenarios	11
2.2 Rim Center	12
2.3 Rim Shell	15
2.4 Validation	23
2.5 Mechanical Testing	24
3 RESULTS & DISCUSSION	29
3.1 Rim Center Design	29
3.2 Rim Shell	31
3.3 Validation	34
3.4 Production	38
3.5 Mechanical Testing and Verification	39
4 CONCLUSION	47
4.1 Future Work	48

REFERENCES	50
APPENDICES	51
A MODELING, SET-UP, PROCEDURES & RESULTS	53
A.1 Load Scenarios	54
A.2 FEA - validation Setup	59
A.3 Material Optimization Setup	72
A.4 Topology Optimization Setup	96
A.5 FEM validation Results	101
A.6 Mechanical Testing Results	108
A.7 Reaction Forces on tire - estimated from log data - Half Endurance	113
A.8 Rim Shell Production - Pictures	114
A.9 2014 Layup - used to benchmark Optimized layup	124
B MACHINE DRAWINGS	125
B.1 Machine Drawings Rim Center	126
B.2 Machine Drawing - Molds	127
B.3 Machine Drawings Rim Shell	129
B.4 Base dimensions of Test jig	131
C MEASURING REPORTS & STANDARDS	132
C.1 Measuring Raport Rim Center	133
C.2 Measuring Raport Rim Shell - inner contour	135
C.3 Measuring Raport Rim Shell - outer contour	136
C.4 ETRTO standard for drop center and hump design	137
D DATASHEETS	139
D.1 Strain gauge FRA-5-11-3L	140
D.2 Aluminum 7075 (7075-T651)	142
D.3 Hexcel 6376 - Resin Properties	145
D.4 Hexcel 6376 - Weave Properties	147
D.5 Hexcel 6376 - Unidirectional Properties	149
D.6 Frekote B-15	151
D.7 Frekote 700 NC	153
E SCIENCE IN THE AGE OF EXPERIENCE CONFERENCE	155

Listing of figures

1.1.1 Simplified quarter model	2
1.1.2 Simplified rim	2
1.1.3 Plot of how the distribution between inner and outer mass effect equivalent mass	3
1.1.4 Continental C16 7J-13 rim 80kPa - Camber sensitivity	4
1.3.1 2-piece concept, Revolve NTNU 2014	6
1.3.2 1-piece concept, GreenTeam 2013	6
1.3.3 Monoblock CFRP rim, The Koenigsegg Carbon Fiber Wheel	6
1.3.4 2-piece full CFRP concept, Revolve NTNU 2016	7
1.4.1 Weave types 5 harness sating weave & Unidirectional-fibers	8
2.2.1 Illustration of design space for Rim Center	13
2.3.1 Work flow - Material Optimization	16
2.3.2 Segmentation of the Rim Shell	17
2.3.3 2-piece positive mold design	18
2.3.4 Illustration of Autoclave prepreg Casting process	18
2.3.5 Production documentation for Rim Shell	19
2.3.6 Joint designs for CFRP layup	20
2.3.7 Layup production of Rim Shell	21
2.3.8 Bagging of CFRP Rim Shell	21
2.3.9 Curing cycle for Hexcel 6376 prepreg	22
2.3.10 Demoulding of Rim Shell	22
2.5.1 Mechanical testing - set-up	24
2.5.2 Illustration of a 3-axis strain gauge rosette	24
2.5.3 Illustration of strain gauge positions and placement of displacement sensors	25
2.5.4 Mounting of strain gauge on Rim Shell	25
2.5.5 Ramp for Vertical Load during quasi static testing of Rim	26
2.5.6 Fixture jig for applying vertical loads during mechanical testing	27

3.1.1 Resulting cross-section of TO rim center	29
3.1.2 Raw data from Topology Optimization performed in Tosca	30
3.1.3 Iterations from Tosca Structure of the 9 spoke rim center	30
3.1.4 Draft analysis of TO design and regenerated machinable designs	31
3.2.1 All CFRP Layup Optimization iterations presented in a mass vs. strain energy plot	32
3.2.2 Sorted layup iterations with strain energy in ascending order	32
3.3.1 Validation results from FEA performed in Abaqus	35
3.3.2 Most stressed section of rim center	36
3.3.3 Stress spectrum for most stressed section of the Rim Center	36
3.3.4 Whole stress cycles for half endurance counted with Rainflow counting	37
3.4.1 Production results	38
3.4.2 Final assembled wheel	39
3.5.1 Comparison of axial strain between FEA and mechanical testing of rim shell	40
3.5.2 Comparison of hoop strain between FEA and mechanical testing of rim shell	40
3.5.3 Comparison of displacement at inner bead between FEA and mechanical testing	41
3.5.4 Comparison of displacement at outer bead between FEA and mechanical testing	41
3.5.5 Comparison of axial strain between FEA and mechanical testing of rim shell subjected to a vertical load of 200 kg	42
3.5.6 Comparison of hoop strain between FEA and mechanical testing of rim shell subjected to a vertical load of 200 kg	42
3.5.7 Dynamical loading of wheel with a vertical loading of 180-200 kg	43
3.5.8 Ebd at testing in Karlsruhe ,Germany	44
3.5.9 Tire changing performed with a tire changing machine	45

Listing of tables

1.1.1 Parameters for Quarter Model	2
1.3.1 Pro and cons of concepts CFRP concepts	7
2.1.1 Quasi static load scenarios for warm tires	12
2.2.1 Design constrains for the center	13
2.2.2 Topology Optimization Set-up	14
2.3.1 Design requirements for the shells	15
3.1.1 Specific stiffness for the 2 different center designs,normalized respect to topology optimized design	31
3.2.1 Layup Result from Material Optimization	33
3.2.2 Performance of optimized layup compared to a aluminum shell and the 2014 layup	33
3.3.1 Validation result including non-linear effects	34
3.3.2 Fatigue properties of Rim Center	37
3.5.1 Error contribution in Mechanical Testing	43

Abbreviations

α	Ratio between m_{out} & m_{in}
ε	Micro Strain
ω	Rotational velocity of rim
E	Elastic Modulus
E_t	Total energy stored in the rim
f_x	Reaction force on tire - Longitudinal direction
f_y	Reaction force on tire - Lateral direction
f_z	Reaction force on tire - Vertical direction
G	Shear Modulus
I	Rotational inertia of rim
m	Total mass of rim
m_e	Equivalent mass
m_{in}	Mass of rim center
m_{out}	Mass of rim shell
N_i	Cycles of stress causing failure at each stress amplitude
n_i	Cycles of reversed stress amplitude
ν	Poisson Ratio
5HS	5 Harness Satin

CAD Computer Aided Design

CAM Computer Aided Manufacturing

CF Carbon Fiber

CFRP Carbon Fiber Reinforced Polymer

CM Center Mount

CMM Coordinate Measuring Machine

CNC Computer Numerical Control

CS Center Shell

DA Drapability Analysis

ETRTO European Tyre and Rim Technical Organisation

FEA Finite Element Analysis

FEM Finite Element Model

FS Formula Student

IB Inner Bead

ID Inner Drop

IF Inner Flange

MO Material Optimization

OB Outer Bead

OD Outer Drop

OF Outer Flange

SBD Simulation Based Design

TO Topology Optimization

UD Unidirectional

There are two really innovative forms of motorsport left: Formula One and Formula Student.

Ross Brawn

1

Introduction

The motorsport industry is constantly working to improve the performance of their cars by looking into advanced materials and manufacturing methods. Key factors to improved performance of a race car are to reduce mass and compliance. The wheel is one of the most important components where mass and stiffness affect the performance of a race car the most. The effect of unsprung and rotational mass is well known as well as how the compliance affects the handling predictability.

In terms of tackling the above challenges with appropriate material choice, there is no material that can compete with carbon fiber-reinforced polymers (CFRP) when it comes to reducing weight in the automotive industry. CFRP has excellent qualities when it comes to strength, weight, and formability. Carbon Fiber composites have been used for a long time in Formula 1 and other extreme sports as their unique stiffness and tunability to specific load cases allows to limit material use and hence to reduce mass. The mechanical property advantage is paired with low investment requirements for production and ease to shape these materials routinely into complex aerodynamic shapes. Due to the polymeric nature, CFRPs are superior for corrosion and energy uptake in high-speed crashes. The main advantage of utilizing fiber composites is the possibility to produce a tailor-made material with the desired geometry for a specified application. It is not a surprise that the unsprung and rotational mass problem in race cars is a ideal scenario for the use of CFRPs. In 2013, Koenigsegg made the world's first hollow, one piece, super light carbon fiber wheel, using their proprietary method named Aircore™ Technology[1]. This wheel is about 40 % lighter and 60 % stiffer than a commercial aluminium alloy race rim.

1.1 PERFORMANCE OF A WHEEL

The performance of a wheel is crucial for a race car. The interaction between suspension, rim, tire, and road can be what makes your team win or lose. The weight and stiffness of the rim is very important for the performance of the suspension and the overall vehicle dynamics. In this section, there will be a short introduction on how weight and stiffness are influencing the vehicle performance, the key motivational background of this thesis.

1.1.1 UNSPRUNG MASS

By using a quarter model of the car to simulate a bump, it can be illustrated easily how the unsprung mass impacts the air time of the wheel and the suspension travel. Parameters used for the quarter model ((Figure 1.1.1) is found in table 1.1.1). A bump is modeled as an extreme case, when the wheel leaves the bump with a characteristics initial velocity of 3 m/s, while the chassis is staying still. The simulation shows that doubling the unsprung mass, doubles the air time of the wheel and increases the suspension travel by 85.7 % .

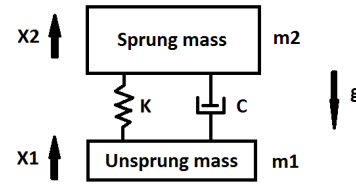


Figure 1.1.1: Simplified quarter model
leaves the bump with a characteristics initial velocity of 3 m/s, while the chassis is staying still. The simulation shows that doubling the unsprung mass, doubles the air time of the wheel and increases the suspension travel by 85.7 % .

Table 1.1.1: Parameters for Quarter Model

Case	m_1 [kg]	m_2 [kg]	k [N/mm]	$g[m/s^2]$
1	6.8	60	35	9.81
2	13.6	60	35	9.81

1.1.2 CONCEPT OF EQUIVALENT MASS

The effect of rotational inertia affects the car during braking, acceleration and overall handling properties. One way to compare the effect of rotational inertia is to introduce the concept of equivalent mass. The total energy stored in the rim is a combination of its translational kinetic energy and its rotational kinetic energy, $E_t = \frac{1}{2}mv^2 + \frac{1}{2}I\omega^2$. Expressing the total energy as the non-rotating energy of some equivalent mass m_e , the equivalent mass can be simplified to [2]:

$$m_e = m + I\omega^2 \quad (1.1)$$

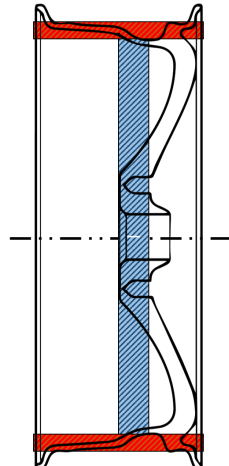


Figure 1.1.2: Simplified rim

Simplifying the rim to a solid disk and a cylindrical shell (Fig: 1.1.2) and defining α as the ratio between outer mass and the inner mass, m_{out} and m_{in} :

$$\alpha = \frac{m_{out}}{m_{out} + m_{in}} \quad (1.2)$$

Then the relation between equivalent mass and sprung-mass is:

$$m_e = m \left(1 + \frac{\alpha + 1}{2}\right) \quad (1.3)$$

Reducing rotational mass is 1.5 - 2.0 times more effective than reducing the same amount of "static mass" (fig: 1.1.3).

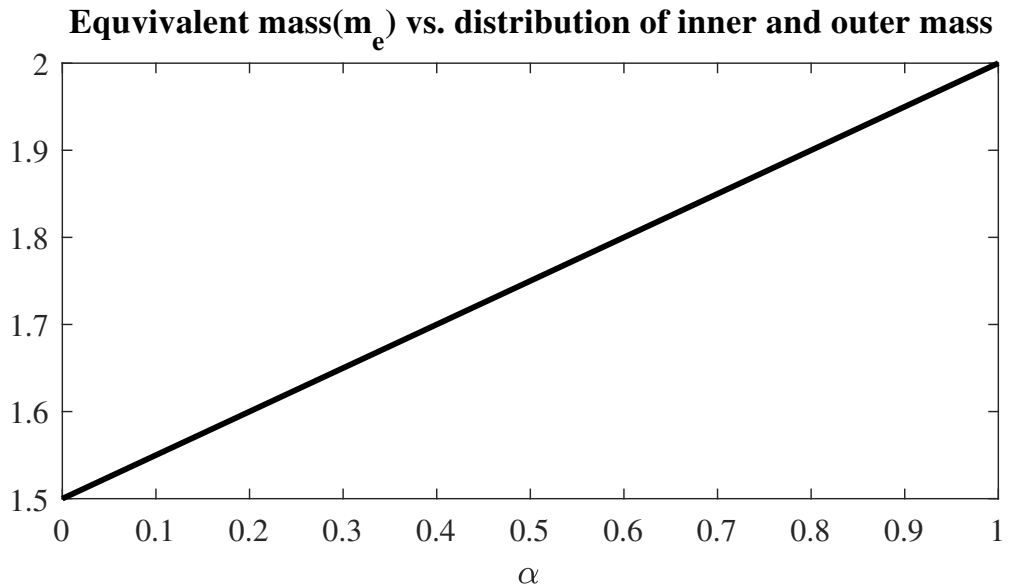


Figure 1.1.3: Plot of how the distribution between inner and outer mass effect equivalent mass

1.1.3 STIFFNESS

Rim stiffness influences the vehicle dynamics, both in terms of possible camber gain and delay of load transfer. The stiffness versus mass can be looked at as a compromise where the performance of the wheel is directly affected by both parameters. By looking at the camber sensitivity in Figure 1.1.4 it is possible to understand how the stiffness of the rim affects the vehicle performance. Following the curves from Figure 1.1.4 we see that the tires actually increase the lateral capacity with camber going in the right direction. This means that if the tire leans in the turn, (negative camber on outer and positive camber on inner tire) camber thrust will give positive effects. The car is turning both right and left, and the most important criteria is that the outer wheel, which have the greatest load, cannot have positive camber, which a flexible rim could contribute to. A stiffer rim could give a quicker load transfer between tire and suspension, which will make transients faster.

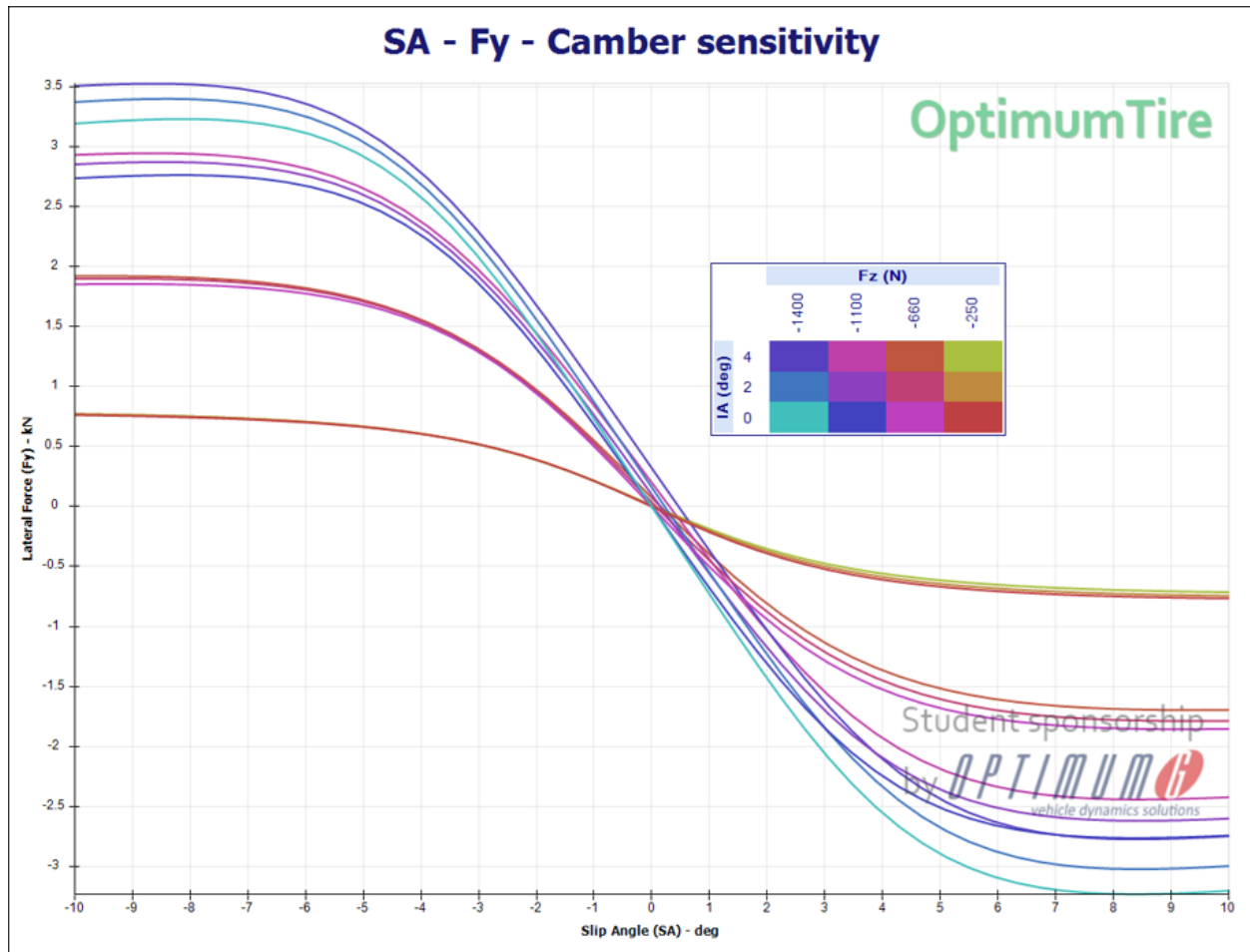


Figure 1.1.4: Continental C16 7J-13 rim 80kPa - Camber sensitivity estimated by Jon Martin Haaland[3]

With this motivational background, this thesis reports the development of a unique CFRP race rim for the 2017 Revolve student race car ELD.

1.2 REVOLVE NTNU AND TEAM ROLE

Revolve NTNU is an independent student organization at the Norwegian University of Science and Technology. In one year, the team completes a full product development process in order to produce a fully functional race car to compete in one of the largest engineering competitions for students in the world, the Formula Student (FS). I was part of the suspension group, where my main task was to develop and produce the wheels for the 2017 car.

This thesis will introduce the reader to the entire product development process of this rim, from the initial design considerations and the reasoning of the multi-material choices, to the developed algorithm for the CFRP layup, the material optimization with weight target procedure as well as the production, the use in the race car competition and the mechanical testing in static and dynamic load case scenarios. This thesis is hence an elaborate work involving overlaps between product design, development of simulation tools and production challenges. In the ambit of the extend of the work, the writer wants to keep the information restricted to the novelties developed within this thesis without spending too much time on revisiting the basic concepts and theory this work is based on. Hence the writer requires the reader to have a basic understanding on:

- Finite Element Method (FEM)
- Topology Optimization (TO)
- Computer Aided Design (CAD)
- Application of FEA in Abaqus for both isotropic and anisotropic materials.
- Carbon Fiber Reinforced Polymer (CFRP)
- Basic Racecar Vehicle Dynamic

1.3 RIM CONCEPTS

1.3.1 2-PIECE CFRP SHELL WITH ALLOY CENTER

The multi-piece rim consists of two separate carbon fiber reinforced plastic wheel shells, which hold the tire and are joined by an alloy metal center connecting the wheel assembly. One of the advantages of having a multi-piece rim is that the tire could be mounted while assembling the rim. This eliminates the use of conventional tire mounting machines that pull the sidewalls of the tires over the flanges on the rims. Sometimes this requires a lot of force which could shatter or permanently damage the brittle CFRP rims, as seen in the competitions.

1.3.2 1-PIECE CFRP SHELL WITH ALLOY CENTER

The 1-piece or single-piece shell solution is quite similar to the latter solution. The production is potentially more difficult but can result in a lighter solution as less carbon is needed. Fewer discontinuities in the layup could benefit in a stiffer rim. However, it would not be possible to mount the tire without a tire changing machine. Furthermore, if the drop center is not designed properly, the flange could be susceptible to cracking or might experience high damage making the rim unsafe to run. To prevent this, a possible solution is to add more fibers around the flanges and dimension the rim for the loads related to mounting, resulting in a heavier solution. For this reason, the drop center should be carefully designed.

1.3.3 MONOBLOCK CFRP WHEEL

The monoblock CFRP rim is the lightest and stiffest solution. It can be produced using CFRP only, or by introducing the use of a core, resulting in a sandwich type structure. In 2013 Koenigsegg made the world's first hollow, one-piece and super light carbon fiber wheel, using a proprietary method developed named Aircore™ Technology[1]. Another way to produce a hollow, or a complete CFRP wheel, is to experiment with an air bladder or a 3D-printed core subsequently melted or dissolved and drained out through shear-pin holes or valve steam holes. Again, this solution would have the same issues related to the tire mounting as the previous solution. It is also the most complex and expensive solution discussed here with respect to production.



Figure 1.3.1: 2-piece concept, Revolve NTNU 2014 [4]



Figure 1.3.2: 1-piece concept, GreenTeam 2013[5]



Figure 1.3.3: Monoblock CFRP rim, The Koenigsegg Carbon Fiber Wheel[6]

1.3.4 2-PIECE FULL CFRP WHEEL

The 2-piece full CFRP solution is quite similar to the monoblock solution, but it consists of two separate parts. The 2 pieces can be joined through bolts or adhesives. If bolted, the same mounting situation as in the 2-piece shell arises. Weight and stiffness advantages close to the monoblock design, however, arise especially if glued. This solution is almost as complex as the monoblock CFRP, but is simplified by splitting up the layup, since the rim produced in two pieces, making it faster to produce.



Figure 1.3.4: 2-piece full CFRP concept, Revolve NTNU 2016

Table 1.3.1: Pro and cons of concepts CFRP concepts

	2-piece CFRP shell with alloy center	2-piece full CFRP wheel	1-piece CFRP shell with alloy center	Monoblock CFRP wheel
Must	Quality assurance	++	-	++
	Production, time, & cost	++	-	++
	Ability to hold pressure	-	-	++
Should	Assembly of rim	-	-	+
	Stiffness	-	+	+
	Weight	-	++	++
++ Superior		+ Good	- Poor	

1.4 CFRP LAYUP

Carbon Fiber is usually arranged to a filament before it is woven into a fabric or into a branch of unidirectional (UD)fibers. A satin weave or more specific a 5 Harness satin weave (5HS) which is found to the left in the Figure 1.4.1, usually has a weft with the same amount fibers in both principal directions resulting in the same properties in both principle directions. An UD weave illustrated right in the Figure 1.4.1, has most of its fiber in the first principle direction, this gives the UD more strength in one direction (typical $E_1 \simeq 25 \cdot E_2$). Using UD in strategical places can save weight by making use of the nonisotropic strength properties. However, UD layups are not as flexible as a weave, since they have most of the fibers in one direction, which more or less limits their use to curved surfaces in the the principal direction only.

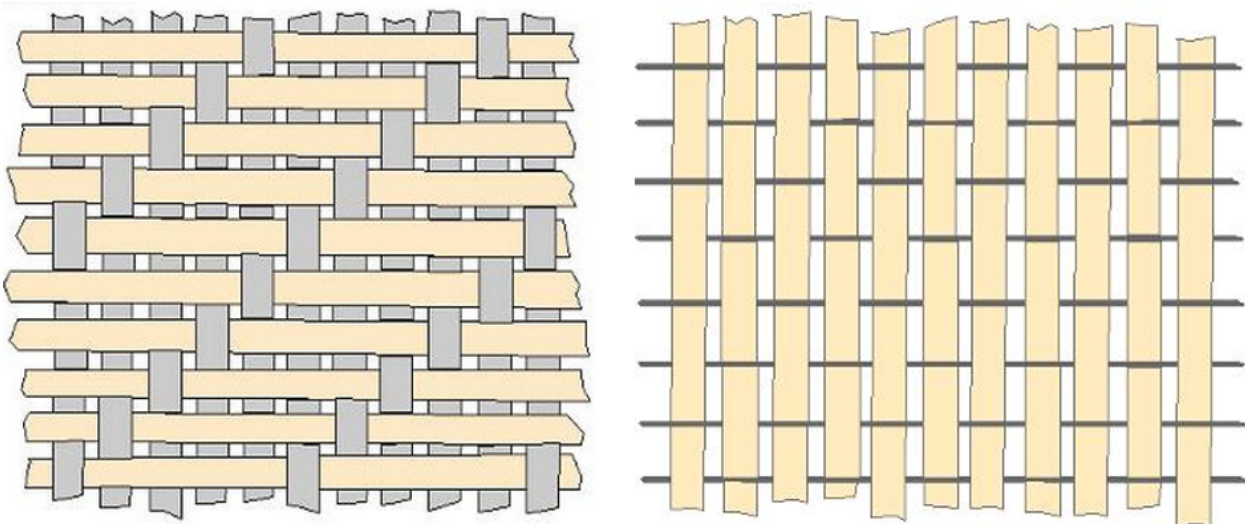


Figure 1.4.1: Weave types: left 5 harness sating weave , right Unidirectional-fibers [7]

1.4.1 MODELING OF CFRP LAMINATES

A laminate consists of two or more lamina/plies bonded together in one single structural element. Modeling of composite laminates are often conducted utilizing the Classic Laminate Theory (CLT). The basic assumptions of CLT are based on Kirchhoff Hypothesis [8]:

1. straight lines normal to the mid-surface remain straight after deformation
2. straight lines normal to the mid-surface remain normal to the mid-surface after deformation
3. the thickness of the plate does not change during a deformation

CLT also assumes perfect bonded layers with infinitesimally thin non-deformable bonding agents. Any out-of-plane stresses would subject a lamina to unnatural stresses, as the lamina can only resist significant stresses in the fibre direction. This modeling technique is not accurate for composites if the laminate is thick

or the transverse shear modulus G_{23} of one or more lamina are small, in which case the shear deformation may be underestimated [9]. For thin composite shells with materials of high shear modulus, it will give an accurate representation.

1.5 STRUCTURAL OPTIMIZATION & SIMULATION DRIVEN DESIGN

Topology optimization (TO) is getting more and more attention especially in engineering problems, where low mass and high stiffness is essential for high performance. TO is a mathematical method with the goal to maximize the performance of a system by optimizing the material distribution within a given design space. The material distribution is optimized with respect to given loads, boundary conditions and constraints. The performance is usually the boundary condition/constraint in TO, e.g minimizing compliance and reducing the mass. TO of isotropic materials is purely geometrical. Here we are looking at composites, i.e. CFRP, which has anisotropic properties. The aim is to use similar approaches, yet not for optimizing the outer dimensions of the component but its internal composition and layup; the routine hence becomes a material optimization (MO). As the reader will go through this thesis, it will become evident that this approach opens new roads towards simulation based composite and likely other multimaterial based optimization.

1.6 PREVIOUS WORK AND MOTIVATION

Based on the previous work done in my project work fall semester 2016/2017 [10], where different wheel concepts were explored, a Hybrid Aluminum Carbon Fiber Composite Wheel has been chosen as the overall best concept (See Table 1.3.1). The hybrid rim is divided into two pieces, consisting of an aluminum center and a CFRP rim shell. A machinable aluminum center reduces the CFRP production time and manufacturing risk considerably. The CFRP shell, in contrast, reduces the mass where it has most impact on performance. This allows the production of a CFRP with reduced complexity. The goal of the thesis is to develop, implement and apply a simulation-driven material optimization approach to develop a fully working race wheel where boundary conditions are set such that maximum number of iterations and hence a wide solution space is possible without constraining the algorithm to known design solution from previous engineering experience. Where the biggest challenge will be to develop a method for implementing Simulation-driven Design approach for Material Optimization.

Manufacturing is more than just putting parts together. It's coming up with ideas, testing principles and perfecting the engineering, as well as final assembly.

James Dyson

2

Methods and Procedure

2.1 LOAD SCENARIOS

The load distribution on the rim was estimated from the reaction forces acting on the tire. Reaction forces from the tires were obtained from tire data considering load transfer and power limit calculated by Jon Martin Haaland, responsible for vehicle dynamics in the team. Together with Jon Martin Haaland and the suspension group, a common load case was decided, where the dynamic loads of the tire were divided into 6 quasi static load cases illustrated in Table 2.1.1 [3]. From this, a correlation between reaction forces and load distribution on the tire rim interaction was established. The load distribution on a rim consist of mainly 4 different cases; static tire pressure, lateral loads, vertical loads and torque due to acceleration/braking. Inflation pressure works laterally on the rim flanges and prevents the tire from slipping and causing debeading. The reactions forces are assumed to have a linear distribution and work equally on each side. The vertical loading was simplified by using a cosine function. This simplification is valid and can be traced back to Hertz in 1882 [11]. For the cornering, brake and acceleration loads, a model was established that is based on the work of Jesuette and Thives [12]. All the load distributions are derived in Appendix A.1

Table 2.1.1: Quasi static load scenarios for warm tires [3]

		Front Wheels				
Cornering (110 kph)		Acceleration	Brake (110 kph)	3g Bump	2g Bump + Cornering (110 kph)	2g Bump + Brake (110 kph)
Inside Wh. Outside Wh.						
F_x	0 N	0 N	462 N	2797 N	0 N	0 N
F_y	574 N	2907 N	0 N	0 N	2907 N	0 N
F_z	241 N	1959 N	482 N	1762 N	1688 N	3084 N
Rear Wheels						
Cornering (110 kph)		Acceleration	Brake (110 kph)	3g Bump	2g Bump + Cornering (110 kph)	2g Bump + Brake (110 kph)
Inside Wh. Outside Wh.						
F_x	0 N	0 N	2420 N	1275 N	0 N	0 N
F_y	832 N	2968 N	0 N	0 N	2968 N	0 N
F_z	358 N	2122 N	1302 N	578 N	1903 N	3390 N

Reaction forces: F_x - longitudinal dir. , F_y - lateral dir. , F_z - vertical dir.

2.2 RIM CENTER

This section will present the methods utilized for design and production of the rim center. Details on the software used will not be presented here. Detailed procedures and setup, the reader is referred to the Appendix A.4. For the design of the rim center, the following software were used, SolidWorks, Abaqus and Tosca Structures. The procedure was divided into four steps:

- 3D-Modeling of the design space in Solidworks
- Building the Finite Element Model in Abaqus
- Setup the topology optimization in Tosca Structures
- Regeneration(3D modeling) of the topology optimized center in SolidWorks

2.2.1 MODELING OF DESIGN SPACE

The design space for the rim center was only restricted by caliper position and the shell size. Geometry and the dimensions of the design space are found in Figure 2.2.1 and were defined by the design constraint found in table 2.2.1. A manufacturing constraint was introduced since the center should be machineable.

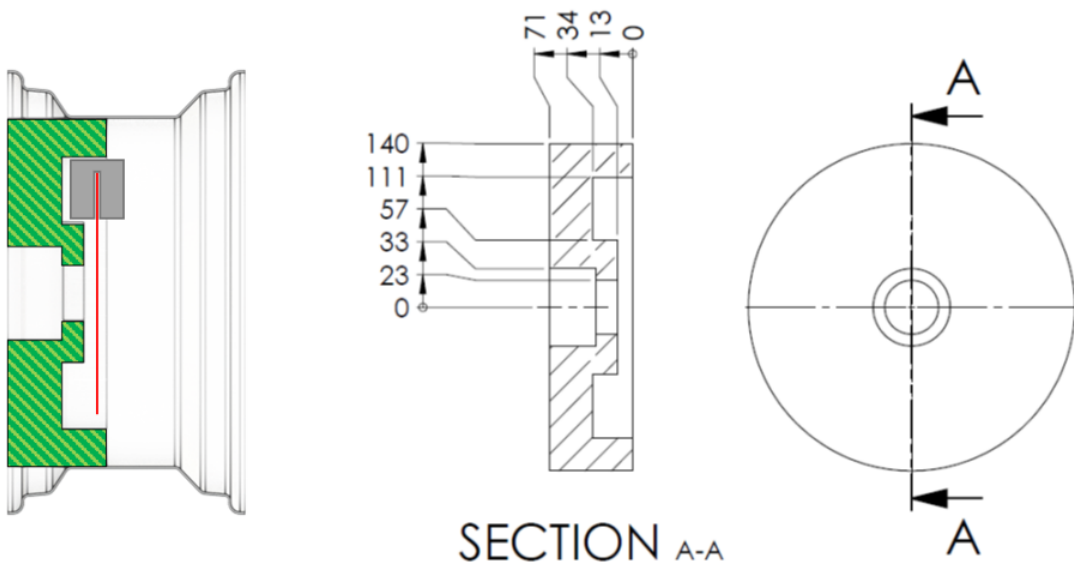


Figure 2.2.1: Illustration of design space for Rim Center

Table 2.2.1: Design constrains for the center

#	Description	Value
1.	Outer diameter	$\varnothing 280$
2.	Center hole diameter for axle	46 mm
3.	Chamfer in center compatible with retaining nut	Must
4.	6 x 6 mm modular bolt circle for aligning studs on hub	$\varnothing 61$
5.	Positive offset, center depth from outer shell contact surface	36 mm
6.	Material type	AL 7075-T651
7.	Production method	Machining
8.	Max mass per center	1 kg
9.	Clearance for internal components	<2mm

2.2.2 FE-MODEL

The FE-model for the topology optimization was simplified by modeling the design space for one spoke of the rim center.

MESH

The finite element mesh was constructed out of 8-node linear brick elements with reduced integration and hourglass control (C3D8R-elements). A structured mesh control was selected with a target approximate

global mesh size of 2 mm. The material was modeled as a linear elastic material with two constants E-moduli and poison ratios, respectively. It was applied to a geometry with a homogeneous section. Material constants for the applied material (AL 7075-T651) are found in the Appendix D.2.

LOADS AND INTERACTIONS

The loads were simplified and assumed to act equally on each spoke. Loads were applied on a dummy shell with simplified tie interaction between the shell and the design space. All boundary conditions were applied to the center lock with a kinematic coupling to the contact surfaces, where the hub and the center nut interact. The loads were defined by 2 independent quasi-static load scenarios defined with linear perturbation steps.

2.2.3 TOPOLOGY OPTIMIZATION

The topology optimization set-up is presented in Table 2.2.2. The optimization task was to minimize the strain energy of the design space under a weight target. The design space is partitioned into both non-design elements and design elements. The non-design elements are located in the center lock region. These elements are not modified during TO and hence called frozen elements in Tosca. Tosca structure does not contain machining as a implemented production constraint. This was approximated, applying the 3-axis milling constraint via a forging constraint acting from both sides in axial direction combined with rotational symmetry.

The weight constraint was set to below 1 kg. The information on finite elements, i.e. the raw data generated by the TO was modified using TOSCA.SMOOTH to smooth the surface. This created an iso-surface of elements, where intermediate densities are equal or greater than 0.3 (default).

Table 2.2.2: Topology Optimization Set-up

Material	Aluminium (7075-T651)
Element Type	Structured hexahedral
Abaqus Load Definition	Brake/acceleration & Cornering
Design Response	Strain energy (all steps),Weight
Objective Function	Minimize Strain Energy
Constraint	Weight Target
Geometric Constraints	Frozen sections, Forging
Design Cycles	50

2.2.4 COMPUTER NUMERICAL CONTROL MACHINING

The manufacturing of the rim center was done with Computer Numerical Control (CNC) machining. This process was outsourced to Mjøs Metallvarefabrikk located in Lonevåg near Bergen. The machining was done on specifications which are found in the Appendix B.1. This CNC machining process consisted of three main steps:

- Programming the machine paths in Computer Aided Manufacturing (CAM) software
- Setup and machining
- Validation of geometric tolerances, done with a Coordinate-measuring machine (CMM)

2.3 RIM SHELL

This section presents the methods utilized for design and production of the rim shell. The main focus is on the method developed for the Material Optimization. Details on the application and software used, will not be presented here. Detailed procedure and set-up can be found in the Appendix A.3. For the material CFRP layup optimization, the following software were used: Isight, Matlab and Abaqus. The work-flow is illustrated in Figure 2.3.1. Isight was used for the optimization strategy linking the different software packages together -> Matlab generated ply text-files in a format suitable to Abaqus based on variables from Isight -> Abaqus performed the FEA simulation of the rim, and uses a pre. python-script to read the layup files from Matlab and then a post. python-script to read the result values, which consisted of the total strain energy for each load case.

2.3.1 3D-MODELING OF RIM SHELL

The Shell geometry was limited geometrically by the suspension geometry, brake system (Table 2.3.1) and standards recommended by the tire manufacturer Continental. The standard is defined by ETRTO – The European Tyre and Rim Technical Organisation. The ETRTO standard for drop center and hump design is found in the Appendix C.4.

Table 2.3.1: Design requirements for the shells

#	Description	Value
1.	Compatible with Continental FormulaStudent C16 7J-13	Must
2.	Min. internal diameter (caliper, suspension and upright clearance)	Ø 280 mm
3.	Max shell weight	0.8 kg
4.	Drop center and bead designed according to ETRTO standard	Must
5.	Material choice	Hexcel 6376; UD & 5H

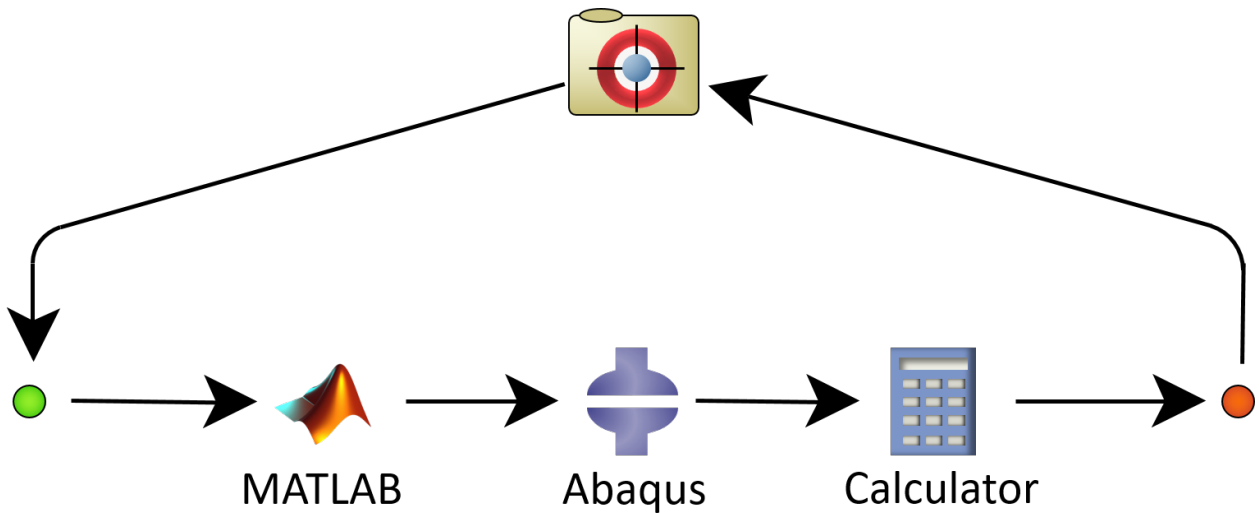


Figure 2.3.1: Work flow - Material Optimization

2.3.2 FE-MODEL

The composite shell was modeled with conventional shell elements with linear elastic properties. The properties of a single lamina was defined by 6 independent lamina constants: $E_1, E_2, \nu_{12}, G_{12}, G_{13}, G_{23}$. Material properties are found in the Appendix. Full composite layup properties were found by stacking every individual ply together and assigning their respective angles. This was done with the composite module in Abaqus.

MESH

The finite element mesh was constructed out of 4-node doubly curved thin linear shell elements with reduced integration, hourglass control and finite membrane strains (S4R-elements). A structured mesh control was selected with a target approximate global mesh size of 5 mm.

LOADS AND INTERACTIONS

Loads were applied to the shell with surface traction following the pressure distribution derived in Appendix A.1 All boundary conditions were applied to the center lock with a kinematic coupling to the contact surfaces where the hub and the center nut interact. The loads were defined by 2 independent quasi-static load scenarios defined with linear perturbation steps.

2.3.3 MATERIAL OPTIMIZATION

The optimization procedure was based on two load cases; cornering and braking. The optimization constraint is the total mass of the shell, and is set as the optimization target. The weight target was set according such that the total weight would be around 10 % lighter than the wheel assembly (rim and tire) of the 2016

car of Revolve NTNU. The optimization contains one objective, which is minimizing strain energy for each load case. Minimizing strain energy is the same as maximizing stiffness. Due to a limited amount of available UD-fibers from the sponsors, a second constraint was added, which was a limit of maximum UD-fiber in square meter per rim shell.

SEGMENTATION AND PARAMETERS

Segmentation of the rim shell was based on anisotropic loads and drapeability properties. The shell was exposed to higher loads on the inner part of the rim and near the interaction points of the rim center. Double curved surfaces were separated from single curved due to the difference in drapeability properties of the layups. The design variable was based on dividing the rim into 8 sections (see Figure 2.3.2). Each section has a range of different design variables, orientations and number of layers. For the sections IB, CM, CS and OB the optimization procedure included a material selection, where a 5 harness satin weave (5HS) CFRP and a unidirectional (UD) CFRP available. All variables and parameters used for the MO is found in Appendix A.3 Table A.3.2.

OPTIMIZATION ALGORITHM

The optimization is based on an evolutionary optimization algorithm. It is well-suited for non-linear and discontinuous design spaces. Another important factor is that it also works well for long running simulations, which is the case for this problem. Evol is an evolution strategy based on the works of Rechenberg and Schwefel[13], which mutates designs by adding a normally distributed random value to each design variable. The mutation strength (standard deviation of the normal distribution) is self-adaptive and changes during the optimization process. The evolution optimization has three stop criteria; converged, reached ultimate iteration or more than n failed iterations.

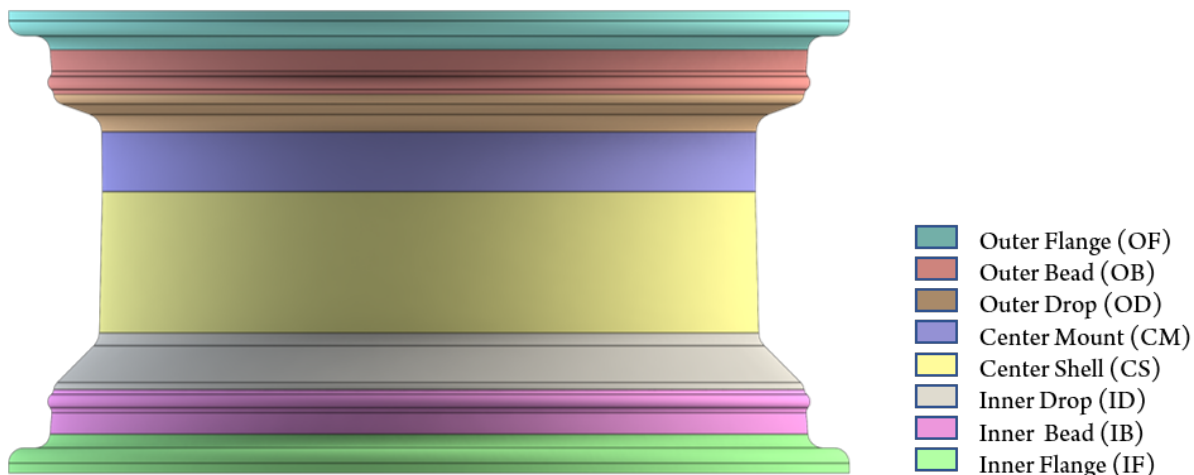


Figure 2.3.2: Segmentation of the Rim Shell

2.3.4 CARBON FIBER REINFORCED POLYMER LAMINATE PRODUCTION

The production of the shells was accomplished with the use of carbon fiber with pre-impregnated active resin (CF-prepreg). The production was divided into tree phases:

- Pre-production of the Shell
 - Drapeability analysis (DA) and ply segmentation
 - CNC cutting of each plies based on DA
- Production of the Shell
- Post-production of the shell
 - Trimming and CNC machining of mounting holes

Shells were manufactured by hand, by the author himself. This was done a with 2-piece aluminum moulds that were bolted together (Figure 2.3.3). The moulds were treated with a release agent before manufacturing the layup. After finishing the layup, the mould was bagged, set under vacuum, and then cured in an autoclave (Figure 2.3.4) subjected to heat and pressure. A high quality part with high surface finish, low resin content and excellent structural performance was obtained. Detailed pictures from the production are found in Appendix A.8.

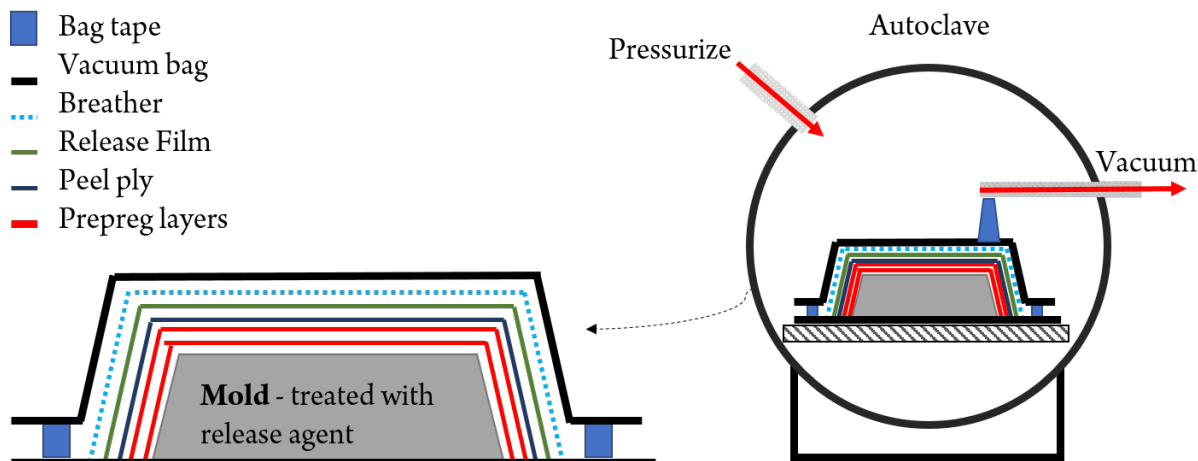


Figure 2.3.4: Illustration of Autoclave prepreg Casting process

PLY SEGMENTATION AND CNC-CUTTING

Form and segmentation of each ply were designed according to a drapeability analysis. For the drapeability analysis, Simens NX and Fibersim were used. The focus on the segmentation for the first layer was to have the biggest and most continuous layer possible. On the rest of the layers, the aim was to minimize angle deviation due to double curvature and to avoid joints on same spots and rather have overlapping joints, see Figure 2.3.6. Based on the drapeability analysis, production manuals(see Figure 2.3.5) were compiled. They contain ply-number, sequence, orientation, placement and material. Each ply was CNC-cut according to the simulated shape in FiberSim. All plies were marked and sorted after ply-number and sequence for each rim. The unidirectional fiber is very brittle and was handled extra carefully by placing on stiff cardboard.

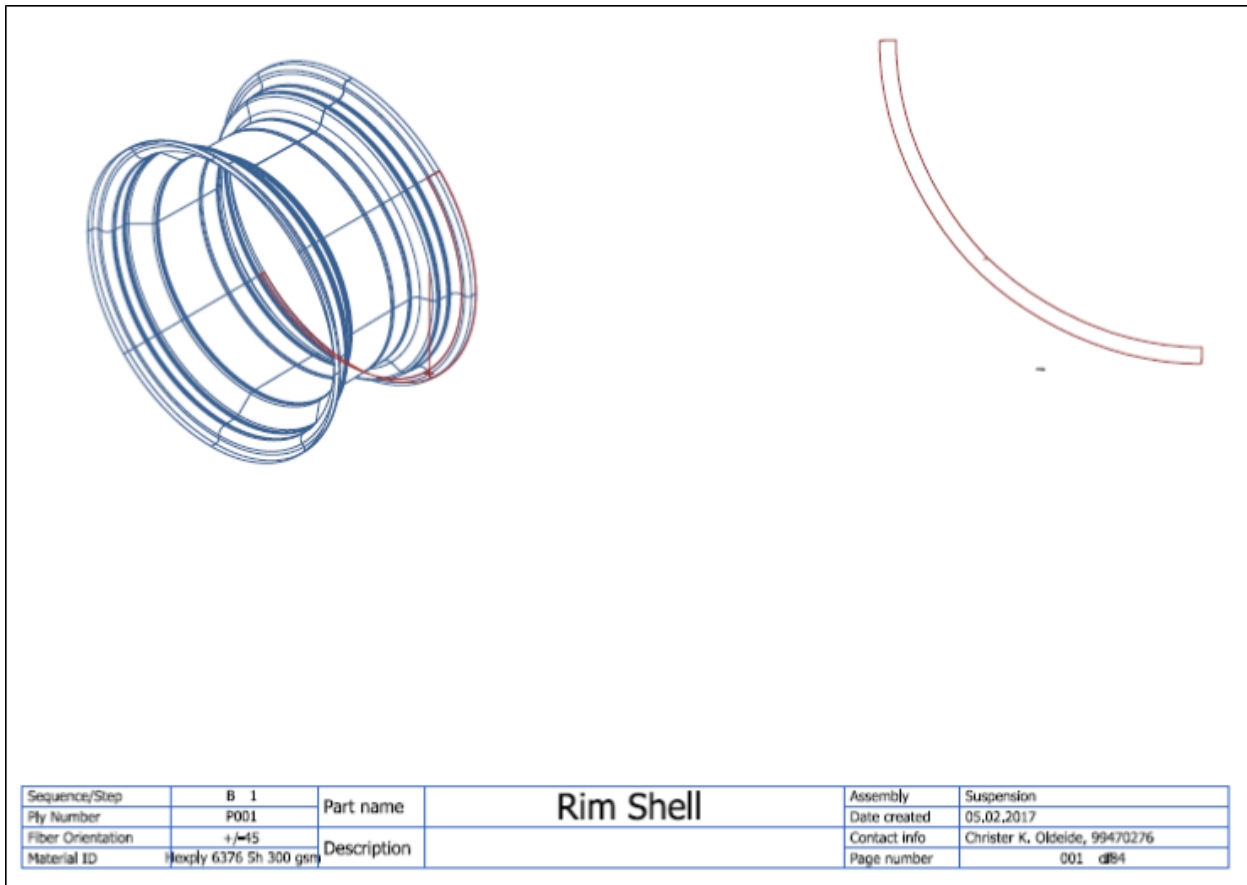
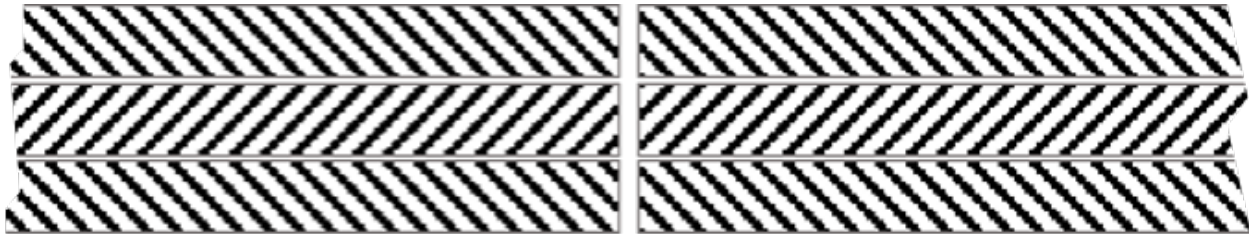
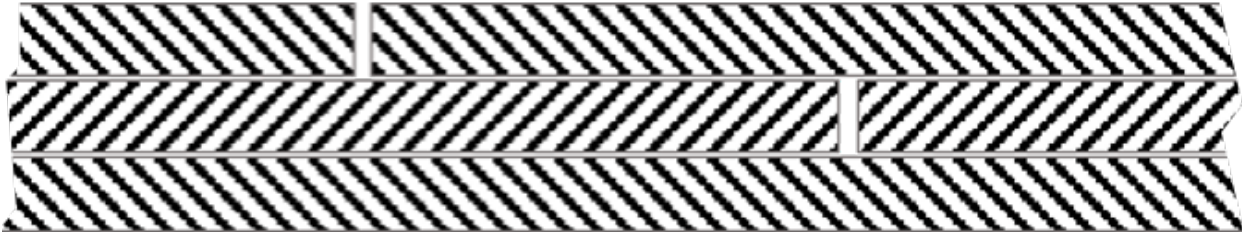


Figure 2.3.5: Production documentation for Rim Shell



Non-overlapping Joints



Overlapping Joints

Figure 2.3.6: Joint designs for CFRP layup

MOULD DESIGN

Positive mould design was chosen due to high curing temperature, which led to high thermal expansion. The contribution of thermal expansion was assumed to be linear and uniform. The moulds were CNC machined at Molstad Modellfabrikk according to the specifications found in Appendix B.2. After machining, the moulds were wet-sanded, starting with p400 and performing final sanding with p2000. After wet-sanding, the moulds were polished and cleaned with acetone. The moulds were then treated with two layers of sealer to fill remaining pores. They were then coated with 5 layers of release agent. The process was repeated for every cast. The application of sealer and release agents was done according to the datasheet found in Appendix D.6-D.7

LAYUP

The layup was done manually by hand according to the documentation made in Fibersim. Firstly, the inner backing on the ply was removed, the outer backing was kept during forming of the ply to minimize distortion. On the first layer a heat gun was used to make the epoxy stick better to the mould (Application of initial ply is seen in Figure 2.3.7 a)). Each layer was shifted 15° to ensure overlapping joints. Two different prepgres were used, a 5HS weave and a UD-fiber. Applying the UD-fiber (Figure 2.3.7 b)) was done extra carefully as this material is sensible for tears and requires an exact placement according to draping analysis to minimize tears and bridges. Between every first and second layer, a debulking (Figure 2.3.7 c)) step of 20 min was executed to minimize bridging and to ensure proper bonding between each layers. After the

last layer was debulked, a layer of peel ply (Orange fabric in Figure 2.3.7 d) was added. The peel ply removes excessive epoxy and is usually used to make an even surface finish with high surface roughness suited for bonding. For the rim shell, the peel ply was applied to save weight and improve the sealing properties between the tire and rim shell.



Figure 2.3.7: a) Initial ply, b) Application of UD-ply, c) Debulking of Rim Shell, d) Application of peel ply

BAGGING

After the peel ply was applied, a release film was added as seen in Figure 2.3.8. In this application, the release film has two functions; isolate the laminate from foreign bodies and prevent the breather from absorbing epoxy. After the release film, a layer of breather was applied around the whole mould, extra layers was added to every sharp edge to reduce the risk of bag burst during curing. The heat rate allowed during curing was determined by the temperature of the mould. To control the heat rate during a curing, a temperature sensor was placed between the laminate and the mould. A high temperature tube bag was chosen only requiring a seal on each end reducing the risk of leakage and bag failure during curing. The bag was sealed with a high temperature proof Vacuum Bag Sealant Tape. Two vacuum ports were placed on top of the mould, one for ensuring vacuum during curing and one for monitoring. Before curing, all bags were evacuated and checked for leakages leading to a pressure drop of more than 0.05 bar in 5 minutes.

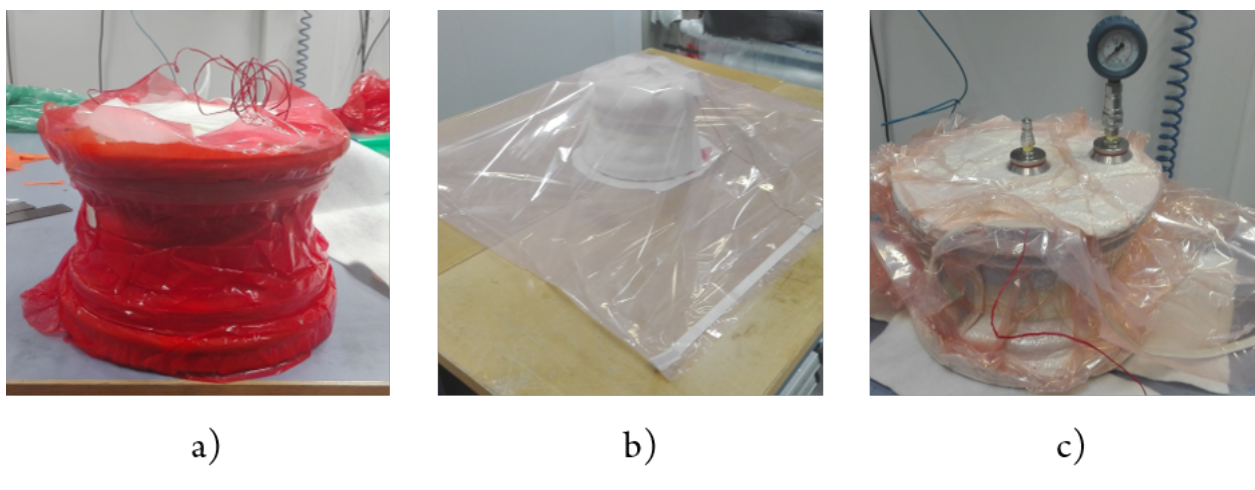


Figure 2.3.8: a) Finished application of release film, b) Bagging of Rim Shell, c) Vacuum test of bag

AUTOCLAVE CURING

The control program for curing the rim shell was set-up according to recommended curing procedure found in Appendix D.3 and is illustrated in Figure 2.3.9. To compensate for the reduced heat rate caused by the high heat capacity of the aluminum mould the temperature set point in the Autoclave was set to 190 °C (maximum allowed for Hexcel 6376).

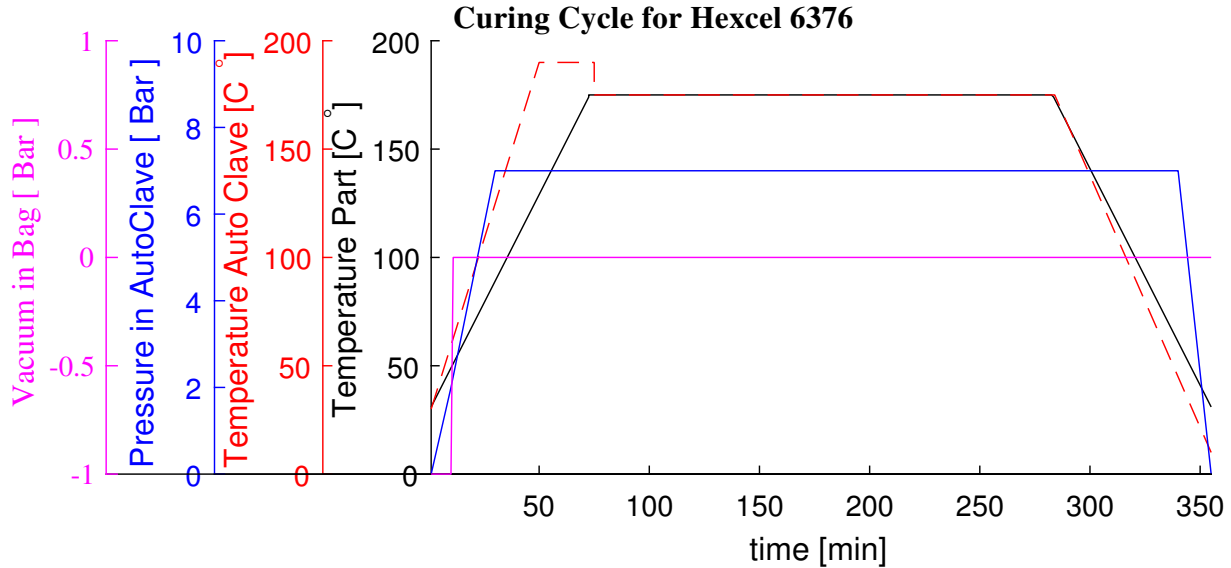


Figure 2.3.9: Curing cycle for Hexcel 6376 prepreg

DEMOULDING & CNC-MACHINING

After curing the used bag, release film and peel ply were removed from the cured rim shell before demoulding (Figure 2.3.10). The rim shell was then machined by Kongsberg Gruppen (KOG) at the Kongsberg Defence Systems (KDS) department in accordance with specifications found in Appendix B.3.

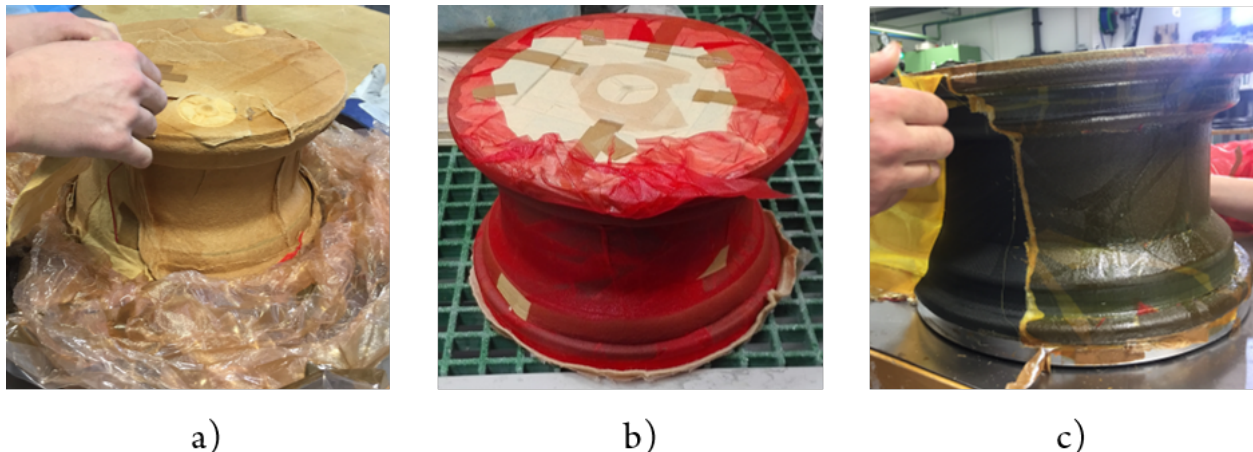


Figure 2.3.10: a) Removing of vacuum bag and breather after curing, b) Removing of release film after curing, c) Removing of peel ply after curing

2.4 VALIDATION

To validate the assembled wheel design (Rim shell and Rim center), an FE-model including non-linear effects was constructed. This section will not go into details concerning applications and software. Complete software set-up and applications used in Abaqus can be found in Appendix A.2.

2.4.1 FEM VALIDATION

Modeling of the rim center and rim shell was based on FE-models described in Section 2.2.2 & 2.3.2. Interactions and loads were changed to give a more accurate representation of the physical model. To include the non-linear effects from the pre-tension in bolts and center-lock, the linear perturbation step was changed to a static general step.

MESH

The same mesh procedure as in the previous model was used but with a mesh refinement near the contact regions.

LOADS AND INTERACTIONS

In addition to load scenarios defined in Appendix A.1, the interaction between the rim center and rim shell was modeled with contacts and bolts, the adhesive used to seal the rim was neglected. To include the pretension on the center lock, a dummy hub was modeled. This dummy hub was also applied to all boundary conditions.

2.5 MECHANICAL TESTING

This section will explain mechanical set-up, fixtures, and measurements needed for verifying laminate modeling and loads for the FE-model in Abaqus.

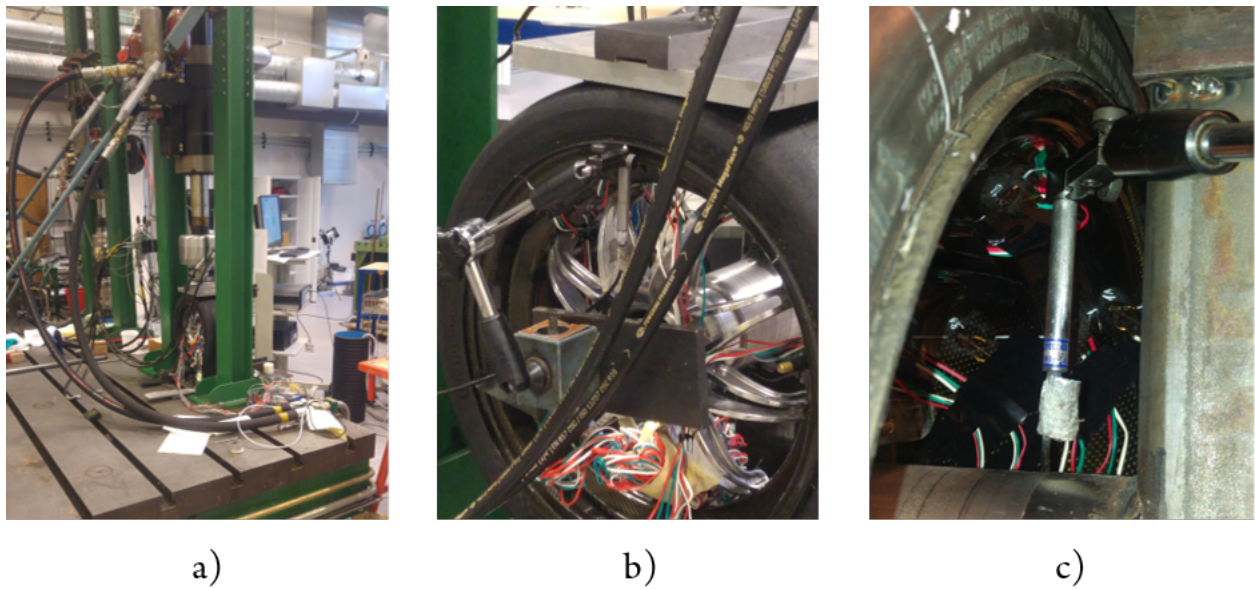


Figure 2.5.1: Mechanical testing: a) set-up of fixture in hydraulic load applicator, b) Placement of inductive displacement sensor for outer bead, c) Placement of inductive displacement sensor for inner bead.

2.5.1 MEASUREMENT

The measuring of the strains and displacements was done digitally and logged according to the applied load. To measure the applied load, a load cell with a range up to 2 tonne was used.

STRAIN

3-axis strain gauges were used to measure the strains along the axis illustrated in Figure 2.5.2. Five strain gauges were placed along the profile of the rim (the type of strain gauges can be found in Appendix D.1). They were placed according to the five red lines in Figure 2.5.3 following the coordinate system in the Figure.

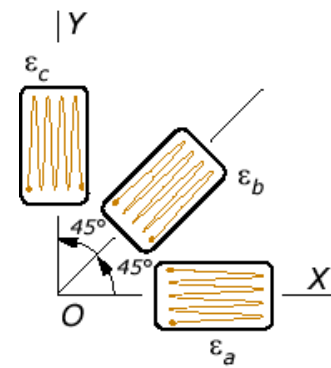


Figure 2.5.2: Illustration of a 3-axis strain gauge rosette [14]

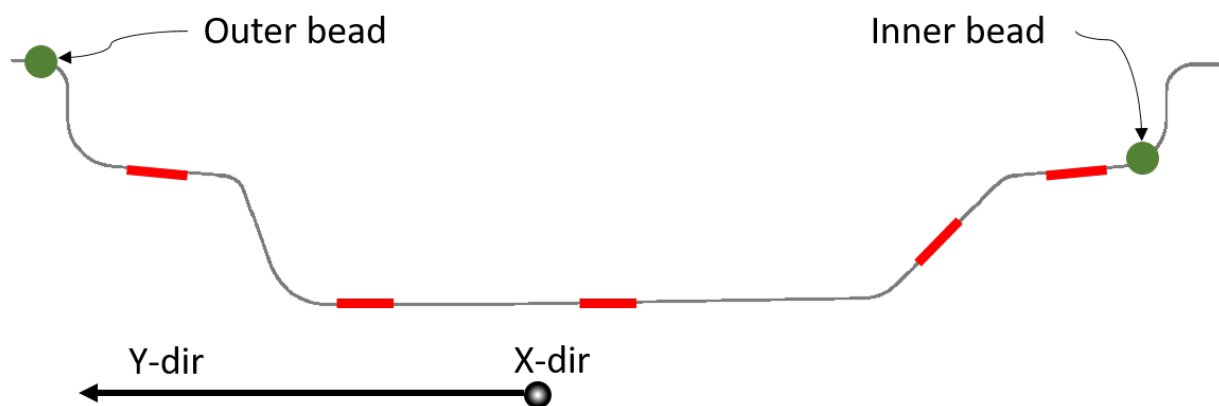


Figure 2.5.3: Illustration of strain gauge positions and placement of displacement sensors

The surface, where strain gauges were mounted, was sanded with a sand paper and cleaned with acetone before the gauge was glued with an adhesive specialized for this application. In Figure 2.5.4 picture a), a strain gauge is glued to the rim, picture b) shows the strain gauge after it is glued in place, picture c) shows all the strain gauges mounted in place.

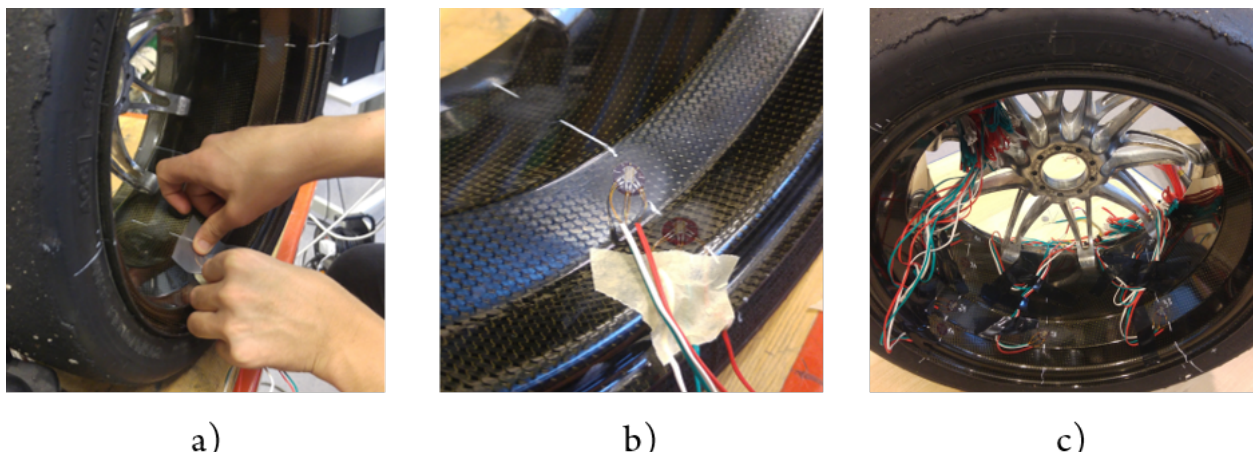


Figure 2.5.4: a) Gluing of strain gauge, b) Strain gauge mounted in place, c) Strain gauges mounted and organized

DISPLACEMENT

Both, the displacement on the inner and outer bead was measured as illustrated in Figure 2.5.3 by the green circles. The sensor was mounted with a magnetic holder as showed picture b) and c) in Figure 2.5.1. To reduce the measuring error coming from compliance of the rig, the magnetic holders were mounted as near the center lock as possible.

2.5.2 TEST PROCEDURE

The mechanical testing of the rim was divided in 3 load cases, inflation pressure, vertical load and dynamical load. Inflation pressure is the simplest load case to replicate in Abaqus and was therefore used to benchmark the laminate modeling of the rim shell. The vertical load case was done to benchmark the modeling of the vertical load case and the modeling of the interaction between the rim center and the rim shell. The dynamical load case was executed to see whether the quasi-static load scenarios were appropriately chosen.

INFLATION PRESSURE

The inflation pressure load was calibrated to zero at the values of the strain gauges obtained at 0 bar over-pressure in the wheel. The pressure was then increased to 2 bar and the strain gauge was measured for 60 seconds. The pressure was then decreased to 1.5 bar and measured again for 60 seconds. The same procedure was repeated for 1.0, 0.75, 0.5 and 0.25 bar. This test was then repeated 3 times for acquiring an appropriate amount of data for comparing.

VERTICAL LOAD

For the vertical load case, the vertical load was set to 3g bump, which is a vertical load of around 2000 N. Both strains and displacement of inner and outer bead were of interest during this test. The vertical load was applied according to Figure 2.5.5 and repeated 3 times. This procedure was done with the rim oriented around the axial direction at three different angles. First, such that the strain gauge was oriented at top and then shifted to 90° and 180°, respectively. This was done to acquire a better understanding of the load distribution around the wheel.

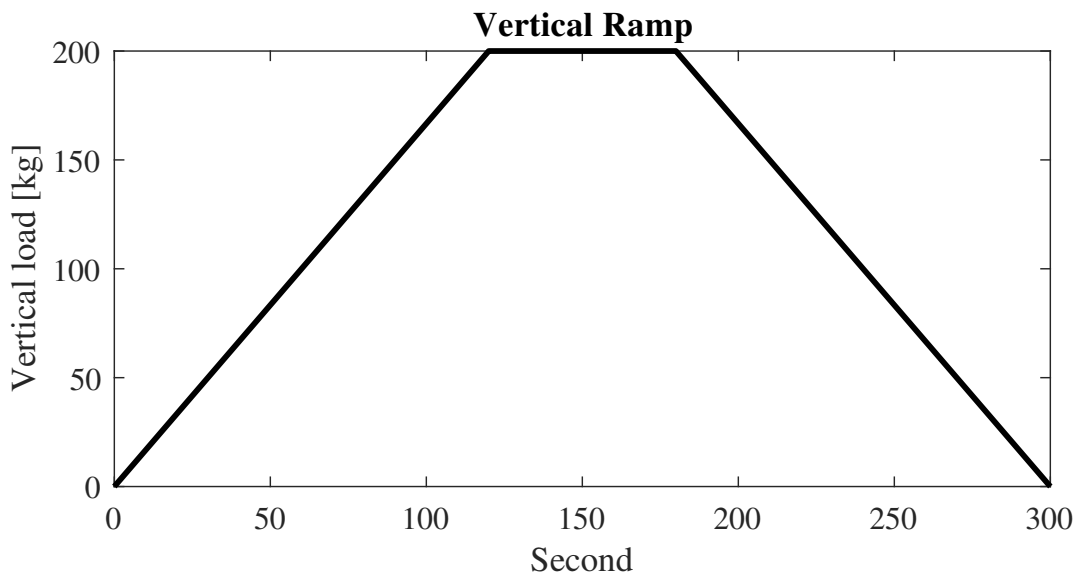


Figure 2.5.5: Ramp for Vertical Load during quasi static testing of Rim

DYNAMICAL LOADS

For the dynamical loads, the vertical load was applied with a square wave function ranging from 180-200 kg. The dynamical load was applied with different frequencies ranging from 0.5-8 Hz. Displacements and strains were logged for each load case.

2.5.3 MECHANICAL SET-UP

A fixture jig made of steel was designed to keep the wheel in place during mechanical testing. To mount the wheel, a simplified hub with the same center locking mechanism as on the race car was created. The rig was designed to have a stiffness giving a displacement at the hub of less than 1% of the estimated displacement of the rim . Machine drawings of fixture jig is found in Appendix B.4.

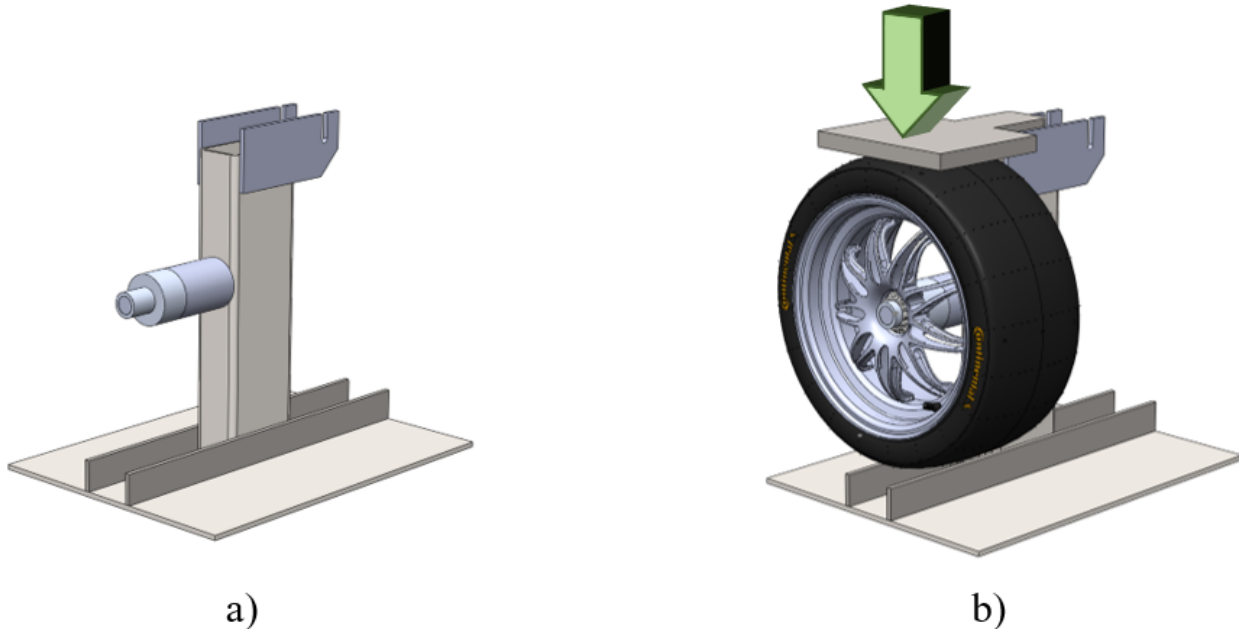


Figure 2.5.6: Fixture jig for applying vertical loads during mechanical testing: a) Illustration of test jig b) Illustration of wheel mounted in test jig, green arrow illustrate vertical load

Failure is central to engineering. Every single calculation that an engineer makes is a failure calculation. Successful engineering is all about understanding how things break or fail.

Henry Petroski

3

Results & Discussion

3.1 RIM CENTER DESIGN

3.1.1 TOPOLOGY OPTIMIZATION

The resulting raw geometry from the topology optimization carried out in Tosca is found in Figure 3.1.4. After 38 iterations, the optimization converged and the mass and strain energy is plotted in Figure 3.1.3. The raw geometry is presented in figure 3.1.2, one can see that the forging production constraint gives a good starting point for a machinable design. The cross-section in Figure 3.1.1 a) shows that all the available design space (Figure 3.1.1 b)) in x-y plane is used near the center-lock, definition of design space is found in Chapter 2 Section 2.2.1. This is not that odd since the cornering load case is one of the biggest. This is in line with many commercial racing center lock rims.

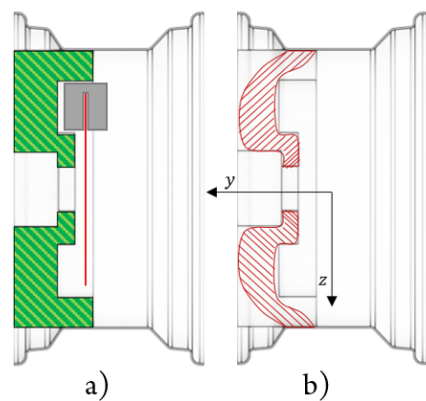


Figure 3.1.1: a) Design space for rim center b) Cross-section of Topology Rim Center

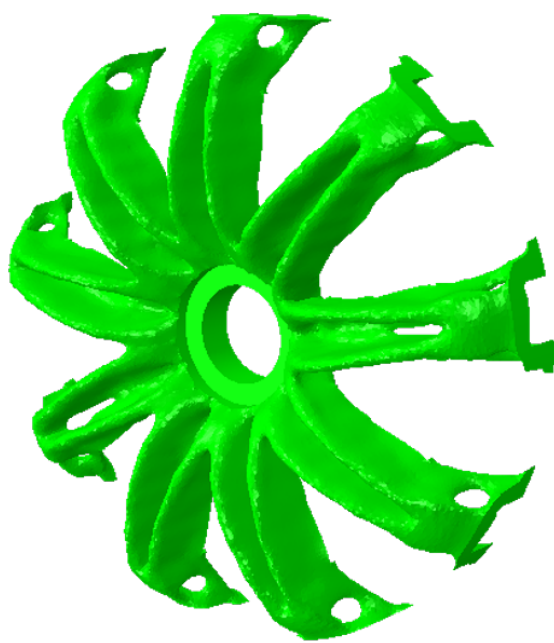


Figure 3.1.2: Raw data from Topology Optimization performed in Tosca

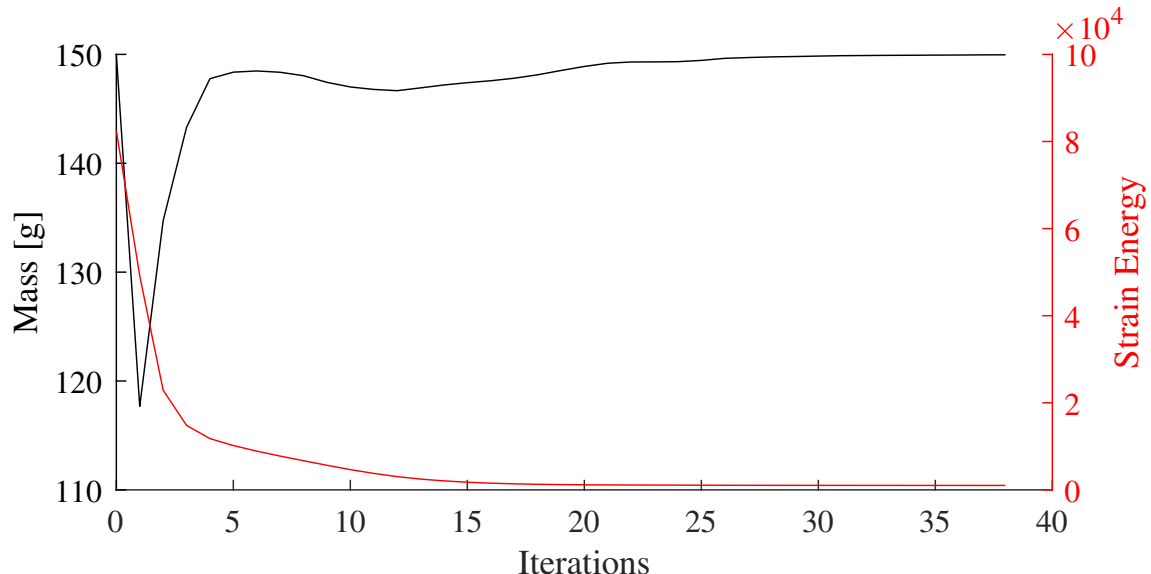


Figure 3.1.3: Iterations from Tosca Structure of the 9 spoke rim center

3.1.2 REGENERATION

A draft analysis, (Figure 3.1.4 a)) shows all positive (green) and negative (red) draft angles. The negative draft is undesirable for a 3-axis machinable design. Two regenerated machinable designs are presented in

figure 3.1.4, see Chapter 2 Section 2.2.3 for machining constraints. Both of the designs use the same cross-section as the TO, figure 3.1.1. The data in Table 3.1.1 is the relative specific stiffness of the regenerated designs with respect to the raw data obtained from TO. The 5-axis design has a specific stiffness of 18 % higher than the TO design and 44.9 % higher than the 3-axis design. The 3-axis design has a lower relative specific stiffness mainly due to a through hole bolted connection which results in a less optimal geometry near the interference to the shell. The 5-axis design has higher relative specific stiffness, this is because it has a greater design freedom than the TO and the 3-axis design.

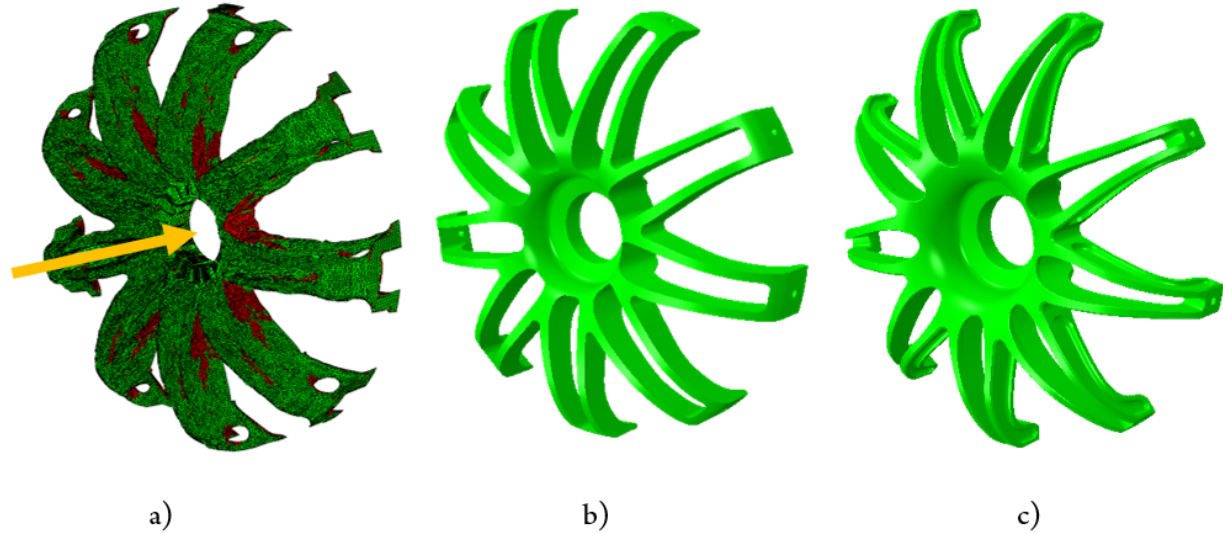


Figure 3.1.4: a) Draft analysis of TO design. Regenerated designs: b) subject to 3-axis and c) subject to 5-axis machining constraint

Table 3.1.1: Specific stiffness for the 2 different center designs, normalized respect to topology optimized design

Design	3-axis	5-axis	Difference
Mass[g]	1021	910	12.2 %
Lateral deflection [mm]	0.93	0.73	27.4 %
Specific stiffness	81.4	118	44.9 %

100 = specific stiffness of TO

3.2 RIM SHELL

The CFRP Layup optimization result is presented in figure 3.2.1. The figure shows the mass to strain energy for all optimization iterations. Iteration 1-500 result in a mean mass of 818.0 g with a standard deviation of 110.7 g, iteration 500-1500 provide a mean mass of 781.2 g and a standard deviation of 80.1 g, and the

last iterations yield a mean mass of 717.1 g and a standard deviation of 43.3 g. In the beginning of the optimization, the mass had a large deviation and is random. The deviation of the mass is getting lower for each data set, and the mean mass tends to converge around the target mass of 700 g, see Chapter 2 Section 2.3.3 for weight target. The evolution-based layup optimization converged after 3699 iterations, with a resulting mass of 710 g. In figure 3.2.2 the layup iterations are sorted with strain energy in ascending order. Looking at mass plotted in black, one can see that there is a clear trend at the lower bound between mass and strain energy. No extreme values at the lower bound is a good indication of convergence.

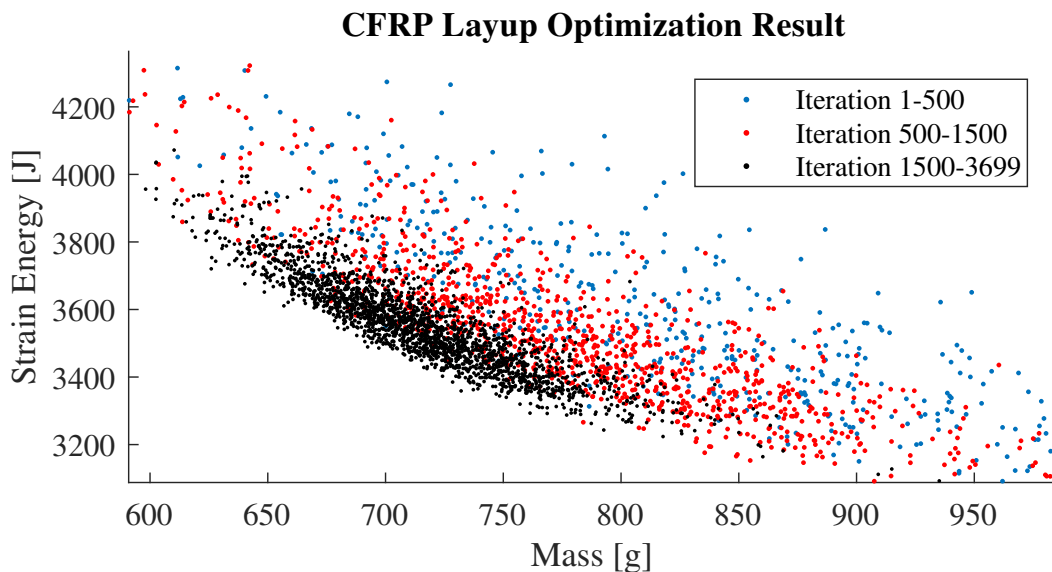


Figure 3.2.1: All CFRP Layup Optimization iterations presented in a mass vs. strain energy plot

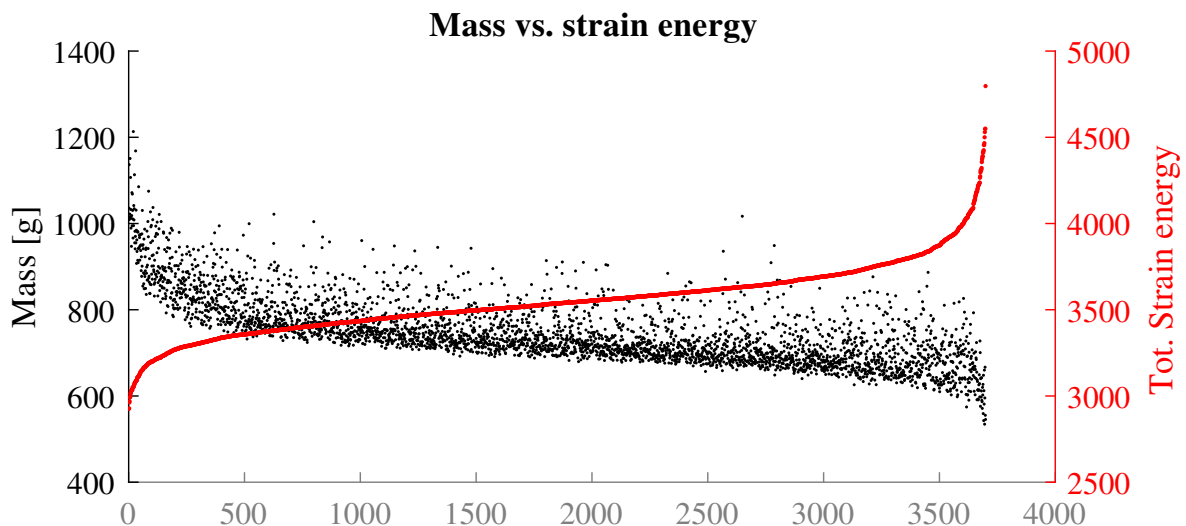


Figure 3.2.2: Sorted layup iterations with strain energy in ascending order

The resulting layup is presented in Table 3.2.1. Notation of segmentation is illustrated in Chapter 2 Section 2.3.3 Figure 2.3.2. Each row in the table represents one layer on the laminate. The layup stacking is not typical in engineering practice, there is no symmetry in the thickness. However, there seems to appear a pattern where the UD-Fiber are arranged in complementing pairs, similar to a balanced laminate. The optimization has prioritized more plies, close to where the center is mounted to the rim shell, i.e. on the center mount (CM) section see Chapter 2, Section 2.3.3. This priority can be explained by the unsymmetrical loads the rim shell is subjected to and that interaction between the Rim center will lead to some form of stress concentrations.

Table 3.2.1: Layup Result from Material Optimization

Ply.	OF	OB	OD	CM	CS	ID	IB	IF
1	S 45	S 45	S 45	S 45	S 45	S 45	S 45	S 45
2	S 45	S o	S o	S o	S o	S 45	U -75	S o
3	S o	U -30	S o	U 30	U 30	S o	S o	S 45
4	S o	U o	S 45	U -30	U -30	S o	S 45	S o
5	S o	U 30	S o	U -60	U -60	S o	U o	S o
6	S 45	S 45	S 45	U o	U o	S o	U 75	S o
7	-	S o	S o	U 60	U 60	S o	U o	S 45
8	-	-	-	U o	S o	S o	S o	S o
9	-	-	-	S 45	-	S 45	-	-
10	-	-	-	S o	-	-	-	-
11	-	-	-	S 45	-	-	-	-

S - Satin weave U - Unidirectional

3.2.1 PERFORMANCE OF OPTIMIZED LAYUP

In Table 3.2.2 the performance of the layup is compared to an aluminum shell and a shell with the layup developed for the CFRP rim for the 2014 Revolve NTNU car. The aluminum shell has a thickness of 3.18 mm, which is the same thickness as formula student aluminum rim sold by K2W Precision Inc.[\[15\]](#). All shells have the same shell geometry. The layup of the 2014 shell is found in Appendix A.9.

Table 3.2.2: Performance of optimized layup compared to a aluminum shell and the 2014 layup

Design	Mass [g]	Lateral Deflection [mm] (cornering@110km/h)	Specific Stiffness	Rotational Inertia [gmm ²]
Shell with Optimized layup	700	1.476	100.0	$1.7 \cdot 10^7$
Aluminum Shell	2150	0.856	56.1	$5.3 \cdot 10^7$
Shell with 2014 layup	600	1.901	90.6	$1.5 \cdot 10^7$

Specific Stiffness Normalized to Optimal layup

The optimized layup has a specific stiffness of around 45 % higher than the aluminum shell with a decreased rotational inertia of nearly 70 %. Compared to the 2014 layup, the optimized layup has an increased specific stiffness of almost 10% and 23% lower lateral deflection with only 10 % higher rotational inertia.

3.3 VALIDATION

In Table 3.3.1 max stress, deflection and safety factors for all load cases are presented. This validation model includes non-linear effects like contact and pre-tension on bolts and the center lock. The connection of the rim center to the rim shell was done as described in Chapter 2 Section 2.4.1. In Figure 3.3.1, the FEA results for the cornering load case is presented, together with a detail view of pretension effects. The Von-Mises stresses in cornering on the center is lower than 50 MPa for most of the center and 115 MPa on a small region for the heaviest loaded spokes. The maximum shell stress in cornering is 51.8 MPa and has 0.187 according to Tsai-Wu failure criterion where 1 is failure. The lowest safety factor for the centerpiece is 3.43 against yield, and 0.235 for the shell according to Tsai-Wu failure criterion. The overall low stresses indicate that the overall stiffness is high. FEM results for all load cases are found in Appendix A.5.

Table 3.3.1: Validation result including non-linear effects

Load case	f_x [N]	f_y [N]	f_z [N]	Max shell stress [MPa]	Max center Mises [MPa]	Deflection mag. [mm]	Shell	Center
							Tsai-Wu Failure Criterion	Safety Factor
Turn	-	2968	2122	51.8	115	2.27	0.187	4.78
Brake	2876	-	1895	57.3	133	0.96	0.132	4.11
3g bump	-	-	1903	58.1	64.2	0.811	0.118	8.56
2g bump +turn	-	2968	3390	66.9	137.93	2.82	0.235	3.99
2g bump +brake	2876	-	3020	54.6	160.35	1.39	0.196	3.43

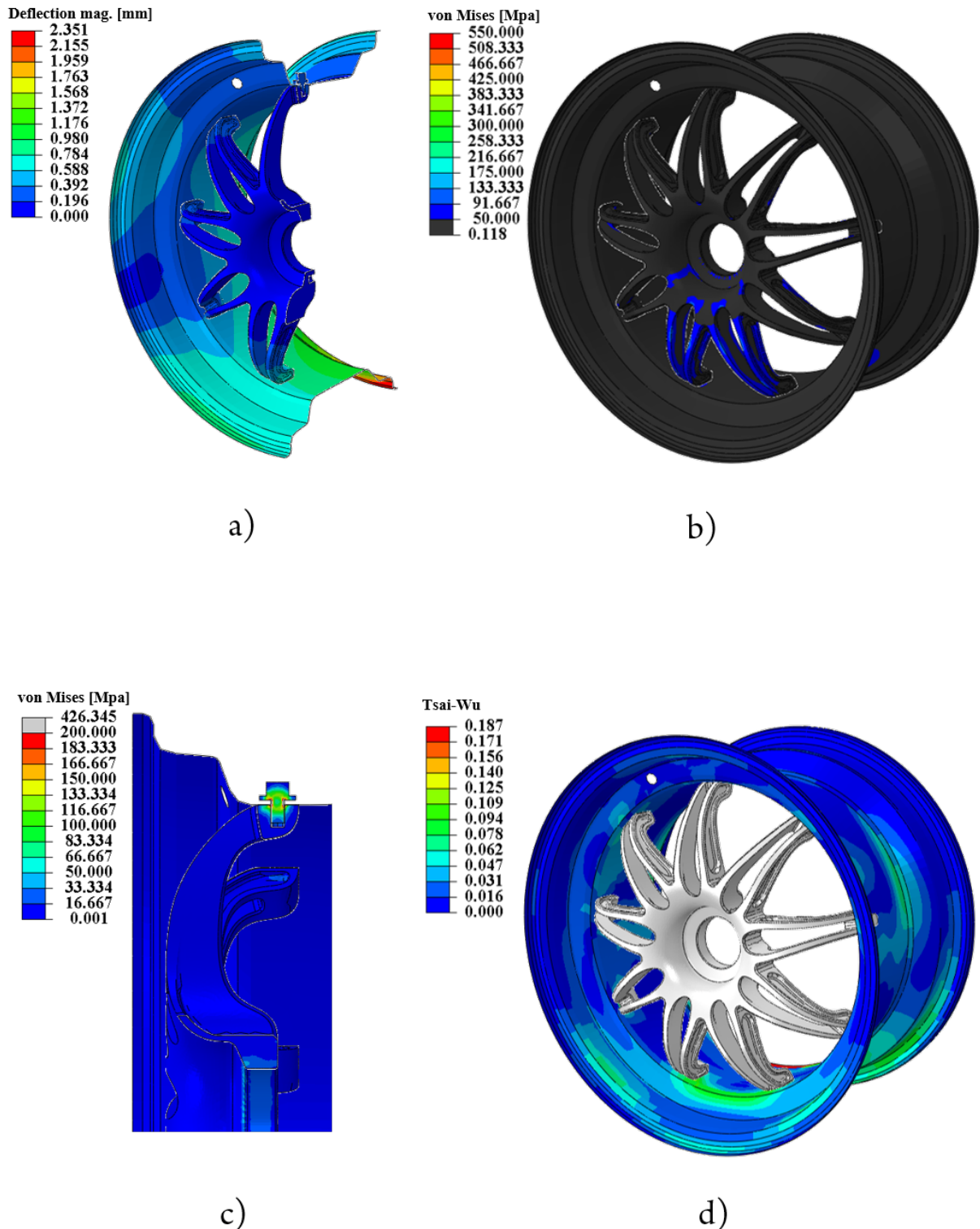


Figure 3.3.1: Validation results from Abaqus: a) Deflection magnitude in cornering @110km/h. b) Von-mises stress on center in cornering @110km/h. c) Pretension on center lock and bolts. d) Tsai-Wu failure criterion on shell in cornering @110km/h

3.3.1 FATIGUE PROPERTIES RIM CENTER

The stress spectrum for the most stressed section of the rim is presented in Figure 3.3.3, the most stressed section is found in Figure 3.3.2. This is the stress spectrum based on half endurance (11 km), where the loads are coming from actual log-data (Appendix A.7). The stress spectrum is estimated from FEA in Abaqus and a linear regression performed in MatLab.

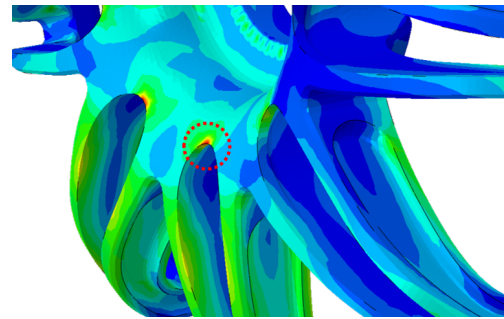


Figure 3.3.2: Most stressed section of rim center

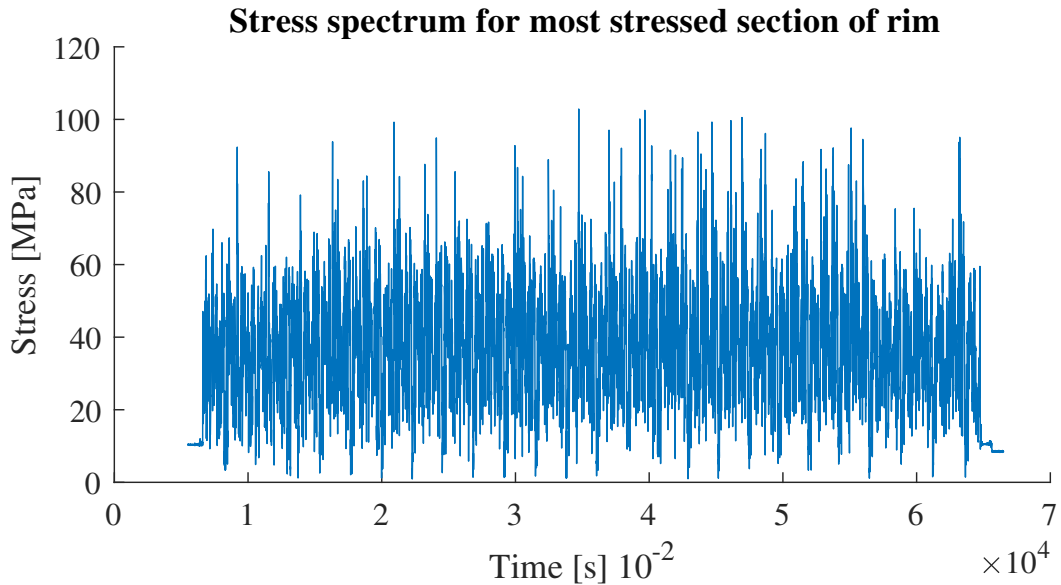


Figure 3.3.3: Stress spectrum for most stressed section of the Rim Center

In Figure 3.3.4, the whole stress cycles based on Standardized ‘Rainflow’ algorithm (ASTM E1049 [16]) is presented. Based on these stress cycles and the SN-curve found in the Appendix D.2, the fatigue properties of the rear and the front rim center are presented in Table 3.3.2. The Palmgren-Miner linear damage rule, or damage index predicts fatigue failure of the component when the summation of the cycles of reversed stress amplitude, n_i , to the cycles of stress causing failure at each stress amplitude, N_i , equals unity, i.e., $\sum_i n_i/N_i = 1$ [17]. Number of endurance run before failure is estimated by the inverse of the damage index for one endurance.

Table 3.3.2: Fatigue properties of Rim Center

#	Rear Rim Center	Front Rim Center
Damage Index		
(Minor damage rule for one endurance)	0.006	0.009
Number of endurance before failure	166	110

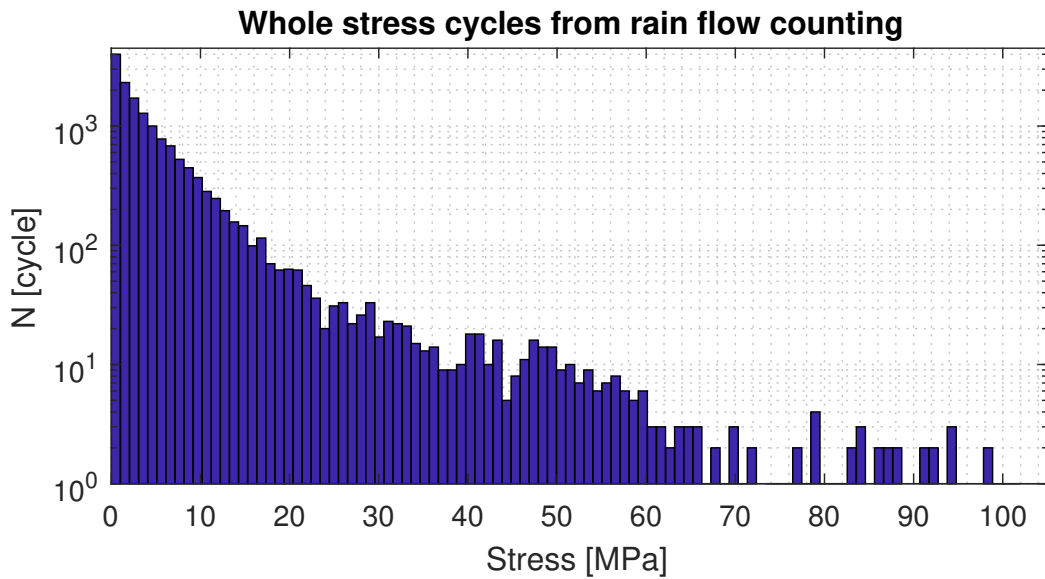


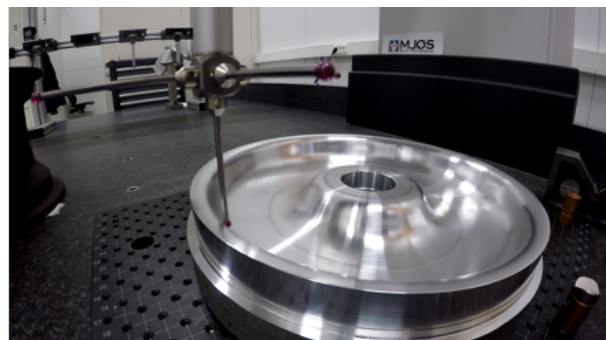
Figure 3.3.4: Whole stress cycles for half endurance counted with Rainflow counting

Looking at the fatigue data, one can see that fatigue is not an issue for the wheel center. This is a good indication that the optimization has worked since a design optimized for stiffness should indicate in general overall low stress. The front rim, which has the lowest fatigue life, is estimated to last 110 endurances, which is equivalent to around 2400 km racing distance, which is way over the requirement for a Formula Student race car.

3.4 PRODUCTION



a)



b)



c)



d)

Figure 3.4.1: a) 5-axis milling of Rim Center, b) Control of specified tolerances on coordinate measuring machine(CMM) during production c) Rim Shell before Autoclave curing, d) Rim Shell at weight after curing and demolding

In Figure 3.4.1, the manufacturing of the rim center and the rim shell is presented. Picture: a) shows the rim center during the last machining step, where the pockets are milled. Picture: b) shows the probing of the rim center after the last lathe operation. Picture: c) shows the rim shell ready for autoclave curing. Picture: d) shows the finished rim shell after demoulding with a resulting weight of 710 g. The final assembled wheel is presented in Figure 3.4.2. Measuring reports for both rim center and rim shell are found in Appendix C.1. The rim shell was measured to have a roundness of 50 µm at the rim center interference. The final assembled rim was measured to have a run out of 50 µm. Overall, the production went well and resulted in high quality parts proving that the manufacturing design specifications applied in the optimization step were successful.



Figure 3.4.2: Final assembled wheel

3.5 MECHANICAL TESTING AND VERIFICATION

Axial strain and hoop strain for inflation pressure of 2 bar are presented in Figure 3.5.1 & 3.5.2. The experimental strain data from the strain gauge is plotted with respect to the strain calculated in Abaqus. Modeling of the inflation pressure is the simplest and most documented load scenario. There is a clear relationship between the physical data and the simulation in FEA. This indicates that the modeled laminate represents the physical laminate well.

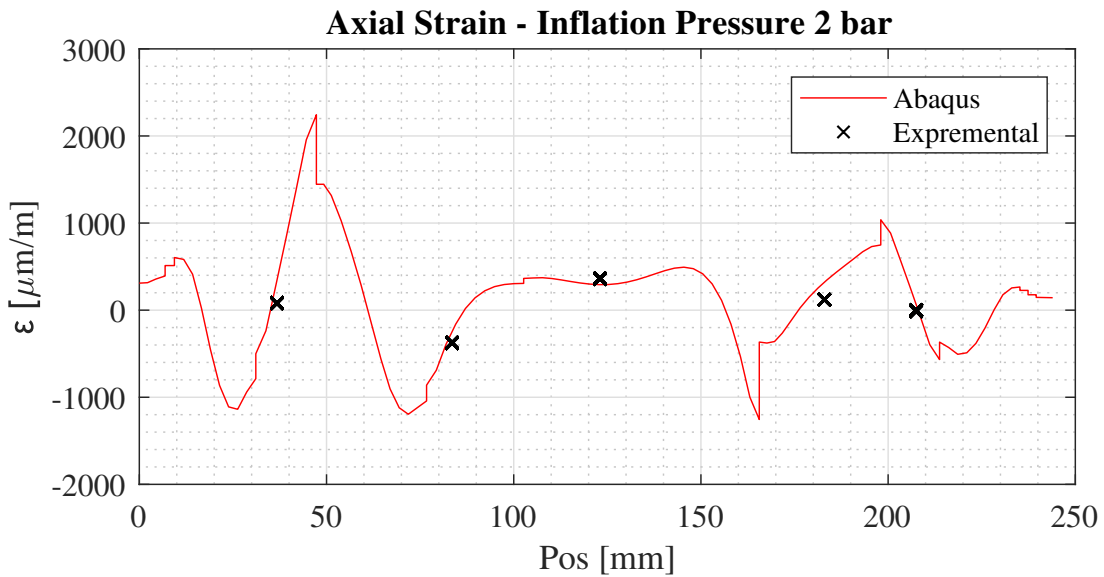


Figure 3.5.1: Comparison of axial strain between FEA and mechanical testing of rim shell

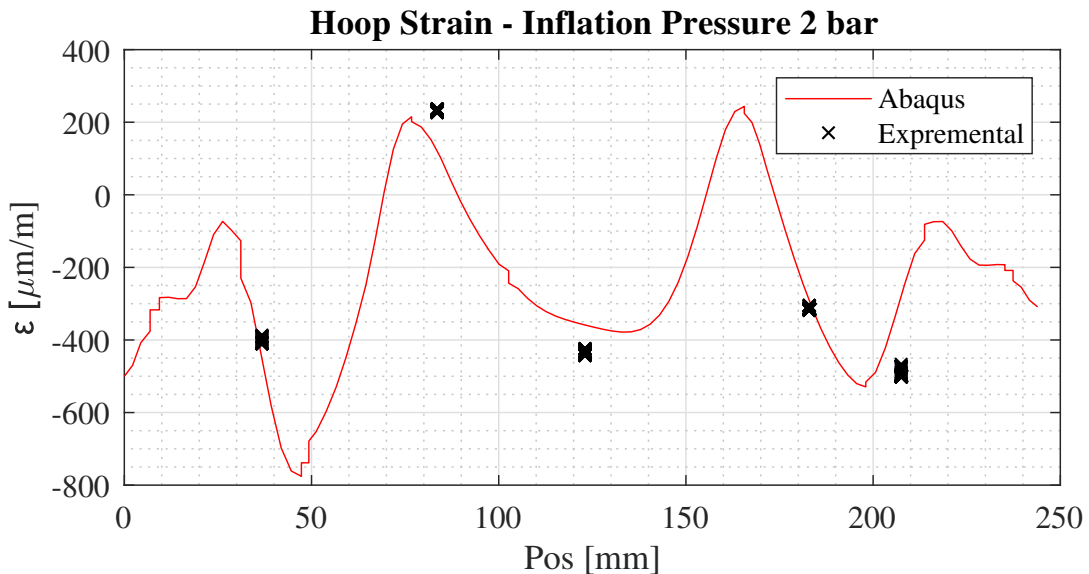


Figure 3.5.2: Comparison of hoop strain between FEA and mechanical testing of rim shell

In figure 3.5.3 & 3.5.4, the displacement of the inner and outer bead during vertical loading is presented. The modeled displacement resembles the physical one with a difference of maximum 15.6 %. The deflection slope changes around 1100 N. The slope has a negative change in the outer bead and a positive change in the inner bead. This non-linearity could be caused by tire behavior or deformation and misalignment of the fixture.

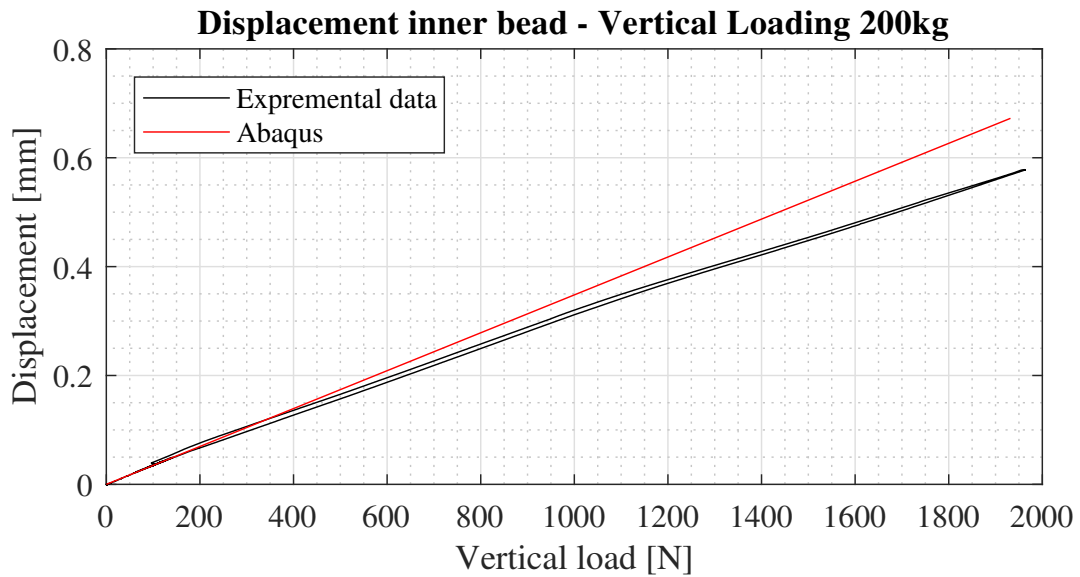


Figure 3.5.3: Comparison of displacement at inner bead between FEA and mechanical testing with a vertical loading of 200 kg

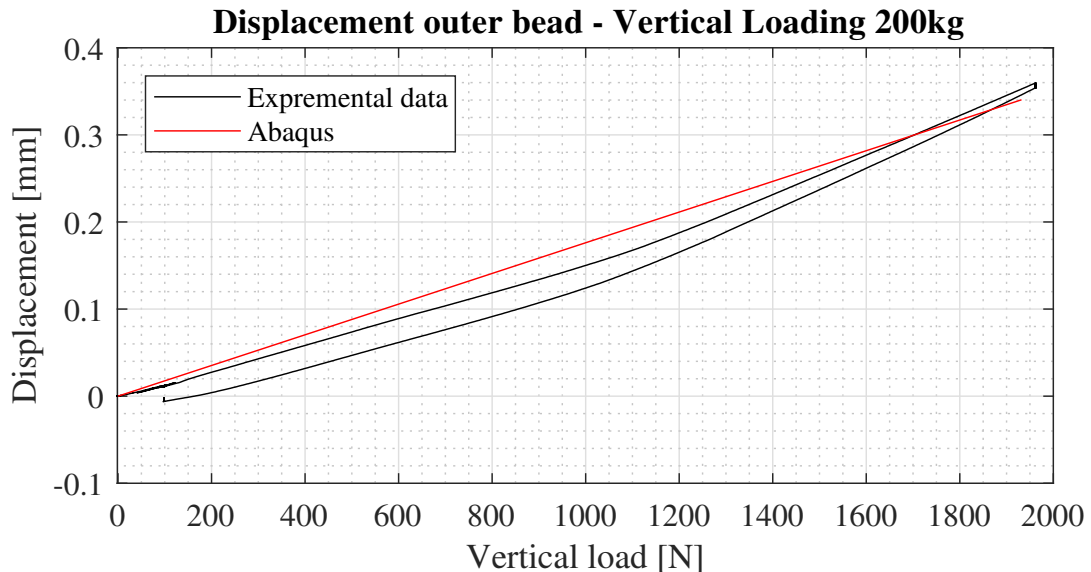


Figure 3.5.4: Comparison of displacement at outer bead between FEA and mechanical testing with a vertical loading of 200 kg

Axial and hoop strain for vertical loading is presented in Figure 3.5.5 & 3.5.6. The strain from the experimental testing matches the model well. Axial strain near the interference with the tire is significantly lower on the physical test, nearly a factor of 11. The tire load is modeled as a surface traction on FEM, which does

not take into account the extra stiffness the physical tire will give to the bead. The vertical load model seems to represent well the overall physical load but tends to overestimate the axial load near the interaction with the tire.

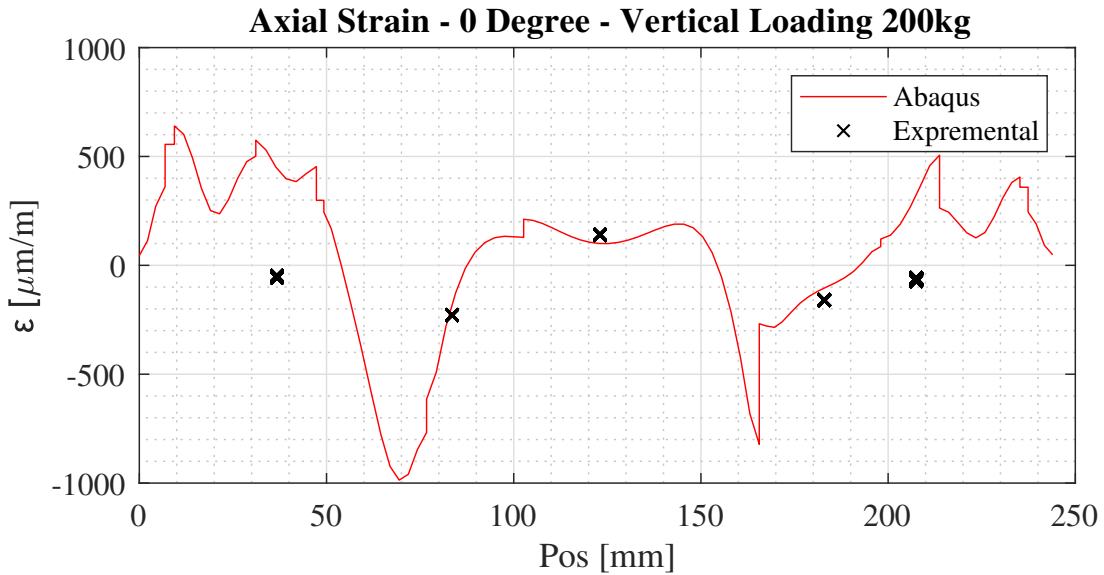


Figure 3.5.5: Comparison of axial strain between FEA and mechanical testing of rim shell subjected to a vertical load of 200 kg

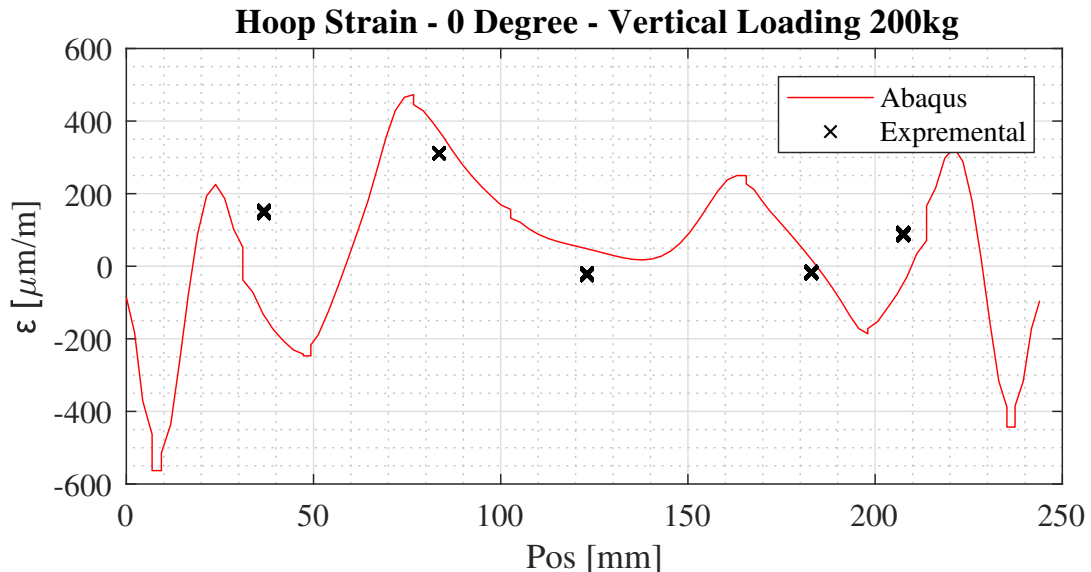


Figure 3.5.6: Comparison of hoop strain between FEA and mechanical testing of rim shell subjected to a vertical load of 200 kg

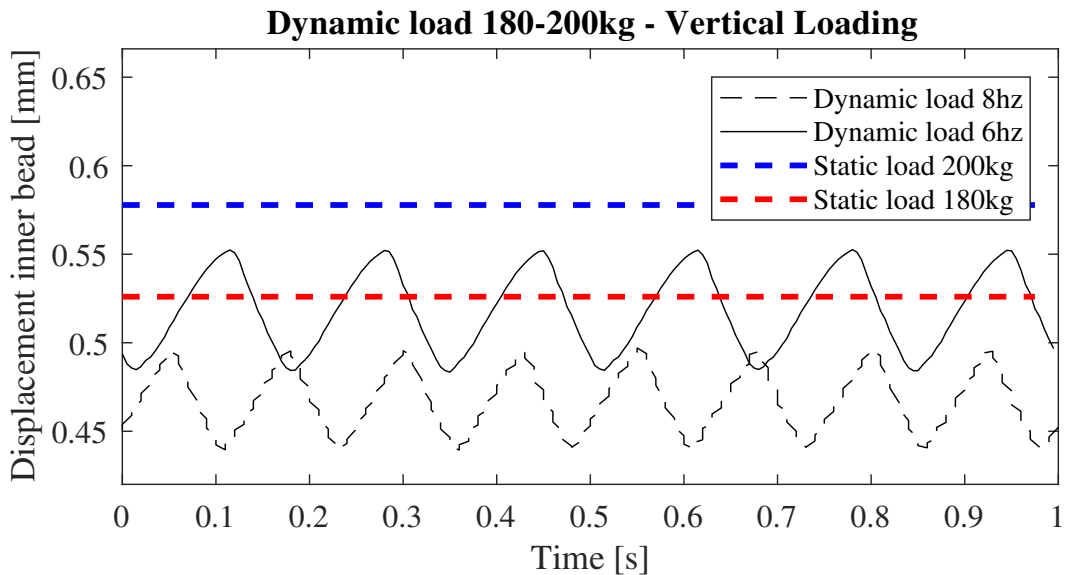


Figure 3.5.7: Dynamical loading of wheel with a vertical loading of 180-200 kg

In Figure 3.5.7 data from the dynamic testing is presented. Displacement for the static loading is higher than for the dynamic loading. The displacement is lowest for the dynamic loading with the highest frequency. The tire has damping properties, which lower the displacement for dynamic loads. For quasi-static loads scenarios, this damping effect can be neglected. This indicates that modeling loads as quasi-static for dimensioning and design of the rim are conservative and applicable. All test results are found in Appendix A.6.

Table 3.5.1: Error contribution in Mechanical Testing

Source of Error	Magnitude of Error	Correctability
Jig Compliance	Small	Easy
Inaccuracy of Jig	Medium	Moderate
Load path in Tire	Unknown	Hard
Positioning of Strain Gauge	Small	Easy
Missalignment of Strain Gauge axis	Medium	Moderate
Inaccuracy of measurements from Strain Gauge	Neglectable	Easy
Positioning of Displacement Sensor	Medium	Moderate
Inaccuracy of measurements from Displacement Sensor	Small	Easy
Inaccuracy of measurements from Load Cell	Small	Moderate

In Table 3.5.1 some possible contributions to errors for the mechanical testing are listed. Various of

tire inflation pressures were tested. Displacement at inner and outer bead varied for the tests done at 0.5, 0.75, and 1.0 bar. Tests done at 1.0 bar and above gave same displacement. This could be explained by the deformation of the tire that is greater for lower pressure, which could result in an uneven load distribution as the load applicator could touch the sidewalls of the tire. Some tests were done by adjusting the angle of the load applicator, a change of 0.2 degree shifted 0.05 mm between the inner and the outer bead displacement at the vertical load of 200 kg. This indicates that the angle of loading has a big impact on the load path in the tire. The sources of error during testing are not fully understood, and should be investigated further.

3.5.1 FIELD TESTING

All 3 sets of the rims worked and performed well during testing and the 2 Formula Student(FS) competitions; Formula Student Germany and Formula Student Spain. In Figure 3.5.8 ELD is in Germany at the Karlsruhe Institute of Technology FS teams' test facilities. The wheels did not leak air, which is one the most common problems for FS-wheels. Normally, tire changes are time-consuming due to the need for a sealant between the tire and the rim. The rough surface finish coming from the peel ply used in the casting process for rim shell had excellent sealing properties to the tire. This eliminated the need for a sealant, saving both weight and time. In total 8 sets of tires were used, all tire changes were performed on a tire changing machine. In Figure 3.5.9, a picture of a tire change is presented. None of the rims experienced any issues during this process and were not subjected to any cracks or delamination. Delamination and cracks on tire flanges are one of most common failure of one-piece rim shells during the competition.



Figure 3.5.8: Eld at testing in Karlsruhe ,Germany



Figure 3.5.9: Tire changing performed with a tire changing machine

*Scientists investigate that which already is;
Engineers create that which has never been.*

Albert Einstein

4

Conclusion

Formula student is a perfect environment to test and explore new ways of high performance product design and manufacturing. The access to an excellent network of industrial partners, software solutions and university labs and competences puts one on the forefront of engineering practice development. This report presents the first entire process development of a segmented Formula student wheel with Topology optimized aluminum center and optimized CFRP rim shell. The design considerations are outlined allowing an ideal balance between manufacturability (center), inertia and stiffness (rim). for the rim, an evolution based algorithm was developed and presented in this work that allows to iterate through millions of different layups to find the optimum with minimum compliance under a certain weight target. The weight target of 710 g was met giving a deflection of maximum 2.27 mm in two quasi static critical load scenarios. The entire wheel was validated under 6 quasi static load conditions including bolt forces, center lock connection and full contact as well as fatigue properties. The report further described the production process, where the rim was fabricated by the author himself exactly meeting dimensions and weight target. The manufactured wheels performed well in race conditions; tire changes worked seamlessly as no additional sealing was required due to the manufactured CFRP surfaces that were air tight. Mechanical tests on the wheel showed the perfect agreement between the simulation and the experimental results with the local strain discrepancies ranging from 4.7 % to 21.3 % in load cases of inflation pressure (2 bar). The largest discrepancy was found in large static loads up to 200 kg, where the discrepancy for the total deformation was 15.6 %. The impacts of dynamic loads were negligible due to the damping behavior of the tire. This shows

that simulation based design is a feasible approach to infuse innovation into next generation high performing products and presents, to the best of the author's knowledge, the first evolution based composite layup optimization inked to an entire product development process all the way to testing and application. This could be beneficial in a wide range of composite material applications, where key aspects of this procedure could be further improved.

4.1 FUTURE WORK

A novel simulation Driven Design approach has been developed and used to design and manufacture fully working and high performing set of wheels for a formula style race car. A design approach with minimal influence by an engineer is not better than the task given to the computer. Yet, the design success is subject to defining proper inputs than in a conventional design process. This implementation of a simulation Driven Design approach for composite material optimization shows promising results, regarding the possibility to design a high-performance composite layup by only defining geometry, loads and boundary conditions. To the best of my knowledge, I have not seen any successful composite designs with a similar design approach. The method works well as it is now, but there is a great potential for the improvement of this process avoiding steps, where the Evolution based algorithm may not be appropriate for the task. A suggestion would be to use the evolution based algorithm for the first iterations and then switching over to a gradient based algorithm. Another improvement that should be investigated is segmentation of the layup, this is done manually and by experience for now. Implementing a segmentation optimization could improve the performance of the design considerably. This could also be combined with a production constraint like drapability, which could give the design a variable segmentation for each layer. This could improve both design performance and manufacturability.

References

- [1] E.Astrén. Koenigsegg reinvents the wheel, 2013.
<http://koenigsegg.com/koenigsegg-reinvents-wheel/>, accessed: 2016-12-10.
- [2] S.Mason. Rotational Inertia of a Rim, 2016.
<http://stephenmason.com/cars/rotationalinertia.html>, accessed: 2016-11-29.
- [3] J.M.Haaland. Vehicle Dynamics Simulation for setting up a Four-Wheel Independent Drive Electric Race Car. Master's thesis, The Norwegian University of Science and Technology, 2017.
- [4] H.Sølvberg. Carbon Fiber Composite Wheels for Formula Student. Master's thesis, The Norwegian University of Science and Technology, 2014.
- [5] Greenteam Uni Stuttgart. Eo711-4 (2012/2013), 2017.
<https://www.greenteam-stuttgart.de/en/eo711-4-20122013/>, accessed: 2017-18-01.
- [6] Carbon Fiber Gear, a dpitMedia Company. The Koenigsegg Carbon Fiber Wheel is So Light You Can Throw It Around, 2017.
<https://blog.carbonfibergear.com/the-koenigsegg-carbon-fiber-wheel-is-so-light-you-can-throw-it-around>, accessed: 2017-29-11.
- [7] Fibermax Composites. Weaving Styles, © Copyright 2002 - 2014.
https://www.fibermaxcomposites.com/shop/index_files/weavingstylesandpatterns.php, accessed: 2017-07-04.
- [8] T.D.Barry. Study of a Post Structure in Composite Material for Rail Line Electrification Assembly, 2011.
http://bibing.us.es/proyectos/abreprojy/70301/fichero/5_Laminate+Theory.pdf,
accessed: 2017-10-11.
- [9] E.J.Barbero. *Finite Element Analysis of Composite Materials Using Abaqus*. CRC Press, 2013.
- [10] C.K.Oldeide. Design and analysis of CFRP wheels for a formula student race car. Project work, 2016.
- [11] H.Hertz. *The Contact of Elastic Solids*. Macmillan, 1896.
- [12] J.P.Jesuette and M.Theves. Finite Element Analysis of Tire/Tire Interface Forces Under Braking and Cornering Loads². *Tire Science and Technology*, Vol.20(2):83–105., April-June 1992.
- [13] Dassault Systèmes. *Isight documentation*. ©Dassault Systèmes, 2006.

- [14] eFunda. Strain Rosette for Strain Measurement.
http://www.efunda.com/formulae/solid_mechanics/mat_mechanics/strain_gage_rosette.cfm, accessed: 2017-10-11.
- [15] K2W Precision Inc. FormulaSAERacing Wheels, Geometrical specification:, 2017.
<http://keizerwheels.com/wp-content/uploads/2015/03/Kosmo-Series.zip>, accessed: 2017-14-11.
- [16] ASTM International. Standard Practices for Cycle Counting in Fatigue Analysis.
<https://www.astm.org/Standards/E1049.htm>, accessed: 2017-8-11.
- [17] J.J.Kauzlarich. The Palmgren-Miner rule derived. *Tribological Design of Machine Elements, Proceedings of the 15th Leeds-Lyon Symposium on Tribology held at Bodington Hall, The University of Leeds*, 14:175–179, 1989.
- [18] J.C.Stearns. *An investigation of stress and displacement distribution in a aliminum alloy automobile rim*. PhD thesis, The University of Akron, 2000.
- [19] J.Montgomery. Boundary Condition Influences on Shank Stress in 3D Solid Bolt Simulation . *2008 Abaqus Users' Conference*, page 18, may 2002.
- [20] Dassault Sys-temes. Isight & the SIMULIA Execution Engine, Process automation and design exploration., 2016.
<http://www.3ds.com/products-services/simulia/products/isight-simulia-execution-engine/>, accessed: 2016-12-04.
- [21] Dassault Systèmes. *Abaqus 6.14 Documentation: Abaqus/CAE User's Manual, 9.5.5 Creating and running a macro*. ©Dassault Systèmes, 2014.

Appendices

A

Modeling, Set-Up, Procedures & Results

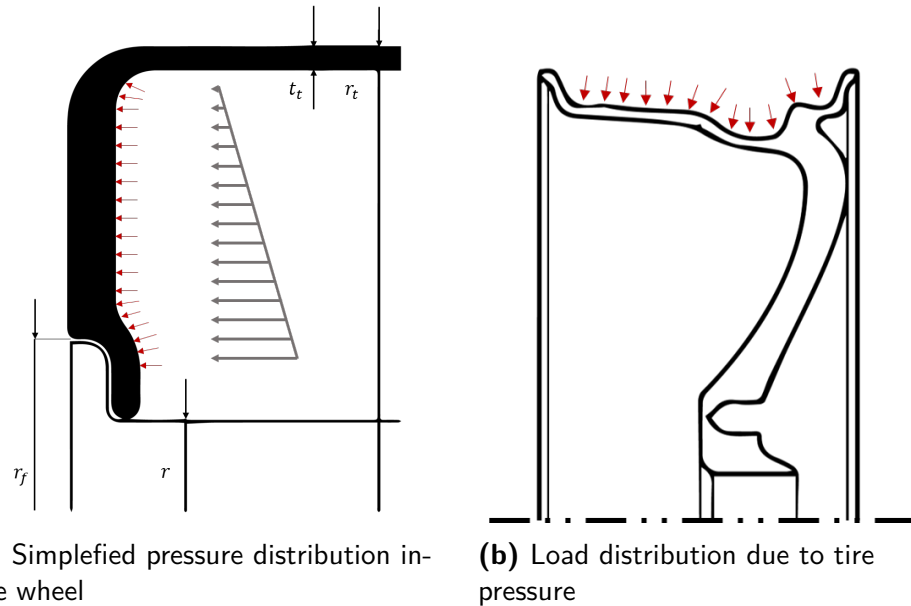
A.1 LOAD SCENARIOS

TIRE PRESSURE

Inflation pressure works laterally on the rim flanges and prevents the tire from slipping and causing debonding. The reactions forces (grey arrows in fig:(a)) which balancing the pressure that acts on the tire's sidewall (red arrows in fig:(a)) are assumed to have a linear distribution and that they work equally on each side, then the resultant force F_{flange} working on each side are given:

$$F_{flange} = \frac{\pi((r_t - t_t)^2 - r^2)P}{2} \quad (\text{A.1})$$

On the rest of the rim there is an even distributed pressure illustrated in Figure (b).



BUMP LOAD

There are known methodologies for modeling the load on the rim due to the weight of the vehicle. Both the eye bar link and the cosine function are accepted models and have been studied by a range of tire companies. The simplifying of the load using a cosine function can be traced back to Hertz in 1882 [11]. John C. Stearns [18] did a study where he investigated different load methodologies in FEA and compared them to a experiment of the real rim under going the same load condition. He investigated the cosine, eye bar and a Fourier series expansion of the contact patch loading. The cosine function was found to predict the experimental data best, this methodology will be used in further analysis. The cosine methodology

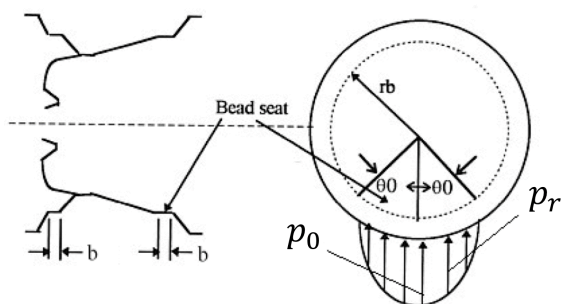


Figure A.1.2: Radial Loading Schematic [18]

is done by assuming that the bead pressure have a cosine function distribution mode within a central angle of 40° in a circumferential direction as shown in Figure A.1.2 Then the distributed pressure, p_r , is given as:

$$p_r = p_o \cdot \cos\left(\frac{\pi}{2} \cdot \frac{\theta}{\theta_o}\right) \quad (\text{A.2})$$

Setting up a integral of (A.2) the total radial load, f_z , can be found:

$$f_z = b \int_{-\theta_o}^{\theta_o} p_o \cdot r_b d\theta \quad (\text{A.3})$$

Substituting (A.2) into (A.3),

$$f_z = b \int_{-\theta_o}^{\theta_o} p_o \cdot r_b \cdot \cos\left(\frac{\pi}{2\theta_o} \cdot \theta\right) d\theta \quad (\text{A.4})$$

Integration and solving for p_o leads to:

$$p_o = \frac{f_z \cdot \pi}{b \cdot r_b \cdot 4 \cdot \theta_o} \quad (\text{A.5})$$

BRAKING AND ACCELERATION

The loads during braking and acceleration is quite similar. Braking will usually be the most critical load for most vehicles. Braking is limited by tire capacity and acceleration is usually limited by motor power. The max load working on the tires can be calculated from tire capacity and power limit. Acceleration/deceleration of the wheels involves tangential shear forces between the tire/rim-interface. Jesuette & Thive did a study where they investigated the interface forces under braking and cornering loads by FEA. The distribution profile of the shear stresses along the rim flange was extracted from the result found by Jesuette & Thive [12].

This was then used to do a sin-regression of the extracted data and by normalizing the curve:

$$y = 0.71 + 0.31 \cdot \sin(0.017x + 1.9) \quad (\text{A.6})$$

Assuming that the pressure p for a race car rim follow the same curve multiplied with a constant p_o , then:

$$p = p_o \cdot (0.71 + 0.31 \cdot \sin(0.017\theta + 1.9)) \quad (\text{A.7})$$

The constant p_o can be found by including the force working on the tires while braking f_x :

$$f_x = p_o \cdot b \cdot \pi \cdot 2r_b \int_{-\theta_o}^{\theta_o} 0.71 + 0.31 \cdot \sin(0.017\theta + 1.9) d\theta \quad (\text{A.8})$$

Integrating and solving for p_o :

$$p_o = \frac{f_x}{2\pi r_b b \cdot (1.42\theta_o + 6.8878 \sin(0.017\theta_o))} \quad (\text{A.9})$$

CORNERING LOADS

Lateral load during cornering is maybe the most important load case regarding vehicle performance, and also one of the load case involving most energy. Lateral loads impose camber gain which in a extreme case could lead into a positive camber (Figure A.1.4) making all of the suspension geometry work useless. A rim without sufficient stiffness could result in a loss of work efficiency of the tire regarding loss in adhesion between the tire and the ground. The lateral distribution was found by using the same regression procedure as in brake loads, by extracting the pressure distribution from Figure A.1.4, with the assumption that the pressure will follow the cosine distribution illustrated in Figure A.1.7, then p is:

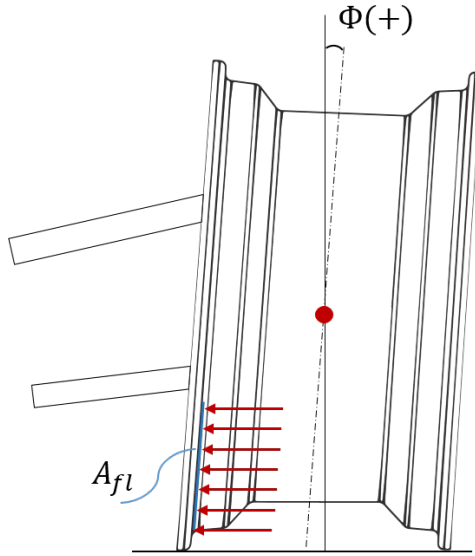


Figure A.1.4: Positive camber gain

$$p = p_o \cdot \cos\left(\frac{\pi\theta}{140}\right) \quad (\text{A.10})$$

The lateral force, f_y , and the areal of the flange were the lateral force is working, A_{fl} , is then used to find p_o :

$$f_y = p_o A_{fl} \int_{-\theta}^{\theta} \cos\left(\frac{\pi\theta}{140}\right) d\theta \quad (\text{A.11})$$

Integrating and solving for p_o :

$$p_o = \frac{f_y \cdot \pi}{280 p_o A_{fl} \cdot \cos\left(\frac{\pi\theta}{140}\right)} \quad (\text{A.12})$$

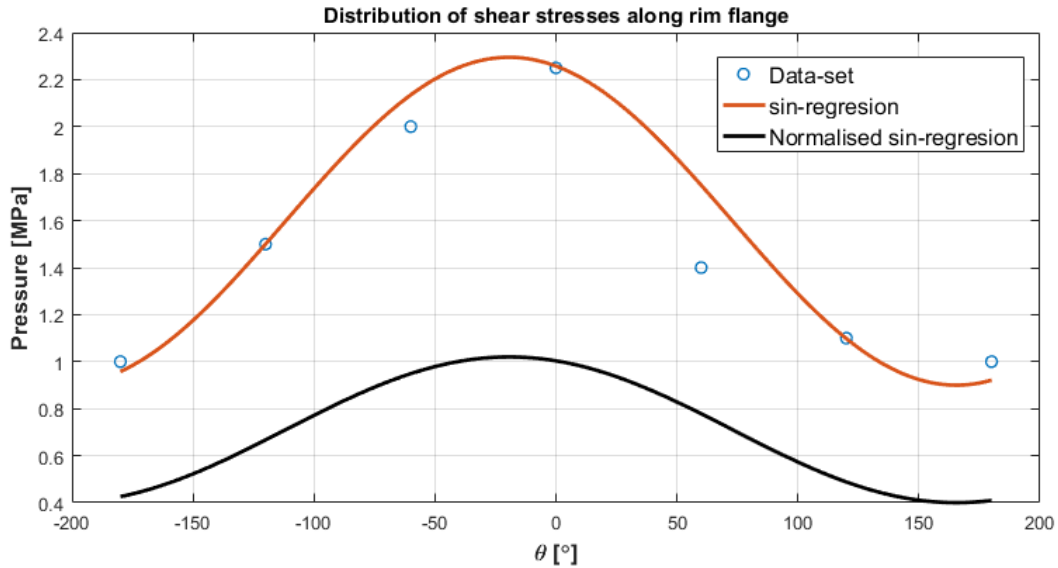


Figure A.1.5: Regression of extracted brake data from Jesuette & Thive [12]

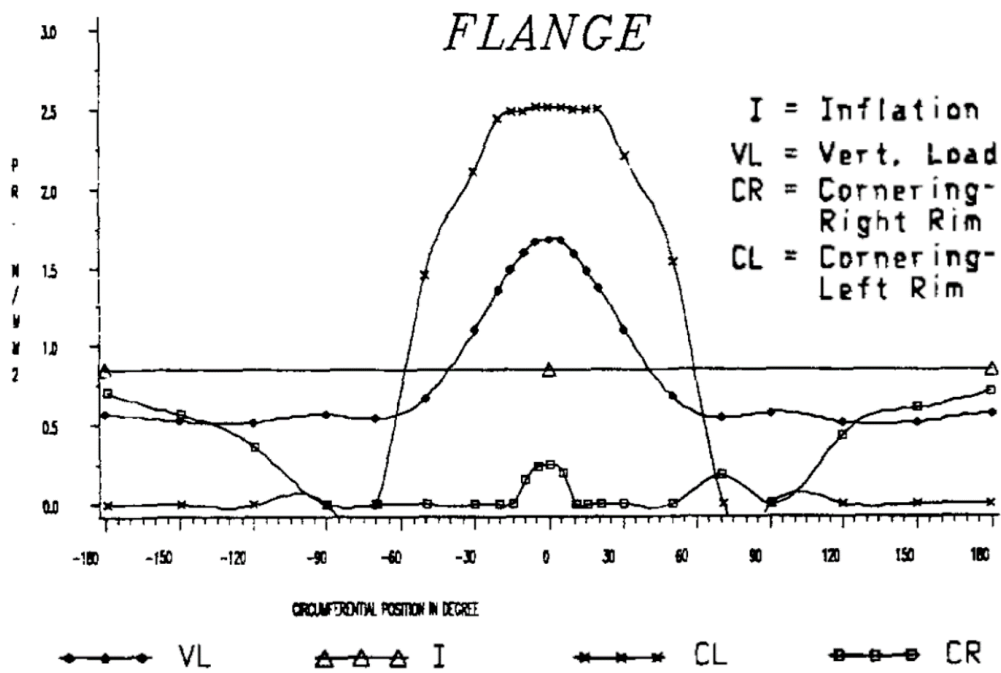


Figure A.1.6: Peak pressure distribution during cornering loads [12]

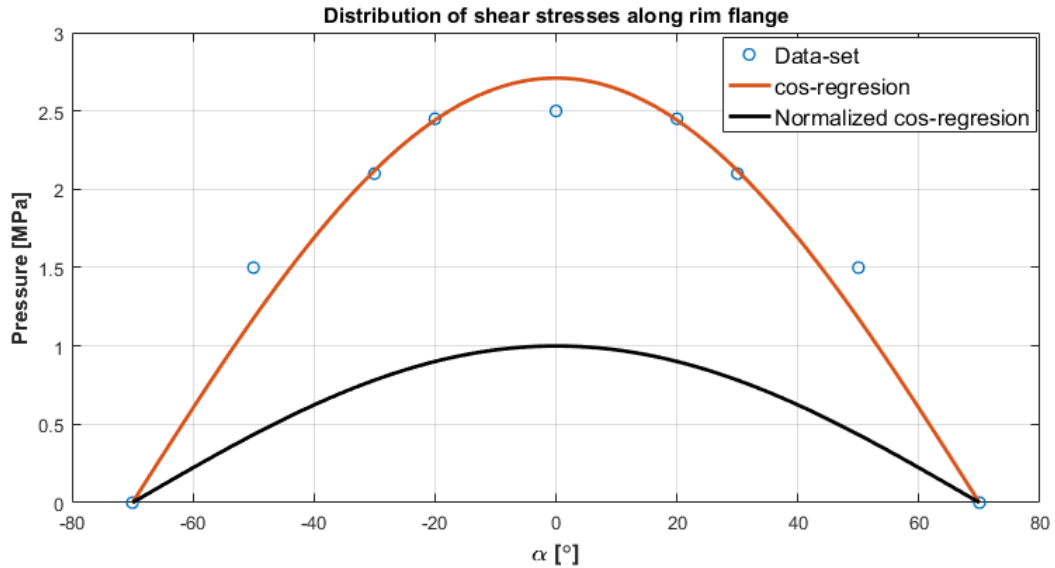


Figure A.1.7: Regression of extracted cornering data from Jesuette & Thive [12]

A.2 FEA - VALIDATION SETUP

This section will follow all the steps done in Abaqus to setup the FE-model for validation of the wheel. It will be structured as the work tree in Abaqus and go through the following items:

- Part
 - Materials
 - Rim shell
 - Rim Center
 - Bolts
 - Hub & center lock
- Assembly
- Step
- Interactions
- Loads
 - Cornering Loads
 - Vertical Loads
 - Brake Loads
 - Pretension in bolts
 - Pretension in Hub & center lock
- Mesh
 - Rim Center
 - Rim Shell
 - Bolts
 - Hub & center lock

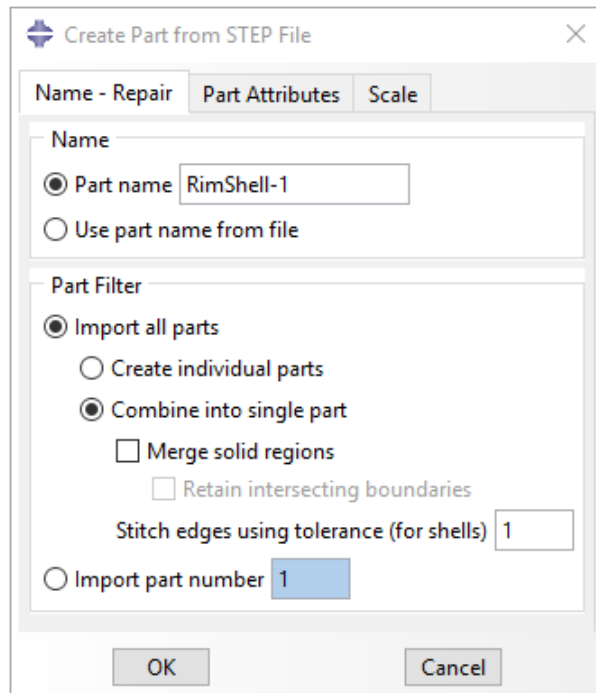


Figure A.2.1

A.2.1 PART

All part geometry was modeled in SolidWorks and imported (Figure A.2.1) to Abaqus with Step file format. Part geometries are found in Figure A.2.2.

A.2.2 PROPERTIES

MATERIALS

Four materials were used for the validation: Steel, Al7075 T6, Hexcels 6376 5HS and Hexcels 6376 UD. All materials were modeled as linear elastic, the metals as isotropic and the composite as lamina. The two laminae were also defined with a failure stress, to calculate Tsai Wu failure criterion. For material data see material data in Appendix D.2 - D.5. All material definitions in Abaqus are found in Figure A.2.3.

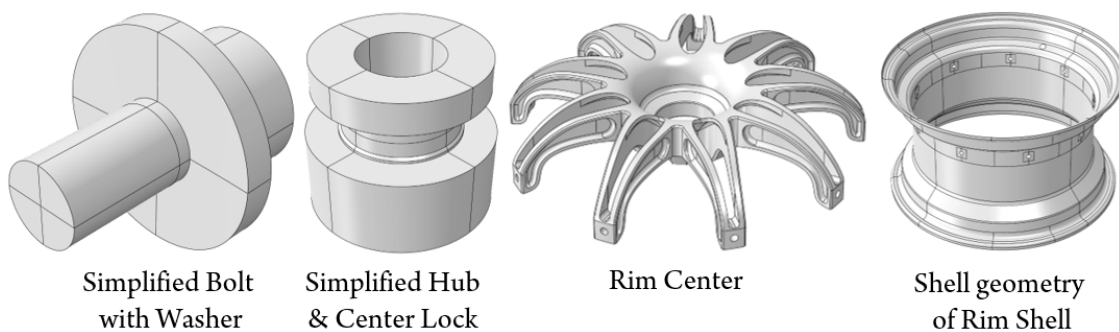


Figure A.2.2

Edit Material

Name: AL7075

Description:

Material Behaviors

Elastic

Type: Isotropic

Use temperature-dependent data

Number of field variables: 0

Moduli time scale (for viscoelasticity): Long-term

No compression

No tension

	Young's Modulus	Poisson's Ratio
1	71500	0.3

Edit Material

Name: Steel

Description:

Material Behaviors

Elastic

Type: Isotropic

Use temperature-dependent data

Number of field variables: 0

Moduli time scale (for viscoelasticity): Long-term

No compression

No tension

	Young's Modulus	Poisson's Ratio
1	200000	0.3

Edit Material

Name: Hexcel 6376 SHS

Description:

Material Behaviors

Elastic

Fail Stress

Type: Lamina

Use temperature-dependent data

Number of field variables: 0

Moduli time scale (for viscoelasticity): Long-term

No compression

No tension

	E1	E2	Nu12	G12	G13	G23
1	67000	67000	0.08	2840	1000	1000

Edit Material

Name: Hexcel 6376 UD

Description:

Material Behaviors

Elastic

Fail Stress

Type: Lamina

Use temperature-dependent data

Number of field variables: 0

Moduli time scale (for viscoelasticity): Long-term

No compression

No tension

	E1	E2	Nu12	G12	G13	G23
1	164000	9000	0.31	6500	6500	6500

Suboption Editor

Fail Stress

Use temperature-dependent data

Number of field variables: 0

Data

	Ten Stress Fiber Dir	Com Stress Fiber Dir	Ten Stress Transv Dir	Com Stress Transv Dir	Shear Strength	Cross-Prod Term Coeff	Stress Limit
1	1006	500	1006	500	55	0	1006

Suboption Editor

Fail Stress

Use temperature-dependent data

Number of field variables: 0

Data

	Ten Stress Fiber Dir	Com Stress Fiber Dir	Ten Stress Transv Dir	Com Stress Transv Dir	Shear Strength	Cross-Prod Term Coeff	Stress Limit
1	2723	1350	111	50	75	0	2723

Figure A.2.3

RIM SHELL

Conventional shell was used to model the composite for the rim shell. This was defined with a composite layup for each of the 8 segment. Shell reference surface and offset was set to bottom surface. Layup orientation was defined with a cylindrical (R, θ, Z) coordinate system with R as the normal. The coordinate system was defined in the center of the rim with the Z-axis in the axial direction. Composite layup for the outer flange segment is found in Figure A.2.4.

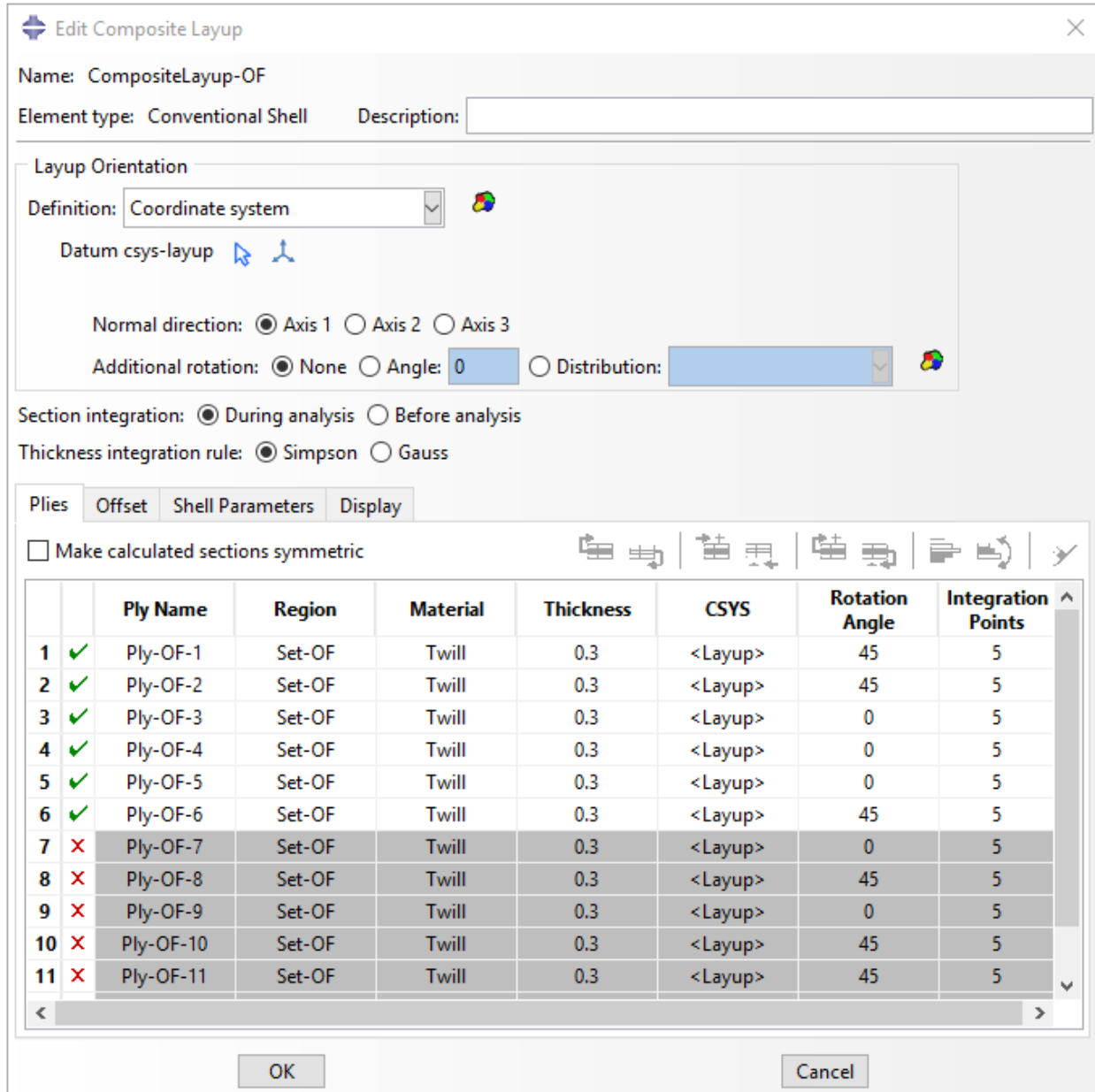


Figure A.2.4

RIM CENTER

Rim Center was modeled with a solid homogeneous section with aluminum as material. This is illustrated in Figure A.2.5.

BOLTS

Bolts was modeled with a solid homogeneous section with steel as material.

HUB & CENTER LOCK

Hub & center lock was modeled with a solid homogeneous section with aluminum as material.

A.2.3 ASSEMBLY

All part was imported with coordinate system according to the main assembly in SolidWorks such that assembly constraint was eliminated. All parts was imported with dependent mesh (mesh on part). See Figure A.2.6. Only one bolt was imported from SolidWorks, and radial pattern was used to copy all the bolts in right place. This was done to reduce work as the mesh and partition procedure is only done for one bolt.

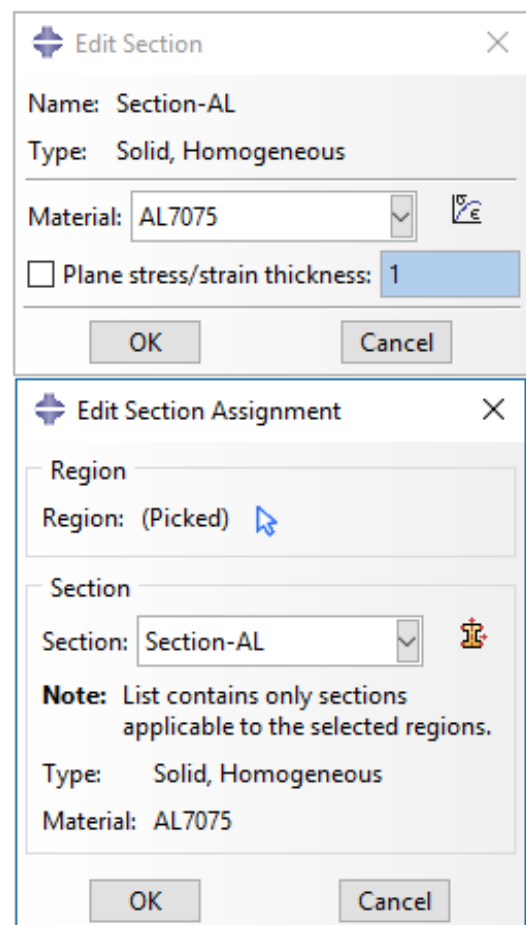


Figure A.2.5

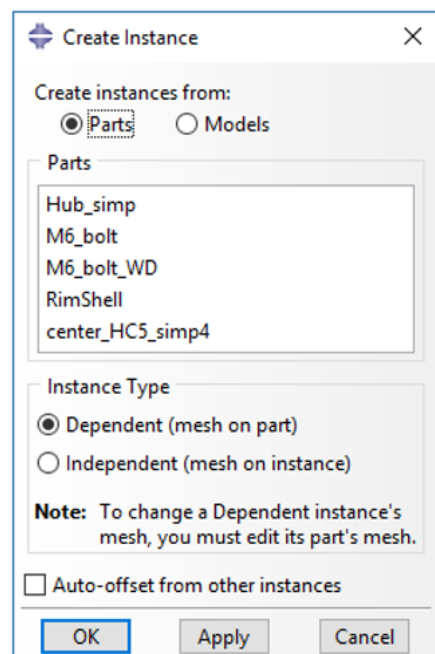


Figure A.2.6

A.2.4 STEP

Two static general steps was used. Step one for applying pretension to bolts and center lock, step two for the given load scenario (Cornering, bump etc. see load scenarios in chapter 2 section 2.1.). Due to contact on curved surfaces the unsymmetrical matrix storage was selected, as this storage have bigger chance to success (drawback slower). See Figure A.2.7 for set-up.

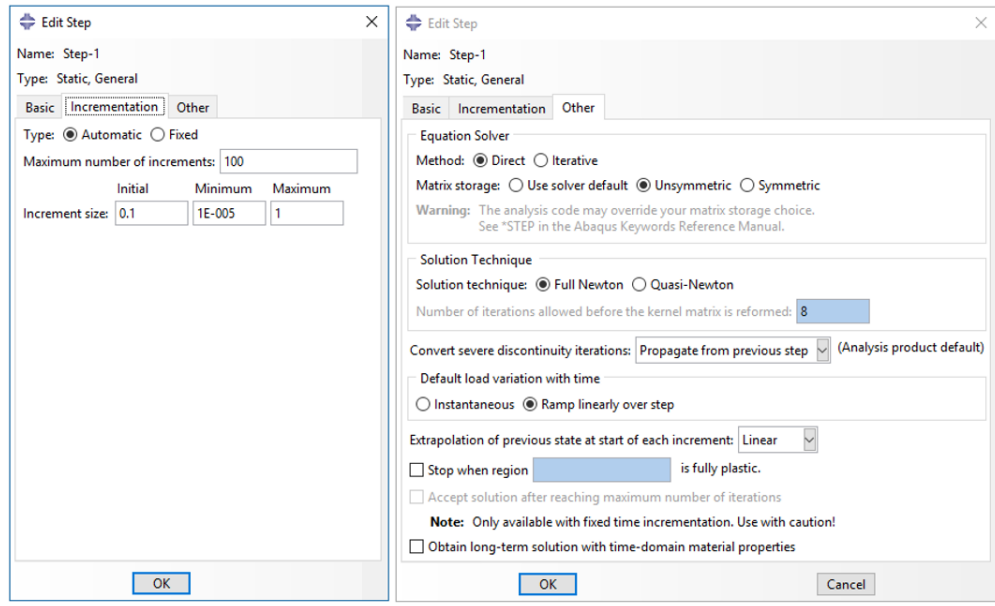


Figure A.2.7

A.2.5 INTERACTIONS

GENERAL CONTACT

General contact was used instead of manually specifying each contact set. General contact setup is found in Figure A.2.9. So reduce solving time every unreasonable surfaces was removed from contact definition. This known as excluded surface pair in Abaqus, red surfaces on the rim in the figure show all excluded surfaces. A contact initialization was used to resolve with strain-free adjustments. Contact properties was set with both tangential and normal behavior, all properties is show in the figure. Bolts was modeled with full lengths, so a surface thickness assignment was added to shell geometry to have the right offset for contact definition between rim shell and bolts. Surface thickness assignment is presented in Figure A.2.8.

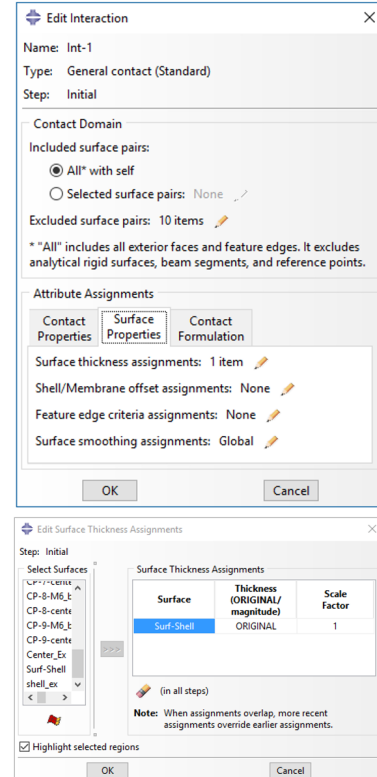


Figure A.2.8

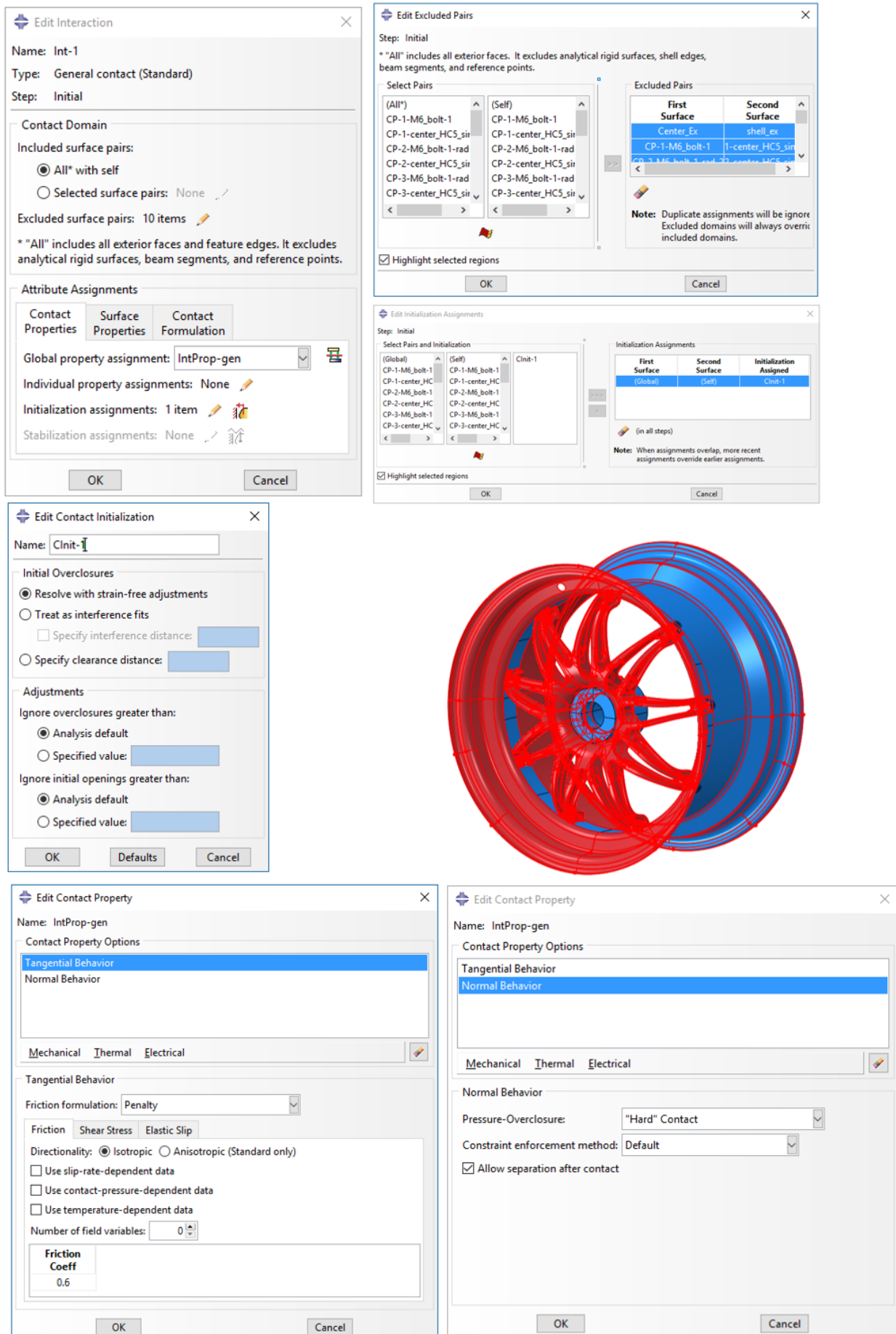


Figure A.2.9

A.2.6 BOLTS

Jerome Montgomery did a study where he compared three modeling techniques for threaded bolt connections with reload. In Figure A.2.10 the stress distribution of tied, smeared and full modeled threads are compared[19]. A tie constraint was used for representing threads interaction between rim center and bolts. This is not best simplification but gives a all right representation of threads respect to computing time. The effect a bolted connection in term of stiffness was the main interest of modeling of the bolts.

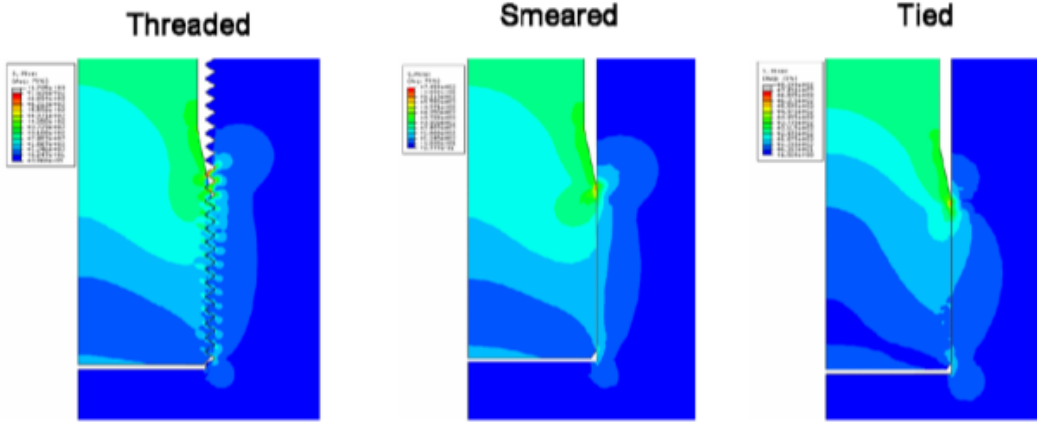


Figure A.2.10: Result from Jerome Montgomery's study [19]

A.2.7 LOADS

This subsection will not go into modeling of each combined load, but only each separate load distribution. See chapter: 2 section: 2.1 for load scenarios. Boundary condition was applied as encastre on the dummy hub.

VERTICAL LOADS

The vertical load distribution is defined on the $a + - 40^\circ$ partition of the inner and outer bead. The load was defined as a surface traction working in Z-direction with distributed by analytic field. The analytic field was based on the vertical distribution defined in Appendix A.1. To apply this equation the cylindrical coordinate system used for the layup orientation was used. See Figure A.2.11 for modeling details related to the vertical load.

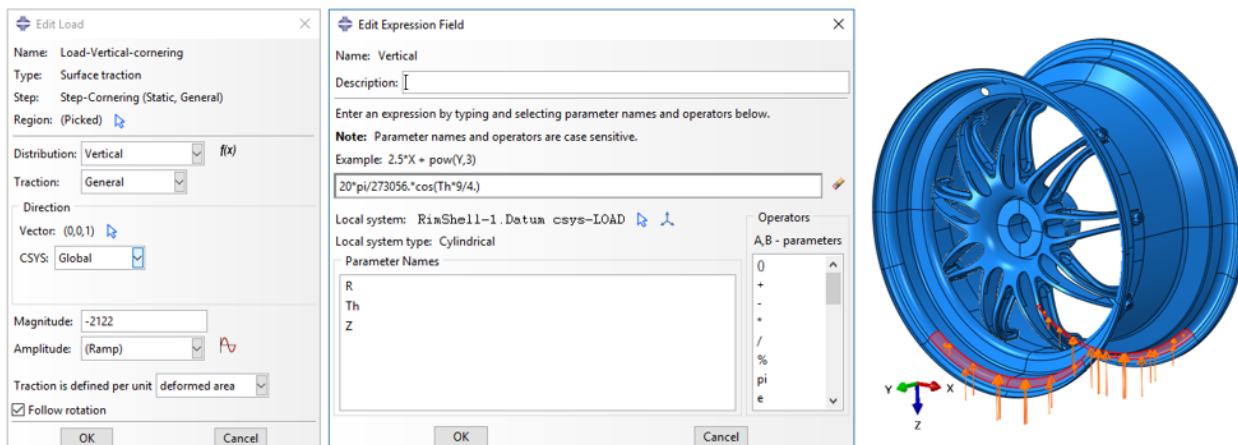


Figure A.2.11

CORNERING LOADS

The vertical load distribution is defined on the $a + -70^\circ$ partition of the inner bead. The load was defined as a surface traction working in Y-direction with distributed by analytic field. The analytic field was based on the lateral distribution defined in Appendix A.1. To apply this equation the cylindrical coordinate system used for the layup orientation was used. See Figure A.2.12 for modeling details related to the cornering load.

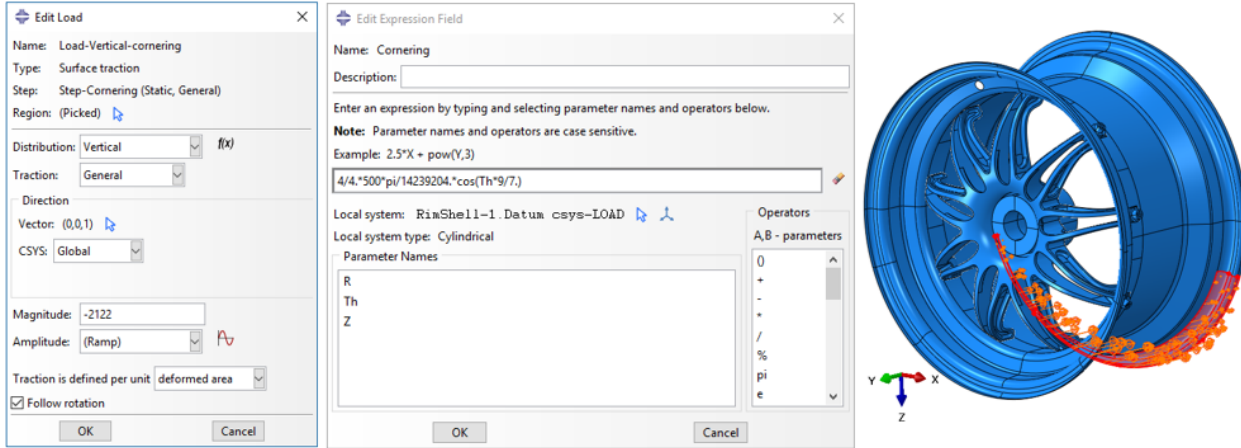


Figure A.2.12

BRAKE LOADS

The brake load distribution is defined on the hole inner and outer bead. The load was defined as a surface traction working as a shear traction distributed by analytic field. The analytic field was based on the brake distribution defined in Appendix A.1. To apply this equation the cylindrical coordinate system used for the layup orientation was used. See Figure A.2.13 for modeling details related to the brake load.

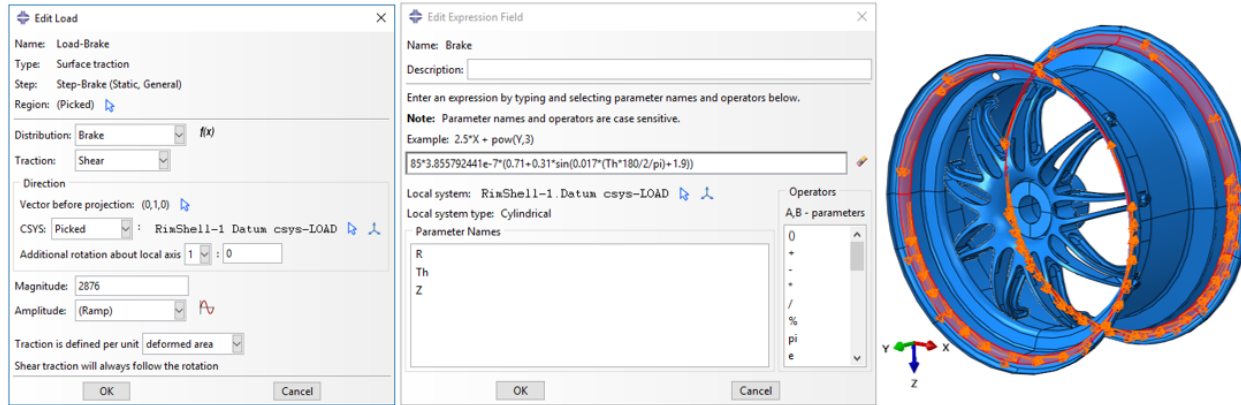


Figure A.2.13

PRETENSION IN BOLTS

Pretension in the bolts was defined with a bolt load on the middle partition between the threads and the bolt head. For definition of a bolt load a center axis in the axial direction of the bolt is needed. The bolt load is applied in the first step before the main load step, in the main load step the bolt is defined with a fixed length. The bolt load is applied with a ramp where 10% of the load is applied during 0.5 of total step time, and rest during the last of the increment. This is done to easier initialize contact when general contact is used, since Abaqus search for all the contact pairs. See Figure A.2.14 for modeling details related to the bolt load.

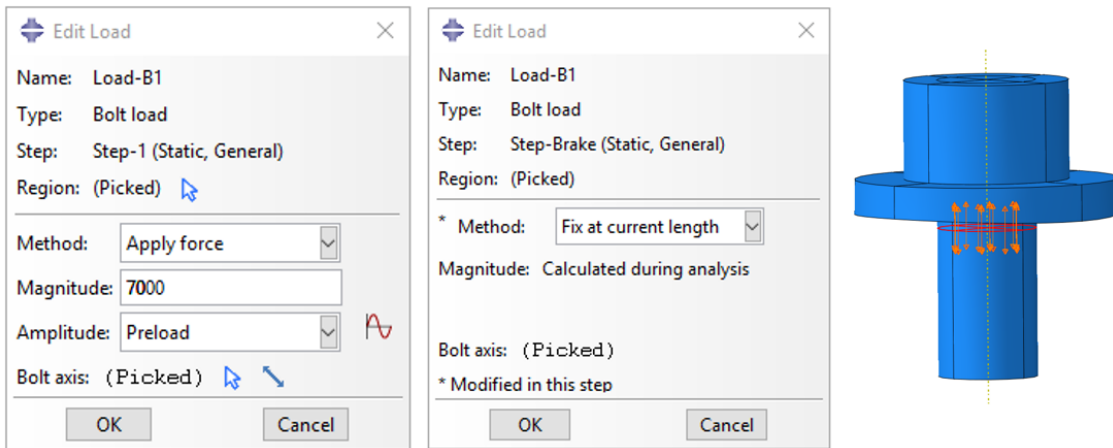


Figure A.2.14

PRETENSION IN HUB & CENTER LOCK

Pretension in the hub & center lock was defined with a bolt load on the middle partition between the threads and the center lock nut. For definition of a bolt load a center axis in the axial direction of the bolt is needed. The bolt load is applied in the first step before the main load step, in the main load step the bolt is defined with a fixed length. The bolt load is applied with a ramp where 10% of the load is applied during 0.5 of total step time, and rest during the last of the increment. This is done to easier initialize contact when general contact is used, since Abaqus search for all the contact pairs. See Figure A.2.15 for modeling details related to the bolt load.

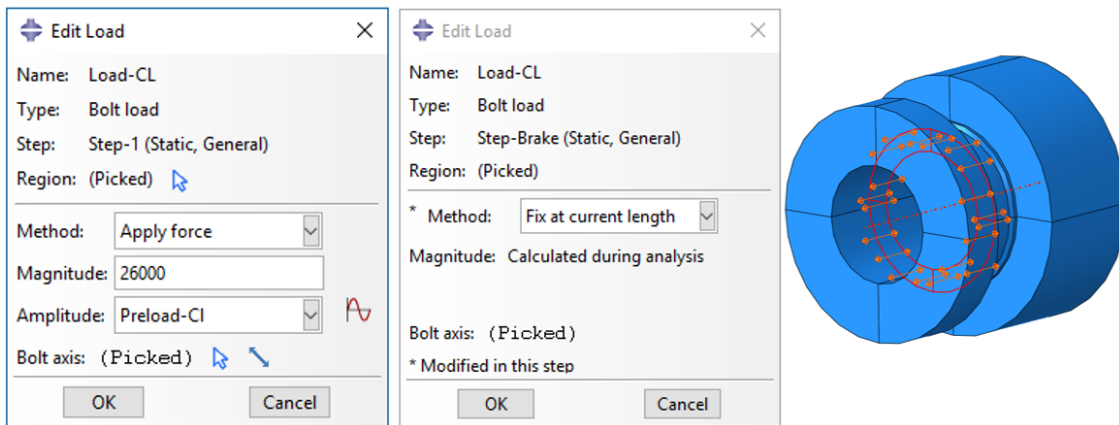


Figure A.2.15

A.2.8 MESH

RIM SHELL

The mesh for the rim shell was made of 4-node doubly curved thin shell elements with reduced integration, hourglass control and finite membrane strains. The element shape is free quad with advancing front as mesh shape algorithm. The global size was set to 5 with a curvature control of 0.05. Mesh refinements was done for all holes in the laminate and to the rim center interaction surfaces. See Figure A.2.16 for details related to mesh.

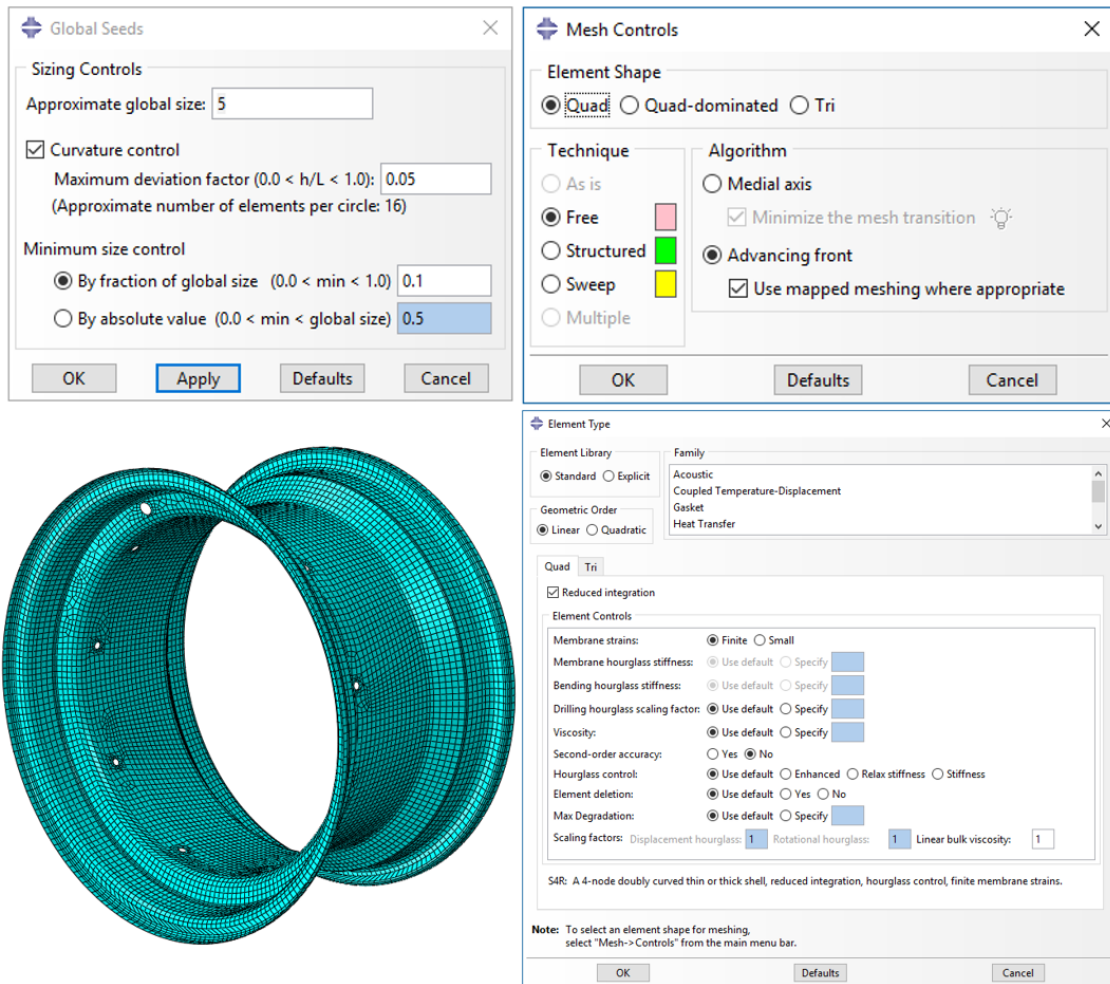


Figure A.2.16

RIM CENTER

The mesh for the rim center was made of 10-node quadratic tetrahedron elements. The element shape is free tet with default shape algorithm. The global size was set to 4 with a curvature control of 0.1. See Figure A.2.17 for details related to mesh.

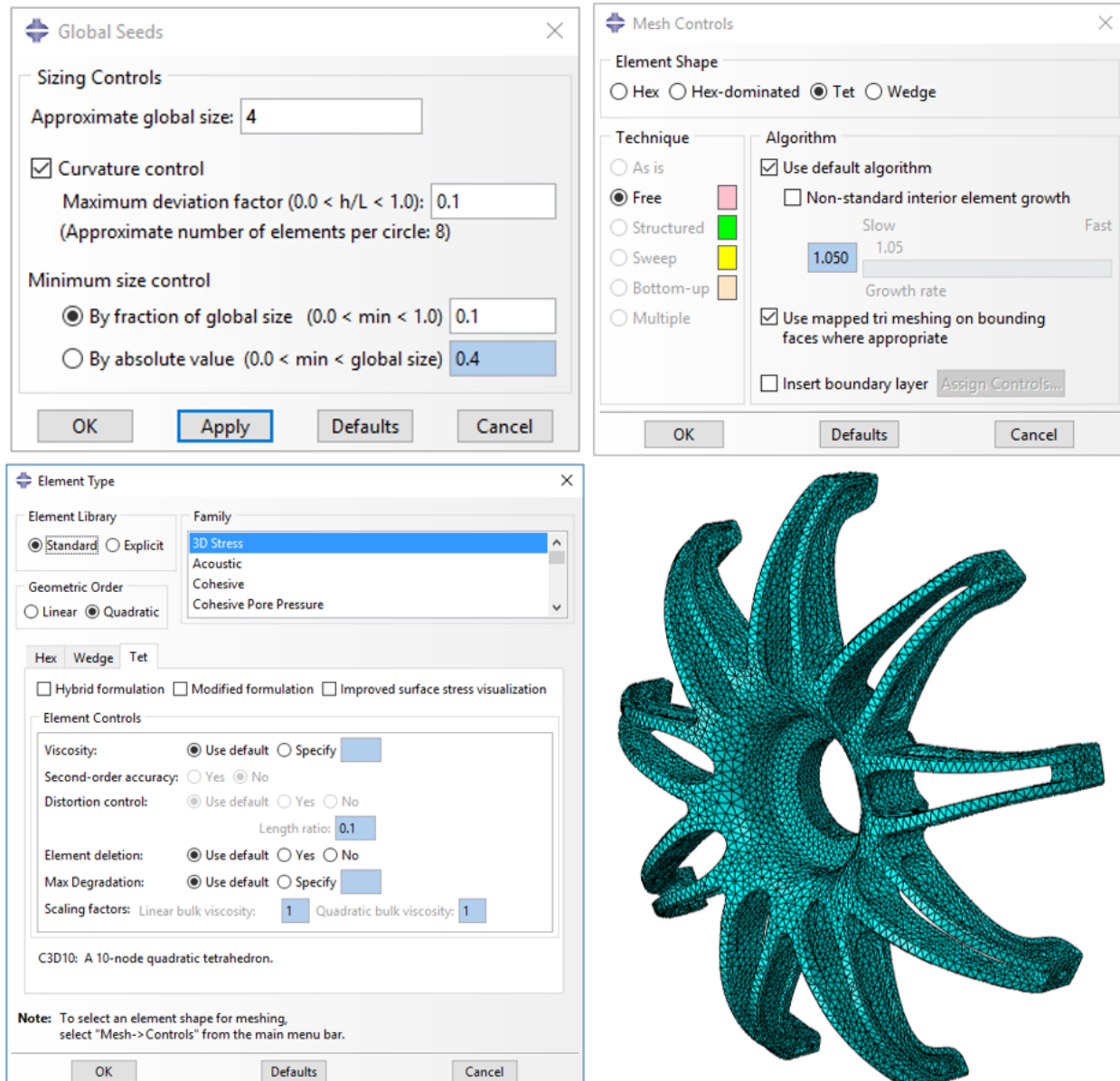


Figure A.2.17

BOLTS

The mesh for the bolts was made of 8-node linear brick elements with reduced integration and hourglass control. The element shape was quad and a combination of structured (green) and sweep (yellow). The global size was set to 1 with a curvature control of 0.1. See Figure A.2.18 for details related to mesh.

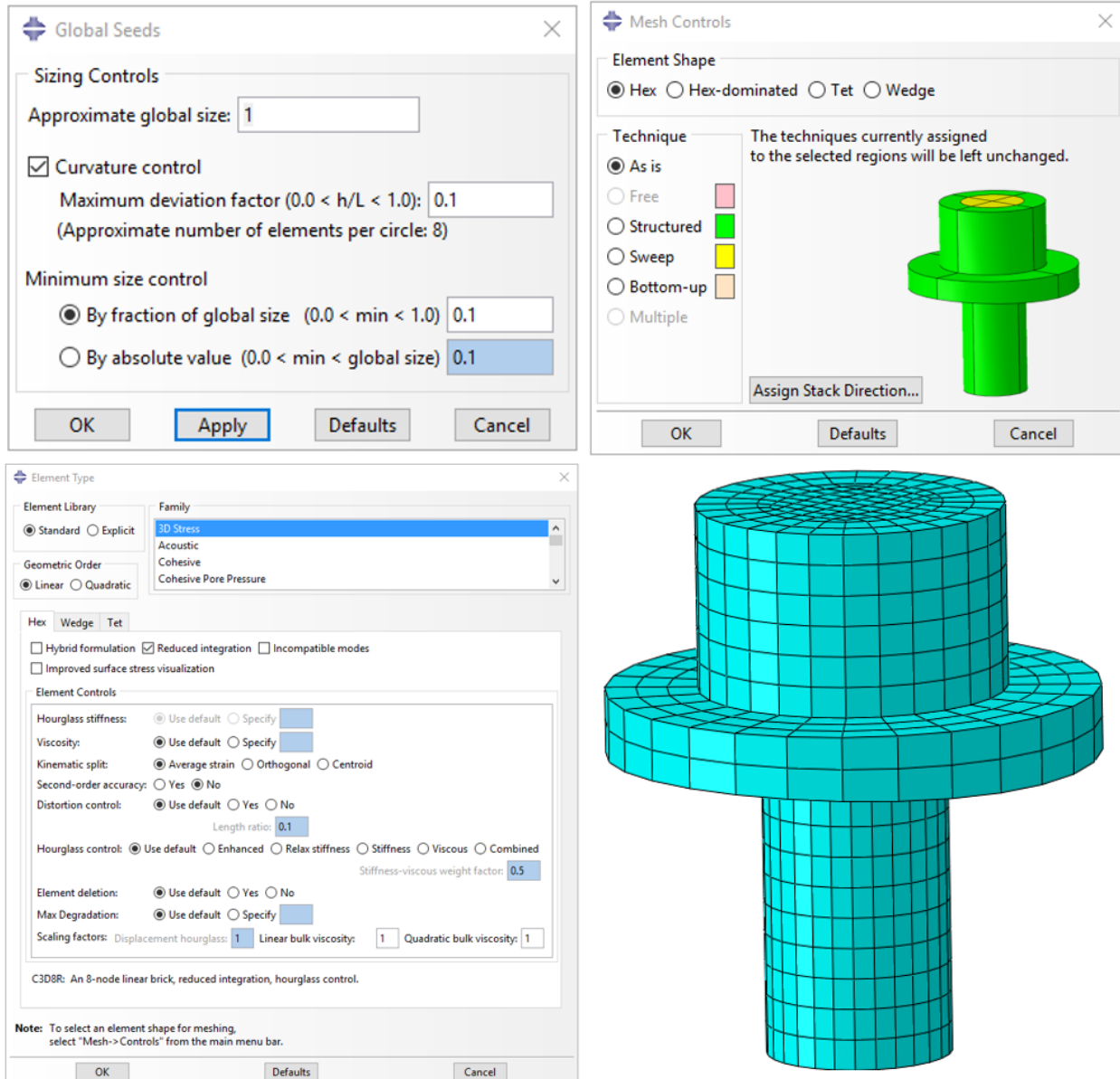


Figure A.2.18

HUB & CENTER LOCK

The mesh for the Hub & center lock was made of 8-node linear brick elements with reduced integration and hourglass control. The element shape was quad and with sweep technique. The global size was set to 3 with a curvature control of 0.05. See Figure A.2.19 for details related to mesh.

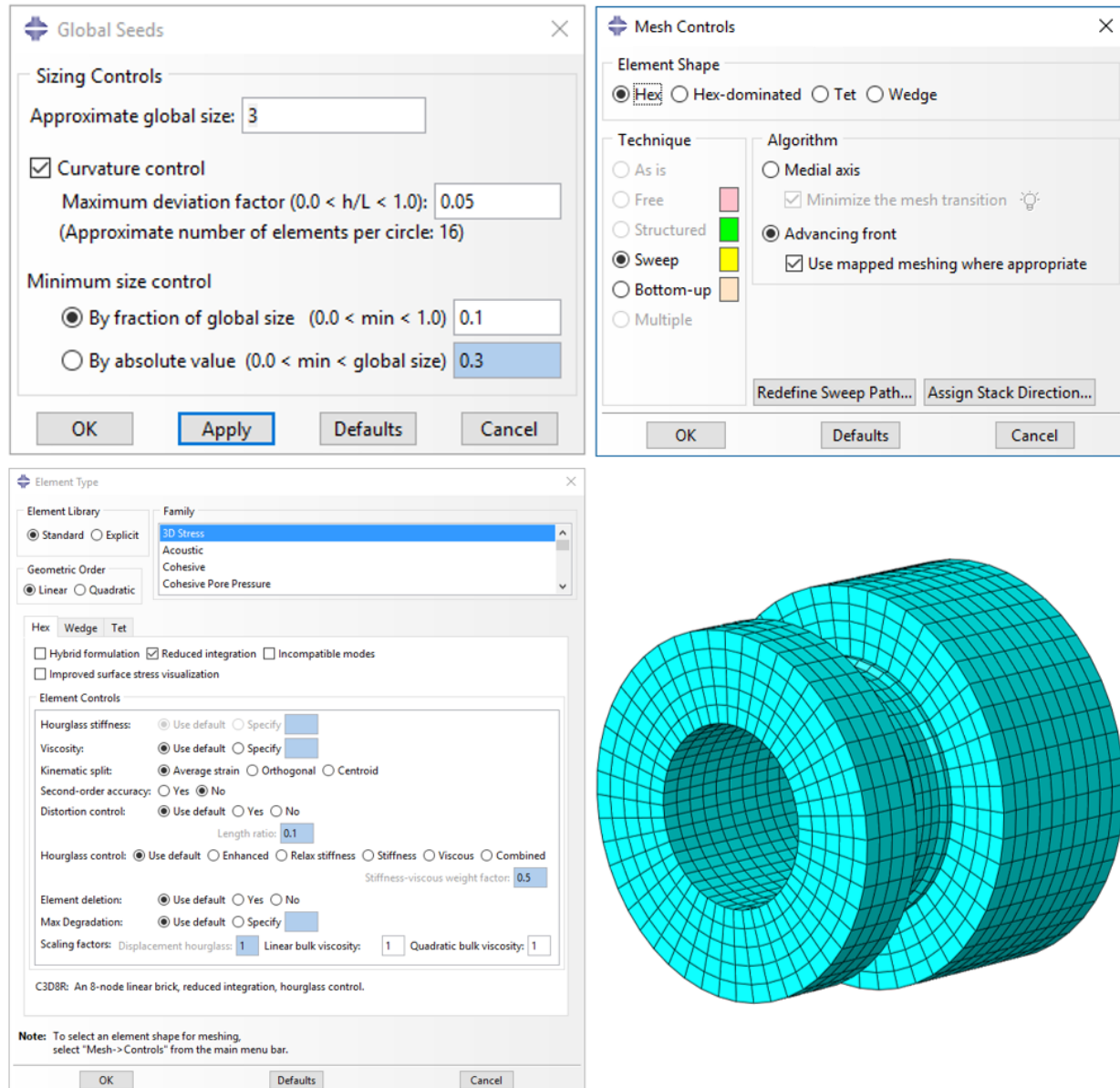


Figure A.2.19

A.3 MATERIAL OPTIMIZATION SETUP

This section will follow all steps done in Isight, Matlab and Abaqus to set up the material optimization. It will be divided and structured as the list under:

- Isight
 - Work-flow
 - Optimization
 - Parameters
- Abaqus
 - Part
 - Step
 - Interactions
 - Macro and scripting
- Codes and Script
 - Matlab Code
 - Abaqus Pre-script
 - Abaqus Post-script

A.3.1 ISIGHT

Isight and the SIMULIA Execution Engine (formerly Fiper) are used to combine multiple cross-disciplinary models and applications together in a simulation process flow, automate their execution across distributed compute resources, explore the resulting design space, and identify the optimal design parameters subject to required constraints[[20](#)].

WORK-FLOW DESCRIPTION

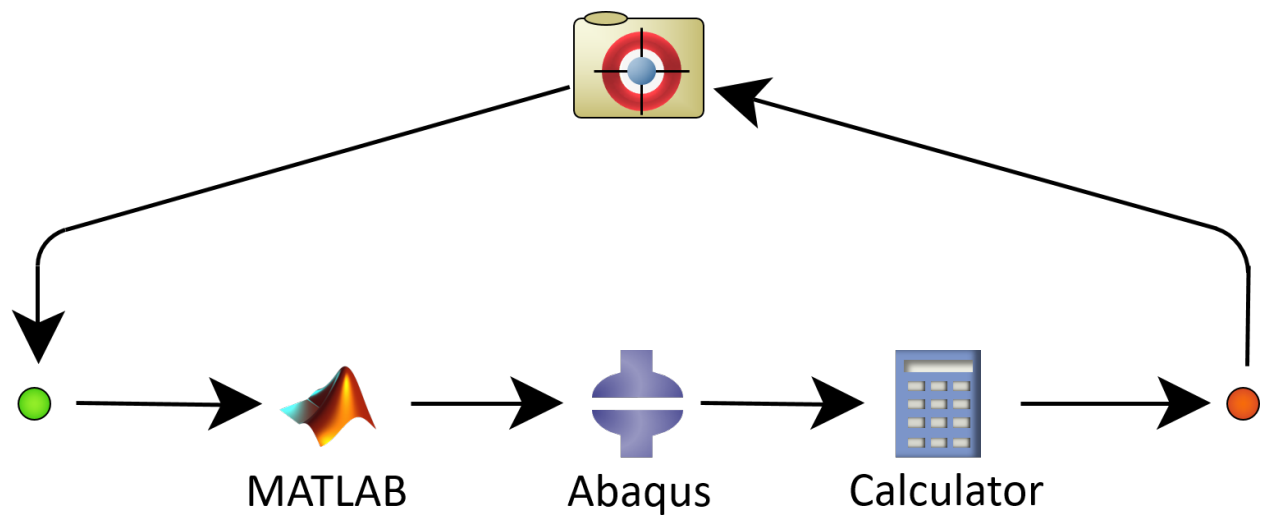


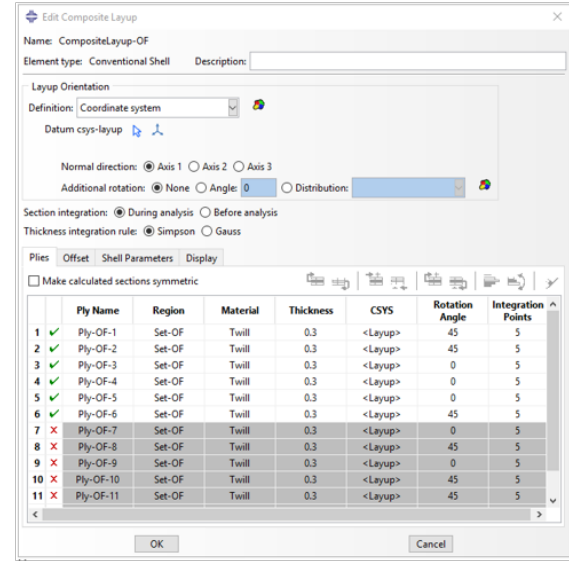
Figure A.3.1

The work-flow used for the material optimization is illustrated in Figure A.3.1. First, the optimizer module (here called Layup optimizer) give Matlab values for each variables consisting; number of plies, orientations and material for all sections. Then Matlab writes 8 text files on the format found in Figure A.3.2 which

is on the same format and have all the information needed for the composite layup editor in Abaqus:A.3.2. Then Abaqus is executed with a prescript written in python. This prescript is constructing a FE-model with layup information from Matlab as input. After the FE-analysis is completed a postscript written python is reading the strain energy, and displacement at the rim flange and outputting the values to the Layup optimizer. The layup optimizer then changes the layup parameters based on the response of the design objectives and the design constraint.

```
0, Ply-OF-1, Set-OF, Twill, 0.3, <Layup>, 45, 5
0, Ply-OF-2, Set-OF, Twill, 0.3, <Layup>, 45, 5
0, Ply-OF-3, Set-OF, Twill, 0.3, <Layup>, 0, 5
0, Ply-OF-4, Set-OF, Twill, 0.3, <Layup>, 0, 5
0, Ply-OF-5, Set-OF, Twill, 0.3, <Layup>, 0, 5
1, Ply-OF-6, Set-OF, Twill, 0.3, <Layup>, 0, 5
1, Ply-OF-7, Set-OF, Twill, 0.3, <Layup>, 0, 5
1, Ply-OF-8, Set-OF, Twill, 0.3, <Layup>, 45, 5
1, Ply-OF-9, Set-OF, Twill, 0.3, <Layup>, 0, 5
1, Ply-OF-10, Set-OF, Twill, 0.3, <Layup>, 45, 5
1, Ply-OF-11, Set-OF, Twill, 0.3, <Layup>, 45, 5
1, Ply-OF-12, Set-OF, Twill, 0.3, <Layup>, 0, 5
1, Ply-OF-13, Set-OF, Twill, 0.3, <Layup>, 0, 5
1, Ply-OF-14, Set-OF, Twill, 0.3, <Layup>, 0, 5
```

Text file formatting



Composite Layup Editor in Abaqus

Figure A.3.2

OPTIMIZATION SET-UP

A evolution based algorithm was used for the optimization, for optimization set-up see Figure A.3.3. The optimization constraints and objectives is found in Table A.3.1. Based on the response of these parameters, Isight updates the variables for each iterations. The variables is updated with goal of fulfilling the design constraint and design objectives. The main goal of the optimization is to hit a weight target of 700 gram and maximize the stiffness by minimizing the strain energy. In addition to this a material-use was set as constraint. This was done as only a limited amount of UD-fibers was available from the sponsors.

Table A.3.1

Design Constraints						
Parameter	Lower Bound	Upper Bound	Target	Scale Factor	Weight Factor	
Square Meter of UD-fiber used per rim		0.3	0.5	0.4	2000.0	0.5
Total mass per Rim Shell	500.0	800.0	700.0	1.42		1.0

Design Objectives				
Parameter	Direction	Target	Scale Factor	Weight Factor
Strain Energy	Minimize	-	0.2922	1.2

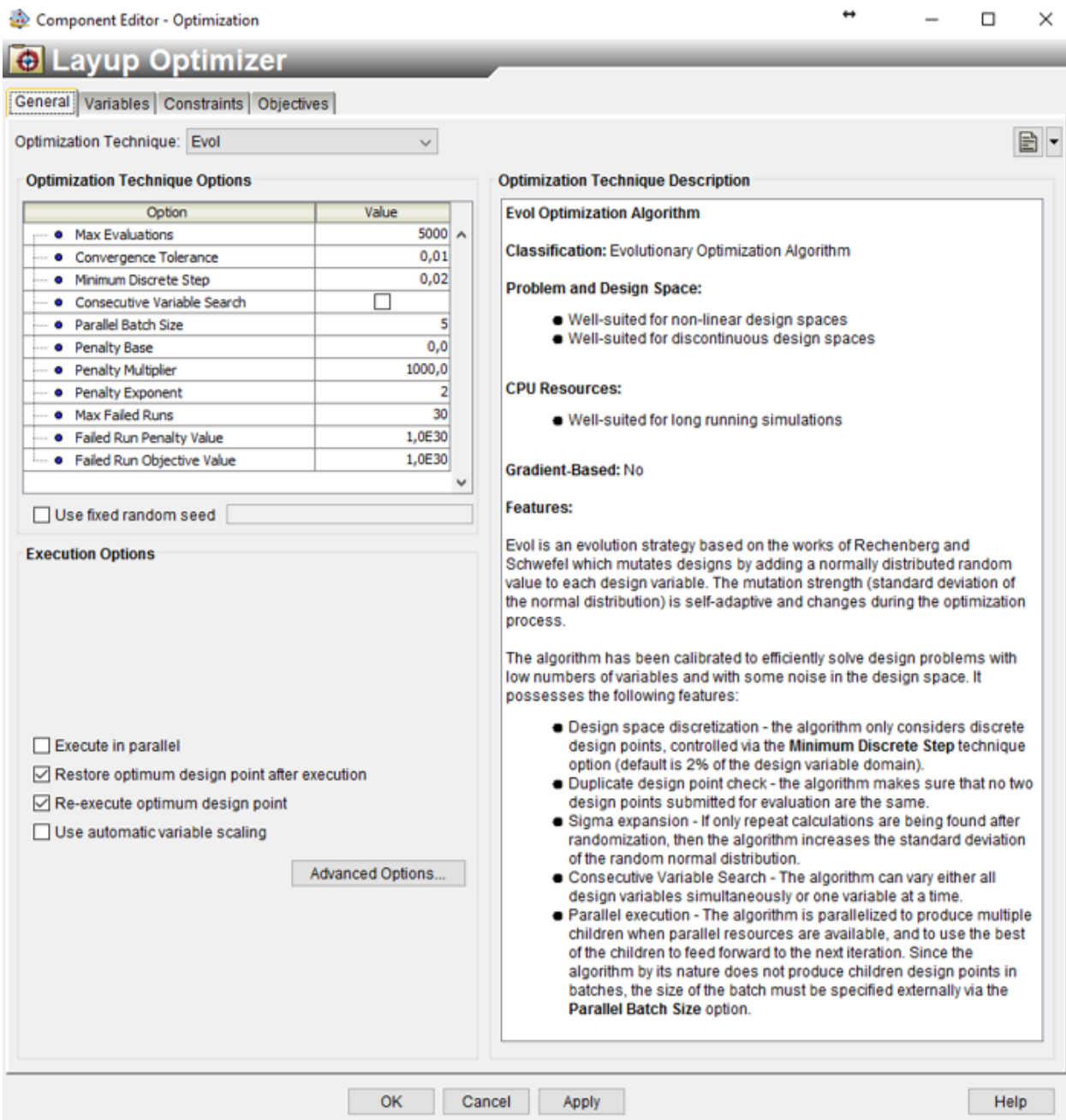


Figure A.3.3

VARIABLES

The variables is based on the segmentation of the rim which is described in chap: 2 section: 2.3.3. Each segment have individual variables which is number of plies, and orientations. In a addition to this variables a material choice (UD & 5HS) was added to segment: OB, CM, CS and IB. Summarized variables is found in Table A.3.2.

Table A.3.2

Segment	Orientations	Number of Layers	Material Choice
OF	0/90 & +-45	5-14	5HS
OB	[-90:15:90]	5-18	UD & 5HS
OD	0/90 & +-45	5-14	5HS
CM	[-90:15:90]	5-18	UD & 5HS
CS	[-90:15:90]	5-18	UD & 5HS
ID	0/90 & +-45	5-14	5HS
IB	[-90:15:90]	5-18	UD & 5HS
IF	0/90 & +-45	5-14	5HS

A.3.2 ABAQUS

This section will only go through the modeling which is different from the modeling described in Appendix A.2 which is the following items in underlined in blue bold text:

- **Part**
- Properties
- Assembly
- **Step**
- **Interactions**
- Loads
- Mesh
- **Macro and Scripting**

PART

The part procedure is the same as in FEA-validation Setup, except the model only have two parts, the Rim center and the Rim shell. The rim shell is simplified and does not include any holes for mounting or for the stem valve. The rim center used for the optimization is a early draft, but it have the baseline as the final rim center. Rim center and rim shell is found in Figure A.3.4.

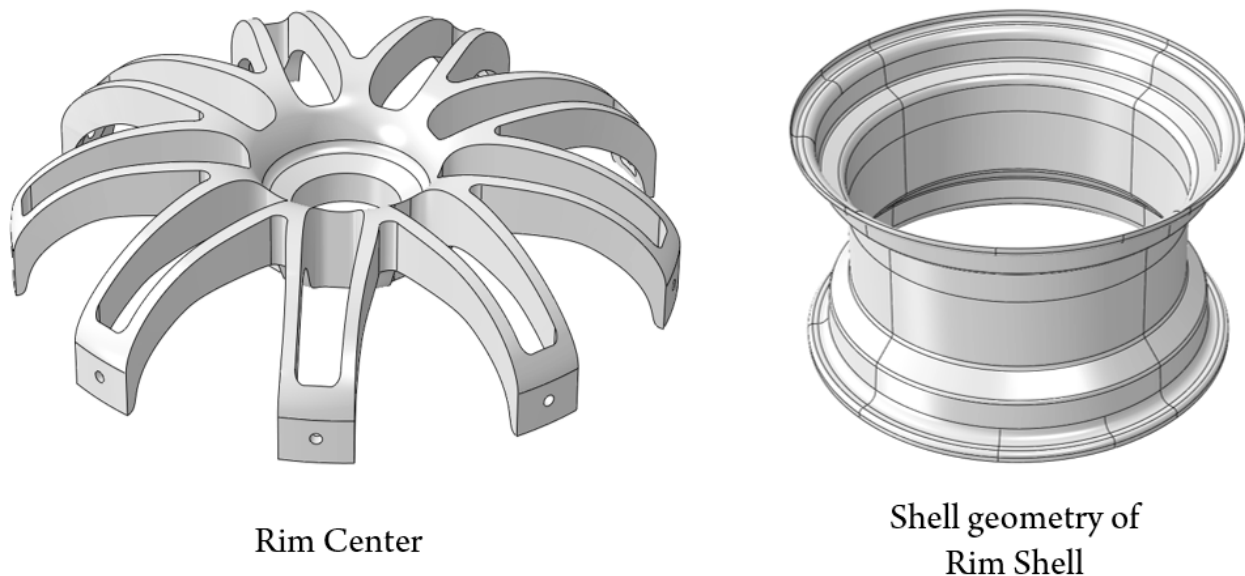


Figure A.3.4

STEP

Two quasi-static linear perturbation steps was used. Step one for cornering at 110km/h and step two for braking at 110km/h. See Figure A.3.5 for set-up.

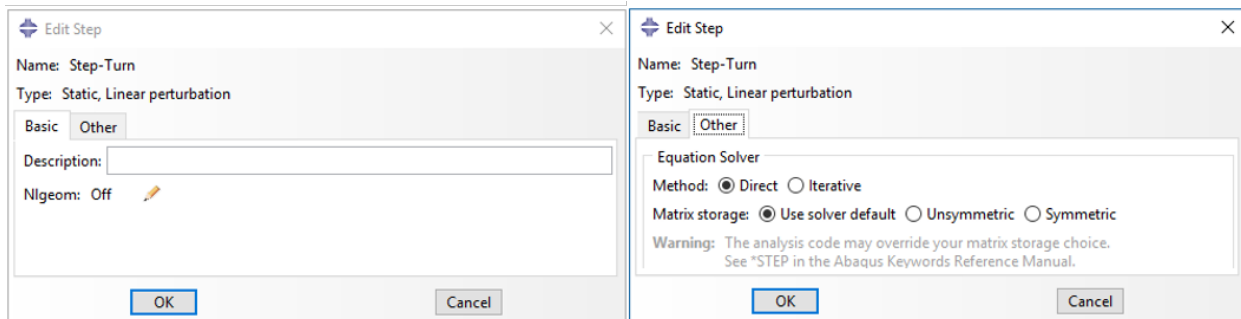
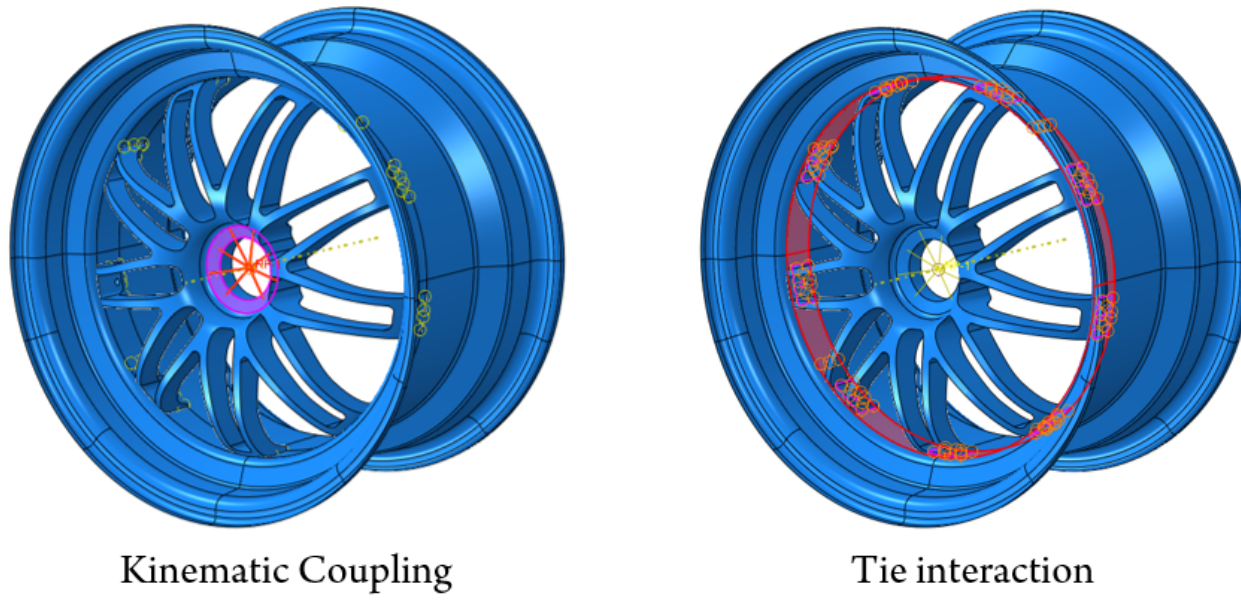


Figure A.3.5

INTERACTIONS

The interactions was simplified to reduce computing time as many design iterations was required by the Evolution based optimization algorithm. The interaction of the hub was simplified with a kinematic coupling constrained in all 6 degree of freedom, which was then encastre and used as boundary condition. The bolted connection between the rim center and the rim shell was simplified with a tie constraint discretized with the surface to surface method. See Figure A.3.6 for coupling and tie set-up.



Kinematic Coupling

Tie interaction

Figure A.3.6

MACRO AND SCRIPTING

Abaqus/CAE can be automated by running Python scripts. Writing these scripts from scratch is not always intuitive. Abaqus have a built in Macro Recorder which allows the user to work in the GUI-enviorment and record that into scripts [21].

First the complete FE-model was built in Abaqus, all steps in the Abaqus work-three was followed as described in the latter sections. Creating of the composite layup was done last with the Macro Recorder on to generate a python code used for the optimization task. This script was then modified to update the layup based on the text file generated by Matlab. This python script is found in Appendix A.3.3.

Another script was created for reading and saving the output values from ODB-result file. This script created without the Macro Recorder and is found in Appendix A.3.3

A.3.3 CODES AND SCRIPTS

MATLAB CODE

```

1 % This script is designed for handling parameters from Isight and writing
2 % them into text files suited for the Abaqus composite layup editor. This
3 % script is only usable for the specific task described in the master
4 % Thesis.
5 % % Parameters for Outer Flange
6 A_of= 31272*10^-6; % m^2
7 double n_of; % Number of plies
8 % double O_of1;
9 O_of1=45;
10 double O_of2;
11 double O_of3;
12 double O_of4;
13 double O_of5;
14 double O_of6;
15 double O_of7;
16 double O_of8;
17 double O_of9;
18 double O_of10;
19 double O_of11;
20 double O_of12;
21 double O_of13;
22 double O_of14;
23 O_of=[O_of1,O_of2,O_of3,O_of4,O_of5,O_of6,O_of7,O_of8,O_of9,O_of10,O_of11,...  
O_of12,O_of13,O_of14]; % Orientations
24 M_of=[1,1,1,1,1,1,1,1,1,1,1,1,1,1,1,1]; % Materials % 1=5HS, UD=0;
25 % % Parameters for OuterBead
26 A_ob= 19247.07 *10^-6; % m^2
27 double n_ob; % Number ob plies
28 O_ob1=45;
29 double O_ob2;
30 double O_ob3;
31 double O_ob4;
32 double O_ob5;
33 double O_ob6;
34 double O_ob7;
35 double O_ob8;
36 double O_ob9;
37 double O_ob10;
38 double O_ob11;
39 double O_ob12;
40 double O_ob13;
41 double O_ob14;
42 double O_ob15;
43 double O_ob16;
44 double O_ob17;
45 double O_ob18;
46 O_ob=[O_ob1,O_ob2,O_ob3,O_ob4,O_ob5,O_ob6,O_ob7,O_ob8,O_ob9,O_ob10,O_ob11,...  
O_ob12,O_ob13,O_ob14,O_ob15,O_ob16,O_ob17,O_ob18]; % Orientation ply1
47 M_ob1=1;
48 double M_ob2;
49 double M_ob3;
50 double M_ob4;
51 double M_ob5;
52 double M_ob6;
```

```

55 double M_ob7;
56 double M_ob8;
57 double M_ob9;
58 double M_ob10;
59 double M_ob11;
60 double M_ob12;
61 double M_ob13;
62 double M_ob14;
63 double M_ob15;
64 double M_ob16;
65 double M_ob17;
66 double M_ob18;
67 M_ob=[M_ob1,M_ob2,M_ob3,M_ob4,M_ob5,M_ob6,M_ob7,M_ob8,M_ob9,M_ob10,M_ob11,...  

68 M_ob12,M_ob13,M_ob14,M_ob15,M_ob16,M_ob17,M_ob18]; % 1=5HS, UD=0;  

69 % % Parameters for Outer Drop
70 A_od=25819.78*10^-6; % m^2
71 double n_od; % Number of plies
72 O_od1=45;
73 double O_od2;
74 double O_od3;
75 double O_od4;
76 double O_od5;
77 double O_od6;
78 double O_od7;
79 double O_od8;
80 double O_od9;
81 double O_od10;
82 double O_od11;
83 double O_od12;
84 double O_od13;
85 double O_od14;
86 O_od=[O_od1,O_od2,O_od3,O_od4,O_od5,O_od6,O_od7,O_od8,O_od9,O_od10,O_od11,...  

87 O_od12,O_od13,O_od14]; % Orientations
88 M_od=[1,1,1,1,1,1,1,1,1,1,1,1,1,1,1,1]; % Materials % 1=5HS, UD=0;
89 % % Parameters for Center Flange
90 A_cf= 23046.38*10^-6; % m^2
91 double n_cf; % Number cf plies
92 O_cf1=45;
93 double O_cf2;
94 double O_cf3;
95 double O_cf4;
96 double O_cf5;
97 double O_cf6;
98 double O_cf7;
99 double O_cf8;
100 double O_cf9;
101 double O_cf10;
102 double O_cf11;
103 double O_cf12;
104 double O_cf13;
105 double O_cf14;
106 double O_cf15;
107 double O_cf16;
108 double O_cf17;
109 double O_cf18;
110 O_cf=[O_cf1,O_cf2,O_cf3,O_cf4,O_cf5,O_cf6,O_cf7,O_cf8,O_cf9,O_cf10,O_cf11,...  

111 O_cf12,O_cf13,O_cf14,O_cf15,O_cf16,O_cf17,O_cf18]; % Orientations
112 M_cf1=1;
113 double M_cf2;
114 double M_cf3;
115 double M_cf4;
116 double M_cf5;
117 double M_cf6;
118 double M_cf7;
119 double M_cf8;
120 double M_cf9;
121 double M_cf10;
122 double M_cf11;
123 double M_cf12;
124 double M_cf13;
125 double M_cf14;

```

```

126 double M_cf15;
127 double M_cf16;
128 double M_cf17;
129 double M_cf18;
130 M_cf=[M_cf1,M_cf2,M_cf3,M_cf4,M_cf5,M_cf6,M_cf7,M_cf8,M_cf9,M_cf10,M_cf11,...  

131 M_cf12,M_cf13,M_cf14,M_cf15,M_cf16,M_cf17,M_cf18]; % 1=5HS, UD=0;
132 % % Parameters for Center Shell
133 A_cs=52808.87*10^-6; % m^2
134 double n_cs; % Number of plies
135 O_cs1=45;
136 double O_cs2;
137 double O_cs3;
138 double O_cs4;
139 double O_cs5;
140 double O_cs6;
141 double O_cs7;
142 double O_cs8;
143 double O_cs9;
144 double O_cs10;
145 double O_cs11;
146 double O_cs12;
147 double O_cs13;
148 double O_cs14;
149 double O_cs15;
150 double O_cs16;
151 double O_cs17;
152 double O_cs18;
153 O_cs=[O_cs1,O_cs2,O_cs3,O_cs4,O_cs5,O_cs6,O_cs7,O_cs8,O_cs9,O_cs10,O_cs11,...  

154 O_cs12,O_cs13,O_cs14,O_cs15,O_cs16,O_cs17,O_cs18]; % Orientations
155 % double M_cs1;
156 M_cs1=1;
157 double M_cs2;
158 double M_cs3;
159 double M_cs4;
160 double M_cs5;
161 double M_cs6;
162 double M_cs7;
163 double M_cs8;
164 double M_cs9;
165 double M_cs10;
166 double M_cs11;
167 double M_cs12;
168 double M_cs13;
169 double M_cs14;
170 double M_cs15;
171 double M_cs16;
172 double M_cs17;
173 double M_cs18;
174 M_cs=[M_cs1,M_cs2,M_cs3,M_cs4,M_cs5,M_cs6,M_cs7,M_cs8,M_cs9,M_cs10,M_cs11,...  

175 M_cs12,M_cs13,M_cs14,M_cs15,M_cs16,M_cs17,M_cs18]; % 1=5HS, UD=0;
176 % % Parameter for Inner Drop
177 A_id=28377.53*10^-6; % m^2
178 double n_id; % Number of plies
179 % double O_id1;
180 O_id1=45;
181 double O_id2;
182 double O_id3;
183 double O_id4;
184 double O_id5;
185 double O_id6;
186 double O_id7;
187 double O_id8;
188 double O_id9;
189 double O_id10;
190 double O_id11;
191 double O_id12;
192 double O_id13;
193 double O_id14;
194 O_id=[O_id1,O_id2,O_id3,O_id4,O_id5,O_id6,O_id7,O_id8,O_id9,O_id10,O_id11,...  

195 O_id12,O_id13,O_id14]; % Orientation
196 M_id=[1,1,1,1,1,1,1,1,1,1,1,1,1,1,1,1]; % Material % 1=5HS, UD=0;

```

```

197
198 % % Paramters for Inner Bead
199 A_ib= 23897.81*10^-6; % m^2
200 double n_ib; % Number of plies
201 O_ib1=45;
202 double O_ib2;
203 double O_ib3;
204 double O_ib4;
205 double O_ib5;
206 double O_ib6;
207 double O_ib7;
208 double O_ib8;
209 double O_ib9;
210 double O_ib10;
211 double O_ib11;
212 double O_ib12;
213 double O_ib13;
214 double O_ib14;
215 double O_ib15;
216 double O_ib16;
217 double O_ib17;
218 double O_ib18;
219 O_ib=[O_ib1,O_ib2,O_ib3,O_ib4,O_ib5,O_ib6,O_ib7,O_ib8,O_ib9,O_ib10,O_ib11,...  

220 O_ib12,O_ib13,O_ib14,O_ib15,O_ib16,O_ib17,O_ib18]; % Orientations
221 M_ib1=1;
222 double M_ib2;
223 double M_ib3;
224 double M_ib4;
225 double M_ib5;
226 double M_ib6;
227 double M_ib7;
228 double M_ib8;
229 double M_ib9;
230 double M_ib10;
231 double M_ib11;
232 double M_ib12;
233 double M_ib13;
234 double M_ib14;
235 double M_ib15;
236 double M_ib16;
237 double M_ib17;
238 double M_ib18;
239 M_ib=[M_ib1,M_ib2,M_ib3,M_ib4,M_ib5,M_ib6,M_ib7,M_ib8,M_ib9,M_ib10,M_ib11,...  

240 M_ib12,M_ib13,M_ib14,M_ib15,M_ib16,M_ib17,M_ib18]; % 1=5HS, UD=0;
241 % % Paramters for InnerFlange
242 A_if=31110.57*10^-6; % m^2
243 double n_if; % Number of plies
244 O_if1=45;
245 double O_if2;
246 double O_if3;
247 double O_if4;
248 double O_if5;
249 double O_if6;
250 double O_if7;
251 double O_if8;
252 double O_if9;
253 double O_if10;
254 double O_if11;
255 double O_if12;
256 double O_if13;
257 double O_if14;
258 O_if=[O_if1,O_if2,O_if3,O_if4,O_if5,O_if6,O_if7,O_if8,O_if9,O_if10,O_if11,...  

259 O_if12,O_if13,O_if14]; % Orientations
260 M_if=[1,1,1,1,1,1,1,1,1,1,1,1,1,1,1,1];% Material % 1=5HS, UD=0;
261 % % Material properties
262 m_5HS=471; % GSM 5HS
263 m_UD=162; % GSM UD
264 t_5HS=( '0.3' ); % Thickness 5HS
265 t_UD=( '0.1' ); % Thickness UD
266 % % Abaqus data
267 int_p=5; % intergration point

```

```

268 ccys=( '<Layup>' );
269 % % OuterFlange
270 filename='OF.txt';
271 reg_set='Set -OF';
272 ply_name='Ply -OF-';
273 fid=fopen(filename , 'w');
274 mass_of=0;
275 for i=1:14
276 if i<=n_of
277 stat=( '0' );
278 ms=1;
279 else
280 stat=( '1' );
281 ms=0;
282 end
283 if M_of(i)==1
284 mat=( '5HS' );
285 t=t_5HS;
286 mass_of=mass_of+m_5HS*A_of*ms;
287 else
288 mat=( 'UD' );
289 t=t_UD;
290 mass_of=mass_of+m_UD*A_of*ms;
291 end
292 fprintf(fid , '% s, % s% d, % s, % s, % s, % s, % d, % d\n' ,stat ,ply_name ,i
293 ,...
294 ,reg_set ,mat ,t ,ccys ,O_of(i) ,int_p);
295 end
296 fclose(fid);
297 % % OuterBead
298 filename='OB.txt';
299 reg_set='Set -OB';
300 ply_name='Ply -OB-';
301 fid=fopen(filename , 'w');
302 mass_ob=0;
303 for i=1:18
304 if i<=n_ob
305 stat=( '0' );
306 ms=1;
307 else
308 stat=( '1' );
309 ms=0;
310 end
311 if M_ob(i)==1
312 mat=( '5HS' );
313 t=t_5HS;
314 mass_ob=mass_ob+m_5HS*A_ob*ms;
315 else
316 mat=( 'UD' );
317 t=t_UD;
318 mass_ob=mass_ob+m_UD*A_ob*ms;
319 end
320 fprintf(fid , '% s, % s% d, % s, % s, % s, % s, % d, % d\n' ,stat ,ply_name ,i
321 ,...
322 ,reg_set ,mat ,t ,ccys ,O_ob(i) ,int_p);
323 end
324 fclose(fid);
325 % % OuterDrop
326 filename='OD.txt';
327 reg_set='Set -OD';
328 ply_name='Ply -OD-';
329 fid=fopen(filename , 'w');
330 mass_od=0;
331 for i=1:14
332 if i<=n_od
333 stat=( '0' );
334 ms=1;
335 else
336 stat=( '1' );
337 ms=0;

```

```

336
337 end
338 if M_of( i )==1
339     mat=( '5HS' );
340     t=t_5HS;
341 else
342     mat=( 'UD' );
343     t=t_UD;
344     mass_od=mass_od+m_5HS*A_od*ms;
345 end
346 fprintf( fid , '% s, % s% d, % s, % s, % s, % s, % d, % d\n' ,stat ,ply_name ,i
347     ,...
348     ,reg_set ,mat ,t ,ccys ,O_od( i ) ,int_p );
349 end
350 fclose( fid );
351 % % CenterFlange
352 filename='CF.txt';
353 reg_set='Set-CF';
354 ply_name='Ply-CF-';
355 fid=fopen( filename , 'w' );
356 mass_cf=0;
357 for i=1:18
358     if i<=n_cf
359         stat=( '0' );
360         ms=1;
361     else
362         stat=( '1' );
363         ms=0;
364     end
365
366     if M_cf( i )==1
367         mat=( '5HS' );
368         t=t_5HS;
369         mass_cf=mass_cf+m_5HS*A_cf*ms;
370     else
371         mat=( 'UD' );
372         t=t_UD;
373         mass_cf=mass_cf+m_UD*A_cf*ms;
374     end
375
376     fprintf( fid , '% s, % s% d, % s, % s, % s, % s, % d, % d\n' ,stat ,ply_name ,i
377     ,...
378     ,reg_set ,mat ,t ,ccys ,O_cf( i ) ,int_p );
379 end
380 fclose( fid );
381 % % CenterShell
382 filename='CS.txt';
383 reg_set='Set-CS';
384 ply_name='Ply-CS-';
385 fid=fopen( filename , 'w' );
386 mass_cs=0;
387 for i=1:18
388     if i<=n_cs
389         stat=( '0' );
390         ms=1;
391     else
392         stat=( '1' );
393         ms=0;
394     end
395     if M_cs( i )==1
396         mat=( '5HS' );
397         t=t_5HS;
398         mass_cs=mass_cs+m_5HS*A_cs*ms;
399     else
400         mat=( 'UD' );
401         t=t_UD;
402         mass_cs=mass_cs+m_UD*A_cs*ms;
403     end
404     fprintf( fid , '% s, % s% d, % s, % s, % s, % s, % d, % d\n' ,stat ,ply_name ,i
        ,...

```

```

405         reg_set ,mat ,t ,ccys ,O_cs( i ) ,int_p );
406     end
407     fclose( fid );
408 % % InnerDrop
409 filename='ID.txt';
410 reg_set='Set-ID';
411 ply_name='Ply-ID-';
412 fid=fopen( filename , 'w' );
413 mass_id=0;
414 for i=1:14
415     if i<=n_id
416         stat=( '0' );
417         ms=1;
418     else
419         stat=( '1' );
420         ms=0;
421     end
422     if M_id( i )==1
423         mat=( '5HS' );
424         t=t_5HS;
425         mass_id=mass_id+m_5HS*A_id*ms;
426     else
427         mat=( 'UD' );
428         t=t_UD;
429         mass_id=mass_id+m_UD*A_id*ms;
430     end
431     fprintf( fid , '% s, % s% d, % s, % s, % s, % d, % d\n' ,stat ,ply_name ,i
432             ,...
433             ,reg_set ,mat ,t ,ccys ,O_id( i ) ,int_p );
434 end
435 fclose( fid );
436 % % InnerBead
437 filename='IB.txt';
438 reg_set='Set-IB';
439 ply_name='Ply-IB-';
440 fid=fopen( filename , 'w' );
441 mass_ib=0;
442 for i=1:18
443     if i<=n_ib
444         stat=( '0' );
445         ms=1;
446     else
447         stat=( '1' );
448         ms=0;
449     end
450     if M_ib( i )==1
451         mat=( '5HS' );
452         t=t_5HS;
453         mass_ib=mass_ib+m_5HS*A_ib*ms;
454     else
455         mat=( 'UD' );
456         t=t_UD;
457         mass_ib=mass_ib+m_UD*A_ib*ms;
458     end
459     fprintf( fid , '% s, % s% d, % s, % s, % s, % d, % d\n' ,stat ,ply_name ,i
460             ,...
461             ,reg_set ,mat ,t ,ccys ,O_ib( i ) ,int_p );
462 end
463 fclose( fid );
464 % % InnerFLange
465 filename='IF.txt';
466 reg_set='Set-IF';
467 ply_name='Ply-IF-';
468 fid=fopen( filename , 'w' );
469 mass_if=0;
470 for i=1:14
471     if i<=n_if
472         stat=( '0' );
473         ms=1;
474     else

```

```

473     stat=( '1' );
474     ms=0;
475   end
476   if M_if( i )==1
477     mat=( '5HS' );
478     t=t_5HS;
479     mass_if=mass_if+m_5HS*A_if*ms;
480   else
481     mat=( 'UD' );
482     t=t_UD;
483     mass_if=mass_if+m_UD*A_if*ms;
484   end
485   fprintf( fid , '% s, % s% d, % s, % s, % s, % s, % d, % d\n' ,stat ,ply_name ,i
486   ,...
487   ,reg_set ,mat ,t ,ccys ,O_if( i ) ,int_p );
488 end
489 mass_tot=mass_of+mass_od+mass_cs+mass_id+mass_if+mass_ob+mass_cf+mass_ib;
490 % total mass of rim
491 AUD=(n_ob-sum(M_ob(1:n_ob)))*A_ob + (n_cf-sum(M_cf(1:n_cf)))*A_cf + ...
492 (n_cs-sum(M_cs(1:n_cs)))*A_cs + (n_ib-sum(M_ib(1:n_ib)))*A_ib;% Total
493 % surface area of UD
494 fclose( fid );

```

ABAQUS PRE-SCRIPT

```

1 # -*- coding: mbcs -*-
2 # Do not delete the following import lines
3 from abaqus import *
4 from abaqusConstants import *
5 import __main__
6
7
8 import section
9 import regionToolset
10 import displayGroupMdbToolset as dgm
11 import part
12 import material
13 import assembly
14 import step
15 import interaction
16 import load
17 import mesh
18 import optimization
19 import job
20 import sketch
21 import visualization
22 import xyPlot
23 import displayGroupOdbToolset as dgo
24 import connectorBehavior
25
26 session.viewports['Viewport: 1'].view.setValues(nearPlane=1076.81,
27 farPlane=1637.08, width=766.687, height=438.824, cameraPosition=(
28 276.033, -1241.47, 482.228), cameraTarget=(96.8227, -26.6858,
29 -0.0612259))
30
31 # REGION OuterFlange
32 layupOrientation = mdb.models['Model-1'].parts['Shell'].datums[23]
33 p = mdb.models['Model-1'].parts['Shell']
34 region1=p.sets['Set-OF']
35 p = mdb.models['Model-1'].parts['Shell']
36 region2=p.sets['Set-OF']
37 p = mdb.models['Model-1'].parts['Shell']
38 region3=p.sets['Set-OF']

```

```

39 p = mdb.models['Model-1'].parts['Shell']
40 region4=p.sets['Set-OF']
41 p = mdb.models['Model-1'].parts['Shell']
42 region5=p.sets['Set-OF']
43 p = mdb.models['Model-1'].parts['Shell']
44 region6=p.sets['Set-OF']
45 p = mdb.models['Model-1'].parts['Shell']
46 region7=p.sets['Set-OF']
47 p = mdb.models['Model-1'].parts['Shell']
48 region8=p.sets['Set-OF']
49 p = mdb.models['Model-1'].parts['Shell']
50 region9=p.sets['Set-OF']
51 p = mdb.models['Model-1'].parts['Shell']
52 region10=p.sets['Set-OF']
53 p = mdb.models['Model-1'].parts['Shell']
54 region11=p.sets['Set-OF']
55 p = mdb.models['Model-1'].parts['Shell']
56 region12=p.sets['Set-OF']
57 p = mdb.models['Model-1'].parts['Shell']
58 region13=p.sets['Set-OF']
59 p = mdb.models['Model-1'].parts['Shell']
60 region14=p.sets['Set-OF']
61 compositeLayup = mdb.models['Model-1'].parts['Shell'].CompositeLayup(
62 name='CompositeLayup-OF', description='', elementType=SHELL,
63 offsetType=BOTTOM_SURFACE, symmetric=False,
64 thicknessAssignment=FROM_SECTION)
65 compositeLayup.Section(preIntegrate=OFF, integrationRule=SIMPSON,
66 thicknessType=UNIFORM, poissonDefinition=DEFAULT, temperature=GRADIENT,
67 useDensity=OFF)
68 compositeLayup.ReferenceOrientation(orientationType=SYSTEM,
69 localCsys=layupOrientation, fieldName='',
70 additionalRotationType=ROTATION_NONE, angle=0.0,
71 additionalRotationField='', axis=AXIS_1)

72
73
74
75 fp = open('D:/temp/13inch/Layup6376/SIM/OF.txt')
76 words= [word.strip() for line in fp.readlines() for word in line.split(',') if
    word.strip()]
77 #print(", ".join(words)) # or 'print(words)' if you want to print out 'words'
    as a list
78
79
80 for i in range(0, 13):
81     s=int(words[i+(i*7)])
82     pn=words[i+1+(i*7)]
83     mat=words[i+3+(i*7)]
84     th=float(words[i+4+(i*7)])
85     om=float(words[i+6+(i*7)])
86     compositeLayup.CompositePly(suppressed=s, plyName=pn,
87     region=region1, material=mat, thicknessType=SPECIFY_THICKNESS,
88     thickness=th, orientationType=SPECIFY_ORIENT, orientationValue=om,
89     additionalRotationType=ROTATION_NONE, additionalRotationField='',
90     axis=AXIS_3, angle=0.0, numIntPoints=5)

91
92 #-----End OuterFlange
93
94 # REGION OuterBead
95 layupOrientation = mdb.models['Model-1'].parts['Shell'].datums[23]

```

```

96 p = mdb.models['Model-1'].parts['Shell']
97 region1=p.sets['Set-OB']
98 p = mdb.models['Model-1'].parts['Shell']
99 region2=p.sets['Set-OB']
100 p = mdb.models['Model-1'].parts['Shell']
101 region3=p.sets['Set-OB']
102 p = mdb.models['Model-1'].parts['Shell']
103 region4=p.sets['Set-OB']
104 p = mdb.models['Model-1'].parts['Shell']
105 region5=p.sets['Set-OB']
106 p = mdb.models['Model-1'].parts['Shell']
107 region6=p.sets['Set-OB']
108 p = mdb.models['Model-1'].parts['Shell']
109 region7=p.sets['Set-OB']
110 p = mdb.models['Model-1'].parts['Shell']
111 region8=p.sets['Set-OB']
112 p = mdb.models['Model-1'].parts['Shell']
113 region9=p.sets['Set-OB']
114 p = mdb.models['Model-1'].parts['Shell']
115 region10=p.sets['Set-OB']
116 p = mdb.models['Model-1'].parts['Shell']
117 region11=p.sets['Set-OB']
118 p = mdb.models['Model-1'].parts['Shell']
119 region12=p.sets['Set-OB']
120 p = mdb.models['Model-1'].parts['Shell']
121 region13=p.sets['Set-OB']
122 p = mdb.models['Model-1'].parts['Shell']
123 region14=p.sets['Set-OB']
124 compositeLayup = mdb.models['Model-1'].parts['Shell'].CompositeLayup(
125 name='CompositeLayup-OB', description='', elementType=SHELL,
126 offsetType=BOTTOM_SURFACE, symmetric=False,
127 thicknessAssignment=FROM_SECTION)
128 compositeLayup.Section(preIntegrate=OFF, integrationRule=SIMPSON,
129 thicknessType=UNIFORM, poissonDefinition=DEFAULT, temperature=GRADIENT,
130 useDensity=OFF)
131 compositeLayup.ReferenceOrientation(orientationType=SYSTEM,
132 localCsys=layupOrientation, fieldName='',
133 additionalRotationType=ROTATION_NONE, angle=0.0,
134 additionalRotationField='', axis=AXIS_1)
135
136
137
138 fp = open('D:/temp/13inch/Layup6376/SIM/OB.txt')
139 words= [word.strip() for line in fp.readlines() for word in line.split(',') if
140 word.strip()]
141 #print(", ".join(words)) # or 'print(words)' if you want to print out 'words'
142 as a list
143
144 for i in range(0, 13):
145     s=int(words[i+(i*7)])
146     pn=words[i+1+(i*7)]
147     mat=words[i+3+(i*7)]
148     th=float(words[i+4+(i*7)])
149     om=float(words[i+6+(i*7)])
150     compositeLayup.CompositePly(suppressed=s, plyName=pn,
151     region=region1, material=mat, thicknessType=SPECIFY_THICKNESS,
152     thickness=th, orientationType=SPECIFY_ORIENT, orientationValue=om,
153     additionalRotationType=ROTATION_NONE, additionalRotationField='',
154     axis=AXIS_3, angle=0.0, numIntPoints=5)

```

```

154
155 #-----End OuterBead
-----  

156
157
158 #Outer Drop
159
160 p = mdb.models['Model-1'].parts['Shell']
161 session.viewports['Viewport: 1'].setValues(displayedObject=p)
162 layupOrientation = mdb.models['Model-1'].parts['Shell'].datums[23]
163 p = mdb.models['Model-1'].parts['Shell']
164 region1=p.sets['Set-OD']
165 p = mdb.models['Model-1'].parts['Shell']
166 region2=p.sets['Set-OD']
167 p = mdb.models['Model-1'].parts['Shell']
168 region3=p.sets['Set-OD']
169 p = mdb.models['Model-1'].parts['Shell']
170 region4=p.sets['Set-OD']
171 p = mdb.models['Model-1'].parts['Shell']
172 region5=p.sets['Set-OD']
173 p = mdb.models['Model-1'].parts['Shell']
174 region6=p.sets['Set-OD']
175 p = mdb.models['Model-1'].parts['Shell']
176 region7=p.sets['Set-OD']
177 p = mdb.models['Model-1'].parts['Shell']
178 region8=p.sets['Set-OD']
179 p = mdb.models['Model-1'].parts['Shell']
180 region9=p.sets['Set-OD']
181 p = mdb.models['Model-1'].parts['Shell']
182 region10=p.sets['Set-OD']
183 p = mdb.models['Model-1'].parts['Shell']
184 region11=p.sets['Set-OD']
185 p = mdb.models['Model-1'].parts['Shell']
186 region12=p.sets['Set-OD']
187 p = mdb.models['Model-1'].parts['Shell']
188 region13=p.sets['Set-OD']
189 p = mdb.models['Model-1'].parts['Shell']
190 region14=p.sets['Set-OD']
191 compositeLayup = mdb.models['Model-1'].parts['Shell'].CompositeLayup(
192 name='CompositeLayup-OD', description='', elementType=SHELL,
193 offsetType=BOTTOM_SURFACE, symmetric=False,
194 thicknessAssignment=FROM_SECTION)
195 compositeLayup.Section(preIntegrate=OFF, integrationRule=SIMPSON,
196 thicknessType=UNIFORM, poissonDefinition=DEFAULT, temperature=GRADIENT,
197 useDensity=OFF)
198 compositeLayup.ReferenceOrientation(orientationType=SYSTEM,
199 localCsys=layupOrientation, fieldName='',
200 additionalRotationType=ROTATION_NONE, angle=0.0,
201 additionalRotationField='', axis=AXIS_1)
202
203 fp = open('D:/temp/13inch/Layup6376/SIM/OD.txt')
204 words= [word.strip() for line in fp.readlines() for word in line.split(',') if
205 word.strip()]
206
207
208 for i in range(0, 13):
209     s=int(words[i+(i*7)])
210     pn=words[i+1+(i*7)]

```

```

211     mat=words[ i+3+(i *7) ]
212     th=float( words[ i+4+(i *7) ] )
213     om=float( words[ i+6+(i *7) ] )
214     compositeLayup.CompositePly( suppressed=s , plyName=pn ,
215       region=region1 , material=mat , thicknessType=SPECIFY_THICKNESS ,
216       thickness=th , orientationType=SPECIFY_ORIENT , orientationValue=om ,
217       additionalRotationType=ROTATION_NONE , additionalRotationField=' ' ,
218       axis=AXIS_3 , angle=0.0 , numIntPoints=5 )
219
220 #-----End OuterDrop
-----
```

```

221
222 # REGION CenterFlange
223 layupOrientation = mdb.models['Model-1'].parts['Shell'].datums[23]
224 p = mdb.models['Model-1'].parts['Shell']
225 region1=p.sets['Set-CF']
226 p = mdb.models['Model-1'].parts['Shell']
227 region2=p.sets['Set-CF']
228 p = mdb.models['Model-1'].parts['Shell']
229 region3=p.sets['Set-CF']
230 p = mdb.models['Model-1'].parts['Shell']
231 region4=p.sets['Set-CF']
232 p = mdb.models['Model-1'].parts['Shell']
233 region5=p.sets['Set-CF']
234 p = mdb.models['Model-1'].parts['Shell']
235 region6=p.sets['Set-CF']
236 p = mdb.models['Model-1'].parts['Shell']
237 region7=p.sets['Set-CF']
238 p = mdb.models['Model-1'].parts['Shell']
239 region8=p.sets['Set-CF']
240 p = mdb.models['Model-1'].parts['Shell']
241 region9=p.sets['Set-CF']
242 p = mdb.models['Model-1'].parts['Shell']
243 region10=p.sets['Set-CF']
244 p = mdb.models['Model-1'].parts['Shell']
245 region11=p.sets['Set-CF']
246 p = mdb.models['Model-1'].parts['Shell']
247 region12=p.sets['Set-CF']
248 p = mdb.models['Model-1'].parts['Shell']
249 region13=p.sets['Set-CF']
250 p = mdb.models['Model-1'].parts['Shell']
251 region14=p.sets['Set-CF']
252 compositeLayup = mdb.models['Model-1'].parts['Shell'].CompositeLayup(
253   name='CompositeLayup-CF' , description=' ' , elementType=SHELL ,
254   offsetType=BOTTOM_SURFACE , symmetric=False ,
255   thicknessAssignment=FROM_SECTION)
256 compositeLayup.Section(preIntegrate=OFF, integrationRule=SIMPSON,
257 thicknessType=UNIFORM, poissonDefinition=DEFAULT, temperature=GRADIENT,
258 useDensity=OFF)
259 compositeLayup.ReferenceOrientation(orientationType=SYSTEM,
260 localCsys=layupOrientation , fieldName=' ' ,
261 additionalRotationType=ROTATION_NONE, angle=0.0 ,
262 additionalRotationField=' ' , axis=AXIS_1)
263
264
265
266 fp = open('D:/temp/13inch/Layup6376/SIM/CF.txt')
267 words= [word.strip() for line in fp.readlines() for word in line.split(',') if
268         word.strip()]
269 #print(", ".join(words)) # or 'print(words)' if you want to print out 'words'
```

```

        as a list

269
270
271 for i in range(0, 13):
272     s=int(words[ i+(i*7) ])
273     pn=words[ i+1+(i*7) ]
274     mat=words[ i+3+(i*7) ]
275     th=float(words[ i+4+(i*7) ])
276     om=float(words[ i+6+(i*7) ])
277     compositeLayup.CompositePly(suppressed=s, plyName=pn,
278                                   region=region1, material=mat, thicknessType=SPECIFY_THICKNESS,
279                                   thickness=th, orientationType=SPECIFY_ORIENT, orientationValue=om,
280                                   additionalRotationType=ROTATION_NONE, additionalRotationField='',
281                                   axis=AXIS_3, angle=0.0, numIntPoints=5)

282
283 #- - - - -End CenterFlange
284
285 #Center Shell
286
287 p = mdb.models['Model-1'].parts['Shell']
288 session.viewports['Viewport: 1'].setValues(displayedObject=p)
289 layupOrientation = mdb.models['Model-1'].parts['Shell'].datums[23]
290 p = mdb.models['Model-1'].parts['Shell']
291 region1=p.sets['Set-CS']
292 p = mdb.models['Model-1'].parts['Shell']
293 region2=p.sets['Set-CS']
294 p = mdb.models['Model-1'].parts['Shell']
295 region3=p.sets['Set-CS']
296 p = mdb.models['Model-1'].parts['Shell']
297 region4=p.sets['Set-CS']
298 p = mdb.models['Model-1'].parts['Shell']
299 region5=p.sets['Set-CS']
300 p = mdb.models['Model-1'].parts['Shell']
301 region6=p.sets['Set-CS']
302 p = mdb.models['Model-1'].parts['Shell']
303 region7=p.sets['Set-CS']
304 p = mdb.models['Model-1'].parts['Shell']
305 region8=p.sets['Set-CS']
306 p = mdb.models['Model-1'].parts['Shell']
307 region9=p.sets['Set-CS']
308 p = mdb.models['Model-1'].parts['Shell']
309 region10=p.sets['Set-CS']
310 p = mdb.models['Model-1'].parts['Shell']
311 region11=p.sets['Set-CS']
312 p = mdb.models['Model-1'].parts['Shell']
313 region12=p.sets['Set-CS']
314 p = mdb.models['Model-1'].parts['Shell']
315 region13=p.sets['Set-CS']
316 p = mdb.models['Model-1'].parts['Shell']
317 region14=p.sets['Set-CS']
318 compositeLayup = mdb.models['Model-1'].parts['Shell'].CompositeLayup(
319     name='CompositeLayup-CS', description='', elementType=SHELL,
320     offsetType=BOTTOM_SURFACE, symmetric=False,
321     thicknessAssignment=FROM_SECTION)
322 compositeLayup.Section(preIntegrate=OFF, integrationRule=SIMPSON,
323 thicknessType=UNIFORM, poissonDefinition=DEFAULT, temperature=GRADIENT,
324 useDensity=OFF)
325 compositeLayup.ReferenceOrientation(orientationType=SYSTEM,
326 localCsys=layupOrientation, fieldName='')

```

```

327 additionalRotationType=ROTATION_NONE, angle=0.0,
328 additionalRotationField=' ', axis=AXIS_1)
329
330 fp = open('D:/temp/13inch/Layup6376/SIM/CS.txt')
331 words= [word.strip() for line in fp.readlines() for word in line.split(',') if
332 word.strip()]
332 #print(", ".join(words)) # or 'print(words)' if you want to print out 'words'
332 as a list
333
334
335 for i in range(0, 13):
336     s=int(words[i+(i*7)])
337     pn=words[i+1+(i*7)]
338     mat=words[i+3+(i*7)]
339     th=float(words[i+4+(i*7)])
340     om=float(words[i+6+(i*7)])
341     compositeLayup.CompositePly(suppressed=s, plyName=pn,
342     region=region1, material=mat, thicknessType=SPECIFY_THICKNESS,
343     thickness=th, orientationType=SPECIFY_ORIENT, orientationValue=om,
344     additionalRotationType=ROTATION_NONE, additionalRotationField=' ',
344     axis=AXIS_3, angle=0.0, numIntPoints=5)
345
346
347 #- - - - -End CenterShell
-----
```

```

348
349
350
351 #Inner drop
352
353 p = mdb.models['Model-1'].parts['Shell']
354 session.viewports['Viewport: 1'].setValues(displayedObject=p)
355 layupOrientation = mdb.models['Model-1'].parts['Shell'].datums[23]
356 p = mdb.models['Model-1'].parts['Shell']
357 region1=p.sets['Set-ID']
358 p = mdb.models['Model-1'].parts['Shell']
359 region2=p.sets['Set-ID']
360 p = mdb.models['Model-1'].parts['Shell']
361 region3=p.sets['Set-ID']
362 p = mdb.models['Model-1'].parts['Shell']
363 region4=p.sets['Set-ID']
364 p = mdb.models['Model-1'].parts['Shell']
365 region5=p.sets['Set-ID']
366 p = mdb.models['Model-1'].parts['Shell']
367 region6=p.sets['Set-ID']
368 p = mdb.models['Model-1'].parts['Shell']
369 region7=p.sets['Set-ID']
370 p = mdb.models['Model-1'].parts['Shell']
371 region8=p.sets['Set-ID']
372 p = mdb.models['Model-1'].parts['Shell']
373 region9=p.sets['Set-ID']
374 p = mdb.models['Model-1'].parts['Shell']
375 region10=p.sets['Set-ID']
376 p = mdb.models['Model-1'].parts['Shell']
377 region11=p.sets['Set-ID']
378 p = mdb.models['Model-1'].parts['Shell']
379 region12=p.sets['Set-ID']
380 p = mdb.models['Model-1'].parts['Shell']
381 region13=p.sets['Set-ID']
382 p = mdb.models['Model-1'].parts['Shell']
383 region14=p.sets['Set-ID']
```

```

384 compositeLayup = mdb.models['Model-1'].parts['Shell'].CompositeLayup(
385     name='CompositeLayup-ID', description='', elementType=SHELL,
386     offsetType=BOTTOM_SURFACE, symmetric=False,
387     thicknessAssignment=FROM_SECTION)
388 compositeLayup.Section(preIntegrate=OFF, integrationRule=SIMPSON,
389     thicknessType=UNIFORM, poissonDefinition=DEFAULT, temperature=GRADIENT,
390     useDensity=OFF)
391 compositeLayup.ReferenceOrientation(orientationType=SYSTEM,
392     localCsys=layupOrientation, fieldName='',
393     additionalRotationType=ROTATION_NONE, angle=0.0,
394     additionalRotationField='', axis=AXIS_1)
395
396
397
398 fp = open('D:/temp/13inch/Layup6376/SIM/ID.txt')
399 words= [word.strip() for line in fp.readlines() for word in line.split(',') if
        word.strip()]
400 #print(", ".join(words)) # or 'print(words)' if you want to print out 'words'
        as a list
401
402
403 for i in range(0, 13):
404     s=int(words[i+(i*7)])
405     pn=words[i+1+(i*7)]
406     mat=words[i+3+(i*7)]
407     th=float(words[i+4+(i*7)])
408     om=float(words[i+6+(i*7)])
409     compositeLayup.CompositePly(suppressed=s, plyName=pn,
410         region=region1, material=mat, thicknessType=SPECIFY_THICKNESS,
411         thickness=th, orientationType=SPECIFY_ORIENT, orientationValue=om,
412         additionalRotationType=ROTATION_NONE, additionalRotationField='',
413         axis=AXIS_3, angle=0.0, numIntPoints=5)
414
415 #-----End InnerDrop
416
417
418 # REGION InnerBead
419 layupOrientation = mdb.models['Model-1'].parts['Shell'].datums[23]
420 p = mdb.models['Model-1'].parts['Shell']
421 region1=p.sets['Set-IB']
422 p = mdb.models['Model-1'].parts['Shell']
423 region2=p.sets['Set-IB']
424 p = mdb.models['Model-1'].parts['Shell']
425 region3=p.sets['Set-IB']
426 p = mdb.models['Model-1'].parts['Shell']
427 region4=p.sets['Set-IB']
428 p = mdb.models['Model-1'].parts['Shell']
429 region5=p.sets['Set-IB']
430 p = mdb.models['Model-1'].parts['Shell']
431 region6=p.sets['Set-IB']
432 p = mdb.models['Model-1'].parts['Shell']
433 region7=p.sets['Set-IB']
434 p = mdb.models['Model-1'].parts['Shell']
435 region8=p.sets['Set-IB']
436 p = mdb.models['Model-1'].parts['Shell']
437 region9=p.sets['Set-IB']
438 p = mdb.models['Model-1'].parts['Shell']
439 region10=p.sets['Set-IB']
440 p = mdb.models['Model-1'].parts['Shell']

```

```

441 region11=p.sets['Set-IB']
442 p = mdb.models['Model-1'].parts['Shell']
443 region12=p.sets['Set-IB']
444 p = mdb.models['Model-1'].parts['Shell']
445 region13=p.sets['Set-IB']
446 p = mdb.models['Model-1'].parts['Shell']
447 region14=p.sets['Set-IB']
448 compositeLayup = mdb.models['Model-1'].parts['Shell'].CompositeLayup(
449     name='CompositeLayup-IB', description='', elementType=SHELL,
450     offsetType=BOTTOM_SURFACE, symmetric=False,
451     thicknessAssignment=FROM_SECTION)
452 compositeLayup.Section(preIntegrate=OFF, integrationRule=SIMPSON,
453     thicknessType=UNIFORM, poissonDefinition=DEFAULT, temperature=GRADIENT,
454     useDensity=OFF)
455 compositeLayup.ReferenceOrientation(orientationType=SYSTEM,
456     localCsys=layupOrientation, fieldName='',
457     additionalRotationType=ROTATION_NONE, angle=0.0,
458     additionalRotationField='', axis=AXIS_1)
459
460
461
462 fp = open('D:/temp/13inch/Layup6376/SIM/IB.txt')
463 words= [word.strip() for line in fp.readlines() for word in line.split(',') if
464         word.strip()]
465 #print(", ".join(words)) # or 'print(words)' if you want to print out 'words'
466 # as a list
467
468 for i in range(0, 13):
469     s=int(words[i+(i*7)])
470     pn=words[i+1+(i*7)]
471     mat=words[i+3+(i*7)]
472     th=float(words[i+4+(i*7)])
473     om=float(words[i+6+(i*7)])
474     compositeLayup.CompositePly(suppressed=s, plyName=pn,
475         region=region1, material=mat, thicknessType=SPECIFY_THICKNESS,
476         thickness=th, orientationType=SPECIFY_ORIENT, orientationValue=om,
477         additionalRotationType=ROTATION_NONE, additionalRotationField='',
478         axis=AXIS_3, angle=0.0, numIntPoints=5)
479
480
481 #InneFlange
482
483 p = mdb.models['Model-1'].parts['Shell']
484 session.viewports['Viewport: 1'].setValues(displayedObject=p)
485 layupOrientation = mdb.models['Model-1'].parts['Shell'].datums[23]
486 p = mdb.models['Model-1'].parts['Shell']
487 region1=p.sets['Set-IF']
488 p = mdb.models['Model-1'].parts['Shell']
489 region2=p.sets['Set-IF']
490 p = mdb.models['Model-1'].parts['Shell']
491 region3=p.sets['Set-IF']
492 p = mdb.models['Model-1'].parts['Shell']
493 region4=p.sets['Set-IF']
494 p = mdb.models['Model-1'].parts['Shell']
495 region5=p.sets['Set-IF']
496 p = mdb.models['Model-1'].parts['Shell']
497 region6=p.sets['Set-IF']

```

```

498 p = mdb.models['Model-1'].parts['Shell']
499 region7=p.sets['Set-IF']
500 p = mdb.models['Model-1'].parts['Shell']
501 region8=p.sets['Set-IF']
502 p = mdb.models['Model-1'].parts['Shell']
503 region9=p.sets['Set-IF']
504 p = mdb.models['Model-1'].parts['Shell']
505 region10=p.sets['Set-IF']
506 p = mdb.models['Model-1'].parts['Shell']
507 region11=p.sets['Set-IF']
508 p = mdb.models['Model-1'].parts['Shell']
509 region12=p.sets['Set-IF']
510 p = mdb.models['Model-1'].parts['Shell']
511 region13=p.sets['Set-IF']
512 p = mdb.models['Model-1'].parts['Shell']
513 region14=p.sets['Set-IF']
514 compositeLayup = mdb.models['Model-1'].parts['Shell'].CompositeLayup(
515 name='CompositeLayup-IF', description='', elementType=SHELL,
516 offsetType=BOTTOM_SURFACE, symmetric=False,
517 thicknessAssignment=FROM_SECTION)
518 compositeLayup.Section(preIntegrate=OFF, integrationRule=SIMPSON,
519 thicknessType=UNIFORM, poissonDefinition=DEFAULT, temperature=GRADIENT,
520 useDensity=OFF)
521 compositeLayup.ReferenceOrientation(orientationType=SYSTEM,
522 localCsys=layupOrientation, fieldName='',
523 additionalRotationType=ROTATION_NONE, angle=0.0,
524 additionalRotationField='', axis=AXIS_1)

525
526
527 fp = open('D:/temp/13inch/Layup6376/SIM/IF.txt')
528 words= [word.strip() for line in fp.readlines() for word in line.split(',') if
      word.strip()]
529 #print(" ".join(words)) # or 'print(words)' if you want to print out 'words'
      as a list
530
531
532 for i in range(0, 13):
533     s=int(words[i+(i*7)])
534     pn=words[i+1+(i*7)]
535     mat=words[i+3+(i*7)]
536     th=float(words[i+4+(i*7)])
537     om=float(words[i+6+(i*7)])
538     compositeLayup.CompositePly(suppressed=s, plyName=pn,
539     region=region1, material=mat, thicknessType=SPECIFY_THICKNESS,
540     thickness=th, orientationType=SPECIFY_ORIENT, orientationValue=om,
541     additionalRotationType=ROTATION_NONE, additionalRotationField='',
542     axis=AXIS_3, angle=0.0, numIntPoints=5)
543 #- - - - -End InnerFlange
      - - - - -
544
545 p = mdb.models['Model-1'].parts['Shell']
546 session.viewports['Viewport: 1'].setValues(displayedObject=p)
547
548 a = mdb.models['Model-1'].rootAssembly
549 a.regenerate()

```

ABAQUS POST-SCRIPT

¹ """
² userscript_odb.py

```

3      """
4
5  #
6  #from abaqus import *
7  from abaqusConstants import *
8  import odbAccess
9  from odbAccess import *
10 import __main__
11 import operator
12 import sys
13 import math
14
15 #
16 # S T A R T
17 #
18
19
20 # Open .odb results file
21 odbName = 'Job-layup.odb'
22 myOdb = openOdb( dbName, readOnly=True )
23
24
25 #Create a variable that refers to the last frame of the first step.
26 step = myOdb.steps['Step-Turn']
27 step_brake=myOdb.steps['Step-Brake']
28
29 lastFramebrake = myOdb.steps['Step-Brake'].frames[-1]
30 lastFrame = myOdb.steps['Step-Turn'].frames[-1]
31 displacement=lastFrame.fieldOutputs['U']
32 displacement_brake=lastFramebrake.fieldOutputs['U']
33 #Create a variable that refers to the displacement 'U' in the last frame of
34     the frist step.
35
36 STRAINENERGY=step.historyRegions['Assembly ASSEMBLY'].historyOutputs['ALLSE']
37 STRAINENERGY_brake=step_brake.historyRegions['Assembly ASSEMBLY'].
38     historyOutputs['ALLSE']
39
40
41 #Create a variable that refers to the node located at the flange of the rim (
42     Nodes= NODEID-1)
43 NODE443=myOdb.rootAssembly.instances['SHELL-1'].nodes[442]
44
45 NODE443Displacement=displacement.getSubset(region=NODE443).values[0]
46 N443Disp_brake=displacement_brake.getSubset(region=NODE443).values[0]
47
48 u_turn=NODE443Displacement.data[2]*NODE443Displacement.data[2]+
49     NODE443Displacement.data[1]*NODE443Displacement.data[1]+
50     NODE443Displacement.data[0]*NODE443Displacement.data[0]
51 u_turn=sqrt(u_turn)
52 u_brake=N443Disp_brake.data[2]*N443Disp_brake.data[2]+N443Disp_brake.data[1]*
53     N443Disp_brake.data[1]+N443Disp_brake.data[0]*N443Disp_brake.data[0]
54 u_brake=sqrt(u_brake)
55
56

```

```
57
58 # Write the angle in the output parameters file
59 paramsFile = open ('user_params.txt', 'w')
60 paramsFile.write('Tot_strain_turn'+'\t'+ str(st_turn)+'\n'+ 'Tot_strain_brake' +
61   '\t'+ str(st_brake)+'\n'+ 'U3_flange_turn'+'\t'+ str(u_turn)+'\n'+ 'U3_flange_brake'+'\t'+str(u_brake))
62 paramsFile.close()
```

A.4 TOPOLOGY OPTIMIZATION SETUP

This section will follow all the steps done in Abaqus to setup the FE-model used for the TO in Tosca Structures, together with all steps needed to set up the TO in Tosca Structures. The set-up description will be structured and go through the following items outlined in bold blue text:

- **Part**
- Properties
- Assembly
- **Step**
- **Interactions**
- Loads
- **Mesh**
 - Rim Shell
 - Design space for Rim Center
- **Optimization Task**
 - Design Response
 - Objective Functions
 - Constraints
 - Geometric Restrictions

A.4.1 PART

The part procedure is the same as in FEA-validation Setup, except the model only have two parts, the design space for the rim center and the shell geometry for the rim shell. The design space and the rim shell is modeled as 9th part to reduce computing time. Rim center and rim shell is found in Figure A.4.1.

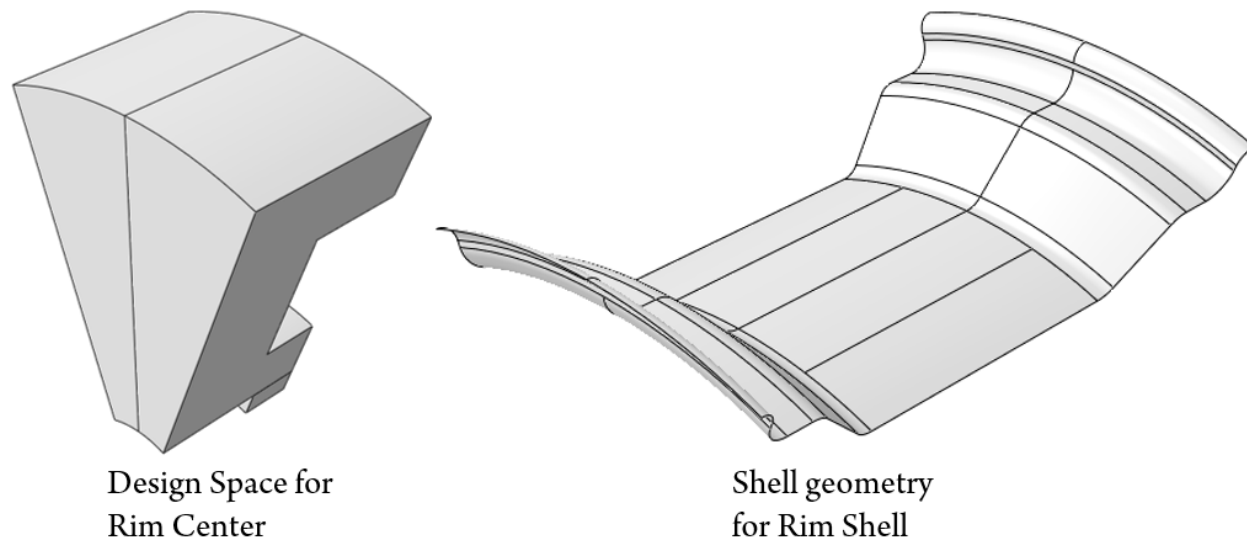


Figure A.4.1

A.4.2 STEP

The step procedure is same as described for the material optimization, Appendix A.3.2

A.4.3 INTERACTIONS

The interactions are similar to the interactions for the material optimization, see Appendix A.3.2. In Figure A.4.2 the interaction set-up is presented.

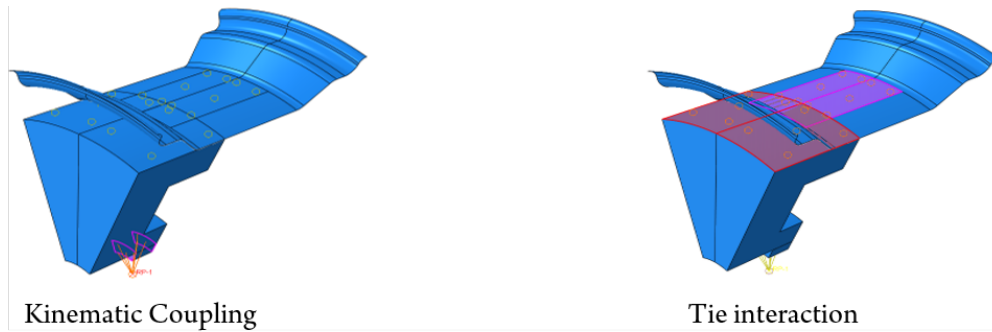


Figure A.4.2

A.4.4 MESH

RIM SHELL

The mesh for the rim shell was made of 4-node doubly curved thin shell elements with reduced integration, hourglass control and finite membrane strains. The element shape is combination of free quad and structured quad. See Figure A.4.3 for details related to mesh.

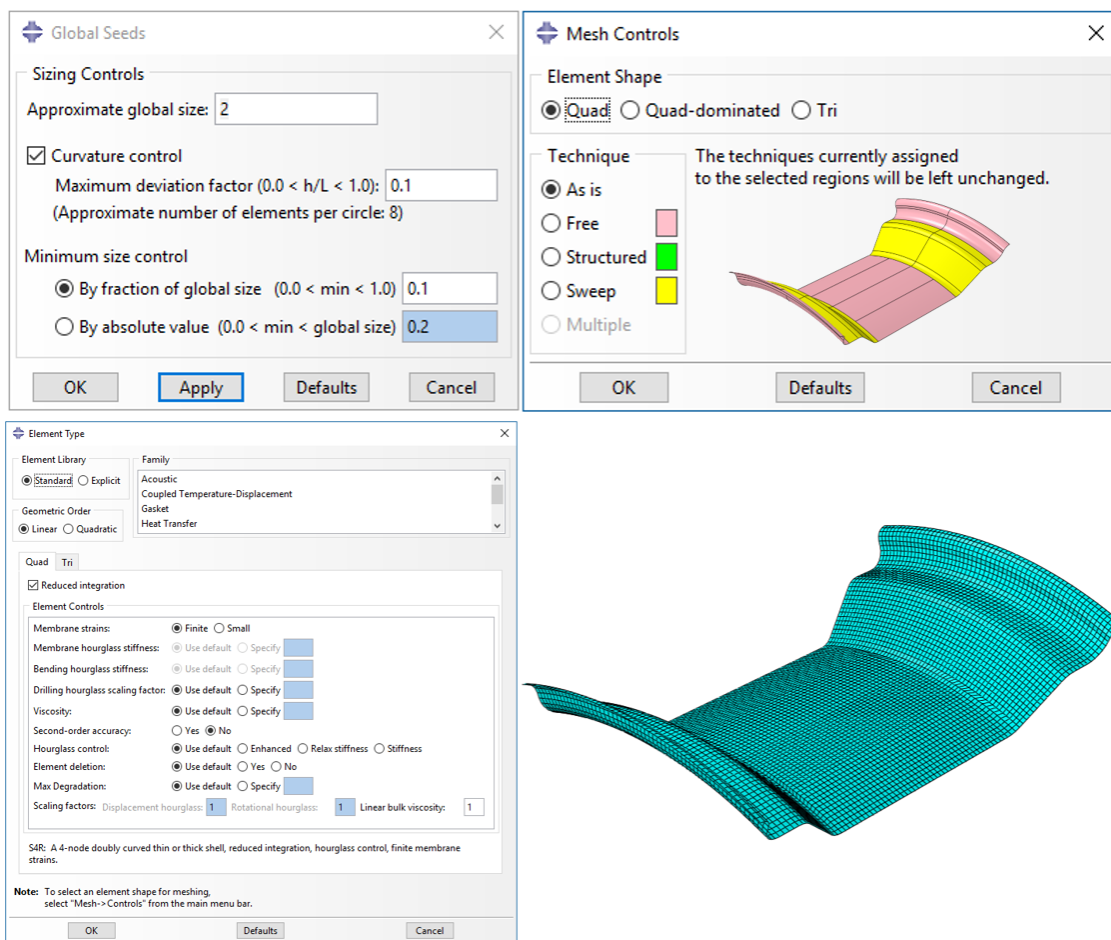


Figure A.4.3

DESIGN SPACE FOR RIM CENTER

The mesh for the design space was made of 8-node linear brick elements with reduced integration and hourglass control. Linear brick element was used instead of tet elements which save computing time as fewer elements are needed for same mesh size. The element shape was quad and a combination of structured (green) and sweep (yellow). The global size was set to 2 with a curvature control of 0.1. See Figure A.4.4 for details related to mesh.

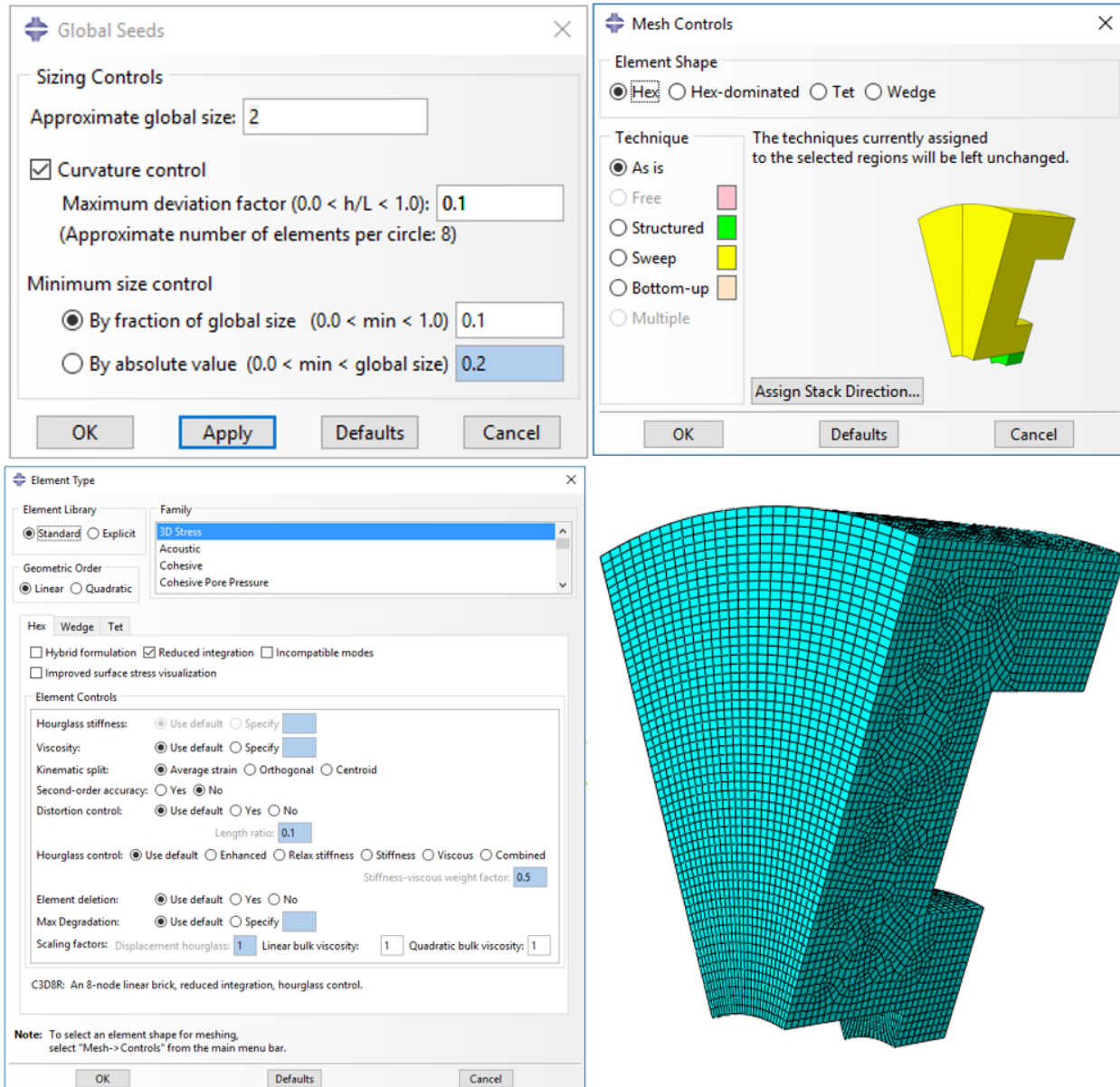


Figure A.4.4

A.4.5 OPTIMIZATION TASK

For the optimization task the whole model was set as region with sensitive-based algorithm. No loads or boundary conditions were set as frozen.

DESIGN RESPONSE

Two different design response was created. Strain Energy for the whole model and weight for the design space. See Figure A.4.5 for design response set-up.

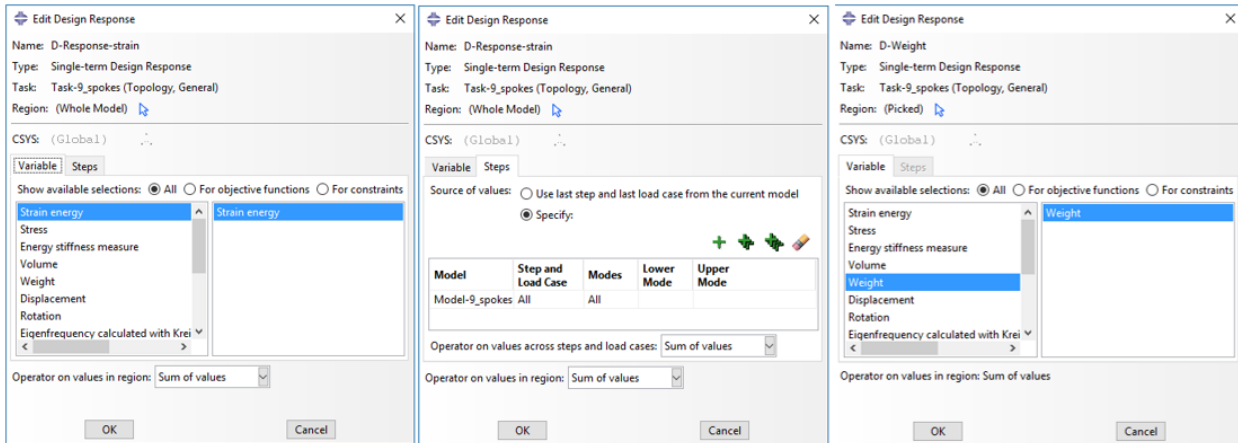


Figure A.4.5

OBJECTIVE FUNCTIONS

The design response strain energy is set as objective function and was set to be minimized. The design response strain energy was set to be the sum of both load case. This means that Tosca would treat both load case equally, and will prioritize stiffness equally for both load case. See Figure A.4.6 for design objective set-up.

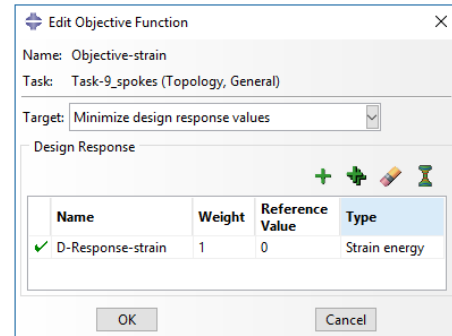


Figure A.4.6

CONSTRAINTS

The weight design response was set as constraint. It was set as a weight target where the weight should less or equal to 150 gram. See Figure A.4.7 for constraint set-up. The design weight target of rim center was less than 1.0 kilogram, which means 111 gram for a 9Th part of the rim. The final target was set to 150 gram, as this gave a more machinable design. The design was then tweaked during regenerating to be less than 1 kilogram.

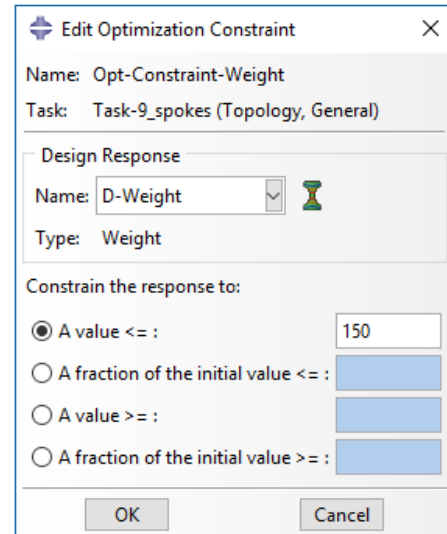


Figure A.4.7

GEOMETRIC RESTRICTIONS

Five geometric restrictions was added to the TO model. The center lock region and the rim shell was frozen. A planar symmetry was added to the design space to ensure that the design is performing the same for both brake and acceleration loads. The planar symmetry set-up is found in Figure A.4.8 To have a 3-axis kind of production constraint, forging constraint was added in both axial directions. Forging set-up is found in Figure A.4.9

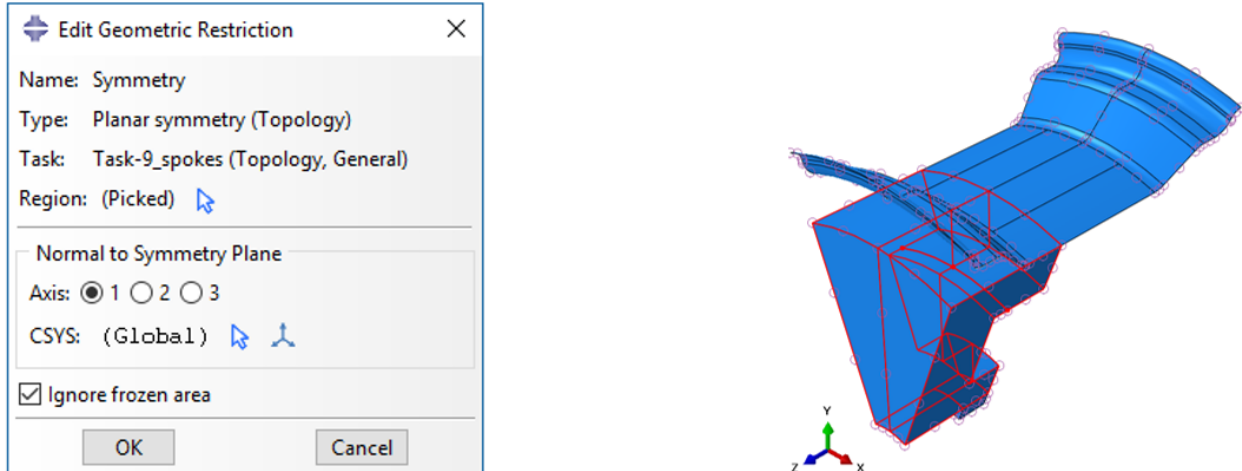


Figure A.4.8

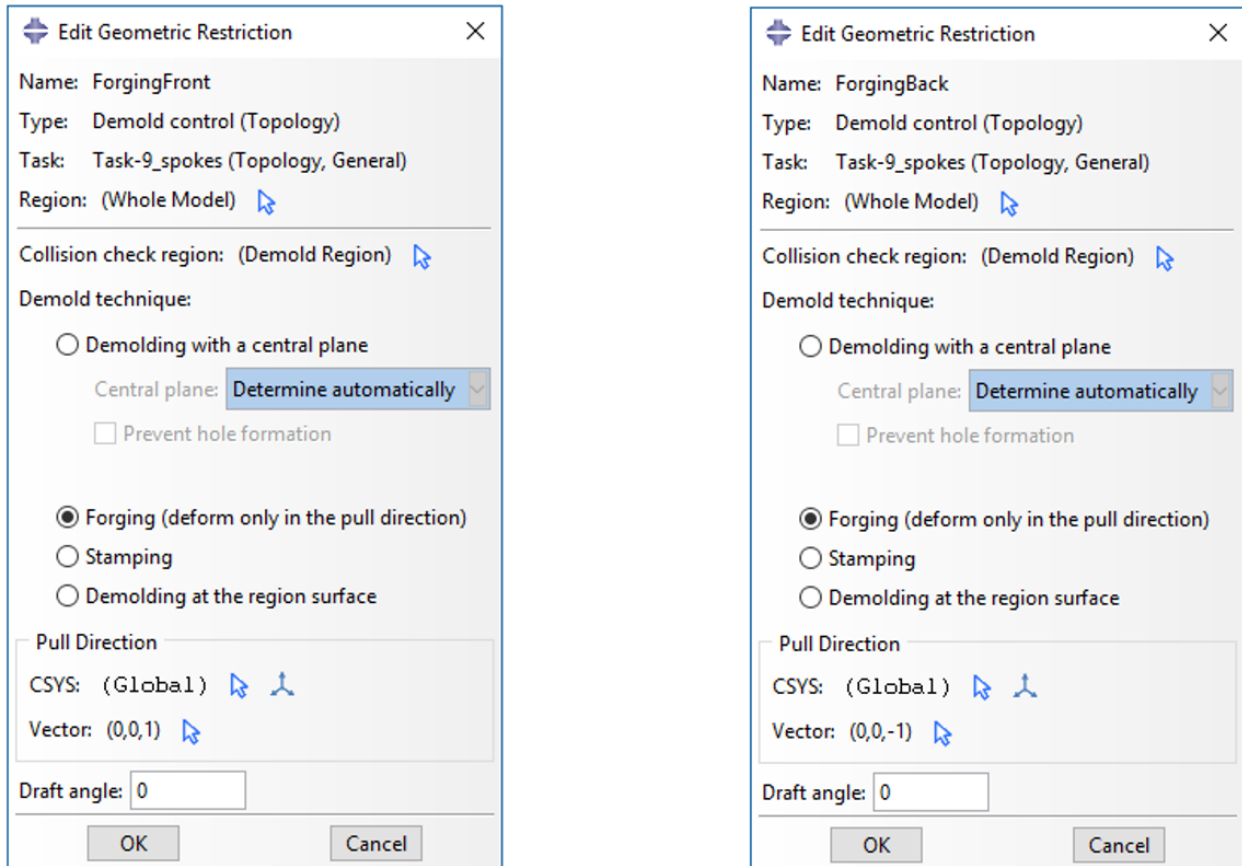
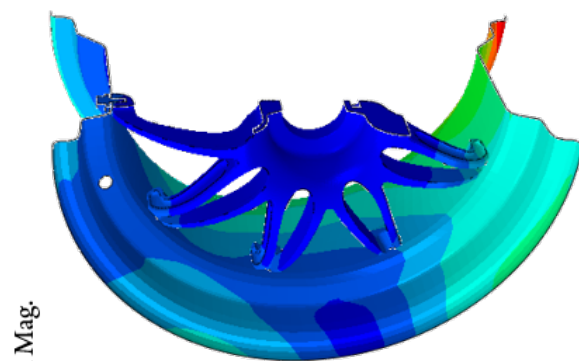
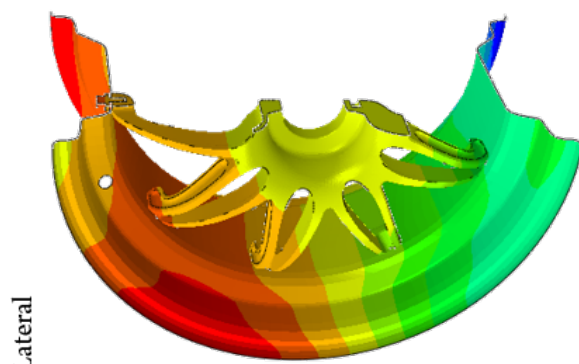
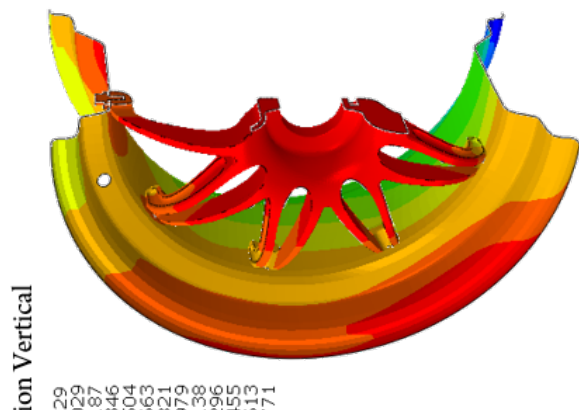
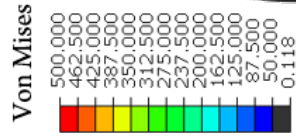
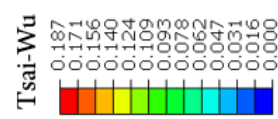
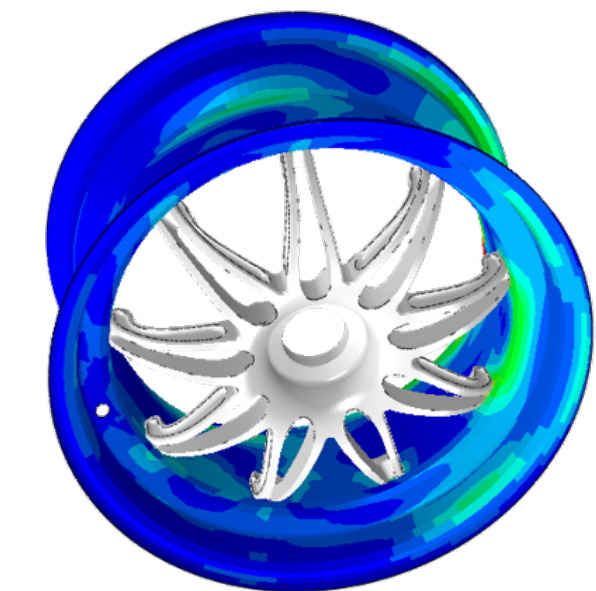


Figure A.4.9

A.5 FEM VALIDATION RESULTS

A.5.1 CORNERING @ 110KM/H

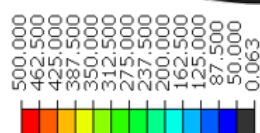


A.5.2 BRAKE @ 110KM/H

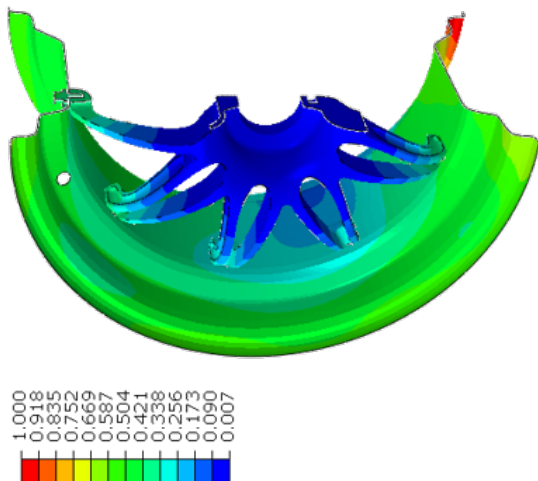
Tsai-Wu



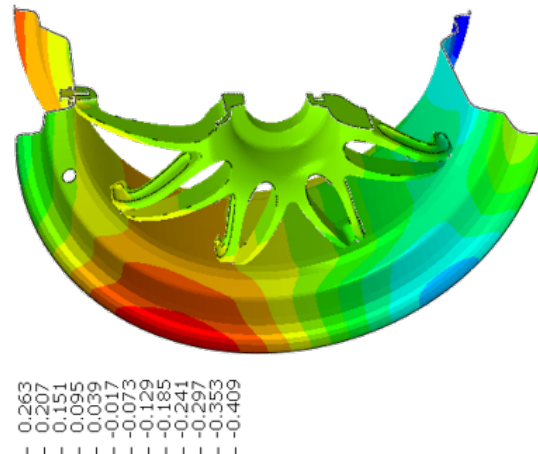
Von Mises



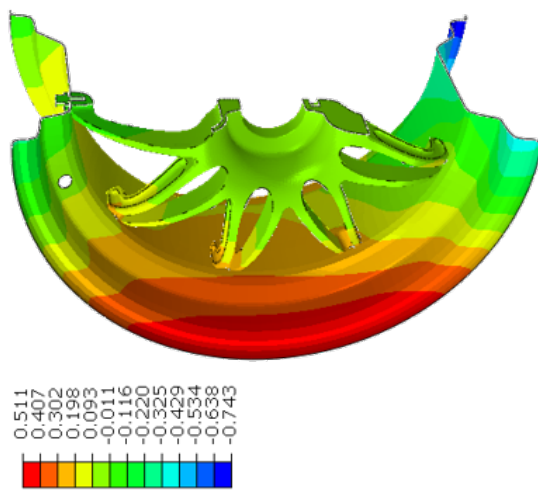
Deflection Mag.



Deflection Lateral

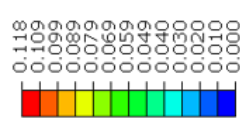


Deflection Vertical

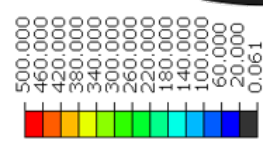


A.5.3 3G BUMP

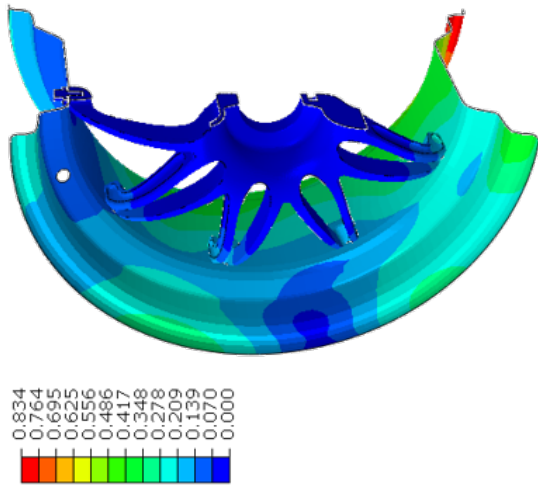
Tsai-Wu



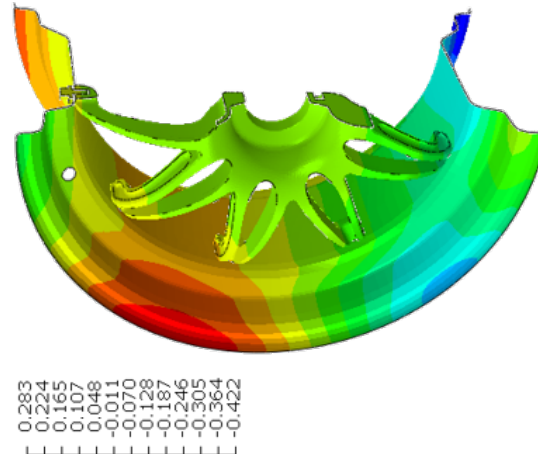
Von Mises



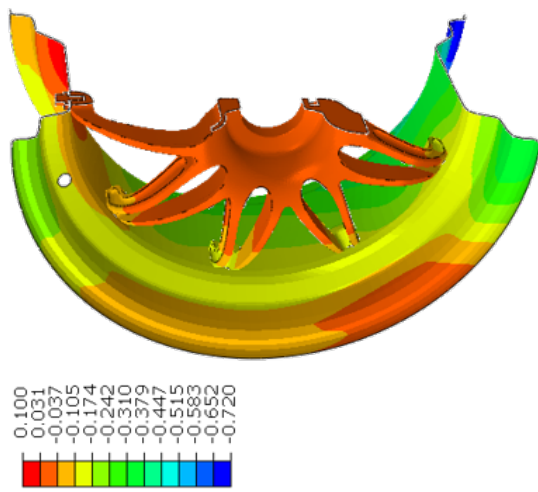
Deflection Mag.



Deflection Lateral

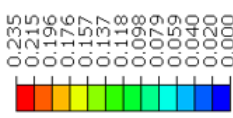


Deflection Vertical

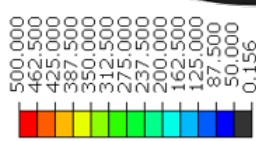


A.5.4 2G BUMP + CORNERING @ 110KM/H

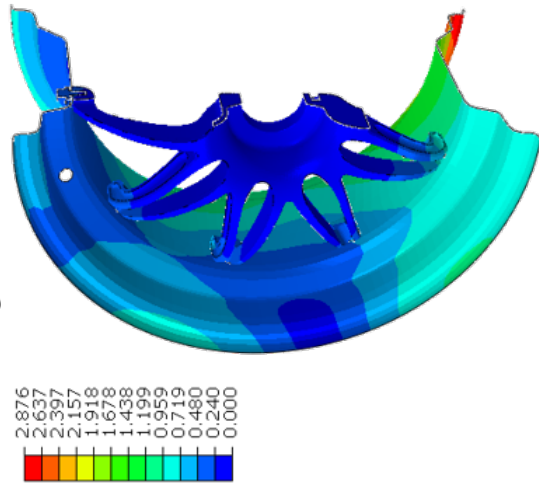
Tsai-Wu



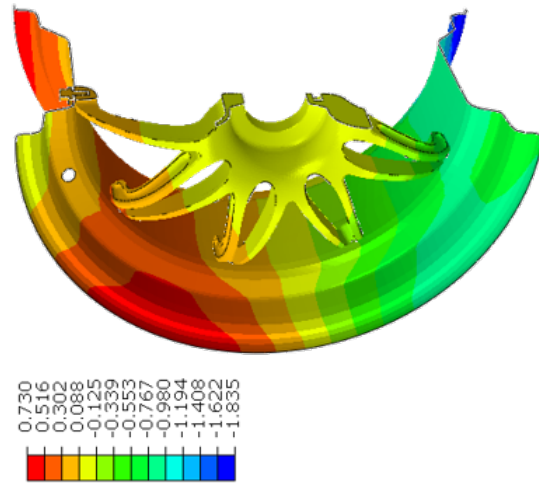
Von Mises



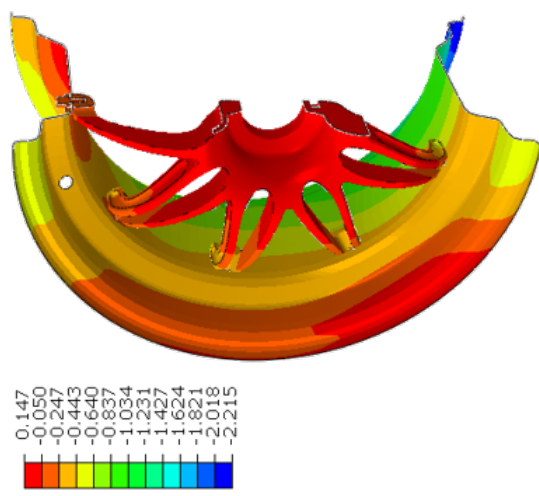
Deflection Mag.

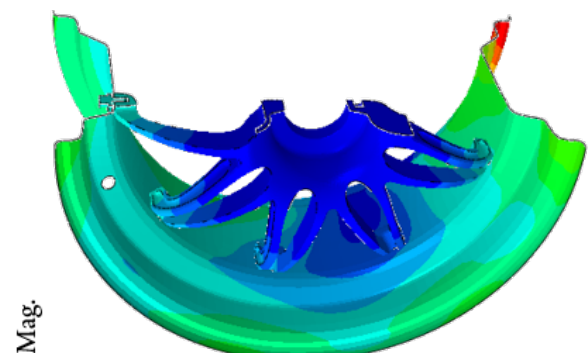
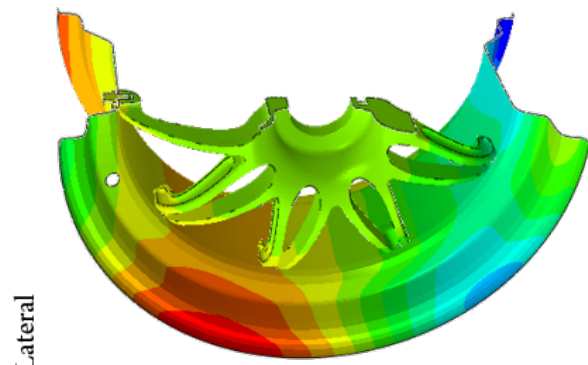
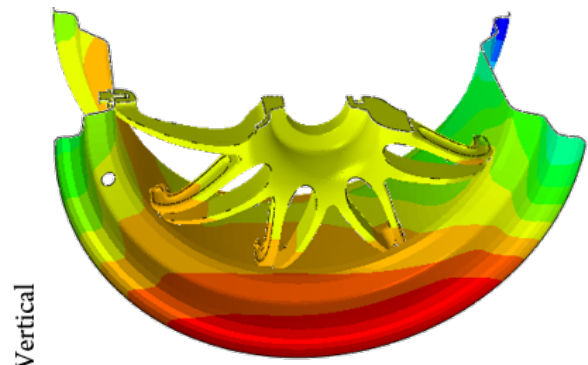
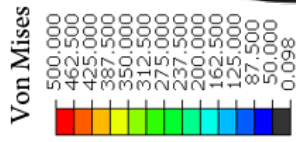
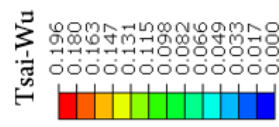
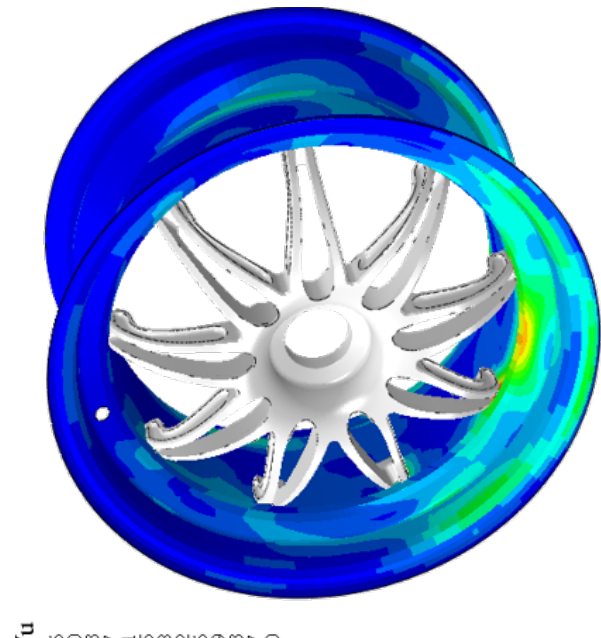


Deflection Lateral

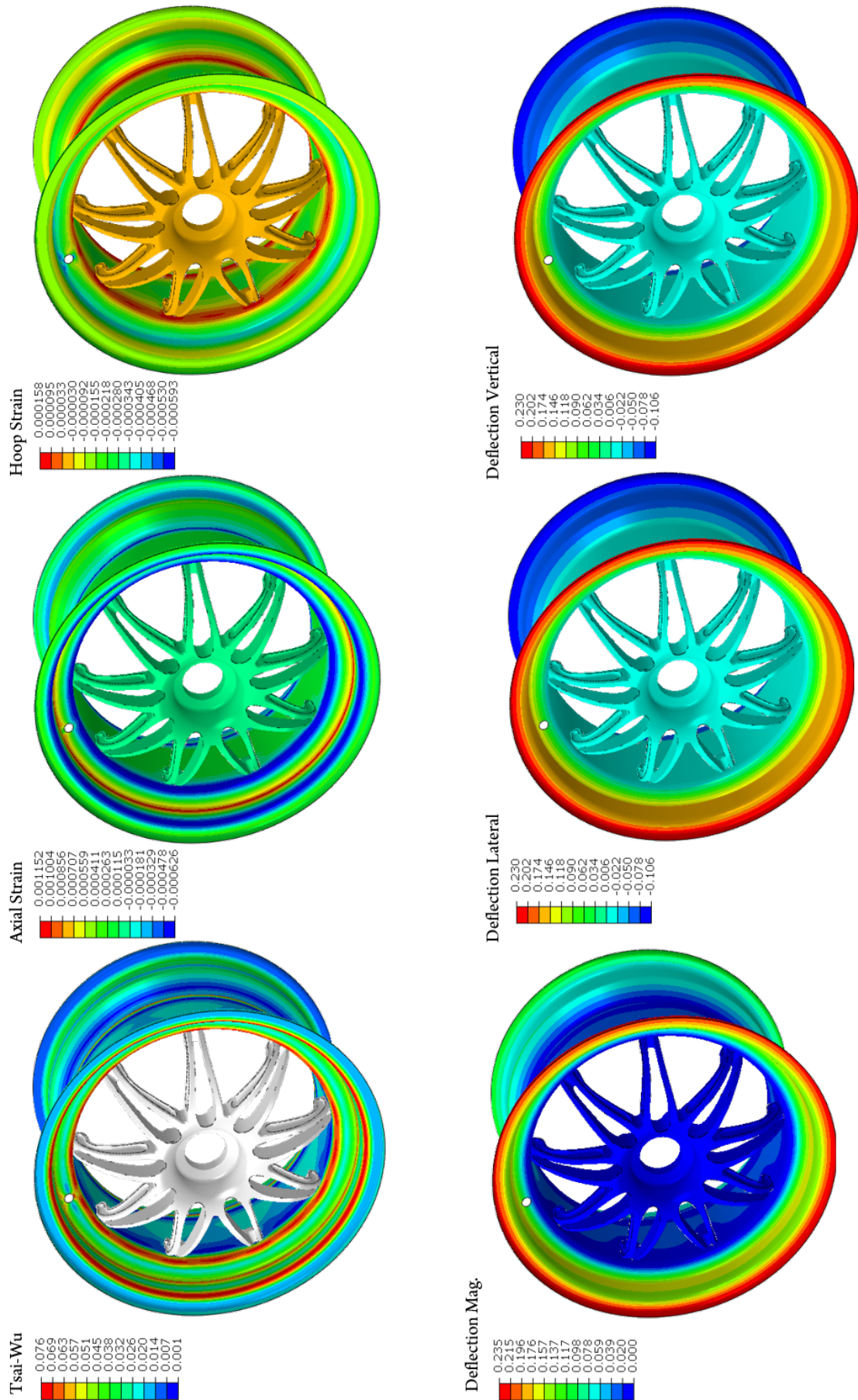


Deflection Vertical

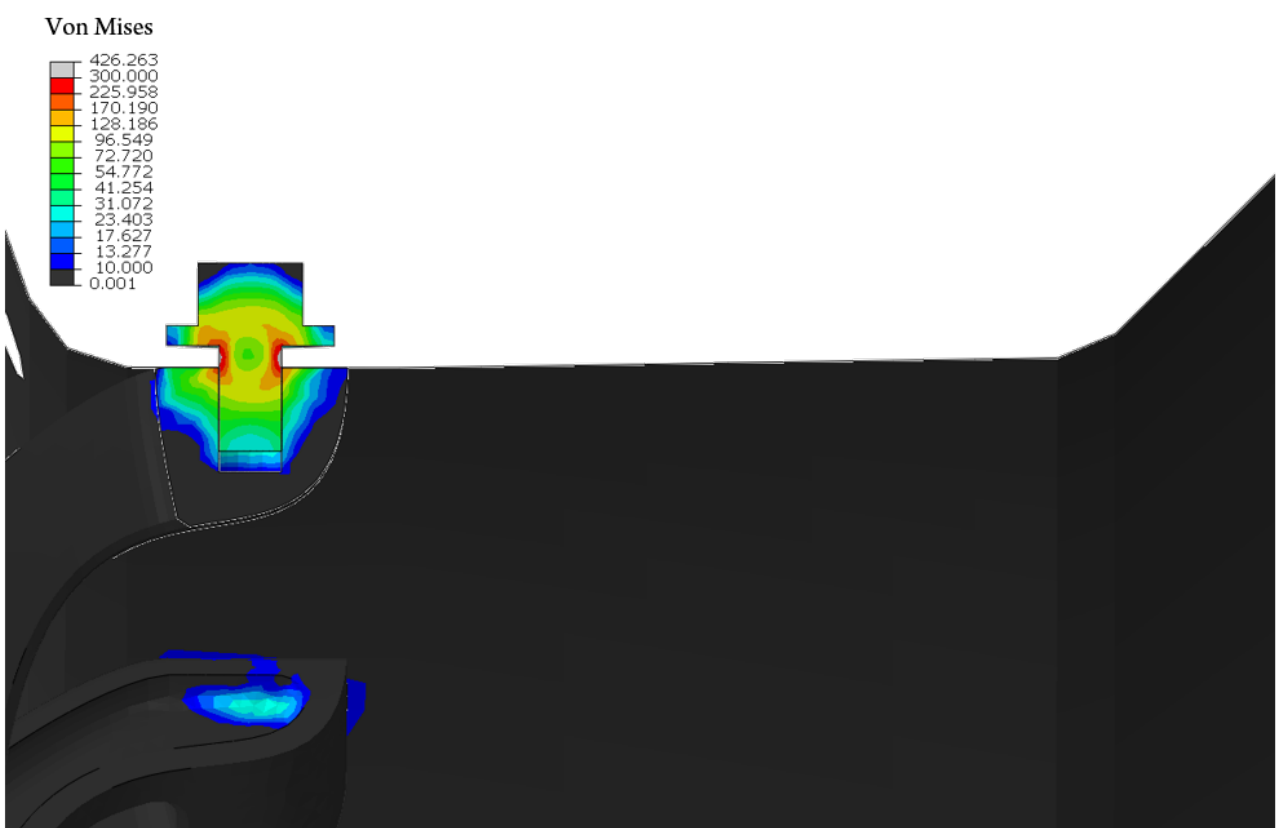
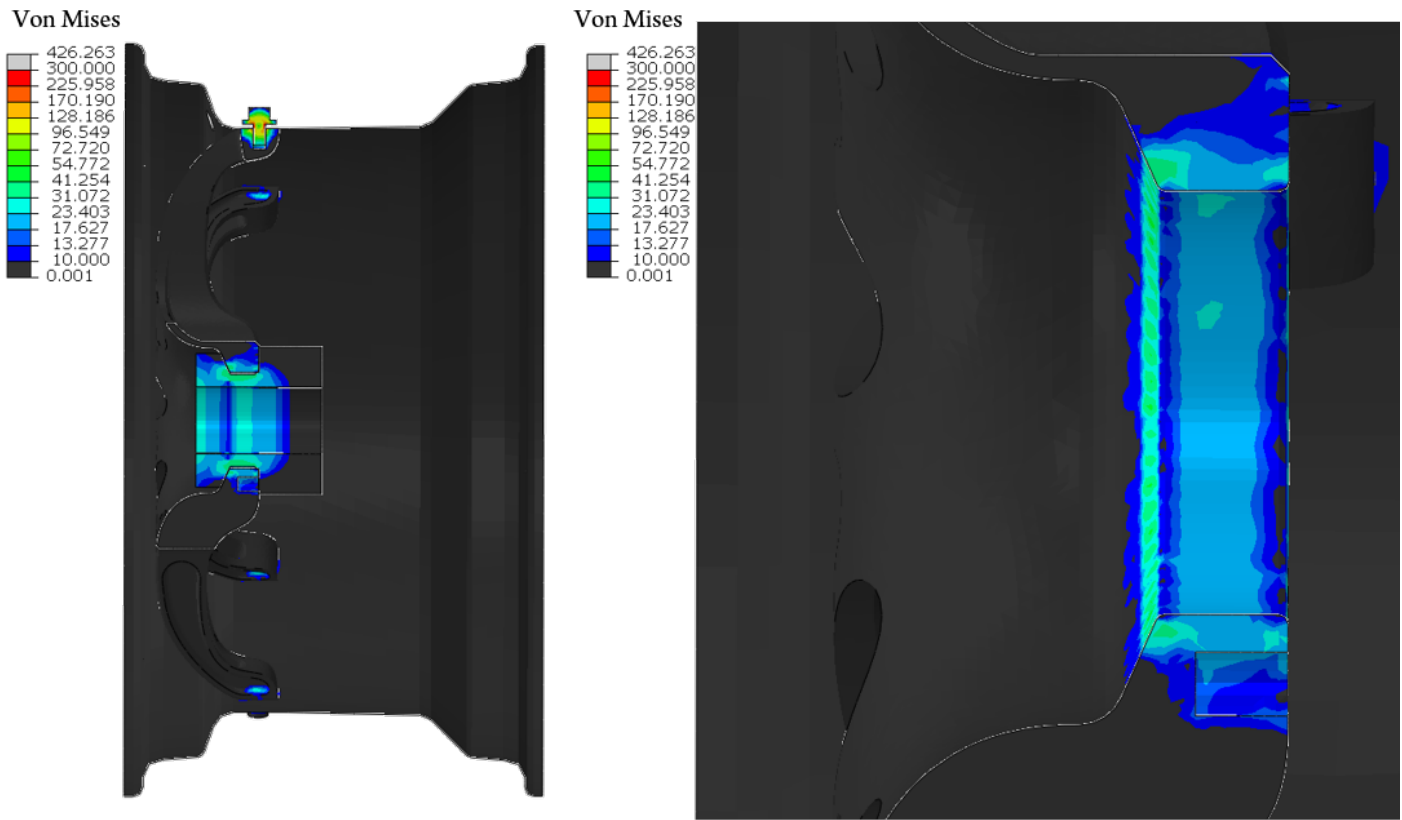




A.5.6 INFLATION PRESSURE 1 BAR



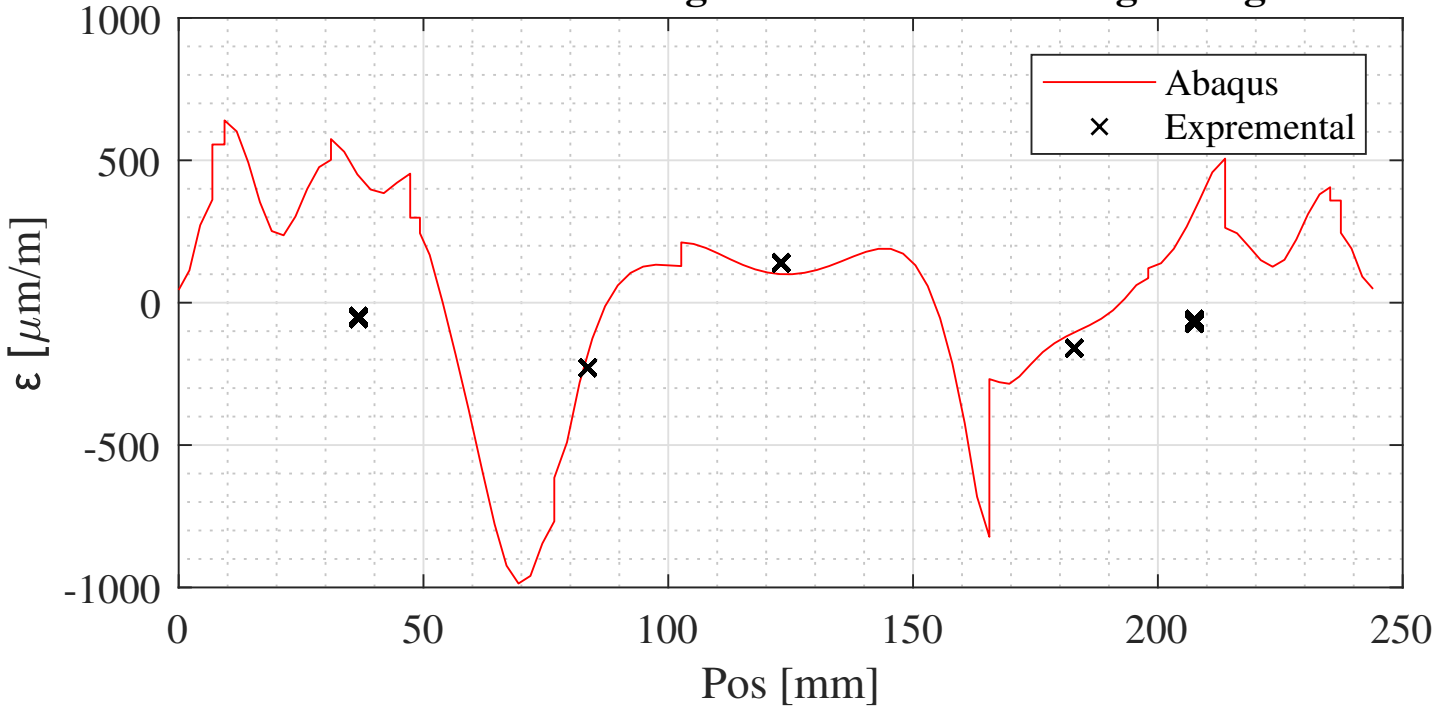
A.5.7 PRETENSION EFFECTS



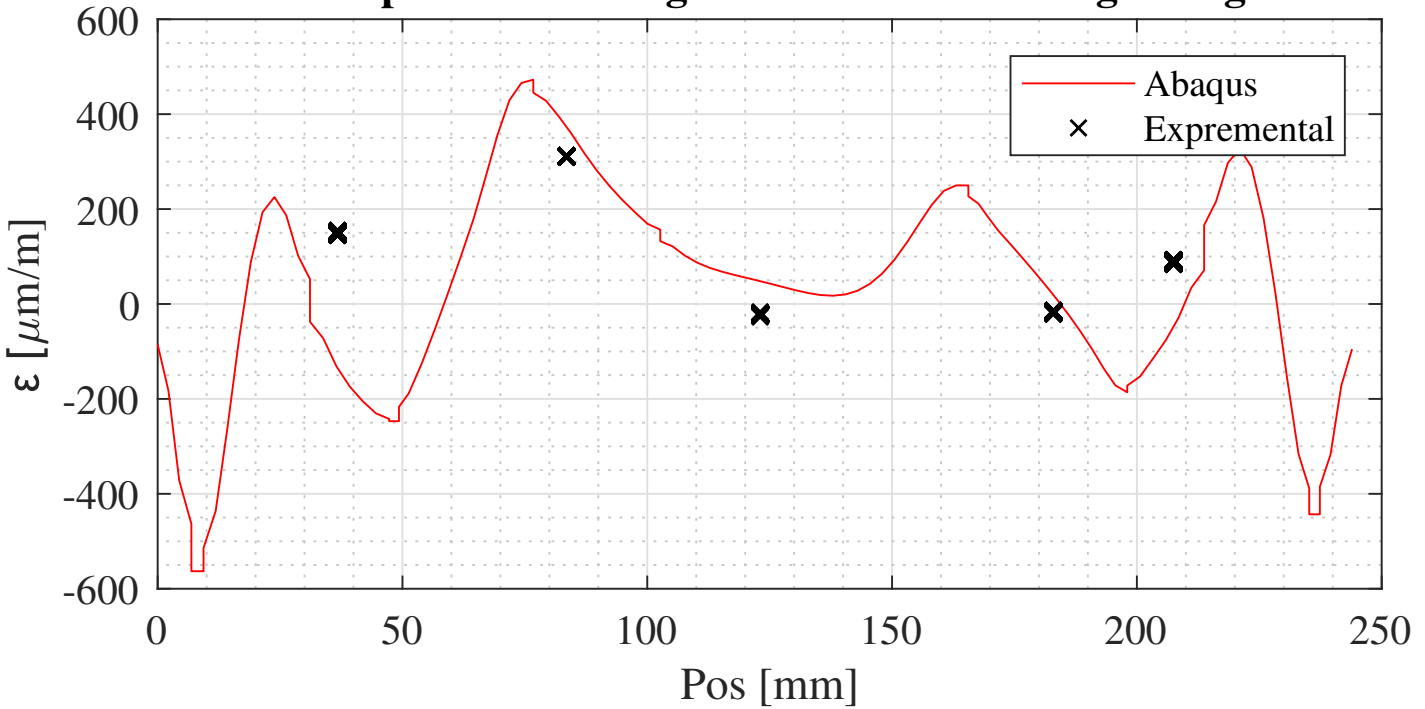
Close up of pretension effect of bolts on Rim Center

A.6 MECHANICAL TESTING RESULTS

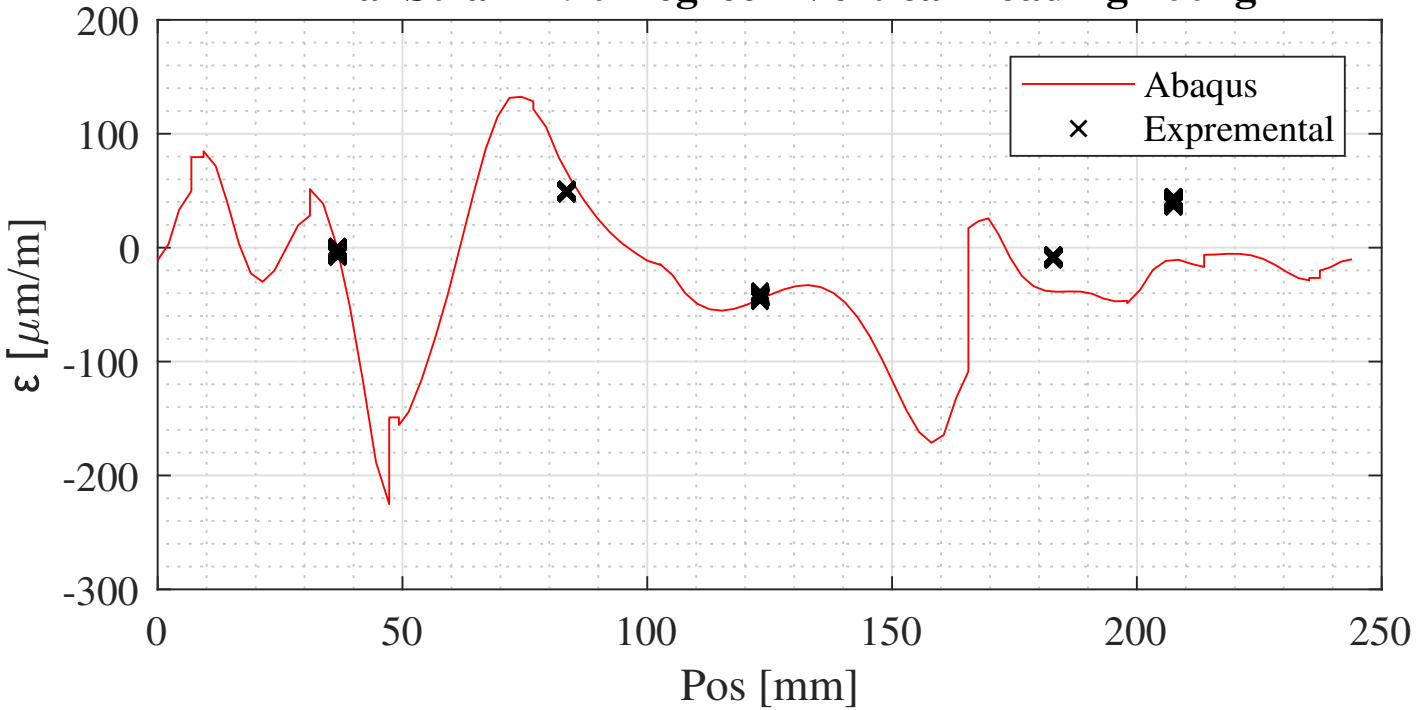
Axial Strain - 0 Degree - Vertical Loading 200kg



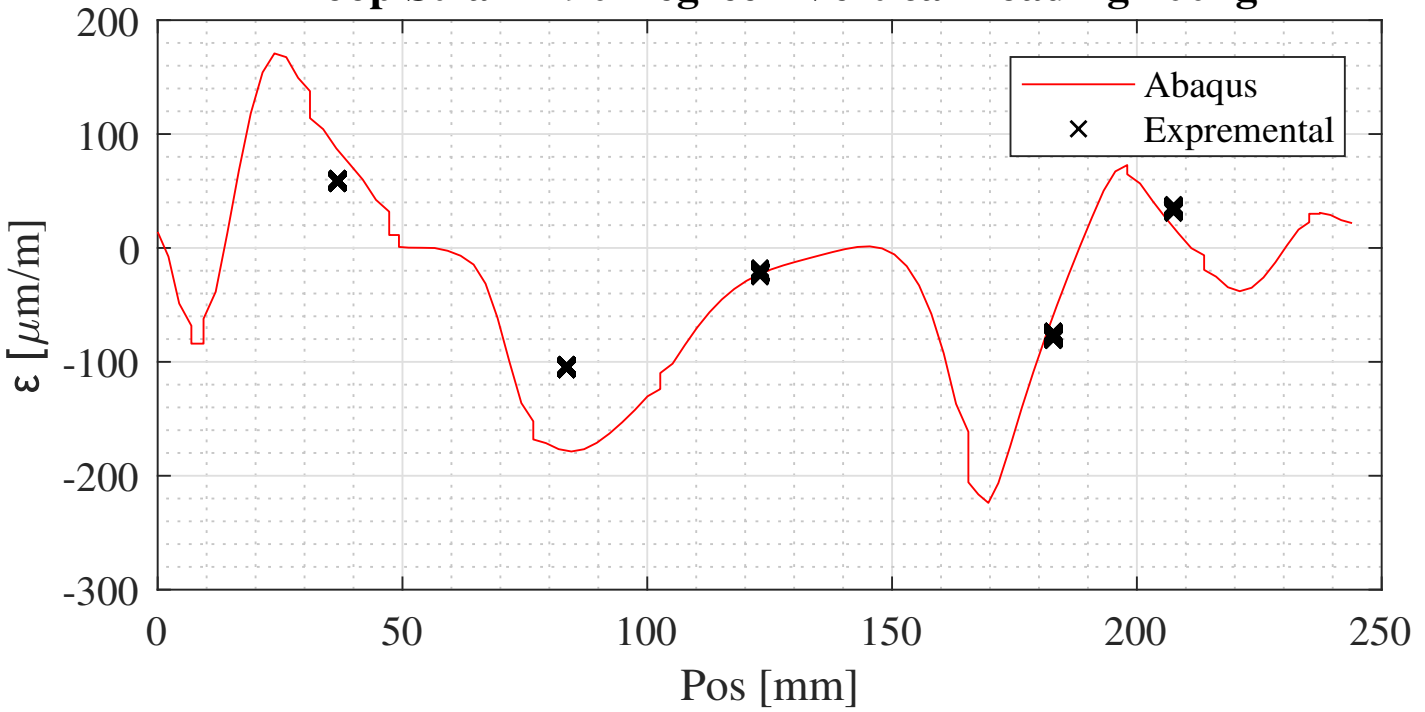
Hoop Strain - 0 Degree - Vertical Loading 200kg



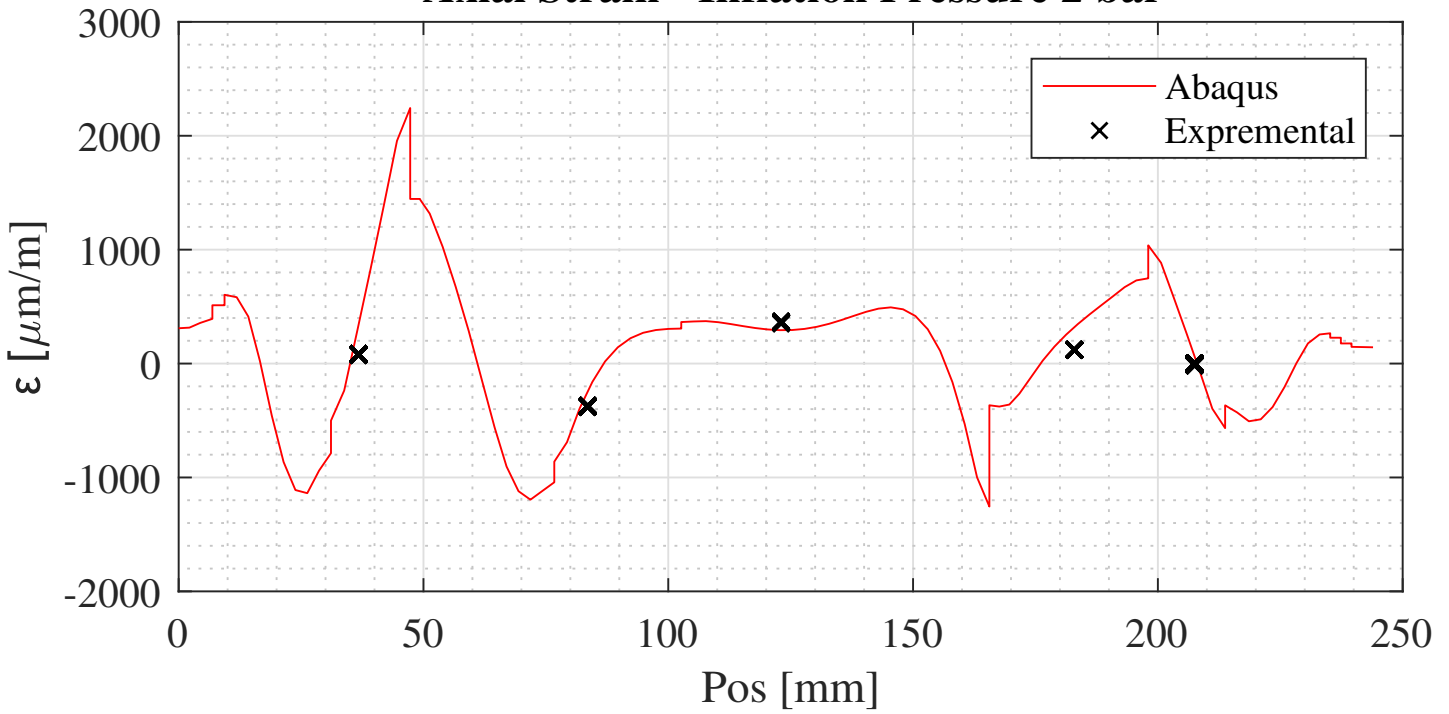
Axial Strain - 90 Degree - Vertical Loading 200kg



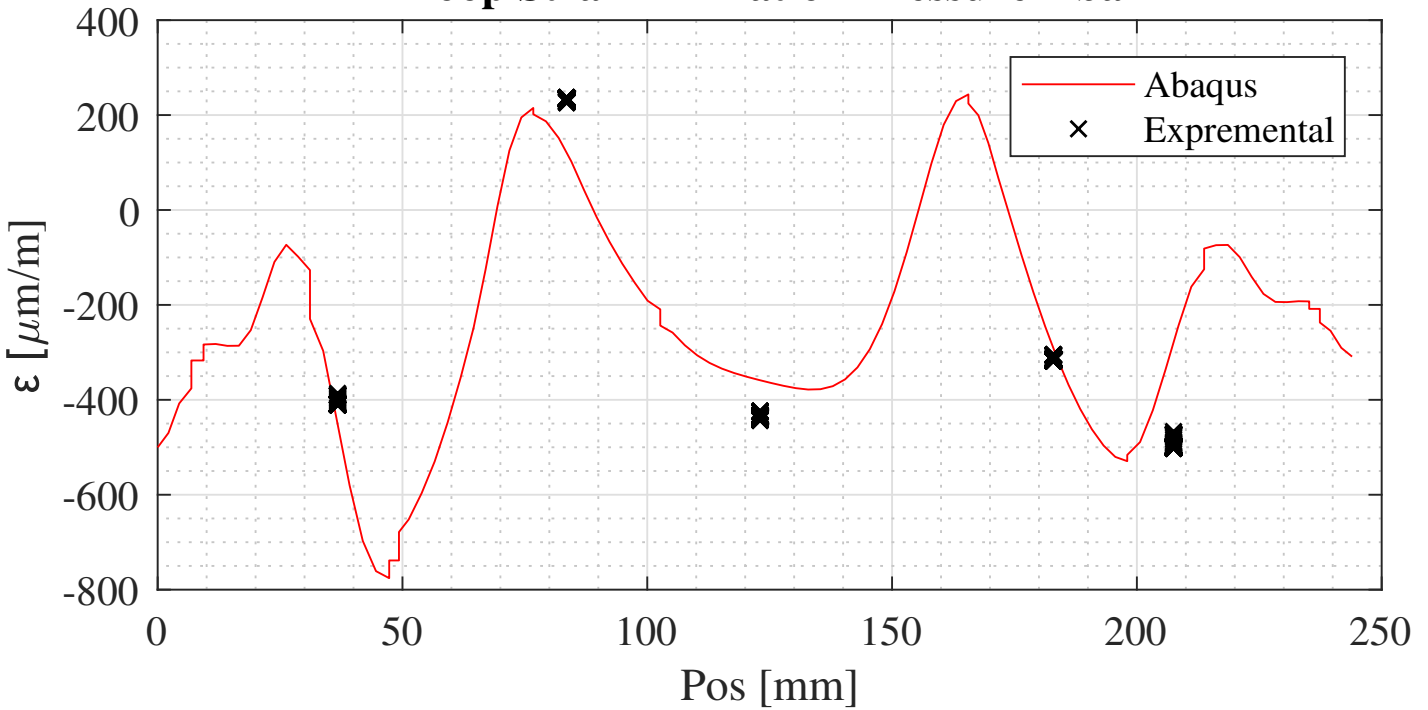
Hoop Strain - 90 Degree - Vertical Loading 200kg



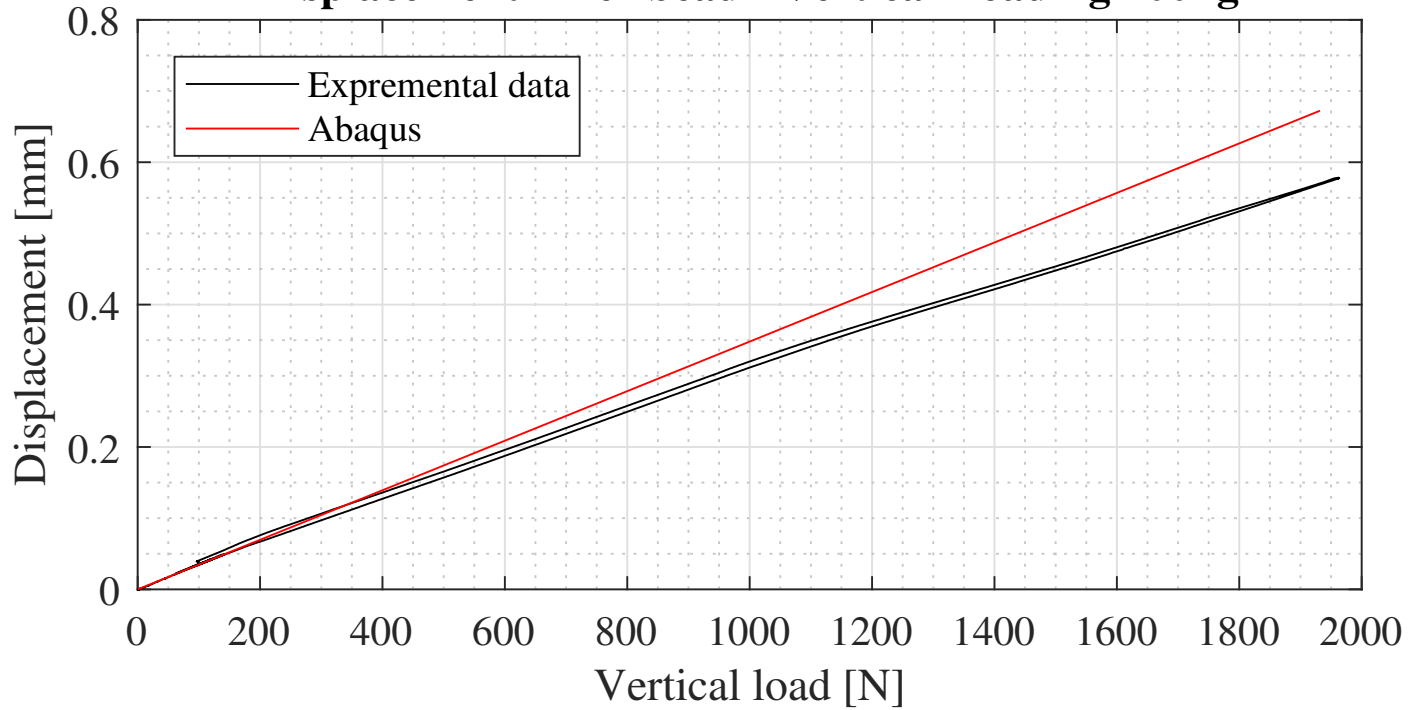
Axial Strain - Inflation Pressure 2 bar



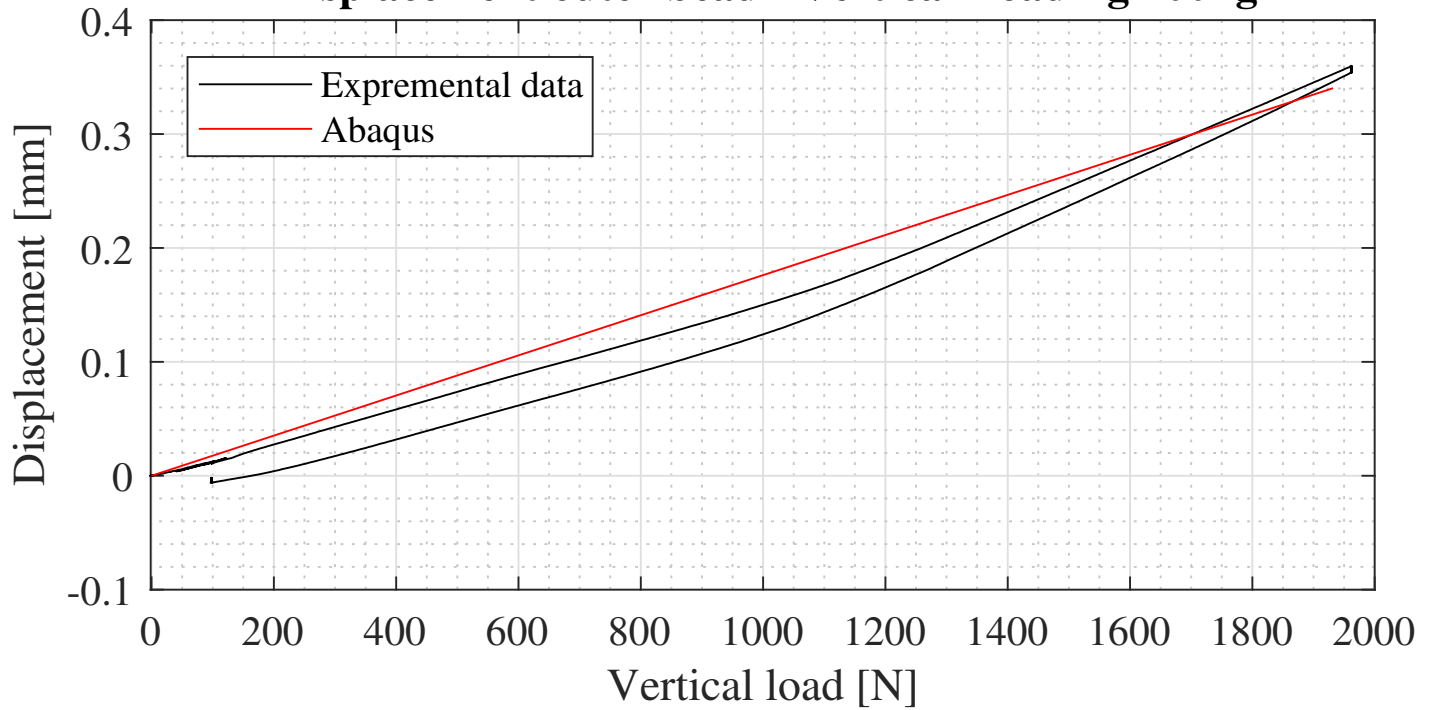
Hoop Strain - Inflation Pressure 2 bar

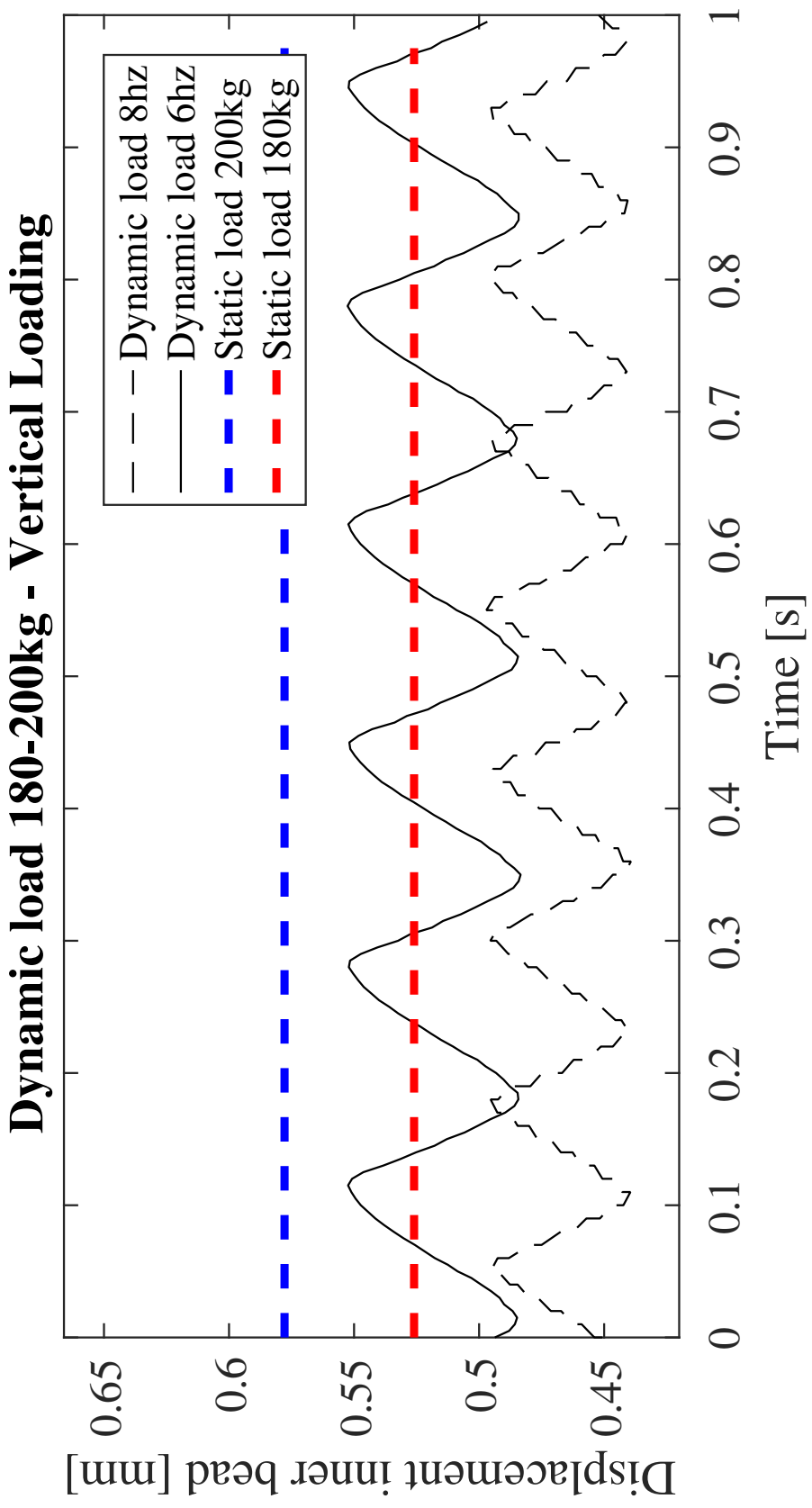


Displacement inner bead - Vertical Loading 200kg



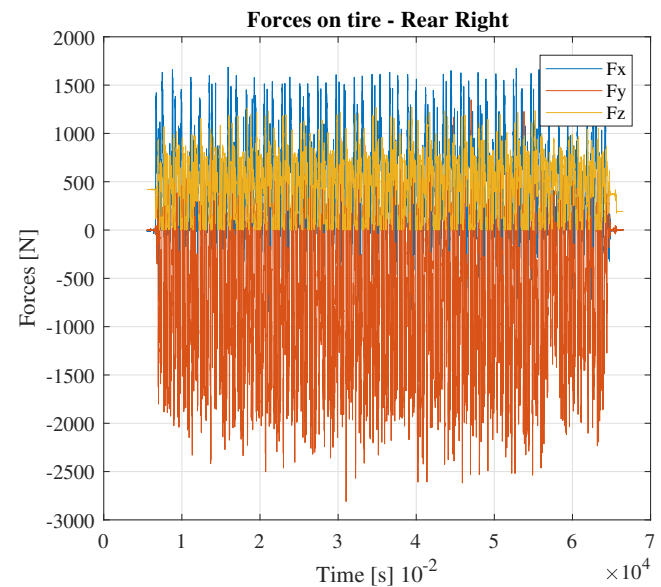
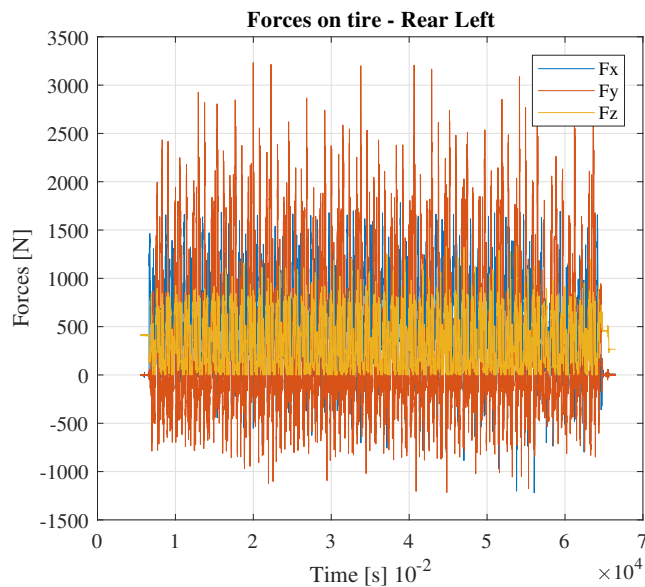
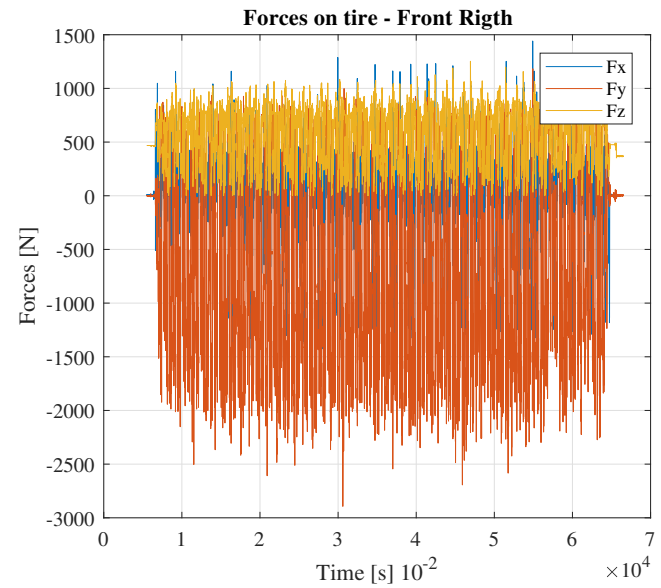
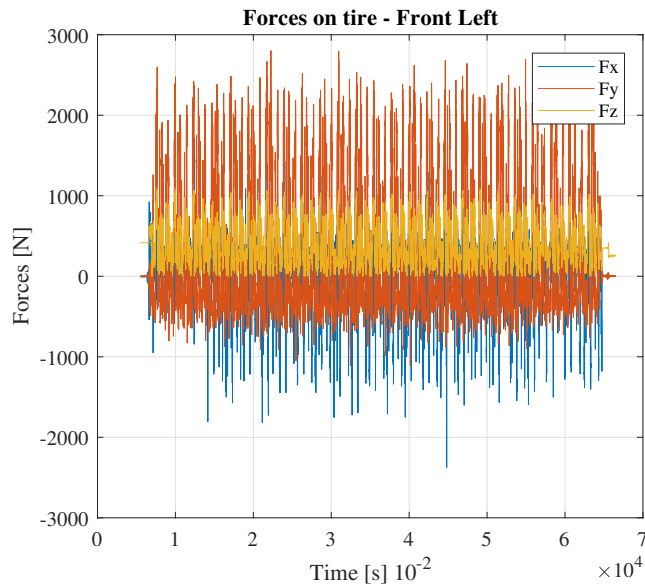
Displacement outer bead - Vertical Loading 200kg





A.7 REACTION FORCES ON TIRE - ESTIMATED FROM LOG DATA - HALF ENDURANCE

The reaction forces on the tire was estimated from damper-position data, accelerometer-data and total mass of car with driver. Lateral and longitudinal forces was balanced by the normal forces working on each tire. The log-data was from testing at Værnes of the 2016 car Gnist.



A.8 RIM SHELL PRODUCTION - PICTURES



Figure A.8.1: Molds after polishing, application of sealer and release agent.



Figure A.8.2: Initial ply added on outer flange

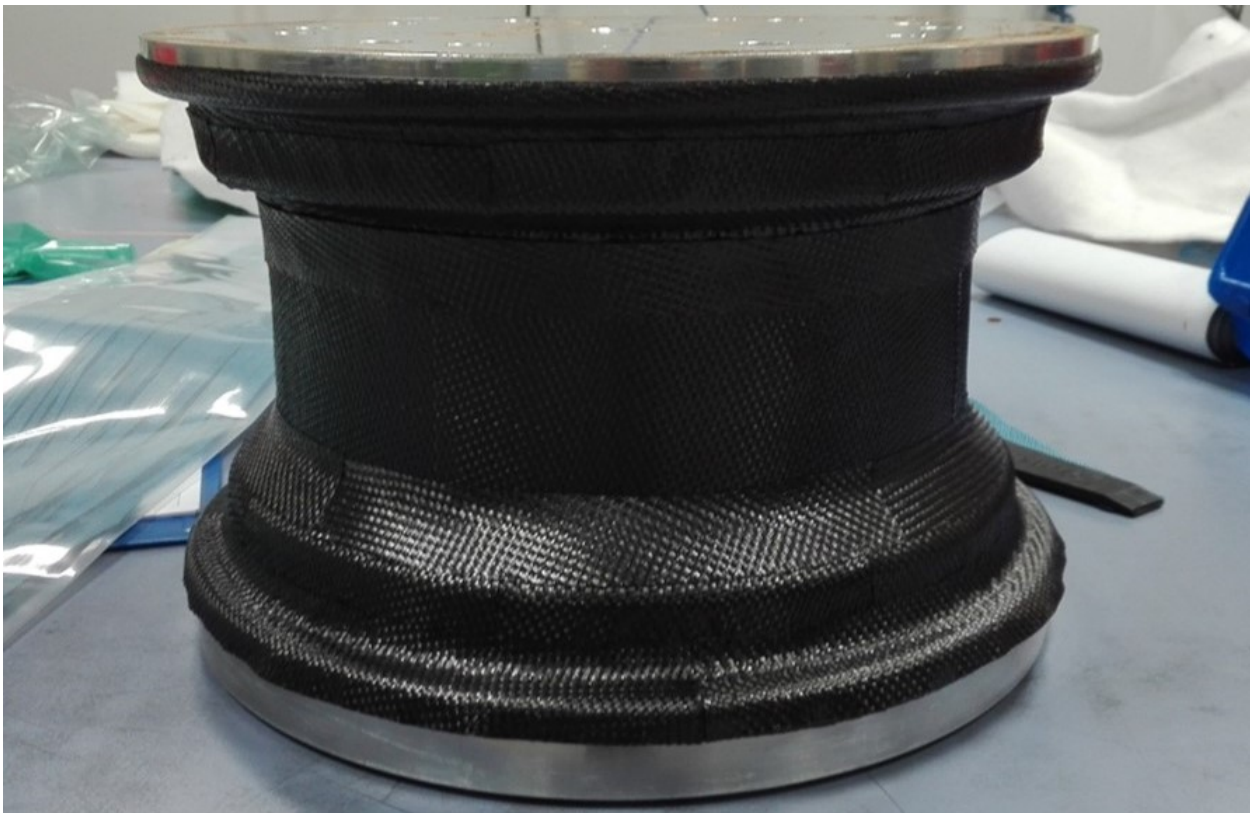


Figure A.8.3: Initial layer before debulking

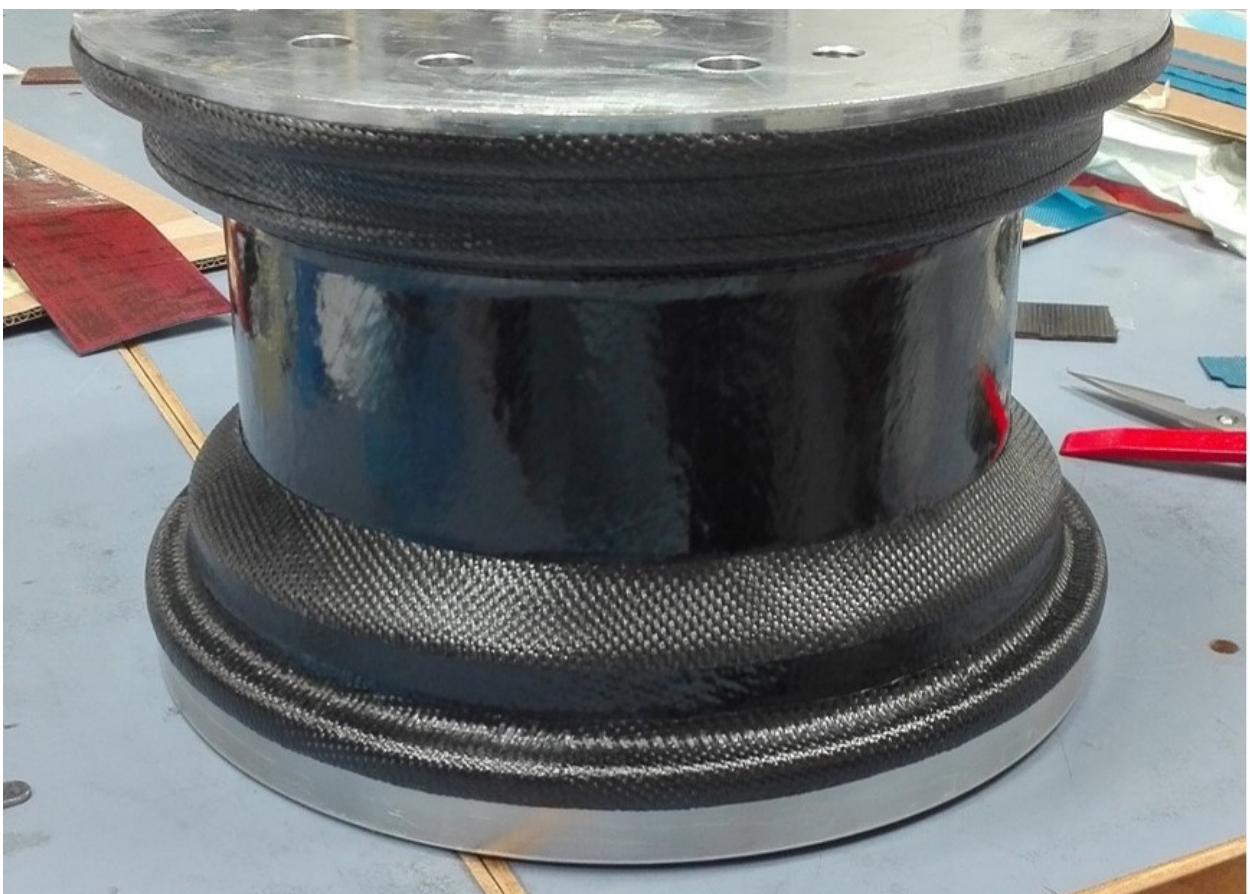


Figure A.8.4: 4 Th layer after debulking



Figure A.8.5: Rim shell under debulking



Figure A.8.6: The hump was created by stacking small stripes of CFRP



Figure A.8.7: Application of peel ply



Figure A.8.8: Left: Bagtape rolled in release film, used to reduce bridging around bead. Right: Temperature sensor, mounted between mold and laminate



Figure A.8.9: Finished application of release film

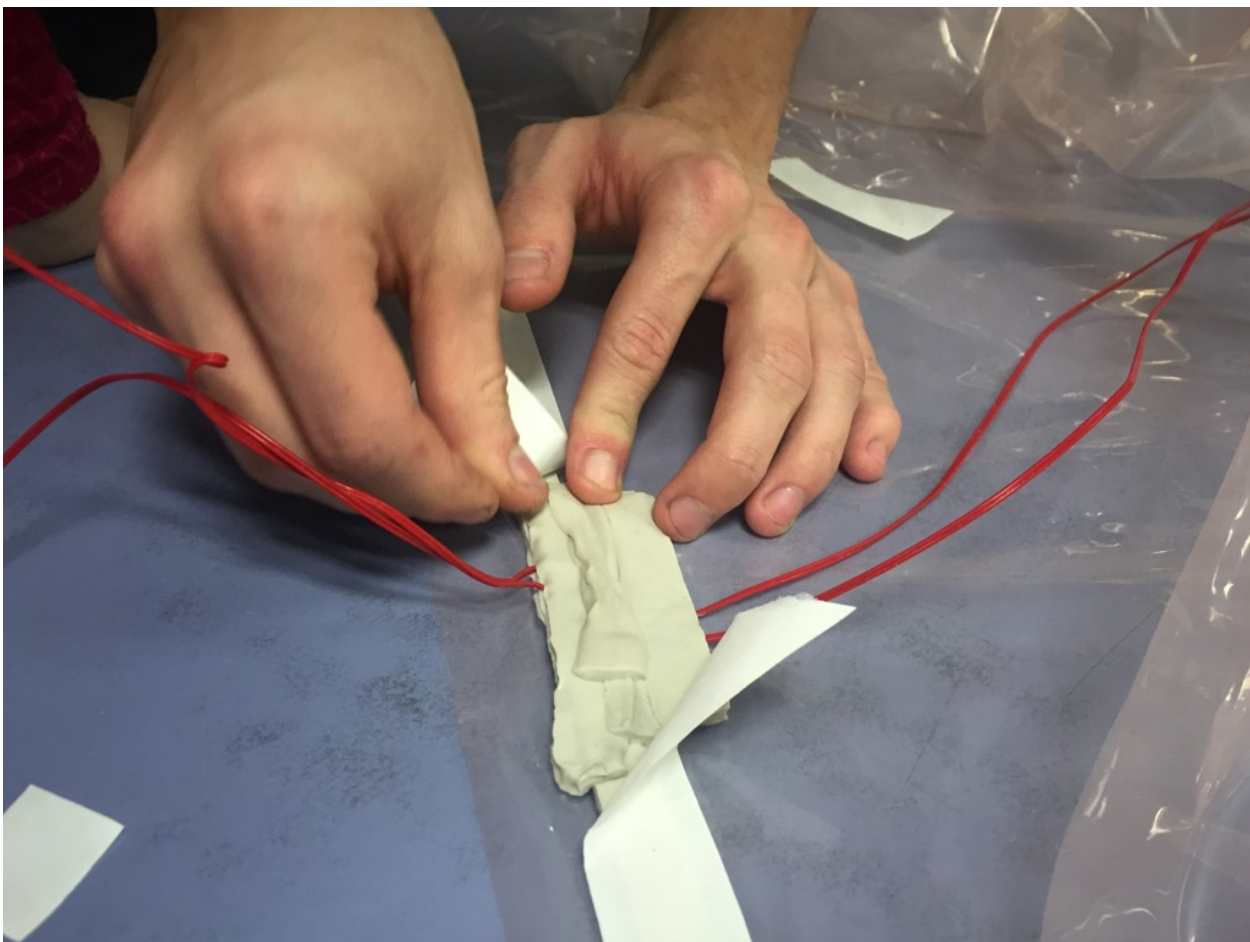


Figure A.8.10: Sealing of temp sensor though tha bag



Figure A.8.11: Vacuum bag ready for sealing

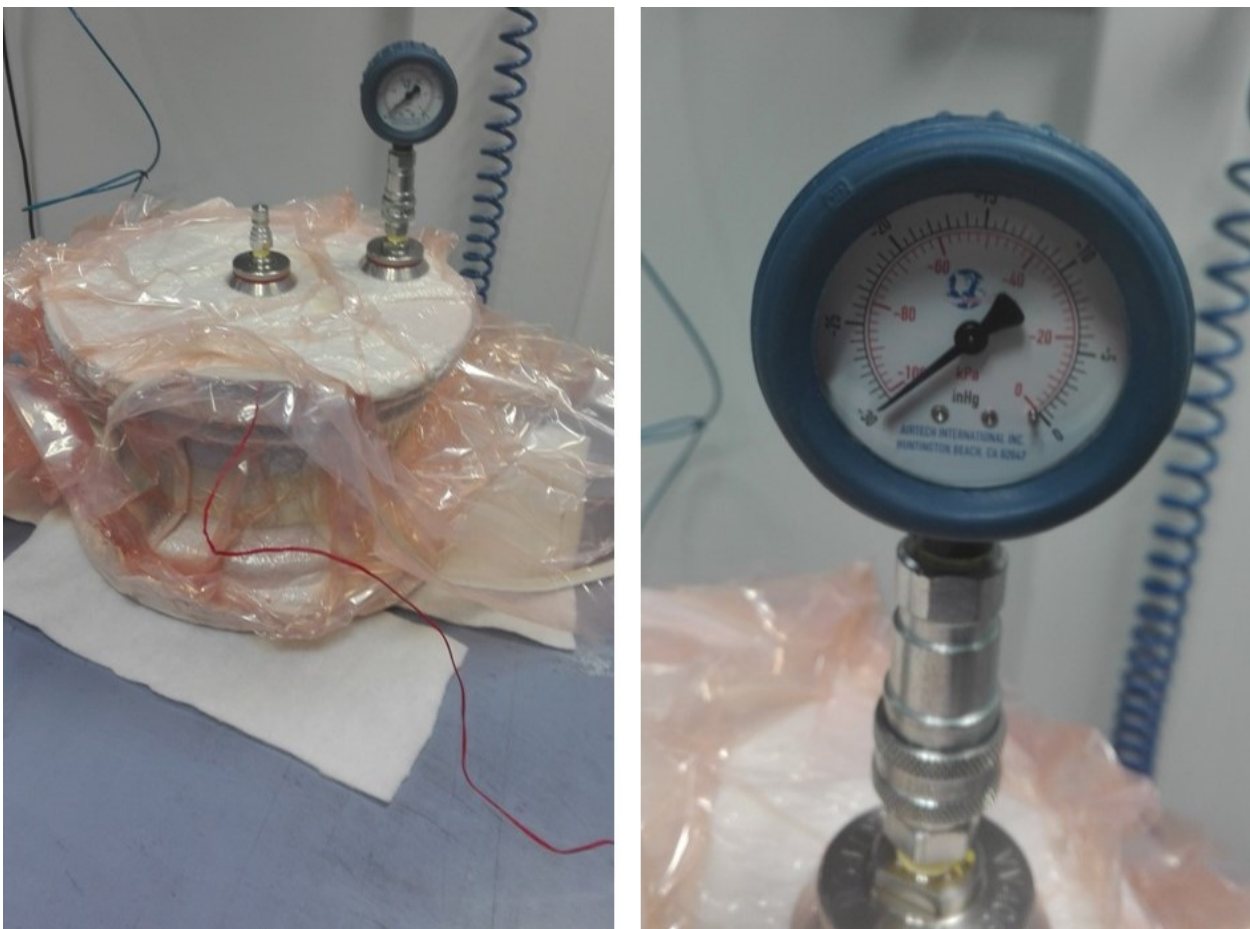


Figure A.8.12: Vacuum leak test



Figure A.8.13: Rim shell ready for autoclave curing

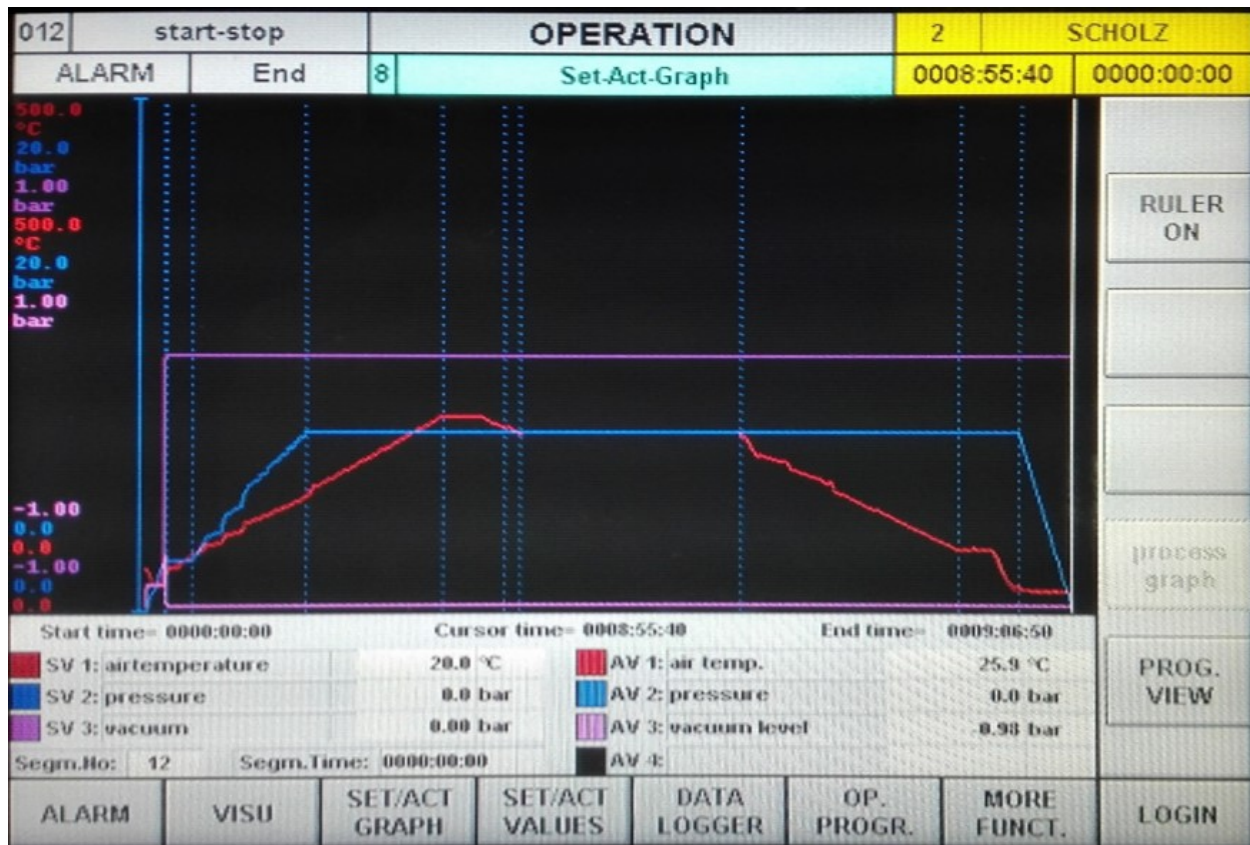


Figure A.8.14: Set-point for autoclave during curing

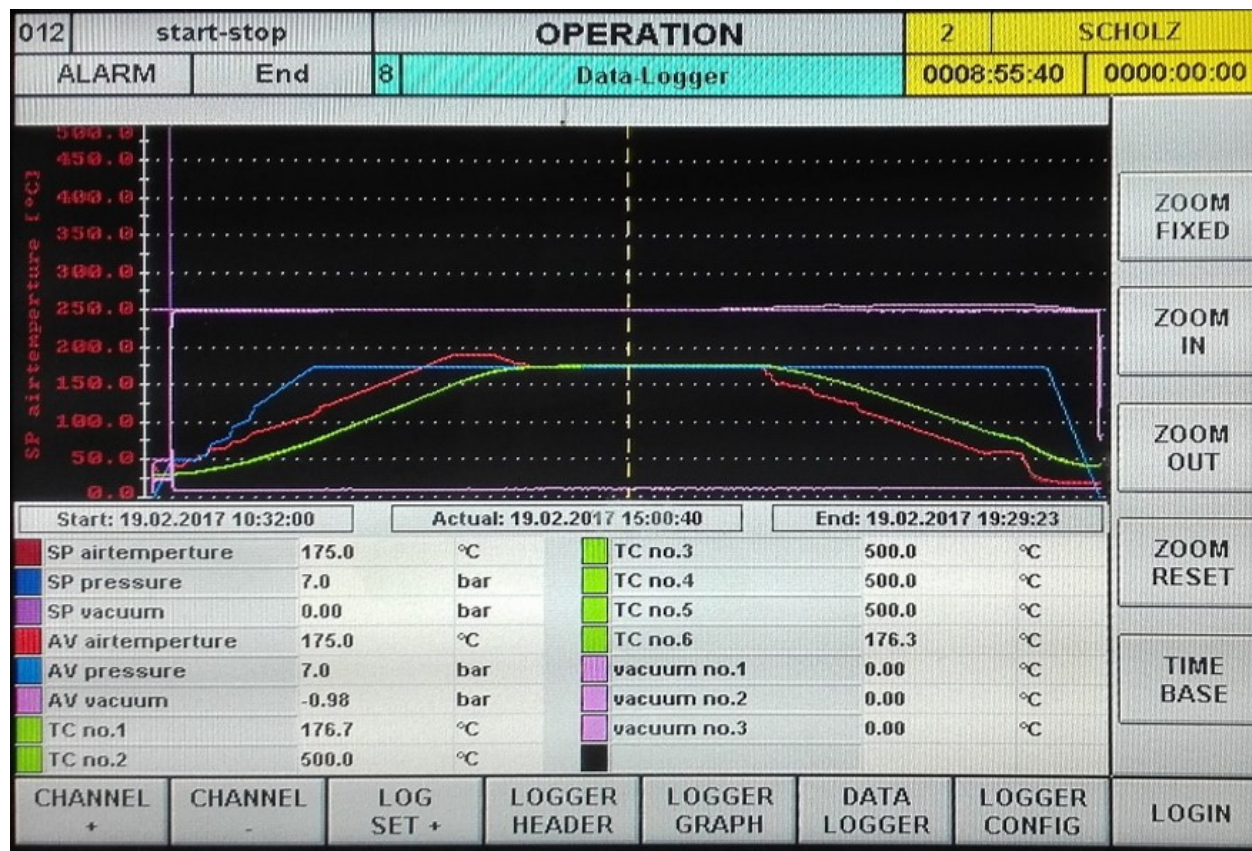


Figure A.8.15: Curing log-data



Figure A.8.16: Rim shell under demoulding



Figure A.8.17: Removal of release film



Figure A.8.18: Removal of peel ply before demoulding

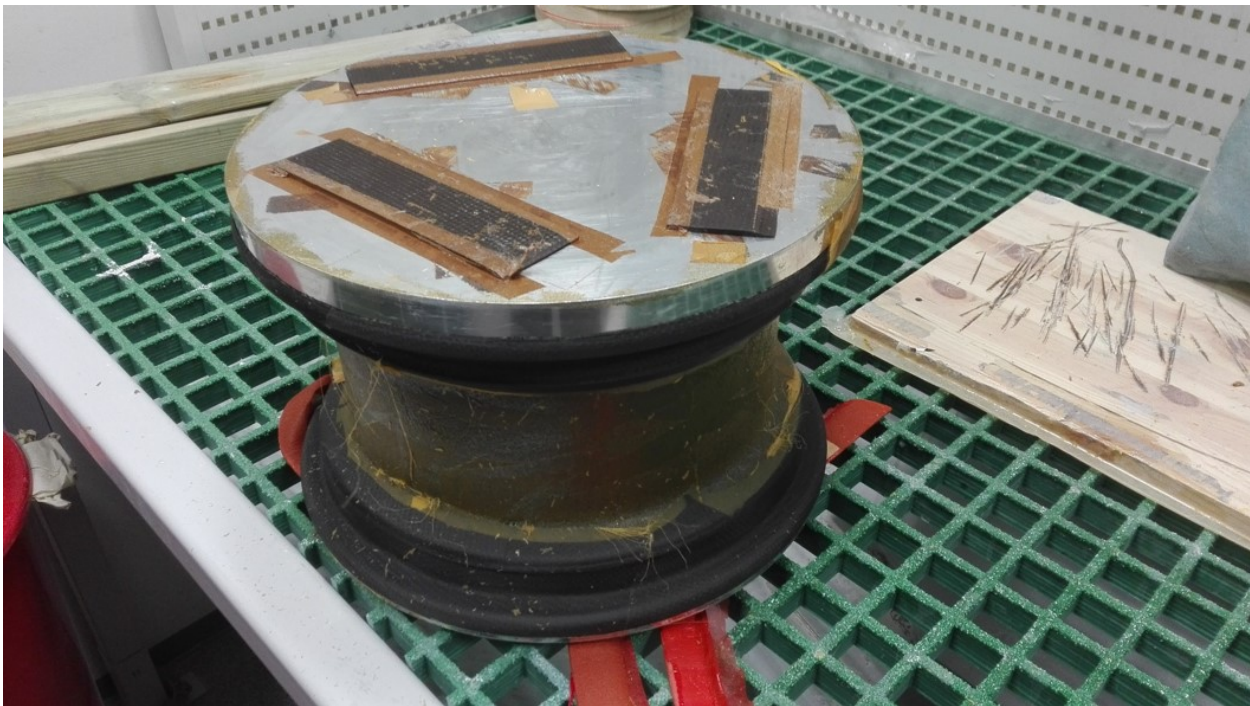


Figure A.8.19



Figure A.8.20: Finished cured and demulded rim shell, here on a scale for controlling the weight

A.9 2014 LAYUP - USED TO BENCHMARK OPTIMIZED LAYUP

Ply.	OF	OB	OD	CM	CS	ID	IB	IF
1	S o	S o	S o	S o	S o	S o	S o	S o
2	S o	S o	S o	U o	U o	S 45	U o	S 45
3	S 45	U 90	S 45	U 90	U 90	S o	U 90	S 45
4	S 45	U 90	S 45	U o	U o	S o	U o	S 45
5	S o	U 90	S o	U 90	U 90	S 45	U 90	S 45
6	S o	U 90	S o	U o	U o	S o	U o	S o
7	-	S o	-	S 45	S 45	-	S 45	-
8	-	S o	-	S o	S o	-	S o	-

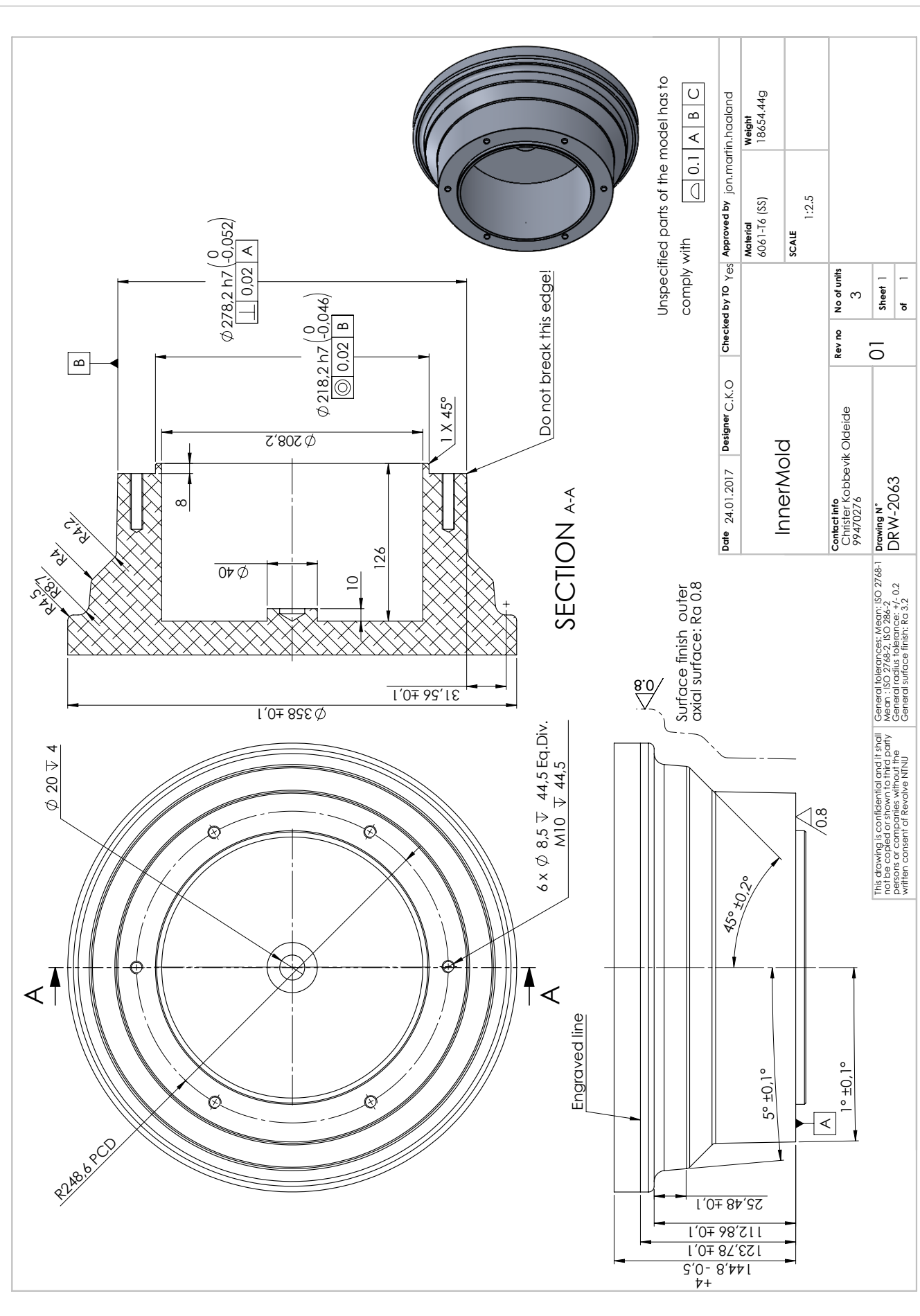
S - Satin weave

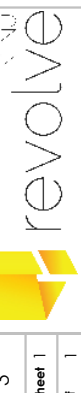
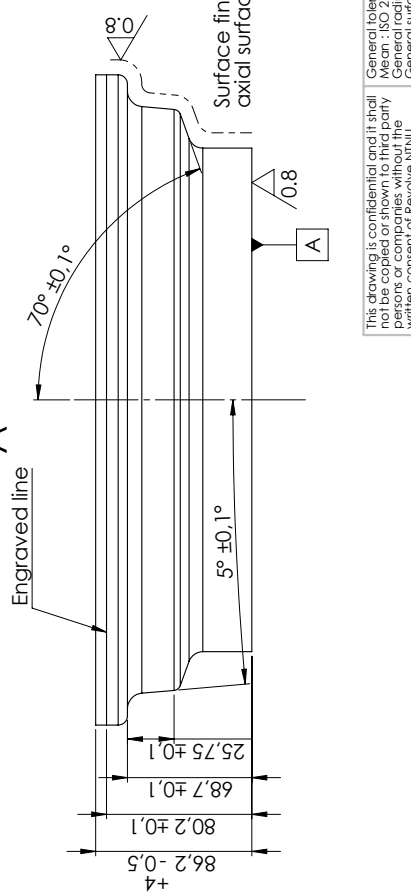
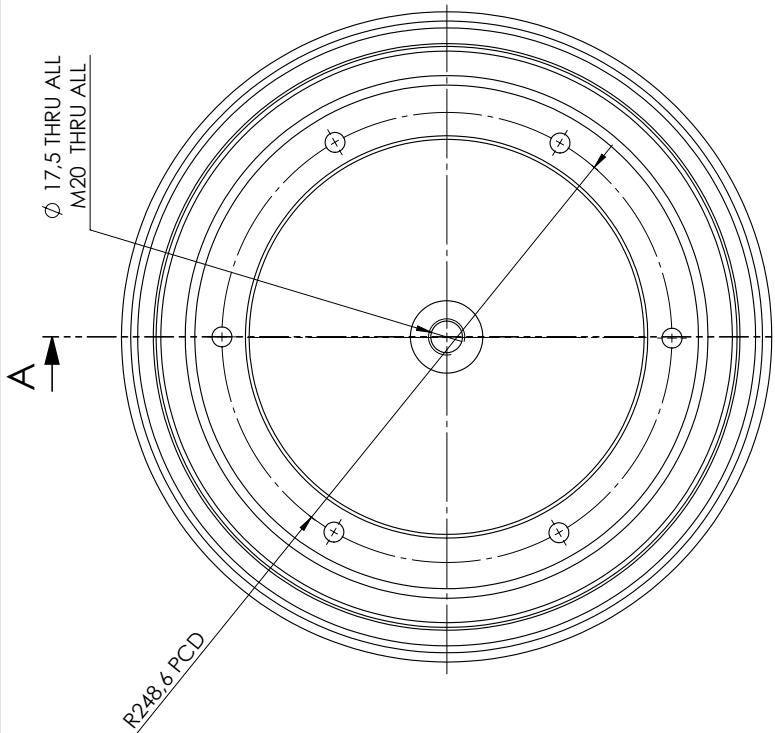
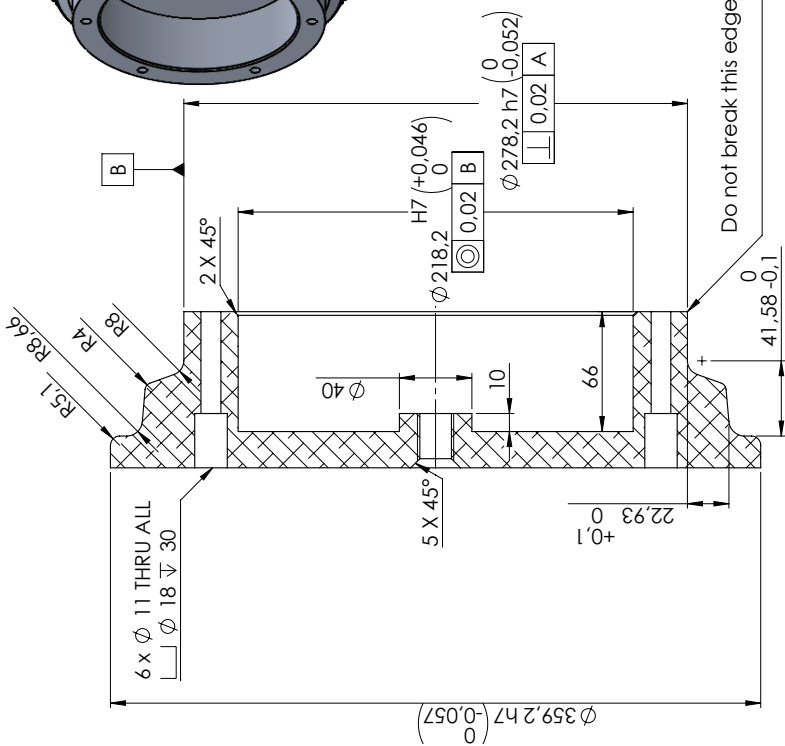
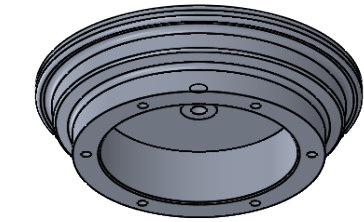
U - Unidirectional

B

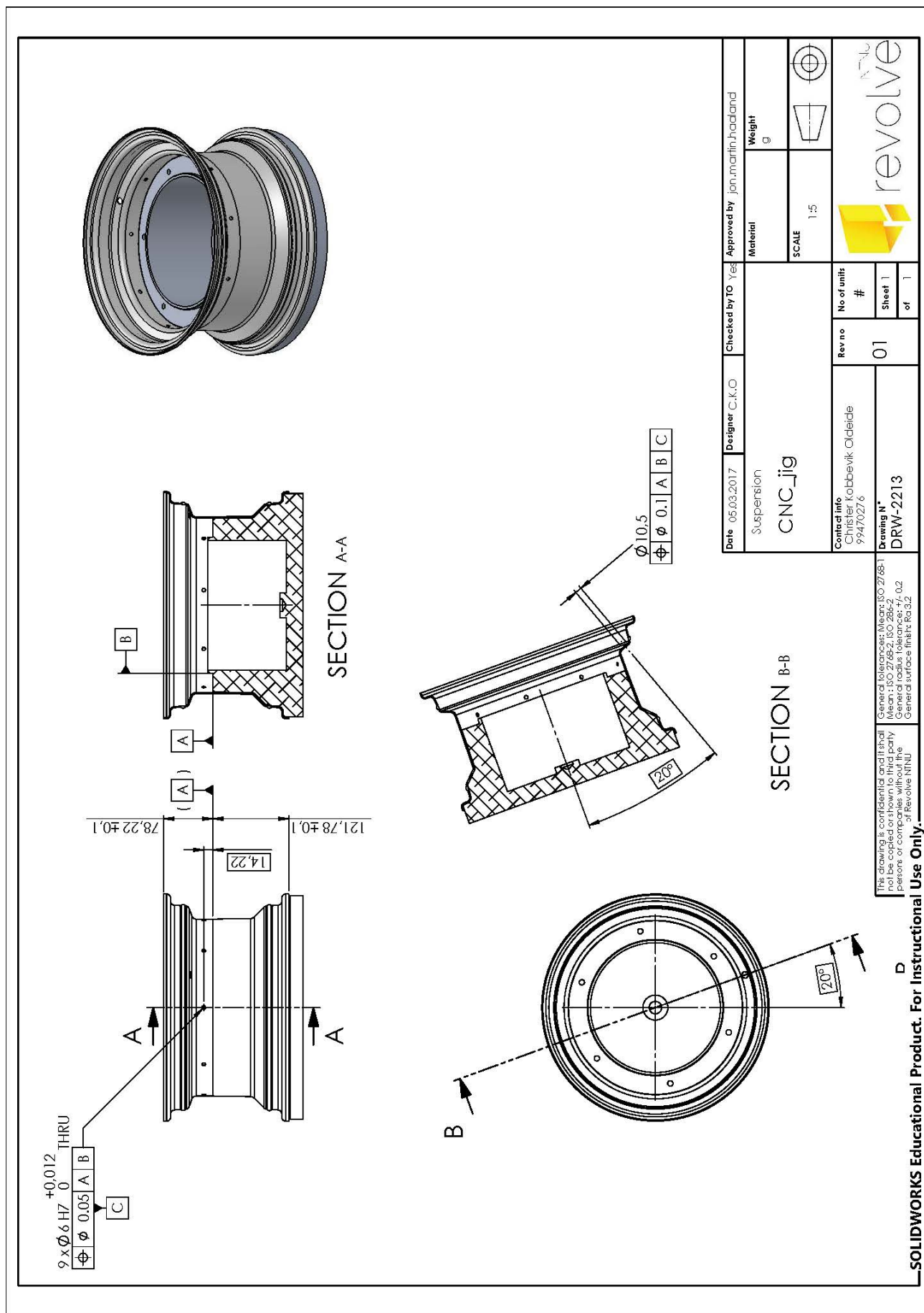
Machine Drawings

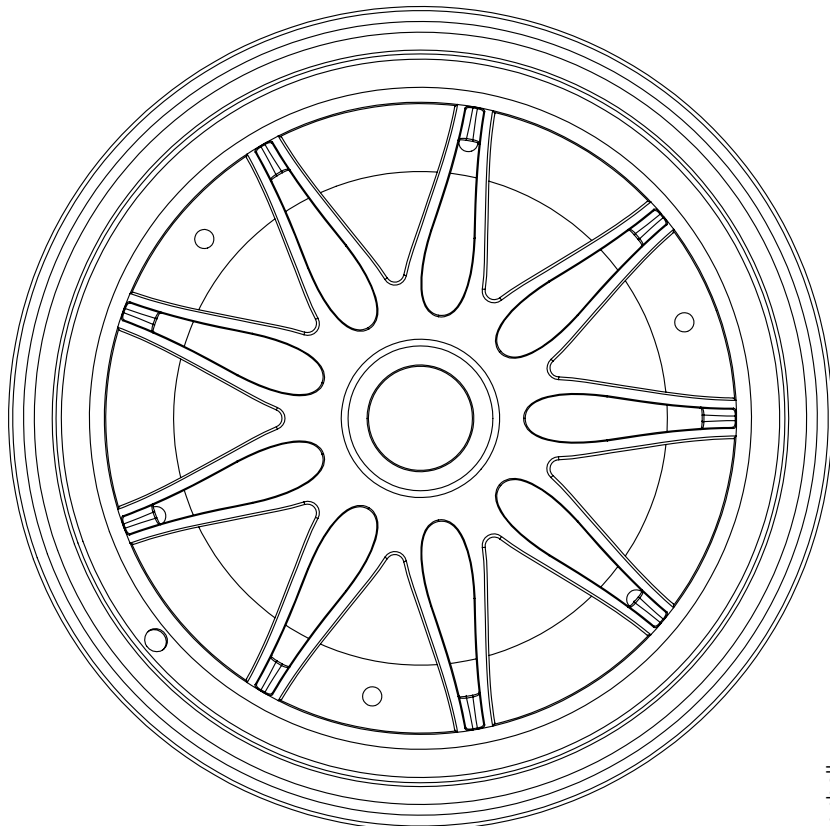
B.2 MACHINE DRAWING - MOLDS



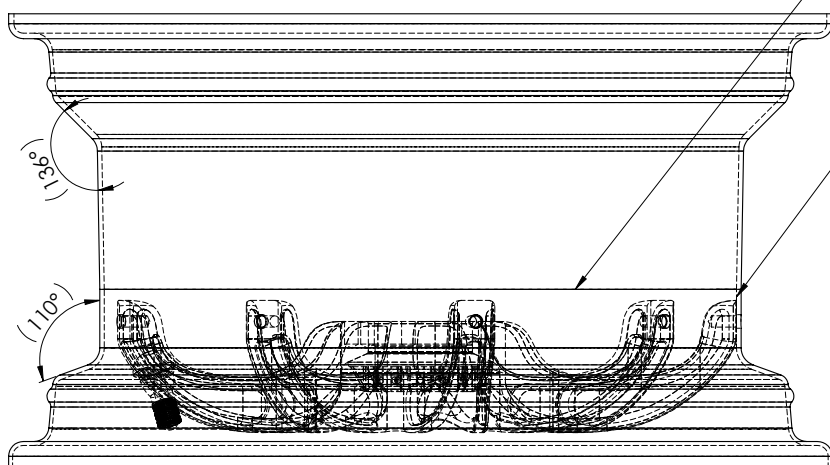


B.3 MACHINE DRAWINGS RIM SHELL





This line is visible on rim shell,
(EPOXY edge)



SOLIDWORKS® 2013 Product. For Instructional Use Only.

General tolerances: Mean: ISO 2768-1
Mean: ISO 2768-2 ISO 286-2
General radius tolerance: +/- 0.2
General surface finish: Ra 3.2

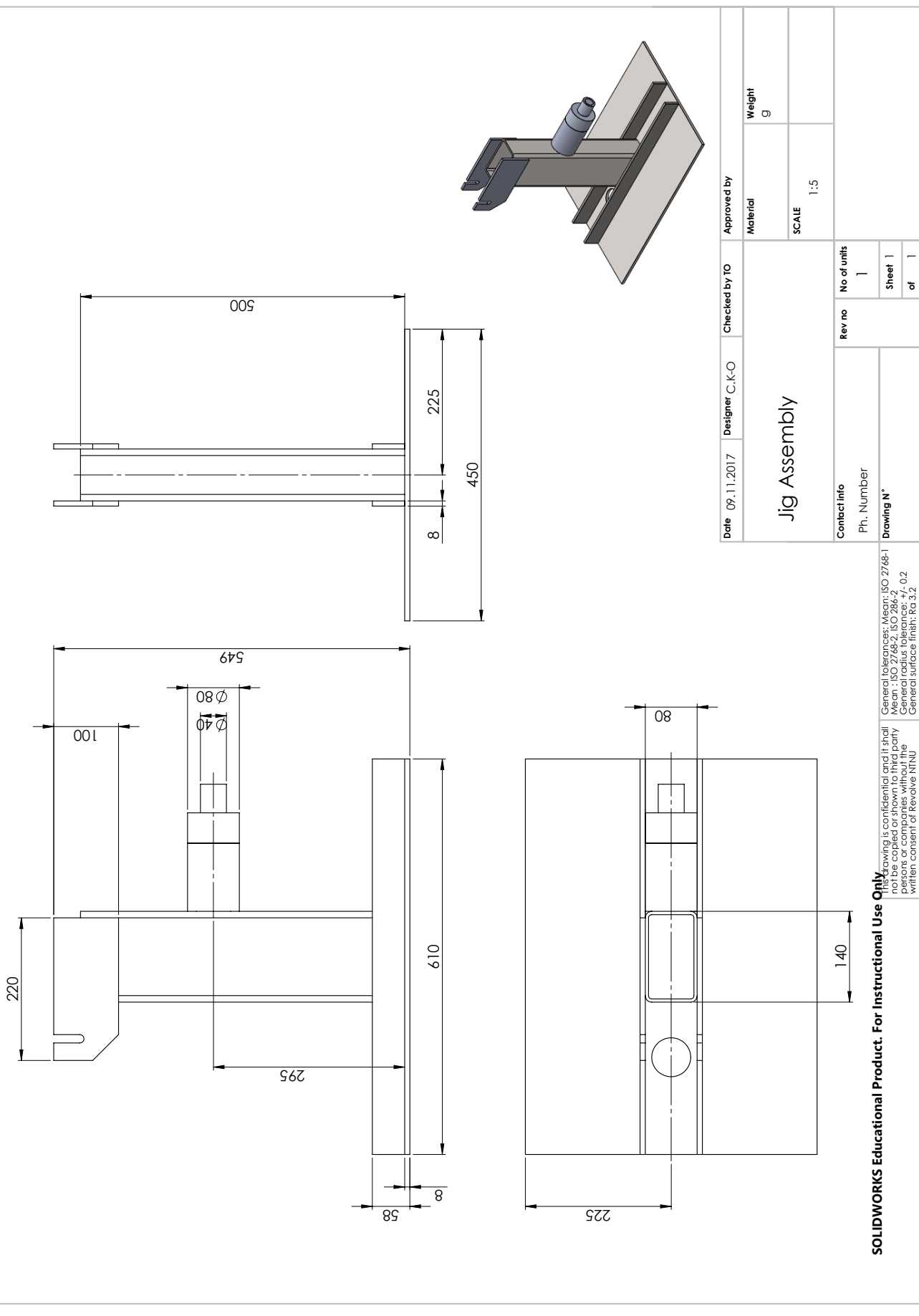
Date	Designer	Checked by	Approved by	Material	Weight
21.02.2017	C.K.O				
				SCALE 1:2	

Rim_ASS
Contact Info
Christen Kobbevik Oldeide
974/0276

Rev no	No of units	#	Sheet 1 of 1
01			

Drawing N°
DRW-2193

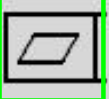
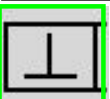
B.4 BASE DIMENSIONS OF TEST JIG



C

Measuring Reports & Standards

C.1 MEASURING RAPORT RIM CENTER

ZEISS Calypso		MJØS METALLVAREFABRIKK AS	ZEISS	
Measurement Plan NTNU DRW2189	Date March 1, 2017	Operation no 40		
Drawing No. DRW2189	Time 9:39:56 am	Order 33112		
Inspector Øystein Nordås	Customer name Øystein	Incremental Part Number 1		
Actual	Nominal	Upper Tol.	Lower Tol.	Deviation
 Overall Result				
All Characteristics: ...in Tolerance: 6				
...Out of tolerance: 0				
...Over Warning Limit: 0				
...Not Calculated: 0				
Total Coord. systems: 0				
...Not Calculated: 0				
Total Text elements: 0				
 Flatness Ref A 0.05	0.001	0.000	0.050	0.001
 Diameter 46H9	46.027	46.000	0.062	- 0.027
 Diameter_Cylinder2	278.722	278.720	0.020	- -0.020 0.002
 Perpendicularity 0.05 to A	0.001	0.000	0.050	0.001
 Cylindricity 0.05	0.016	0.000	0.050	-- 0.016
 Curve Form1 Shape Of Zone: Standard	0.088	0.000	0.100	-- -0.100 0.088

ZEISS Calypso



Measurement Plan
NTNU DRW2189 Opr-50

Date
March 1, 2017

Operation no
1

Drawing No.
* drawingno *

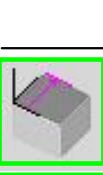
Time
9:41:47 am

Order

Inspector
Øystein Nordås

Customer name
Mjøs Metallvarefabrikk AS

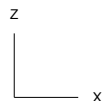
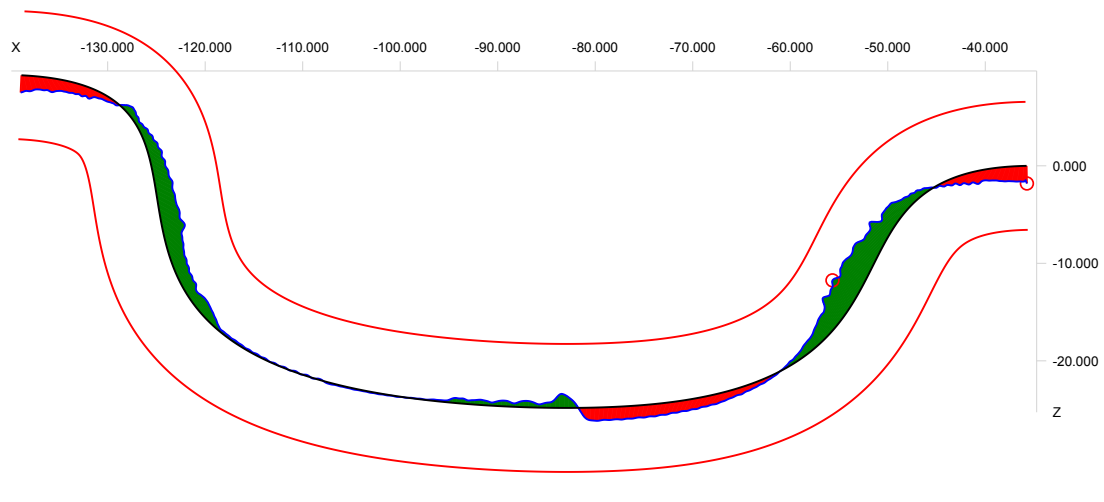
Incremental Part Number
2

	Actual	Nominal	Upper Tol.	Lower Tol.	Deviation
Overall Result					
All Characteristics:	4				
...in Tolerance:	4				
...Out of tolerance:	0				
...Over Warning Limit:	0				
...Not Calculated:	0				
Total Coord. systems:	0				
...Not Calculated:	0				
Total Text elements:	0				
 Y Value_Intersection1	14.002	14.000	0.100	-0.100	0.002
 Profile2	0.027	0.000	0.050		0.027
 Curve Form2 Shape Of Zone: Standard	0.032	0.000	0.100	-0.100	0.032

C.2 MEASURING RAPORT RIM SHELL - INNER CONTOUR

	Calypso 6.0.1202	Carl Zeiss	Date February 28, 2017
Part Number 7	CMM Type ACCURA_2	Drawing No. DRW2189	Order 33112
Department: Operator Signature:	Master		
Meas. Plan Name NTNU DRW2189			

1: Curve Form1



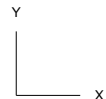
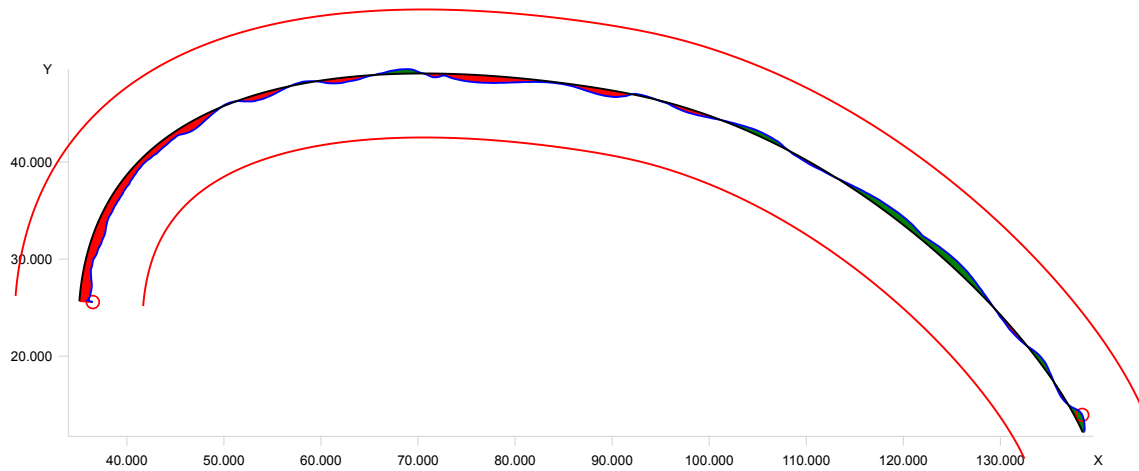
0.1 mm
100 : 1

No	Identifier	Sigma [mm]	Form [mm]	Number of Points	Lower Tol. [mm]	Upper Tol. [mm]	MinInd	Min Dev. [mm]	MaxInd	Max Dev. [mm]
1	Curve Form1	0.019	0.088	1000	-0.100	0.100	998	-0.043	817	0.045
	Best Fit	Translation	X [mm]-0.011	Y [mm]0.000	Z [mm]0.012	Rotation	X 0.000	Y 0.015	Z 0.000	

C.3 MEASURING RAPORT RIM SHELL - OUTER CONTOUR

 Calypso 6.0.1202	Carl Zeiss		Date Order	March 1, 2017
Part Number 2	CMM Type ACCURA_2		Drawing No.	Department: Operator Master Signature:
Meas. Plan Name NTNU DRW2189 Opr-50				

1: Curve Form2



0.1 mm
100 : 1

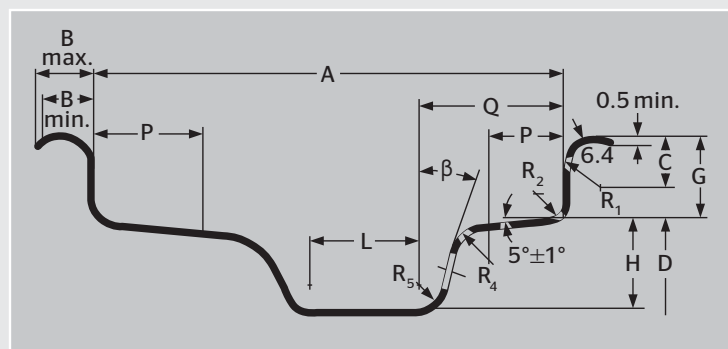
No	Identifier	Sigma [mm]	Form [mm]	Number of Points	Lower Tol. [mm]	Upper Tol. [mm]	MinInd	Min Dev. [mm]	MaxInd	Max Dev. [mm]
1	Curve Form2	0.007	0.032	993	-0.100	0.100	977	-0.021	29	0.011
	Best Fit	Translation	X [mm] 0.000	Y [mm] 0.000	Z [mm] 0.000	Rotation	X 0.000	Y 0.000	Z 0.000	

C.4 ETRTO STANDARD FOR DROP CENTER AND HUMP DESIGN

all tyre brands of Continental 95

R_4 and R_5 : between
4 and 10 mm
 R_5 : not larger than 10 mm

Valve Hole-Ø:
11.5 mm ($11.3_{-0}^{+0.4}$) centrally
in the side of the rim well.
16.0 mm ($15.7_{-0}^{+0.4}$)
only with Ø-Code 15.



Rim Contour	A	Dimensions (mm)											
		Min.	B Max. 1)	G ± 0,6	P	H Min. 2)	L Min.	Q	R ₁ Min.	R ₂ Max.	β Min.		
3.00 B	76				13		16	28			10°		
3.50 B	89				15		19	34					
4.00 B	101.5	10	13	14.1		15			7.5	4.5	13°		
4.50 B	114.5				19.5		22	45					
5.00 B	127												
5.50 B	139.5												
6.00 B	152.5												
3 J	76				13		16	28			10°		
3 ½ J	89				15		19	34					
4 J	101.5												
4 ½ J	114.5												
5 J	127												
5 ½ J	139.5												
6 J	152.5												
6 ½ J	165												
7 J	178												
7 ½ J	190.5												
8 J	203												
8 ½ J	216												
9 J	228.5												
9 ½ J	241.5												
10 J	254												
10 ½ J	266.5												
11 J	279.5												
11 ½ J	292												
12 J	305												
12 ½ J	317.5												

¹⁾ B max. values may be exceeded on rims for light commercial vehicles

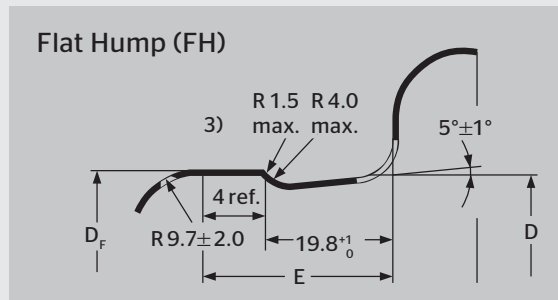
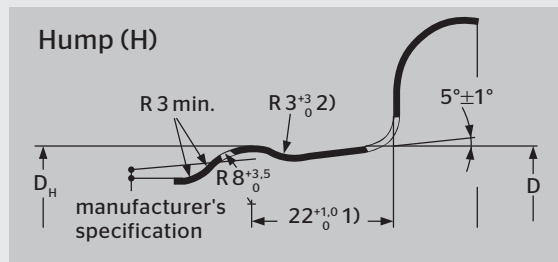
²⁾ Minimum dimensions for well depth (H) and well angle are required for tyre mounting

Rim diameter

Code (ins)	12	13	14	15	16	17	18	19	20	21	22	23	24
D (mm)	304.0	329.4	354.8	380.2	405.6	436.6	462.0	487.4	512.8	538.2	563.6	589.0	614.4

Special rim executions for passenger cars

In many countries safety rims must be used for tubeless radial tyres.



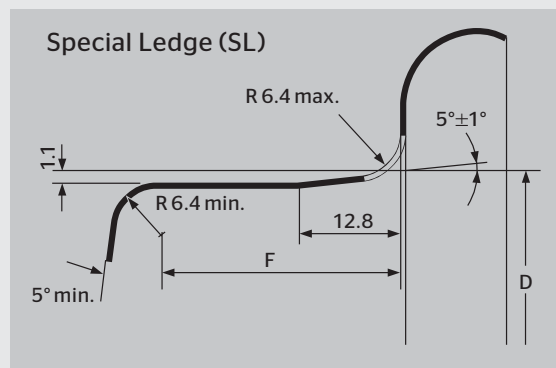
¹⁾ In most car rims 19.8 mm.

²⁾ For B-Rims R = 8.5 mm max. resp. R = 4 ± 1 mm.

³⁾ Deburred.

These **full-drop centre rims with safety shoulders** for cars, estate cars and light trucks are marked with the following codes shown after rim size designation:

- H** = one-sided round hump on outer shoulder (formerly: H 1)
- H2** = double round hump
- FH** = flat hump on outer shoulder (formerly: FHA 1)
- FH2** = double flat hump (formerly: FHA 2)
- CH** = combination hump = flat hump on outer shoulder, round hump on inner shoulder (formerly: FHA-H)
- SL** = special ledge
- EH2/2+** = Extended Hump (with extended hump on both sides)
(see following page)



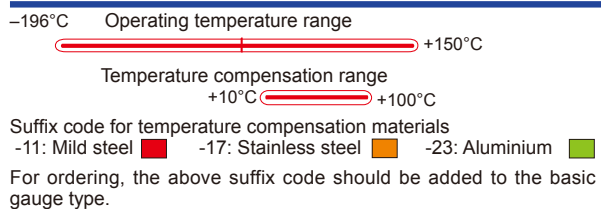
Ledge	Rim diameter Code (ins)	Dimensions (mm)		
		H	FH	
		Circumference $\pi \cdot D_H (+ 0/-3)$	Circumference $\pi \cdot D_F (+ 0/-3)$	E Max.
B	12	957.6	-	-
	13	1037.0	1034.8	24.5
	14	1116.8	1114.6	
J	13	1037.0	1034.8	28.5
	14	1116.8	1114.6	
	15	1196.6	1194.4	
	16	1276.4	1274.2	
	17	1373.8	1371.6	
	18	1453.6	1451.4	
	19	1533.4	1531.2	
	20	1613.2	1611.0	
	21	1693.0	1690.8	
	22	1772.8	1770.6	
	23	1852.6	1850.4	
	24	1932.4	1930.2	

D

Datasheets

D.1 STRAIN GAUGE FRA-5-11-3L

Developing Strain Gauges and Instruments



FOIL STRAIN GAUGES series F

Applicable adhesives

CN	-196 ~ +120°C
P-2	-30 ~ +150°C
EB-2	-60 ~ +150°C

GENERAL USE

Gauge pattern	Basic type	Gauge size L W	Backing L W	Resistance Ω
0°/90° 2-element Rosette Stacked: FCA	M metal G general			
	FCA-1 FCA-2 FCA-3 FCA-5 FCA-6 FCA-10	1 0.7 ϕ 4.5 2 0.9 ϕ 7 3 1.7 ϕ 11 5 1.9 ϕ 12 6 2.4 ϕ 14 10 2.5 ϕ 17		120 120 120 120 120 120
350Ω 0°/90° 2-element Rosette Stacked: FCA				
	FCA-1-350 (x 3) FCA-2-350 (x 3) FCA-5-350 (x 3)	1 1.6 ϕ 8 2 1.9 ϕ 9.5 3 2 ϕ 10 5 1.8 ϕ 10		350 350 350 350
0°/45°/90° 3-element Rosette Stacked: FRA				
	FRA-1 FRA-2 FRA-3 FRA-5 FRA-6 FRA-10	1 0.7 ϕ 4.5 2 0.9 ϕ 7 3 1.7 ϕ 11 5 1.9 ϕ 12 6 2.4 ϕ 14 10 2.5 ϕ 17		120 120 120 120 120 120

FOIL STRAIN GAUGES

series F

Suffix code for temperature compensation materials
 -11: Mild steel -17: Stainless steel -23: Aluminium
 For ordering, the above suffix code should be added to the basic gauge type.

-196°C Operating temperature range +150°C

Temperature compensation range
 +10°C +100°C

Applicable adhesives	CN	-196 ~ +120°C
	P-2	-30 ~ +150°C
	EB-2	-60 ~ +150°C

GENERAL USE

Gauge pattern	Basic type	Gauge size L W	Backing L W	Resistance Ω
Example of type number designation FLA-5 -350 -11 -3LJB/-3LJBT (2-wire/3-wire) Length in meter and type of integral leadwire(* ¹) Self-temperature-compensation number(* ²) Gauge resistance in ohm (Blank for 120Ω) Basic strain gauge type and gauge length	* ¹ : Not mentioned for gauges without leadwire * ² : The following numbers are available for F series gauges -11: Mild steel (11ppm/°C) -17: Stainless steel, Copper alloy (17ppm/°C) -23: Aluminium (23ppm/°C)			
350Ω 0°/45°/90° 3-element Rosette Stacked: FRA				Each package contains 10 gauges.
 FRA-1-350 (x 3) FRA-2-350 FRA-5-350	FRA-1-350 FRA-2-350 FRA-3-350 FRA-5-350	1 1.6 ϕ 8 350 2 1.9 ϕ 9.5 350 3 2 ϕ 10 350 5 1.8 ϕ 10 350		

SPECIAL USE

Gauge pattern	Basic type	Gauge size L W	Backing L W	Resistance Ω
Option F This code is appended to the basic type for strain gauges with lead-free solder in place of leaded solder. Fatigue life of the strain gauge may become shorter by the lead-free solder.	Example of type number designation FLT-05A -11 -350 -F -3LJC -F Option F : LEAD-free soldering of leadwire Option F: LEAD-free soldering of strain gauge Gauge resistance (Blank for 120Ω) Self-temperature-compensation number Basic strain gauge type			
Shearing strain measurement : FLT				Each package contains 10 gauges.
 Gauge Length Gauge backing length	Left 45° FLT-05A Right 45° FLT-05B	0.5 0.66 4 1.3 120 0.5 0.66 4 1.3 120		
Torque measurement : FCT				Each package contains 10 gauges.
 Gauge Length Gauge backing length Gauge base width	 FCT-2 FCT-2-350	2 1.5 8.7 6.5 120 2 1.5 7.6 5.3 350		

D.2 ALUMINUM 7075 (7075-T651)



Aluminum 7075-T6; 7075-T651

Subcategory: 7000 Series Aluminum Alloy; Aluminum Alloy; Metal; Nonferrous Metal

Close Analogs: none

Composition Notes: A Zr + Ti limit of 0.25 percent maximum may be used with this alloy designation for extruded and forged products only, but only when the supplier or producer and the purchaser have mutually so agreed. Agreement may be indicated, for example, by reference to a standard, by letter, by order note, or other means which allow the Zr + Ti limit.

Aluminum content reported is calculated as remainder.

Composition information provided by the Aluminum Association and is not for design.

Key Words: Aluminium 7075-T6; Aluminium 7075-T651, UNS A97075; ISO AlZn5.5MgCu; Aluminium 7075-T6; Aluminium 7075-T651; AA7075-T6

Component	Wt. %
Al	87.1 - 91.4
Cr	0.18 - 0.28
Cu	1.2 - 2
Fe	Max 0.5

Component	Wt. %
Mg	2.1 - 2.9
Mn	Max 0.3
Other, each	Max 0.05
Other, total	Max 0.15

Component	Wt. %
Si	Max 0.4
Ti	Max 0.2
Zn	5.1 - 6.1

Material Notes: General 7075 characteristics and uses (from Alcoa): Very high strength material used for highly stressed structural parts. The T7351 temper offers improved stress-corrosion cracking resistance.

Applications: Aircraft fittings, gears and shafts, fuse parts, meter shafts and gears, missile parts, regulating valve parts, worm gears, keys, aircraft, aerospace and defense applications; bike frames, all terrain vehicle (ATV) sprockets.

Data points with the AA note have been provided by the Aluminum Association, Inc. and are NOT FOR DESIGN.

Physical Properties	Metric	English	Comments
Density	2.81 g/cc	0.102 lb/in³	AA; Typical
Mechanical Properties	Metric	English	Comments
	150	150	AA; Typical; 500

CRP MECCANICA S.r.l.

Sede Legale e Amministrativa/Headquarters and Administration Office

Via Cesare Della Chiesa 21 - 41126 Modena

Tel./Phone +39-059-330544/821135/826025

Fax +39-059-822071/381148

C.F./ P.IVA/Registro Imprese Modena IT00782680367 (VAT number)

Capitale sociale Euro 564.000 i. v.



Hardness, Brinell			g load; 10 mm ball
Hardness, Knoop	191	191	Converted from Brinell Hardness Value
Hardness, Rockwell A	53,50	53,50	Converted from Brinell Hardness Value
Hardness, Rockwell B	87	87	Converted from Brinell Hardness Value
Hardness, Vickers	175	175	Converted from Brinell Hardness Value
Ultimate Tensile Strength	572 MPa	83000 psi	AA; Typical
Tensile Yield Strength	503 MPa	73000 psi	AA; Typical
Elongation at Break	11 %	11 %	AA; Typical; 1/16 in. (1.6 mm) Thickness
Elongation at Break	11 %	11 %	AA; Typical; 1/2 in. (12.7 mm) Diameter
Modulus of Elasticity	71.7 GPa	10400 ksi	AA; Typical; Average of tension and compression. Compression modulus is about 2% greater than tensile modulus.
Poisson's Ratio	0.33	0.33	
Fatigue Strength	159 MPa	23000 psi	AA; 500,000,000 cycles completely reversed stress; RR Moore machine/specimen
Fracture Toughness	20 MPa-m ^{1/2}	18.2 ksi-in ^{1/2}	K(IC) in S-L Direction
Fracture Toughness	25 MPa-m ^{1/2}	22.8 ksi-in ^{1/2}	K(IC) in T-L Direction
Fracture Toughness	29 MPa-m ^{1/2}	26.4 ksi-in ^{1/2}	K(IC) in L-T Direction
Machinability	70 %	70 %	0-100 Scale of Aluminum Alloys
Shear Modulus	26.9 GPa	3900 ksi	
Shear Strength	331 MPa	48000 psi	AA; Typical
Electrical Properties	Metric	English	Comments
Electrical Resistivity	5.15e-006 ohm-cm	5.15e-006 ohm-cm	AA; Typical at 68°F
Thermal Properties	Metric	English	Comments

CRP MECCANICA S.r.l.

Sede Legale e Amministrativa/Headquarters and Administration Office

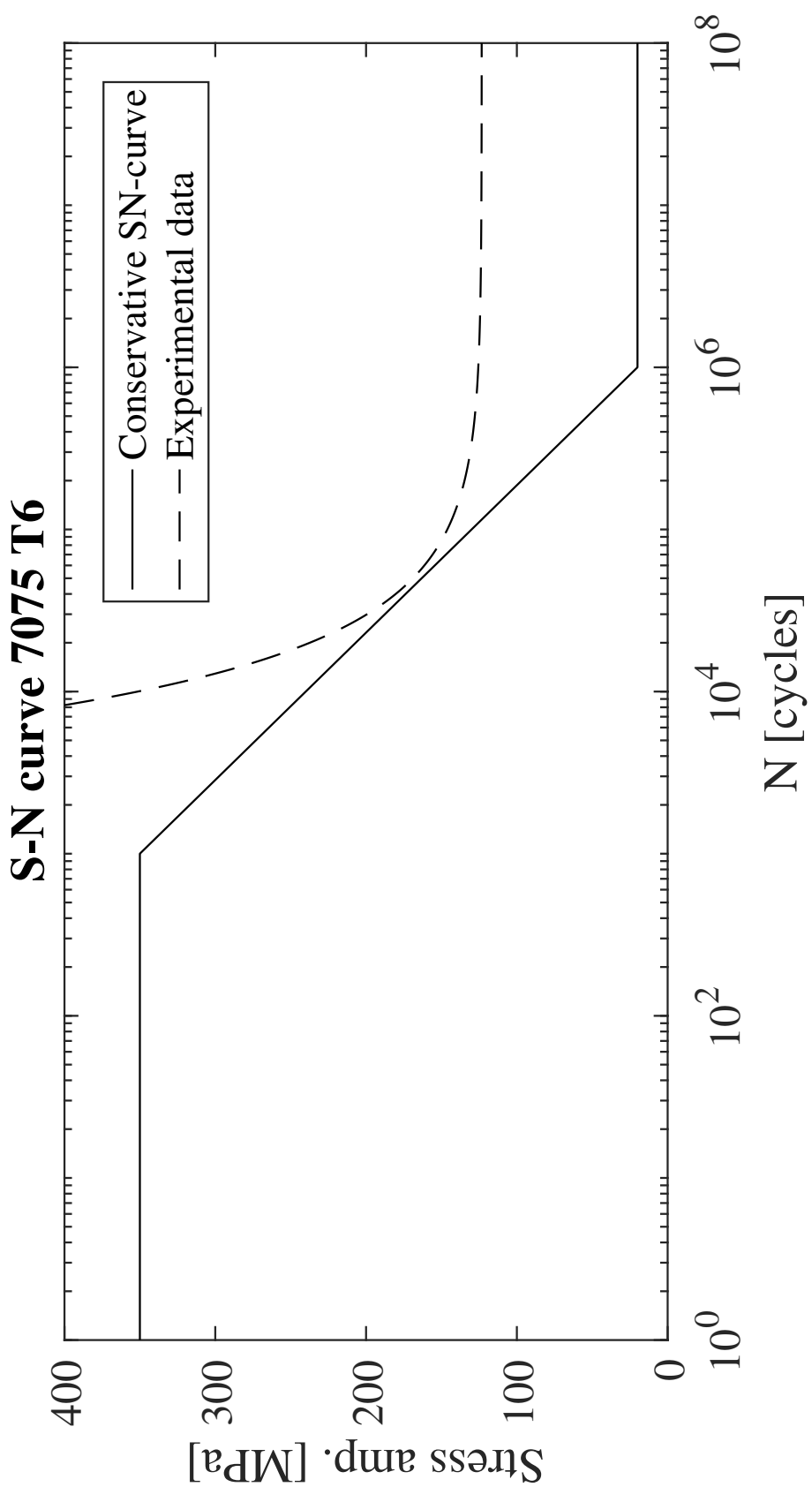
Via Cesare Della Chiesa 21 - 41126 Modena

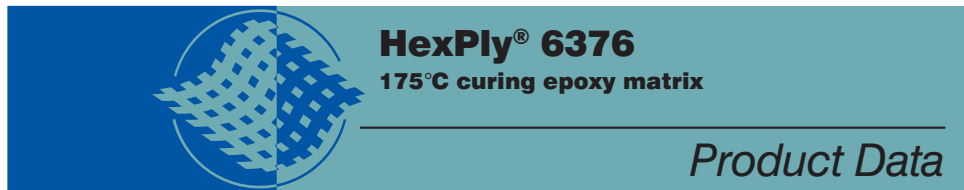
Tel./Phone +39-059-330544/821135/826025

Fax +39-059-822071/381148

C.F./ P.IVA/Registro Imprese Modena IT00782680367 (VAT number)

Capitale sociale Euro 564.000 i. v.





Description

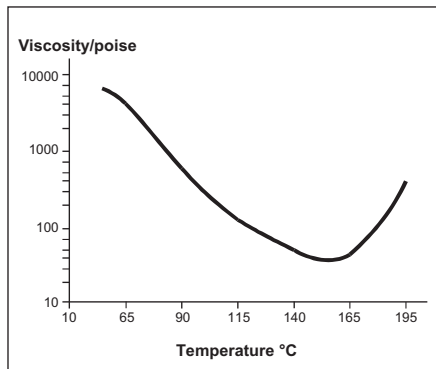
HexPly 6376 is a high performance tough matrix formulated for the fabrication of primary aircraft structures. It offers high impact resistance and damage tolerance for a wide range of high temperature applications.

Benefits and Features

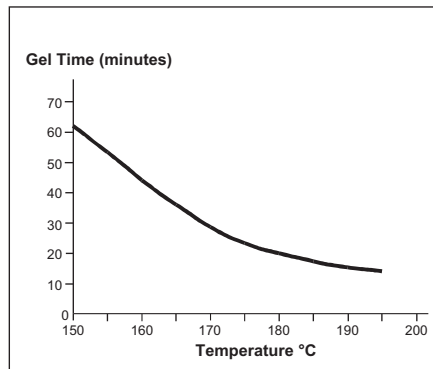
- Excellent toughness and damage tolerance
- Simple straight-up cure cycle
- Controlled matrix flow for ease of processing
- Effective translation of fibre properties
- Good hot/wet properties up to 150°C

Resin Matrix Properties

Rheology



Gel Time





Cured Matrix Properties (cured at 175°C)

		Method
Tensile strength	105 MPa	ISO R527 type 1
Tensile modulus	3.60 GPa	ISO R527 type 1
Tensile strain	3.1%	ISO R527 type 1
Flexural strength	144 MPa	ISO 178
Flexural modulus	4.4 GPa	ISO 178
Toughness G_{ic}	432 J/m ²	Tested in accordance with EGF Task Group on Polymers and Composites protocol.
Cured density	1.31 g/cm ³	

Prepreg Curing Conditions

2 hours at 175°C and 700kN/m² (7 bar) pressure.

Heat up rate 2°C to 5°C.

Components up to 30 mm thick can be cured without a dwell in the schedule provided that the heat-up rate is not more than 3°C/minute. There is no deterioration in performance after 3 times the recommended cure schedule (verified by interlaminar shear strength tests).

Prepreg Storage Life

- Tack Life @ 23°C 10 days (still processable for up to 21 days).
- Guaranteed Shelf Life @ -18°C 6 months (minimum)
- Storage conditions.

HexPly 6376 prepgs should be stored as received in a cool dry place or in a refrigerator. After removal from refrigerator storage, prepreg should be allowed to reach room temperature before opening the polythene bag, thus preventing condensation. (A full reel in its packaging can take up to 48 hours).

Precautions for Use

The usual precautions when handling uncured synthetic resins and fine fibrous materials should be observed, and a Safety Data Sheet is available for this product. The use of clean disposable inert gloves provides protection for the operator and avoids contamination of material and components.

Important

All information is believed to be accurate but is given without acceptance of liability. Users should make their own assessment of the suitability of any product for the purposes required. All sales are made subject to our standard terms of sale which include limitations on liability and other important terms.

©Copyright Hexcel Corporation
Publication FTA051b (March 2007)

For More Information

Hexcel is a leading worldwide supplier of composite materials to aerospace and other demanding industries. Our comprehensive product range includes:

- Carbon Fibre
- RTM Materials
- Honeycomb Cores
- Continuous Fibre Reinforced Thermoplastics
- Carbon, glass, aramid and hybrid prepgs
- Reinforcement Fabrics
- Structural Film Adhesives
- Honeycomb Sandwich Panels
- Special Process Honeycombs

For US quotes, orders and product information call toll-free 1-800-688-7734

For other worldwide sales office telephone numbers and a full address list please go to:

<http://www.hexcel.com/contact/salesoffices>

**Description**

HexPly® 6376C-905-36% is a Epoxy High Strength Carbon Woven prepeg, whereby 6376 is the resin type; 36% is the resin content by weight; 905 is the reinforcement reference and C represents High Strength Carbon fibre. This data sheet is complementary to the 6376 resin data sheet, which should be consulted for additional information.

Reinforcement Data

		0°	90°
Nominal Area Weight	g/m ²	280	140
Composition		5H satin	
Fibre Type		High Strength Carbon 3K	
Nominal Fibre Density	g/cm ³	1,77	

Matrix Properties

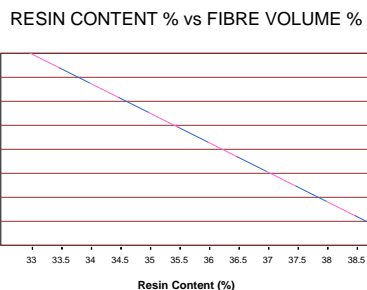
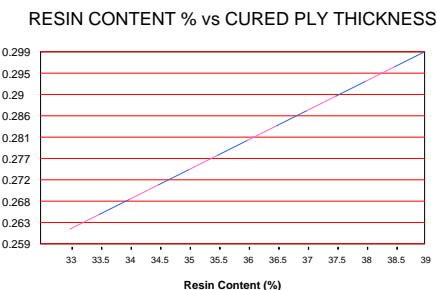
Glass transition temperature of laminate (Cure cycle: 120min @ 175°C)	°C	196 (DMA onset, 5°C/min, 1Hz, 30μm),
Nominal Resin Density	g/cm ³	1,31

Prepreg Data

Nominal Area Weight	g/m ²	438
Nominal Resin Content	weight %	36
Tack Level		Medium

Processing

Cure Cycle	@ 175 °C	120 min
Recommended heat up rate	°C/min	2 - 5°C/min
Pressure gauge	bar	7
The optimum cure cycle, heat up rate and dwell period depend on part size, laminate construction, oven capacity and thermal mass of tool. (See prepreg technology brochure on our website for more information),		

Cured Laminate Properties(nominal composite density 1.57 g/cm³)

The above graphs enable the fibre volume content of a laminate to be estimated using the measured cured ply thickness. The calculation assumes no resin loss.



For other worldwide sales office telephone numbers
and a full address list please go to :
<http://www.hexcel.com/contact/salesoffices>



Mechanical Properties

(Normalised to 60% fibre volume, except for ILSS)

Mechanical Properties are based on 175 °C cure for 120 min, at 7 bar pressure and 0,9 bar vacuum.

Data is the result from several tests on Autoclave cured laminates. Some of the values achieved will have been higher, and some lower, than the figure quoted. These are nominal values.

Warp (RT / Dry)	Tensile	Flexural	ILSS	Compression
Strength (MPa)	1006	-	83	920
Modulus (GPa)	67	-	-	-
Test Method	EN 2561		EN 2563	EN 2850

Prepreg Storage Life

Shelf Life¹: 6 months at -18°C/0°F (from date of manufacture).

¹ Shelf Life: the maximum storage life for HexPly® prepreg, when stored continuously, in a sealed moisture-proof bag, at -18°C/0°F or 5°C/41°F. To accurately establish the exact expiry date, consult the box label.

Out Life²: 21 days at Room Temperature.

² Out Life: the maximum accumulated time allowed at room temperature between removal from the freezer and cure.

Tack Life³: 10 days at Room Temperature.

³ Tack Life: the time, at room temperature, during which prepreg retains enough tack for easy component lay-up.

Prepreg should be stored as received in a cool dry place or in a refrigerator. After removal from refrigerator storage, prepreg should be allowed to reach room temperature before opening the polyethylene bag, thus preventing condensation. (A full reel in its packing can take up to 48 hours).

Precautions for Use

The usual precautions when handling uncured synthetic resins and fine fibrous materials should be observed, and a Safety Data Sheet is available for this product. The use of clean disposable inert gloves provides protection for the operator and avoids contamination of material and components.

Important

All information is believed to be accurate but is given without acceptance of liability. All users should make their own assessment of the suitability of any product for the purposes required. All sales are made subject to our standard terms of sale which include limitations on liability and other terms

® Copyright Hexcel Corporation
HexPly® | 6376C-905-36% | 12/2005 | version : a



For other worldwide sales office telephone numbers
and a full address list please go to :
<http://www.hexcel.com/contact/salesoffices>



HexTow® IM7

Carbon Fiber



Product Data Sheet

HexTow® IM7 carbon fiber is a continuous, high performance, intermediate modulus, PAN based fiber available in 12,000 (12K) filament count tows. This fiber has been surface treated and can be sized to improve its interlaminar shear properties, handling characteristics, and structural properties. It is suggested for use in weaving, prepegging, filament winding, braiding, and pultrusion.

The unique properties of HexTow® IM7 fiber, such as higher tensile strength and modulus, as well as good shear strength, allow structural designers to achieve both higher safety margins for both stiffness and strength critical applications.

IM7-G 12K (0.25%) carbon fiber has been qualified to NMS 818 Carbon Fiber Specification (NCAMP). This allows customers to call out an industry standard, aerospace grade carbon fiber without the need to write and maintain their own specification.

Typical Fiber Properties		U.S. Units	SI Units
Tensile Strength			
6K		800 ksi	5,516 MPa
12K		820 ksi	5,654 MPa
Tensile Modulus (Chord 6000-1000)			
		40.0 Msi	276 GPa
Ultimate Elongation at Failure			
6K		1.9%	1.9%
12K		1.9%	1.9%
Density			
		0.0643 lb/in³	1.78 g/cm³
Weight/Length			
6K		12.5 x 10⁻⁶ lb/in	0.223 g/m
12K		25.0 x 10⁻⁶ lb/in	0.446 g/m
Approximate Yield			
6K		6,674 ft/lb	4.48 m/g
12K		3,337 ft/lb	2.24 m/g
Tow Cross-Sectional Area			
6K		1.94 x 10⁻⁴ in²	0.13 mm²
12K		3.89 x 10⁻⁴ in²	0.25 mm²
Filament Diameter			
		0.203 mil	5.2 microns
Carbon Content			
		95.0%	95.0%
Twist			
		Never Twisted	Never Twisted

Typical HexPly 8552 Composite Properties (at Room Temperature)	U.S. Units	SI Units	Test Method
0° Tensile Strength	395 ksi	2,723 MPa	ASTM D3039
0° Tensile Modulus	23.8 Msi	164 GPa	
0° Tensile Strain	1.6%	1.6%	
0° Flexural Strength	270 ksi	1,862 MPa	ASTM D790
0° Flexural Modulus	22.0 Msi	152 GPa	
0° Short Beam Shear Strength	18.5 ks	128 MPa	ASTM D2344
0° Compressive Strength	245 ksi	1,689 MPa	ASTM Mod. D695
0° Compressive Modulus	21.2 Msi	146 GPa	
0° Open Hole Tensile Strength	62 ksi	427 MPa	
0° Open Hole Compressive Strength	48.8 ksi	336 MPa	ASTM D6484
90° Tensile Strength	16.1 ksi	111 MPa	ASTM D3039
Fiber Volume	60%	60%	



HexTow® IM7 carbon fiber



Product Data Sheet

Yarn/Tow Characteristics	U.S. Units	SI Units
Specific Heat	0.21 Btu/lb-°F	0.21 cal/g-°C
Electrical Resistivity	4.9×10^{-5} ohm-ft	1.5×10^{-3} ohm-cm
Coefficient of Thermal Expansion	-0.36 ppm/°F	-0.64 ppm/°C
Thermal Conductivity	3.12 Btu/hr-ft-°F	5.40 W/m-°K

Carbon Fiber Certification

This carbon fiber is manufactured to Hexcel aerospace grade specification HS-CP-5000. A copy of this specification is available upon request. A Certification of Analysis will be provided with each shipment.

Available Sizing

Sizing compatible with various resin systems, based on application are available to improve handling characteristics and structural properties. Please see additional information on available Sizes on our website or contact our technical team for additional information.

Packaging

Standard packaging of HexTow® IM7 is as follows:

Filament Count	Nominal Weight		Nominal Length	
	(lb)	(kg)	(ft)	(m)
6K	4.0	1.8	26,400	8,050
12K	4.0	1.8	13,350	4,070

Other package sizes may be available on request. The fiber is wound on a 3-inch ID by 11-inch long cardboard tube and overwrapped with plastic film.

Safety Information

Obtain, read, and understand the Material Safety Data Sheet (MSDS) before use of this product.

For more information

Hexcel is a leading worldwide supplier of composite materials to aerospace and industrial markets. Our comprehensive range includes:

- HexTow® carbon fibers
- HexForce® reinforcements
- HiMax™ non-crimp fabrics
- HexPly® prepgres
- HexMC® molding compounds
- HexFlow® RTM resins
- Redux® adhesives
- HexTOOL® tooling materials
- HexWeb® honeycombs
- Acousti-Cap® sound attenuating honeycomb
- Engineered core
- Engineered products

For US quotes, orders and product information call toll-free 1-866-556-2662. For other worldwide sales office telephone numbers and a full address list, please go to:

<http://www.hexcel.com/contact/salesoffice>

©2016 Hexcel Corporation – All rights reserved. Hexcel Corporation and its subsidiaries (“Hexcel”) believe that the technical data and other information provided herein was materially accurate as of the date this document was issued. Hexcel reserves the right to update, revise or modify such technical data and information at any time. Any performance values provided are considered representative but do not and should not constitute a substitute for your own testing of the suitability of our products for your particular purpose. **Hexcel makes no warranty or representation, express or implied, including but not limited to the implied warranties of merchantability and fitness for a particular purpose, and disclaims any liability arising out of or related to, the use of or reliance upon any of the technical data or information contained in this document.**



Loctite® Frekote® B-15™

Known as Frekote B-15

December 2013

PRODUCT DESCRIPTION

Loctite® Frekote® B-15™ provides the following product characteristics:

Technology	Mold Sealer
Appearance	Clear, colorless ^{LMS}
Chemical Type	Solvent Based Polymer
Odor	Solvent
Cure	Room temperature cure
Cured Thermal Stability	≤400 °C
Application	Mold Sealer
Application Temperature	20 to 60 °C
Specific Benefit	<ul style="list-style-type: none"> • No contaminating transfer • High thermal stability • Seals mold porosity, scratches or imperfections

Loctite® Frekote® B-15™ is formulated specifically as a sealer for composite and metal molds with micro porosity problems, small surface scratches or imperfections. Used in conjunction with other Frekote® products, Loctite® Frekote® B-15™ provides an excellent base coat enhancing the release advantages offered.

TYPICAL PROPERTIES OF UNCURED MATERIAL

Specific Gravity @ 25 °C 0.745 to 0.775^{LMS}

Flash Point - See SDS

Release Agent Transfer ≥4^{LMS}

GENERAL INFORMATION

This product is not recommended for use in pure oxygen and/or oxygen rich systems and should not be selected as a sealant for chlorine or other strong oxidizing materials.

For safe handling information on this product, consult the Safety Data Sheet (SDS).

Mold Preparation

Cleaning:

Mold surfaces must be thoroughly cleaned and dried. All traces of prior release must be removed. This may be accomplished by using Loctite® Frekote® PMC or other suitable cleaner. Loctite® Frekote® 915WB™ or light abrasives can be used for heavy build-up.

Directions for use:

1. Loctite® Frekote® B-15™ can be applied to mold surfaces by spraying, brushing, dipping or wiping with a clean, lint free, cotton wiping cloth. When spraying, ensure a dry air source is used or use an airless spray system making sure the nozzles is 20 to 25 cm from the mold surface.
2. Brushing and dipping are effective methods of application, but care should be taken to avoid excessive pooling and to ensure that the part is well drained. Wiping on is the best method of application.
3. Only a thin wet film is required. It is suggested that small areas be coated, working progressively from one mold to the other.
4. Apply a minimum of two coats, allowing 30 minutes between coats.
5. The final coat will cure within 24 hours at 23°C or the cure process can be shortened by baking the mold for 60 minutes at 95°C after ensuring that the mold is dry and all solvents have flashed off.
6. The mold is now ready to be coated with Frekote mold release products. Please refer to individual product data sheets for the proper application of the release agent.

Mold Touch up

Touch up coats with a sealer should only be applied to areas where the mold was repaired. On repaired areas apply the same number of sealer and release agent coats like for the base coating onto new or refurbished molds.

Loctite Material Specification^{LMS}

LMS dated December 18, 2002. Test reports for each batch are available for the indicated properties. LMS test reports include selected QC test parameters considered appropriate to specifications for customer use. Additionally, comprehensive controls are in place to assure product quality and consistency. Special customer specification requirements may be coordinated through Henkel Quality.



Storage

The product is classified as flammable and must be stored in an appropriate manner in compliance with relevant regulations. Do not store near oxidizing agents or combustible materials. Store product in the unopened container in a dry location. Storage information may also be indicated on the product container labelling.

Optimal Storage: 8 °C to 21 °C. Storage below 8 °C or greater than 28 °C can adversely affect product properties.
Material removed from containers may be contaminated during use. Do not return product to the original container. Henkel cannot assume responsibility for product which has been contaminated or stored under conditions other than those previously indicated. If additional information is required, please contact your local Technical Service Center or Customer Service Representative.

Note:

The information provided in this Technical Data Sheet (TDS) including the recommendations for use and application of the product are based on our knowledge and experience of the product as at the date of this TDS. The product can have a variety of different applications as well as differing application and working conditions in your environment that are beyond our control. Henkel is, therefore, not liable for the suitability of our product for the production processes and conditions in respect of which you use them, as well as the intended applications and results. We strongly recommend that you carry out your own prior trials to confirm such suitability of our product.

Any liability in respect of the information in the Technical Data Sheet or any other written or oral recommendation(s) regarding the concerned product is excluded, except if otherwise explicitly agreed and except in relation to death or personal injury caused by our negligence and any liability under any applicable mandatory product liability law.

In case products are delivered by Henkel Belgium NV, Henkel Electronic Materials NV, Henkel Nederland BV, Henkel Technologies France SAS and Henkel France SA please additionally note the following:

In case Henkel would be nevertheless held liable, on whatever legal ground, Henkel's liability will in no event exceed the amount of the concerned delivery.

In case products are delivered by Henkel Colombiana, S.A.S. the following disclaimer is applicable:

The information provided in this Technical Data Sheet (TDS) including the recommendations for use and application of the product are based on our knowledge and experience of the product as at the date of this TDS. Henkel is, therefore, not liable for the suitability of our product for the production processes and conditions in respect of which you use them, as well as the intended applications and results. We strongly recommend that you carry out your own prior trials to confirm such suitability of our product.

Any liability in respect of the information in the Technical Data Sheet or any other written or oral recommendation(s) regarding the concerned product is excluded, except if otherwise explicitly agreed and except in relation to death or personal injury caused by our negligence and any liability under any applicable mandatory product liability law.

In case products are delivered by Henkel Corporation, Resin Technology Group, Inc., or Henkel Canada Corporation, the following disclaimer is applicable:

The data contained herein are furnished for information only and are believed to be reliable. We cannot assume responsibility for the results obtained by others over whose methods we have no control. It is the user's responsibility to determine suitability for the user's purpose of any production methods mentioned herein and to adopt such precautions as may be advisable for the protection of property and of persons against any hazards that may be involved in the handling and use thereof. In light of the foregoing, **Henkel Corporation specifically disclaims all warranties expressed or implied, including warranties of merchantability or fitness for a particular purpose, arising from sale or use of Henkel Corporation's products. Henkel Corporation specifically disclaims any liability for consequential or incidental damages of any kind, including lost profits.** The discussion herein of various processes or compositions is not to be interpreted as representation that they are free from domination of patents owned by others or as a license under any Henkel Corporation patents that may cover such processes or compositions. We recommend that each prospective user test his proposed application before repetitive use, using this data as a guide. This product may be covered by one or more United States or foreign patents or patent applications.

Trademark usage

Except as otherwise noted, all trademarks in this document are trademarks of Henkel Corporation in the U.S. and elsewhere. ® denotes a trademark registered in the U.S. Patent and Trademark Office.

Reference 0.1



LOCTITE® FREKOTE 700-NC™

Known as 700-NC™

January 2015

PRODUCT DESCRIPTION

LOCTITE® FREKOTE 700-NC™ provides the following product characteristics:

Technology	Mold Release
Appearance	Clear, colorless ^{LMS}
Chemical Type	Solvent Based Polymer
Odor	Solvent
Cure	Room temperature cure
Cured Thermal Stability	≤400 °C
Application	Release Coatings
Application Temperature	13 to 135 °C
Specific Benefit	<ul style="list-style-type: none"> • No chlorinated solvents • High gloss finish • High slip • No contaminating transfer • No mold build-up

LOCTITE® FREKOTE 700-NC™ offers excellent release properties for the most demanding applications and is a great all-purpose release agent. LOCTITE® FREKOTE 700-NC™ releases epoxies, polyester resins, thermoplastics, rubber compounds and most other molded polymers.

TYPICAL PROPERTIES OF UNCURED MATERIAL

Specific Gravity @ 25 °C 0.755 to 0.764^{LMS}

Flash Point - See SDS

GENERAL INFORMATION

This product is not recommended for use in pure oxygen and/or oxygen rich systems and should not be selected as a sealant for chlorine or other strong oxidizing materials.

For safe handling information on this product, consult the Safety Data Sheet (SDS).

Mold Preparation

Cleaning:

Mold surfaces must be thoroughly cleaned and dried. All traces of prior release must be removed. This may be accomplished by using Frekote® PMC or other suitable cleaner. Frekote® 915WB™ or light abrasives can be used for heavy build-up.

Sealing New/Repaired Molds:

Occasionally, green or freshly repaired molds are rushed into service prior to complete cure causing an increased amount of free styrene on the mold surface. Fresh or "production line"

repairs, new fiberglass and epoxy molds should be cured per manufacturer's instructions, usually a minimum of 2 -3 weeks at 22°C before starting full-scale production. Fully cured previously unused molds should be sealed before use. This can be accomplished by applying one to two coats of an appropriate Frekote® mold sealer, following the directions for use instructions. Allow full cure of the appropriate Frekote® mold sealer before you apply the first coat of LOCTITE® FREKOTE 700-NC™ as outlined in the directions of use.

Directions for use:

1. LOCTITE® FREKOTE 700-NC™ can be applied to mold surfaces at room temperature up to 135°C by spraying, brushing or wiping with a clean lint-free, cloth. When spraying ensure a dry air source is used or use an airless spray system. Always use in a well ventilated area.
2. Wipe or spray on a smooth, thin, continuous, wet film. Avoid wiping or spraying over the same area that was just coated until the solvent has evaporated. If spraying, hold nozzle 20 to 30cm from mold surface. It is suggested that small areas be coated, working progressively from one side of the mold to the other.
3. Initially, apply 2 to 3 base coats allowing 5 to 10 minutes between coats for solvent evaporation .
4. Allow the final coat to cure for 15 to 20 minutes at 22°C.
5. Maximum releases will be obtained as the mold surface becomes conditioned to LOCTITE® FREKOTE 700-NC™ . Performance can be enhanced by re-coating once, after the first few initial pulls.
6. When any release difficulty is experienced, the area in question can be "touched-up" by re-coating the entire mold surface or just those areas where release difficulty is occurring.
7. **NOTE:** LOCTITE® FREKOTE 700-NC™ is moisture sensitive, keep container tightly closed when not in use. The product should always be used in a well ventilated area.
8. **Precaution:** Users of closed mold systems (rotomolding) must be certain that solvent evaporation is complete and that all solvent vapors have been ventilated from the mold cavity prior to closing the mold. An oil-free compressed air source can be used to assist in evaporation of solvents and ventilation of the mold cavity.



Mold Touch up

Touch up coats should only be applied to areas where poor release is noticed and should be applied using the same method as base coats. This will reduce the possibility of release agent or polymer build-up. The frequency of touch ups will depend on the polymer type, mold configuration, and abrasion parameters.

Loctite Material Specification^{LMS}

LMS dated May 10, 2006. Test reports for each batch are available for the indicated properties. LMS test reports include selected QC test parameters considered appropriate to specifications for customer use. Additionally, comprehensive controls are in place to assure product quality and consistency. Special customer specification requirements may be coordinated through Henkel Quality.

Storage

The product is classified as flammable and must be stored in an appropriate manner in compliance with relevant regulations. Do not store near oxidizing agents or combustible materials. Store product in the unopened container in a dry location. Storage information may also be indicated on the product container labelling.

Optimal Storage: 8 °C to 21 °C. Storage below 8 °C or greater than 28 °C can adversely affect product properties.

Material removed from containers may be contaminated during use. Do not return product to the original container. Henkel cannot assume responsibility for product which has been contaminated or stored under conditions other than those previously indicated. If additional information is required, please contact your local Technical Service Center or Customer Service Representative.

Conversions

(°C x 1.8) + 32 = °F
 kV/mm x 25.4 = V/mil
 mm / 25.4 = inches
 µm / 25.4 = mil
 N x 0.225 = lb
 N/mm x 5.71 = lb/in
 N/mm² x 145 = psi
 MPa x 145 = psi
 N·m x 8.851 = lb·in
 N·m x 0.738 = lb·ft
 N·mm x 0.142 = oz·in
 mPa·s = cP

Note:

The information provided in this Technical Data Sheet (TDS) including the recommendations for use and application of the product are based on our knowledge and experience of the product as at the date of this TDS. The product can have a variety of different applications as well as differing application and working conditions in your environment that are beyond our control. Henkel is, therefore, not liable for the suitability of our product for the production processes and conditions in respect of which you use them, as well as the intended applications and results. We strongly recommend that you carry out your own prior trials to confirm such suitability of our product.

Any liability in respect of the information in the Technical Data Sheet or any other written or oral recommendation(s) regarding the concerned product is excluded, except if otherwise explicitly agreed and except in relation to death or personal injury caused by our negligence and any liability under any applicable mandatory product liability law.

In case products are delivered by Henkel Belgium NV, Henkel Electronic Materials NV, Henkel Nederland BV, Henkel Technologies France SAS and Henkel France SA please additionally note the following:

In case Henkel would be nevertheless held liable, on whatever legal ground, Henkel's liability will in no event exceed the amount of the concerned delivery.

In case products are delivered by Henkel Colombiana, S.A.S. the following disclaimer is applicable:

The information provided in this Technical Data Sheet (TDS) including the recommendations for use and application of the product are based on our knowledge and experience of the product as at the date of this TDS. Henkel is, therefore, not liable for the suitability of our product for the production processes and conditions in respect of which you use them, as well as the intended applications and results. We strongly recommend that you carry out your own prior trials to confirm such suitability of our product.

Any liability in respect of the information in the Technical Data Sheet or any other written or oral recommendation(s) regarding the concerned product is excluded, except if otherwise explicitly agreed and except in relation to death or personal injury caused by our negligence and any liability under any applicable mandatory product liability law.

In case products are delivered by Henkel Corporation, Resin Technology Group, Inc., or Henkel Canada Corporation, the following disclaimer is applicable:

The data contained herein are furnished for information only and are believed to be reliable. We cannot assume responsibility for the results obtained by others over whose methods we have no control. It is the user's responsibility to determine suitability for the user's purpose of any production methods mentioned herein and to adopt such precautions as may be advisable for the protection of property and of persons against any hazards that may be involved in the handling and use thereof. In light of the foregoing, Henkel Corporation specifically disclaims all warranties expressed or implied, including warranties of merchantability or fitness for a particular purpose, arising from sale or use of Henkel Corporation's products. Henkel Corporation specifically disclaims any liability for consequential or incidental damages of any kind, including lost profits. The discussion herein of various processes or compositions is not to be interpreted as representation that they are free from domination of patents owned by others or as a license under any Henkel Corporation patents that may cover such processes or compositions. We recommend that each prospective user test his proposed application before repetitive use, using this data as a guide. This product may be covered by one or more United States or foreign patents or patent applications.

Trademark usage

Except as otherwise noted, all trademarks in this document are trademarks of Henkel Corporation in the U.S. and elsewhere. ® denotes a trademark registered in the U.S. Patent and Trademark Office.

Reference 0.1

E

Science in the Age of Experience Conference



3DEXPERIENCE®

DASSAULT | The 3DEXPERIENCE® Company

CERTIFICATE PARTICIPANT

This certifies that Christer Oldeide, Norwegian University of Science and Technology participated in the

2017 SCIENCE IN THE AGE OF EXPERIENCE

Academic Poster Showcase

and received Favorite of the Conference for
their submission

Charles D Wilcox

Charles WILCOX
Director, SIMULIA Global Academia

Development of Hybrid Aluminum Carbon Fiber Composite Wheels for a Formula Style Race Car

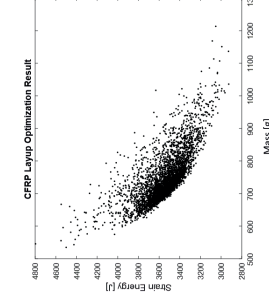
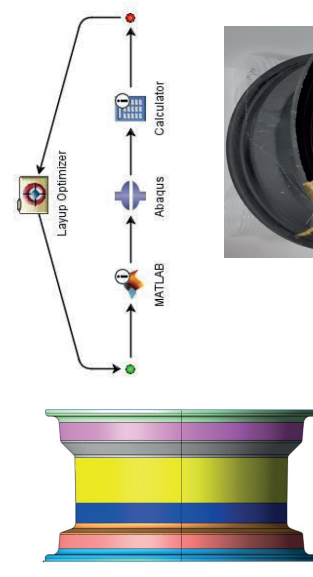
Christe Kobbvik Oldedie^{1,2}, Jørgen Elliesen^{*}, Jan Torgersen²

¹Revolve NTNU, S. P. Andersens veg 5, 7031 NORWAY
²NTNU/MTP, Richard Birkelands vei 2B, NORWAY

Race car applications pose stringent requirements to machine design. Today's requirements necessitate optimizing weight while maximizing stiffness, providing best possible traction while considering all dynamic and static loads during the competition. Working on this year's NTNU race car has introduced Evolution Based Optimization (EBO) and Topology Optimization (TO) into the design process. A hybrid design with a Carbon Fibre Reinforced Plastics (CFRP) shell and an aluminium center was chosen for the wheels. Layup and material choice was optimized in an EBO approach integrating various considerations in a holistic virtual design environment. The aluminium wheel center was TO considering manufacturing constraints and the complete assembled wheel was validated in Abaqus. The entire wheel weighs 1.68 kg while keeping stiffness to the twice of a aluminium racing wheel. The weight exactly matches the optimized design. Simulation based design continues to progress modern product development. Student race cars are a perfect showcase of what is possible and will be an integral part of future engineering.

Rim Shell - Evolutionbased material and layup optimization

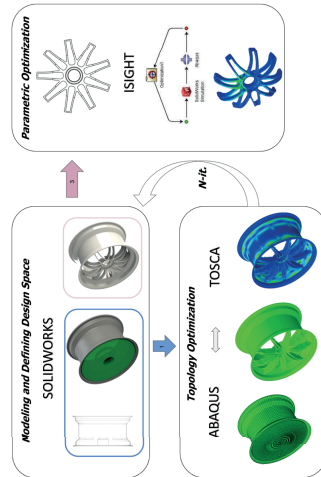
- Loads from tire tests and estimated reaction forces through log data
- Design responses: strain energy (all steps)
- Constraint: Weight target 700 g
- Material use <= 0.4 m² UD
- Design variables: 8 independent zones on shell:
numbers of plies, orientations (90:15:90),
materials (UD, weave)



Validation of assumption made:
 - including non-linear effect from
 pretension of bolts and center lock

Rim Center - Design process

- Optimized with Tosca and Isight (minimizing strain energy and maximizing stiffness)
- Manually optimized for CNC machining
- Weight 920 g





Colophon

THIS THESIS WAS TYPESET using L^AT_EX, originally developed by Leslie Lamport and based on Donald Knuth's T_EX. The body text is set in 11 point Arno Pro, designed by Robert Slimbach in the style of book types from the Aldine Press in Venice, and issued by Adobe in 2007. A template, which can be used to format a PhD thesis with this look and feel, has been released under the permissive MIT (x11) license, and can be found online at github.com/suchow/ or from the author at suchow@post.harvard.edu.